Design and Development of Potential α-Synuclein PET Tracers: Synthesis and Evaluation of Diarylpyrazole- and 2-Styrylbenzothiazole-based Libraries

Dissertation

der Mathematisch-Naturwissenschaftlichen Fakultät
der Eberhard Karls Universität Tübingen
zur Erlangung des Grades eines
Doktors der Naturwissenschaften
(Dr. rer. nat.)

vorgelegt von
Adriana Di Nanni
aus Bari, Italien

Tübingen
2023

Gedruckt mit Genehmigung der Mathematisch-Naturwissenschaftlichen Fakultät der Eberhard Karls Universität Tübingen.

Tag der mündlichen Qualifikation:	19.12.2023
Dekan:	Prof. Dr. Thilo Stehle
1. Berichterstatter:	Prof. Dr. Bernd J. Pichler
2. Berichterstatter:	Prof. Dr. Stefan Laufer

Abstract

Parkinson's disease (PD), multiple system atrophy (MSA), and dementia with Lewy bodies (DLB) are collectively identified as synucleinopathies, a group of neurodegenerative diseases which are defined by the accumulation of α-synuclein (αSYN) fibrils as the characteristic hallmark of pathogenesis. [1] A technique to detect and quantify these aggregates *in vivo* would be critical to the advancement of the field, drastically transforming the understanding, diagnosis and treatment of synucleinopathies. Multiple studies across the recent literature have highlighted some promising αSYN ligands, [2] however no candidate has yet displayed a suitable binding profile to overcome all challenges set by this target and to successfully reach clinical application.

Overall, this study aimed at enhancing the affinity and selectivity of attractive scaffolds from the literature, with the goal of ultimately establishing an αSYN PET tracer.

The rational drug design technique of molecular hybridization was applied to the SIL and MODAG scaffolds to develop a library of diarylpyrazole- (DAP) based hybrid compounds in the pursue of an enhancement of their binding properties. The *in vitro* assessment of DAPs via [^{3}H]SIL26 and [^{3}H]MODAG-001 competition binding assays disproved the original hypothesis for this attachment strategy and demonstrated a shift of selectivity towards amyloid β (Aβ) instead, indicating a theranostic potential for Alzheimer's disease (AD). [3]

The flexibility increase induced by the ring-opening modification on the phenothiazine moiety of DAPs did not result in an enhanced αSYN affinity but instead a complete loss of competition, along with a considerable decrease in Aβ binding. [3]

Simultaneously, this study investigated a 2-styrylbenzothiazole-based library, originating from the αSYN selective fluorescent probe RB1. The lead compound **PFSB** and its less lipophilic derivative **MFSB** were selected from a set of 42 novel compounds for their favorable binding affinity. Both [^{3}H]PiB competition assays and *in vitro* autoradiography on human brain slices demonstrated a remarkable αSYN/Aβ selectivity. Together with the display of blood-brain barrier penetration and brain-uptake in the *in vivo* PET evaluation of [^{18}F]**MFSB**, these findings highlight 2-styrylbenzothiazoles as a potential critical step forward in the development of αSYN radioligands, although requiring further structural optimization to improve their pharmacokinetics as well as the evaluation of off-target binding in direct assays. [4]

The research presented in this thesis overall provides additional insights on the structural features influencing selectivity among neurodegeneration-associated misfolded proteins and describes a novel candidate for the *in vivo* detection of αSYN.

Zusammenfassung

Innerhalb der sogenannten neurodegenerativen Erkrankungen werden die Parkinson-Krankheit, Multiple System-Atrophie und Demenz mit Lewy-Körperchen gemeinsam als Synucleinopathien zusammengefasst, da sie durch die Anhäufung von α-Synuclein (αSYN)-Fibrillen als charakteristisches Merkmal der Pathogenese definieren. [1] Eine Möglichkeit zum Nachweis und zur Quantifizierung dieser Aggregate *in vivo* würde einen enormen Fortschritt auf diesem Gebiet bedeuten und ein besseres Verständnis, frühere und genauere Diagnose und die Entwicklung von Therapien der Synucleinopathien ermöglichen oder begünstigen.

Mehrere Studien in der jüngeren Literatur haben einige vielversprechende αSYN-Liganden als potenzielle Radiotracer identifiziert, [2] bislang hat jedoch noch kein Kandidat ein geeignetes Bindungsprofil gezeigt, um alle Herausforderungen dieses Ziels zu meistern und eine erfolgreiche klinische Anwendung zu erreichen.

Insgesamt zielte diese Arbeit deshalb darauf ab, die Affinität und Selektivität attraktiver Gerüstsubstanzen aus der Literatur zu verbessern, mit dem ultimativen Ziel der Entwicklung eines geeigneten αSYN-PET-Tracers.

Die *Rational Drug Design*-Technik der molekularen Hybridisierung wurde auf die SIL- und MODAG-Gerüste angewandt, um eine Bibliothek von Diarylpyrazol- (DAP) basierten Hybridverbindungen zu generieren, um ihre guten Bindungseigenschaften zu kombinieren. Die *in vitro*-Untersuchung der DAPs mit Hilfe von [^{3}H]SIL26- und [^{3}H]MODAG-001- Kompetitionsbindungsversuchen zeigte leider für die synthetisierten Verbindungen, dass dieser Weg die Affinität zu αSYN nicht verbessert und zeigte stattdessen eine Verschiebung der

Selektivität in Richtung Amyloid β (Aβ), was durch Ähnlichkeit der Verbindungen zu literaturbekannten Verbindungen ein theranostisches Potenzial für die Alzheimer-Krankheit indizieren könnte. [3]

Eine durch die Ringöffnungsmodifikation an der Phenothiazin-Einheit der DAPs induzierte Flexibilitätserhöhung führte nicht zu einer erhöhten αSYN-Affinität, sondern zu einem vollständigen Verlust der Kompetition, zusammen mit einer erheblichen Abnahme der Aβ-Bindung. [3]

Gleichzeitig wurde in dieser Studie eine auf 2-Styrylbenzothiazolen basierende Bibliothek untersucht, die von dem selektiven αSYN-Fluoreszenzliganden RB1 entstanden ist. Die Leitverbindung **PFSB** und ihr weniger lipophiles Derivat **MFSB** wurden aufgrund ihrer günstigen Bindungsaffinität aus einer Reihe von 42 neuen Verbindungen ausgewählt. Sowohl [^{3}H]PiB-Kompetitions-Versuche als auch *in vitro*-Autoradiographie an pathologischen menschlichen Hirnschnitten zeigten eine bemerkenswerte αSYN/Aβ-Selektivität. Zusammen mit dem Nachweis des Überwindens der Blut-Hirn-Schranke und der Aufnahme durch das Gehirn bei der *in vivo*-PET-Bewertung von [^{18}F]**MFSB** unterstreichen diese Ergebnisse, dass 2-Styrylbenzothiazole einen entscheidenden Schritt vorwärts in der Entwicklung von Aβ-selektiven αSYN-Radioliganden darstellen könnten, auch wenn eine weitere strukturelle Optimierung zur Verbesserung ihrer Pharmakokinetik erforderlich ist, sowie die genauere Untersuchung möglicher Off-Target-Bindungen in direkten Assays. [4]

Die in dieser Arbeit vorgestellte Forschung liefert insgesamt zusätzliche Erkenntnisse über die strukturellen Merkmale, die die Selektivität von mit Neurodegeneration verbundenen fehlgefalteten

Proteinen beeinflussen, und beschreibt einen neuen vielversprechenden Kandidaten für den *in vivo*-Nachweis von αSYN.

Abbreviations

3D	Three-dimensional
Aβ	Amyloid β
AD	Alzheimer's disease
A_m	Molar activity
αSYN	α-synuclein
BBB	Blood-brain barrier
B_{max}	Receptor density
CMRF	Copper-mediated radiofluorination
CNS	Central nervous system
CNS MPO	Central nervous system multiparameter optimization
Cryo-EM	Cryogenic electron microscopy
CSF	Cerebrospinal fluid
CT	Computed tomography
DABTA	Diarylbisthiazole
DAP	Diarylpyrazole
DAT	Dopamine transporter
DLB	Dementia with Lewy bodies
DoE	Design of experiments
DPP	3,5-Diphenylpyrazoles
EWG	Electron-withdrawing groups
GCIs	Glial cytoplasmic inclusions
IHC	Immunohistochemistry
K_{222}	Kryptofix 2.2.2
K_d	Dissociation constant
K_i	Inhibitor constant
LBs	Lewy bodies

LNs	Lewy neurites
MDS	International Parkinson and Movement Disorder Society
MRI	Magnetic resonance imaging
mRNA	messenger RNA
MSA	Multiple system atrophy
NAC	Non-amyloid-β-component
NCIs	Neuronal cytoplasmic inclusions
NFT	Neurofibrillary tangles
NMDA	*N*-methyl-D-aspartate
NMR	Nuclear magnetic resonance
NMS	Non-motor symptoms
NSB	Non-specific binding
PD	Parkinson's disease
PDD	Parkinson's disease dementia
PE	Petroleum ether
PET	Positron emission tomography
PLD2	Phospholipase D2
PNS	Peripheral nervous system
pTau	PhosphoTau
RBD	Rapid-eye-movement sleep behavior disorder
RCC	Radiochemical conversion
RCP	Radiochemical purity
RCY	Radiochemical yield
R_f	Retention factor
ROI	Region of interest
SAR	Structure-activity relationship
SB	Specific binding

SEM	Standard error of the mean
SERT	Serotonin transporters
siRNA	Small interfering RNA
S_NAr	Nucleophilic aromatic substitution
SPE	Solid-phase extraction
ssNMR	Solid-state NMR
SUV	Standardized uptake value
SV2A	Synaptic vesicle glycoprotein 2A
TAC	Time-activity curve
TBS	Tris-buffered saline
TH	Tyrosine hydroxylase
ThT	Thioflavin T
TPSA	Topological polar surface area
VMAT2	Vesicular monoamine transporter 2
VOI	Volume of interest
wt	Wild-type

Acknowledgments and disclosure

I declare that I personally wrote this doctoral thesis, under the supervision of Dr. Andreas Maurer, Prof. Dr. Bernd Pichler and Prof. Dr. Stefan Laufer.

This research was mainly carried out at the Department of Preclinical Imaging and Radiopharmacy, Werner Siemens Imaging Center, Eberhard Karls University Tübingen and funded by the European Union's Horizon 2020 research and innovation program under the Marie Skłodowska-Curie grant agreement n° 813528. Additional funding was provided by the Werner Siemens Foundation. Part of the organic synthesis work was carried out at the Department of Drug Design and Pharmacology, Faculty of Health and Medicinal Sciences, University of Copenhagen.

The libraries were designed under the guidance of Dr. Andreas Maurer, Dr. Gregory D. Bowden (GB), Prof. Dr. Umberto M. Battisti and Prof. Dr. Matthias M. Herth. All organic synthesis and compound characterization was performed by Adriana Di Nanni (AD). All radiosyntheses of fluorinated tracers were established and carried out by AD, under the guidance and training of GB and Johannes Kinzler. *In vitro* fibril binding assays, autoradiography and immunohistochemistry experiments, as well as *in vivo* PET/MR scans were performed by Ran Sing Saw (RS), under the supervision of Prof. Dr. Kristina Herfert. Data analysis for the aforementioned biological evaluation was carried out by AD.

The tritium-labeled radioligand [^{3}H]MODAG-001 was provided by MODAG GmbH. [^{3}H]PiB was purchased from RC Tritec AG. The radiolabeling of [^{3}H]SIL26 was performed by Dr. Natasha S. R. Bidesi

and Špela Korat at the Department of Radiology and Nuclear Medicine, Vrije Universiteit Amsterdam under the supervision of Prof. Dr. Matthias M. Herth, Prof Dr. Albert D. Windhorst and Prof. Dr. Daniëlle Vugts. αSYN fibrils were produced and characterized by Dr. Kaare Bjerregaard-Andersen at the Department of Antibody Engineering and Biochemistry, H. Lundbeck A/S. $A\beta_{1-42}$ fibrils were produced and characterized by RS.

Table of Contents

Abstract I

Zusammenfassung III

Abbreviations VI

Acknowledgments and disclosure IX

Introduction 1

1. The aggregation of α-synuclein to fibrils as hallmark of pathogenesis in synucleinopathies 1

1.1 Synucleinopathies: similarities and discrepancies in histopathology and disease progression 1

1.2 αSYN physiological and pathological function 4

1.3 Other neurodegeneration-related misfolded proteins 9

2. Positron emission tomography and the need for an αSYN PET tracer 10

2.1 The basics of positron emission tomography 10

2.2 Radiolabeling procedures 11

2.2.1 The production and processing of fluorine-18 11

2.2.2 Copper-mediated radiofluorination 13

2.3 The *in vivo* imaging of neurodegeneration 14

2.4 The clinical need for an αSYN PET tracer 16

2.4.1 Currently employed imaging targets 17

2.4.2 αSYN-targeted therapies and available biomarkers . 18

2.4.3 Different strategies for the development of a PET tracer 20

3 Development of an αSYN PET tracer: current status and challenges 22

3.1 Requirements for a successful αSYN PET tracer and related challenges 22

3.1.1 Multiple parameters to describe binding affinity 25

3.2 The most promising scaffolds: their advantages and limitations 27

4 Aims of the study 32

4.1 Aim 1: design and development of a library of diarylpyrazoles 33

4.2 Aim 2: design and development of a library of 2-styrylbenzothiazoles 35

Experimental section 37

1. Chemistry 37

1.1 General materials and methods 37

1.2 Synthesis of a library of diarylpyrazoles 38

1.3 Synthesis of a library of 2-styrylbenzothiazoles 67

2. Radiochemistry 119

2.1 Manual synthesis of [^{18}F]PFSB 119

2.2 Automated synthesis of [^{18}F]PFSB and [^{18}F]MFSB 119

2.3 Synthesis of tritium-labeled radioligands 121

3. Biological evaluation 122

3.1 Calculation of BBB score and CNS MPO 122
3.2 Fibril binding assays 123
3.3 Autoradiography and immunohistochemistry 124
3.4 *In vivo* PET/MR imaging 126
Results 128
1. Design and development of a library of diarylpyrazoles 128
2. Design and development of a library of 2-styrylbenzothiazoles 133
2.1 Synthesis of a 2-styrylbenzothiazol-based library and *in vitro* evaluation 133
2.2 Structural optimization 138
2.3 Radiolabeling of [^{18}F]PFSB and [^{18}F]MFSB 141
2.4 *In vitro* autoradiography and *in vivo* PET imaging 142
Discussion 146
1. Design and development of a library of diarylpyrazoles 146
2. Design and development of a library of 2-styrylbenzothiazoles 149
2.1 Synthesis of a 2-styrylbenzothiazol-based library and *in vitro* evaluation 149
2.2 Structural optimization 153
2.3 Radiolabeling of [^{18}F]PFSB and [^{18}F]MFSB 155
2.4 *In vitro* autoradiography and *in vivo* PET imaging 158
3. General conclusion 160

Publications and patent applications 162

References 163

Appendix 176

1. ^{1}H NMR spectra of the tested compounds 176

2. ^{1}H NMR spectra of the radiolabeling precursors 202

Introduction

1. The aggregation of α-synuclein to fibrils as hallmark of pathogenesis in synucleinopathies

1.1 Synucleinopathies: similarities and discrepancies in histopathology and disease progression

Synucleinopathies such as Parkinson's disease (PD), multiple system atrophy (MSA) and dementia with Lewy bodies (DLB) are a group of neurodegenerative diseases which share the aggregation of α-synuclein (αSYN) to fibrils as the hallmark of pathogenesis.

PD-related motor symptoms were firstly observed in 1817 by James Parkinson, who described the disease as a "shaking palsy". [5] The anatomical origin of these symptoms was located in the presence of abnormal inclusions in the brain, illustrated by Lewy in 1912, and the connection between PD and Lewy bodies (LBs) was demonstrated by following studies. [6] A similar degeneration was found in nerve cell processes, [7] consequently named Lewy neurites (LNs). Immunostaining for αSYN identified the protein as the main component of LBs from DLB and idiopathic PD, [8] as well as of LNs from both diseases. [9]

The progress of αSYN aggregates distribution across brain areas in sporadic ***PD*** was outlined by Braak *et al.* as a six-staged neuropathological development (Figure 1). Briefly, PD-related neurodegeneration starts from the olfactory structures, the medulla oblongata and the pontine tegmentum in the presymptomatic stages 1-2, reaches substantia nigra and amygdala in stage 3, and propagates to the temporal lobe in stage 4 and the neocortex in stages 5-6.

Somato-motor symptoms are expected to appear between stage 3 and 4. [10] Following studies from the same group subsequently expanded this model to include other areas of the central and peripheral nervous system (CNS/PNS). Several layers of the spinal cord, as well as para- and sympathetic pre- and post-ganglionic neurons, displayed their involvement in PD progression since stage 2, resulting in the generation of premotor symptoms and pain. [11, 12] The uncovering of αSYN depositions in the vagal nerves gave rise to the "gut theory", which interprets the advancement of LBs-associated neurodegeneration as a result of the gut-brain axis, with the gut microbiome being involved in the regulation of brain functions. [13] To date, this hypothesis is still vastly debated.

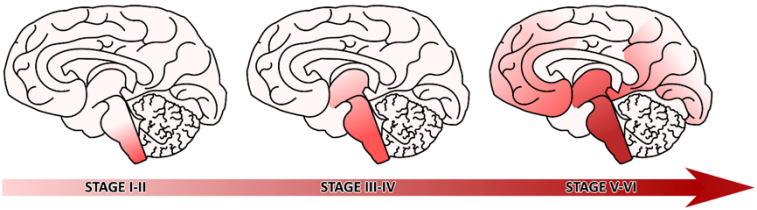

Figure 1. Schematic representation of the six stages of PD-associated neurodegeneration described by Braak et al. Figure generated via Inkscape 1.2.1 in reference to [10].

To explain the sequential spreading of LB pathology across different regions of the nervous system, a prion-like disease model was proposed. [14] Three studies from 2008 simultaneously documented the implantation of embryonic dopaminergic neurons into the brain of PD patients and, in some cases, revealed the propagation of LBs accumulation from host to grafted cells. [15-17] Together with the detection of cell-to-cell transmission from neurons to neural stem cells, [18] these findings led to the hypothesis of αSYN oligomers spreading in a prion-like manner. [19] Subsequent studies supported the neuron-to-neuron transportation hypothesis: αSYN release into the

extracellular space via an exosome-mediated exocytosis process in a calcium-dependent manner and the following uptake by naïve cells were reported. [20, 21]

Similar to PD in its histopathological display of LBs and LNs but also incorporating an early appearance of Alzheimer's disease (AD) -like dementia, ***DLB*** was originally described by Kosaka *et al.* as a combination of various neurodegenerative diseases. [22] Consensus guidelines for the diagnosis of DLB highlighted psychiatric symptoms such as visual hallucinations and fluctuations in cognitive function, as well as REM sleep behavior disorder as early occurring typical features of this disease, together with motor PD-characteristic symptoms. [23, 24] LB pathology was observed as qualitatively analogous to PD but quantitatively dissimilar in its anatomical distribution. [25] Additionally, most DLB cases present an AD-like concentration of amyloid β (Aβ) plaques and, some of them, tau aggregates. [23] As several advanced PD cases exhibit dementia and cognitive impairment too, the general consensus sets the requirement of at least a year of well-established motor-only symptoms before its manifestation for the nosological discrimination of PD dementia (PDD) from DLB. [26, 27]

Compared to the previously discussed synucleinopathies, ***MSA*** reveals a greater discrepancy in histopathological and symptomatic features (Figure 2). MSA was firstly depicted as a conjunction of striatonigral degeneration, [28] olivopontocerebellar atrophy [29] and Shy-Drager syndrome [30] exhibiting abnormal glial cytoplasmic inclusion (GCIs) as pathological hallmark. [31] The ultrastructural examination of GCIs pointed out their significant morphological difference from LBs: Murayama *et al.* described GCIs as granule-associated filaments with diameters of approximately 25 nm, building a network in the middle of oligodendrocytes and occasionally

generating flame-shaped tangle-like structures. [32] Less abundant but morphologically analogous to GCIs, neuronal cytoplasmic inclusions (NCIs) were also identified as a characteristic feature of MSA pathology, [33] particularly frequent in specific regions such as the anterior cingulate cortex and agranular frontal cortex. [34]

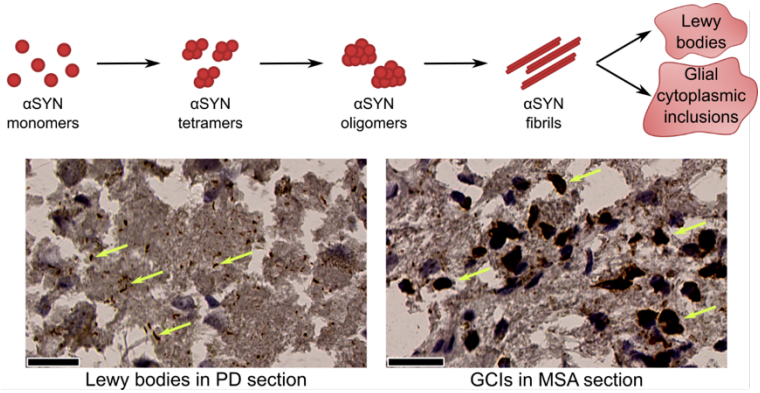

Figure 2. Schematic representation of LBs and GCIs aggregation and immunostained human brain sections from PD (left) and MSA (right) patients. Arrows indicate LBs and GCIs respectively, scale bar: 25 μm. Handling of the brain tissue and acquisition of the immunohistochemistry images are described in the experimental section (paragraph 3.3).

Despite the significant discrepancy in location and morphology which differentiates LBs and LNs from MSA histopathology, a critical factor connects the latter with Lewy body disorders (PD and DLB). Spillantini *et al.* revealed αSYN fibrils are a major component of the filaments detected in frontal cortex and cerebellum of MSA cases, leading to the unification of the diseases discussed above under the comprehensive class of synucleinopathies as a widespread category of neurodegenerative disorders. [1]

1.2 αSYN physiological and pathological function

αSYN was firstly identified as non-amyloid-β-component (NAC) precursor, a peptide of 140 amino acids (Figure 3) found in low

percentages in Aβ plaques in AD brains. [35] It shares the amino-terminal sequence with the two other proteins constituting the synuclein family, whereas the number of repeat regions and the carboxy-terminal region differentiate them into α-, β- and γ-synuclein. [36]

αSYN is physiologically present in the healthy brain, where one of its normal functions is putatively the inhibition of phospholipase D2 (PLD2), [37] affecting the PLD2-catalyzed hydrolysis of phosphatidylcholine into phosphatidic acid and therefore the regulation of the synaptic vesicle cycle. [38] It has also been shown to act similarly to apolipoprotein A1 in the origination of membrane curvature: its insertion in the amphipathic layer generates smaller vesicles and ultimately modulates dopamine release. [39]

Furthermore, it inhibits the activity of tyrosine hydroxylase (TH) by decreasing its phosphorylation. As TH is the rate-limiting enzyme in dopamine biosynthesis, when pathological aggregation reduces the amount of soluble αSYN it consequently alters the homeostasis in dopaminergic cells, leading to cell death. [40]

An interaction with DNA has recently been described, with αSYN modulating its damage response and stimulating its repair function, particularly in the case of double-strand break. [41] A chaperone-like activity has been observed as well, [42] and has been specifically linked to the second acidic repeat carboxy-terminal region, residues 125-140. [43]

Several other αSYN-protein interactions have been proposed, although the impact most of them have on cell physiology remains to be fully understood. [44] The similarity between αSYN and its corresponding zebra finch protein putatively involved in the song learning process, synelfin, suggested a potential connection with

neural plasticity in the human brain. [45] Behavioral studies in αSYN knockout mice corroborated its involvement in learning ability and in working and spatial memory. [46]

Similarly to its physiological function, the conversion of native αSYN into its corresponding toxic species still needs further clarification. Soluble αSYN can exist in the monomeric or tetrameric forms or generate higher-level oligomers, all conformations being in mutual equilibrium. Toxicity comparison between oligomers and fibrils is still widely debated. [47, 48]

The aggregation process into insoluble fibrils may originate from dysfunctional post-translational modifications. [49] For instance, nitration of tyrosine-39 residues (Figure 3) is highly recurrent in LBs. The presence of a relatively bulky group alters folding and function of the protein and reduces its solubility, accelerating fibrillogenesis. [50, 51] The abnormal selective phosphorylation of serine-129 (Figure 3) is also extensively observed and has been shown to promote fibrillation. [52]

Additionally, αSYN defective degradation is putatively involved in the accumulation process. Wild-type (wt) αSYN is typically degraded through a ubiquitin-independent mechanism by the 20S proteasome, [53] which appears to be impaired in substantia nigra of idiopathic PD cases. [54] Instead, toxic species of the protein are a substrate for mono-, di- or tri-ubiquitination, [55] being an additional example of disease-associated post-translational modification.

Furthermore, faster aggregation is detected in the case of carboxy-terminally truncated αSYN proteins. This largely negatively charged region has revealed a down-regulation of self-assembly, therefore modifications in this area, as well as its entire loss, act as a catalytic factor for fibrillogenesis. [56, 57] In fact, the central hydrophobic

domain included in the NAC region is regarded as the essential area for aggregation, particularly involving residues 71-82. [58, 59] In the fibrils structure, the NAC region together with the NAC-adjoining amino-terminal region generally represents the core, whereas the carboxy-terminal region is located peripherally. [57, 60] Nevertheless, all three domains play a role and reciprocally influence their function in oligomerization and fibrillation. [61]

The three-dimensional (3D) structure of recombinant αSYN fibrils was characterized in more detail by cryogenic electron microscopy (cryo-EM) recent studies which described it as a Greek key-like β-sheet architecture and will be further discussed and illustrated in paragraph 3.1. [60, 62-64]

Although the majority of PD cases are sporadic, mutations in the SNCA gene, the gene encoding for αSYN, were identified as a cause for fibrillation, particularly in rare early-onset cases. An A53T point mutation was described by Polymeropoulos *et al.* as an alanine to threonine substitution at position 53 (Figure 3), found in four independent families exhibiting early-onset familial PD. The area where this replacement takes place is expected to organize in an α-helical secondary structure, connected to β-sheet regions. However, the presence of a threonine obstructs the α-helix formation, putatively leading to an extension of the β-sheet conformation and consequently to pathological self-aggregation. [65] Another point mutation was simultaneously identified by Krüger *et al.*: A30P, the alanine to proline substitution at position 30 (Figure 3). Although αSYN is considered a "natively unfolded" protein, lacking a consistent secondary structure, [66] it is speculated that the A30P replacement, as well as A53T, lead to toxic aggregates by affecting the protein conformation. [67] More recent studies have identified additional mutations (E46K, [68] H50Q,

[69] G51D, [70] A53E, [71] A53V [72], Figure 3) along with duplications [73] and triplications [74] of the SNCA gene.

These findings have been used to generate transgenic PD animal models such as the A30P mice, which are currently widely used in αSYN preclinical studies. As these models are not a comprehensive representation of the disease, results need to be cautiously interpreted. However, they have oftentimes proved valuable in the evaluation of potential disease-modifying therapies or putative αSYN PET tracers. [75-77]

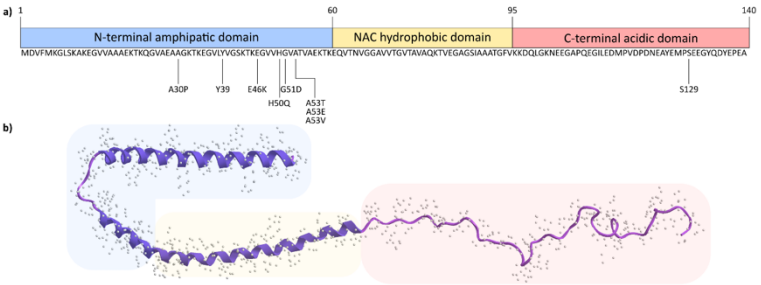

Figure 3. Schematic representation of αSYN structure: a) primary structure, mutation sites and most common site for post-translational modifications are highlighted; b) tertiary structure of monomeric αSYN (PDB ID: 1XQ8, visualized by Chem3D 20.1, PerkinElmer Informatics); N-terminal (blue), NAC (yellow) and C-terminal (red) domains are illustrated by the corresponding colors. Figure generated via Inkscape 1.2.1 in reference to [49].

1.3 Other neurodegeneration-related misfolded proteins

In the complex landscape of neurodegenerative diseases, multiple proteins are associated with the process of misfolding, aggregation and accumulation originating neurodegeneration. In this context, AD is the most widespread cause of dementia, with 90.3 million cases expected worldwide in 2040. [78]

The toxic species generating neuronal lesions in AD patients are identified as Aβ plaques and phosphoTau (pTau) -based neurofibrillary tangles (NFT), whose interaction and synergistic effect in pathology genesis and progression are still under investigation. [79-81]

The development of amyloid plaques originates from the cleavage of the amyloid precursor protein resulting in $A\beta_{1\text{-}40}$ and $A\beta_{1\text{-}42}$ peptides that progressively self-aggregate into oligomers, fibrils, and ultimately plaques. (Figure 4). [82] Concurrently with this process, pTau proteins deposit into NFT. Tau is a microtubule-associated protein which is found to be vastly hyperphosphorylated in AD tissue. Similarly to the previously discussed pathological aggregation of αSYN, this post-translational modification reshapes the physiological state of the monomers, triggering fibrillation and ultimately leading to NFTs. [82]

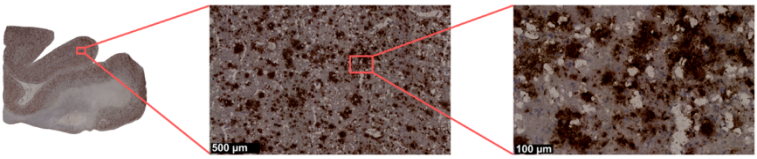

Figure 4. Identification of Aβ plaques in immunostained human brain sections from AD patients. Handling of the brain tissue and acquisition of the immunohistochemistry image are described in the experimental section (paragraph 3.3).

2. Positron emission tomography and the need for an αSYN PET tracer

2.1 The basics of positron emission tomography

Positron emission tomography (PET) is a quantitative *in vivo* imaging technique which relies on the detection of radiotracers to investigate biological processes. This approach is based on the "tracer principle", as firstly suggested by de Hevesy, who was awarded a Nobel prize in 1943 for the use of "radioactive indicators" in the study of biochemical pathways. [83]

Positron emitters are radioisotopes whose decay mainly occurs through the transformation of a proton (P^+) into a neutron (N), with simultaneous emission of a positron (β^+) and a neutrino (v) and release of the exceeding energy (E): $P^+ \rightarrow N + \beta^+ + v + E$. The positron, together with an electron from the surrounding tissue, eventually generates a short-lived positronium. Positron and electron annihilate each other, generating two gamma rays moving in opposite directions with an energy of 511 keV each. When two detectors located on opposite sides of the ring-shaped set of scintillation crystals simultaneously register two gamma rays, a "coincidence" is recorded which indicates the straight line where the annihilation happened, as illustrated in Figure 5. The optical signal received by the crystals is transmitted to photomultiplier tubes and from all recorded data 3D images are mathematically reconstructed. The PET data is typically paired with anatomic information acquired by computed tomography (CT) or magnetic resonance imaging (MRI) to provide the final image. [84]

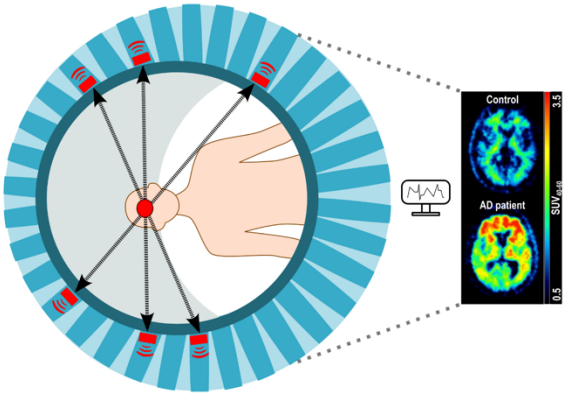

Figure 5. Illustration of the signal generated by β^+ emission in the uptake region and the recording of coincidences along a straight line by the crystal detectors in the ring-shaped PET scanner. The signal is reconstructed into a color-coded image representing the tracer uptake. Figure generated via Inkscape 1.2.1, [^{11}C]PiB brain scan image adapted from [85].

The most commonly employed radioisotopes for the labeling of small molecules are carbon-11 and fluorine-18. Although their short half-lives (20.4 min and 109.7 min respectively) raise the need for an on-site cyclotron production and rapid radiolabeling processes, their usage is favored because of reduced patient radiation dose. Albeit carbon atoms are ubiquitously present in biologically active molecules while fluorine addition produces a structural modification that might affect the affinity to the target, the latter is considered “the radionuclide of choice”: fluorine-18 allows for relatively longer handling time as well as high image resolution due to its short positron linear range in tissues. [86]

2.2 Radiolabeling procedures

2.2.1 The production and processing of fluorine-18

Multiple approaches are available for the cyclotron production of fluorine-18 and its insertion into the desired molecule. Overall,

radiofluorination can be carried out via electrophilic or nucleophilic agents.

Historically, fluorine-18 was produced from the bombardment of ^{20}Ne or $^{18}O_2$/Kr gas targets (nuclear reaction: $^{20}Ne(d,\alpha)^{18}F$ or $^{18}O(p,n)^{18}F$, respectively), affording a highly reactive $[^{18}F]F_2$ that could be employed in electrophilic substitutions. This technique being a carrier-added procedure requiring ^{19}F-fluorine gas to recover the produced fluorine-18 from the target walls, its major drawback was the low specific activity (Bq/kg) of the resulting radioligands. [87, 88]

Despite the substantially reduced reactivity, nucleophilic radiofluorinations are currently widely preferred in the radiochemistry field due to higher regiospecificity and lower carrier content. The nucleophilic source is produced in the form of $[^{18}F]F^-$: the bombardment of the liquid target $[^{18}O]H_2O$ affords an aqueous $[^{18}F]HF$ solution via an $^{18}O(p,n)^{18}F$ nuclear reaction. The fluoride atom, being vastly solvated by water molecules, requires further processing for its reactivity to be enhanced before the actual radiolabeling reaction. The standard approach involves trapping of the fluoride onto an SPE (solid-phase extraction) cartridge through ion-exchange interactions with polymer-bound R_4N^+ salts, followed by elution of a $[^{18}F]F^-$-complex, typically with Kryptofix 2.2.2 (K_{222}). An additional step of azeotropic drying by means of a more volatile solvent (typically MeCN) is performed to ensure water content is decreased to the furthest extent (Figure 6). [87] Variations to this procedure may be required depending on the planned radiolabeling approach (e.g. base-sensitive catalysis).

Due to the scarce reactivity of the fluoride-18 source, multiple novel radiofluorination strategies have been explored in the last decade in order to establish a more efficient tracer production. The synthetic procedure employed for the labeling of the radioligands evaluated in

the research hereafter presented brings emphasis to the copper-mediated radiofluorinations (CMRF), which will be briefly discussed in the following paragraph.

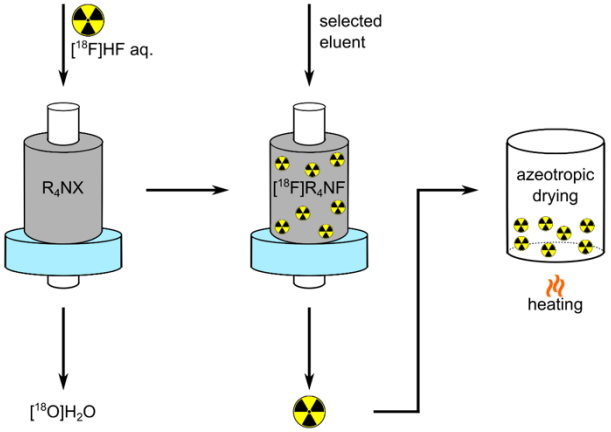

Figure 6. Schematic representation of the standard $[^{18}F]F^-$ processing via QMA trapping and azeotropic drying. Figure generated via Inkscape 1.2.1.

2.2.2 Copper-mediated radiofluorination

Direct fluorination of aromatic rings is most commonly performed via S_NAr (nucleophilic aromatic substitution) reactions. However, this approach requires the arenes to be activated, typically by *ortho*- or *para*-substitution with electron-withdrawing groups (EWG), narrowing the reaction scope for its application (Figure 7). Several strategies overcoming this limitation have been described in the literature, such as the labeling of a prosthetic group prior to its coupling with the desired scaffold, the use of bulkier leaving groups, or the transition-metals catalysis. [87] Among the proposed techniques, the CMRF of aryl boronate esters stands out for its vast reaction scope (Figure 7), as well as the employment of readily accessible and air- and moisture-stable precursors. [89]

According to the proposed mechanism, CMRF relies on the dual role of the $Cu(OTf)_2$ catalyst, which promotes the formation of a Cu(II)-organometallic complex and then oxidize it to the corresponding Cu(III) complex. Reductive elimination generates the final product. [90]

Extensive research recently focused on the evaluation and optimization of CMRF conditions, pointing out the high sensitivity of this strategy to minor changes in the reaction environment. Mossine *et al*. investigated the impact of copper source, reagents mixing order and fluoride elution techniques, [91, 92] developing a custom-made $[^{18}F]F^-$ processing involving a tailored cartridge preconditioning method and a base-free eluting solution. [93] In following design-of-experiments (DoE) studies, Bowden *et al*. evaluated the influence that precursor-, catalyst-, pyridine, solvent- and co-solvent-load have on reaction performance, as well as the temperature and the presence of air and/or argon. Their findings pointed out the challenge of a comprehensive optimization of CMRF, as different precursors may require distinct condition adaptations. [94-96]

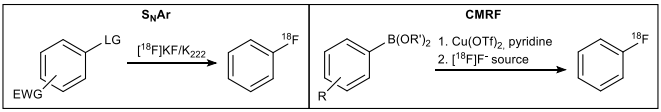

Figure 7. Different strategies for the radiofluorination of aromatic rings: comparison between the S_NAr general synthetic approach (left) and the recently developed CMRF (right).

2.3 The *in vivo* imaging of neurodegeneration

The most widespread clinical use of PET in the last four decades has been the oncological application of $[^{18}F]$FDG (2-deoxy-2-fluoroglucose, Figure 8), which partially undergoes the cellular glucose metabolism, getting trapped in the cell and highlighting tissues where this process

is pathologically increased. [97] However, several efforts have also been focused on the *in vivo* PET imaging of neurodegeneration.

Initially, [^{18}F]FDG was applied to the diagnosis of dementia [98] on the grounds that reduced glucose consumption reflects decreased synaptic density. [99] More recent research has focused on the development of tracers that specifically target aggregates of the misfolded proteins Aβ, tau and αSYN. The first compound to successfully pave the way towards imaging of neurodegeneration was the carbon-11 labeled thioflavin T- (ThT) derivative known as PiB (Pittsburgh compound B, Figure 8), the gold-standard for the preclinical imaging of Aβ plaques. [100, 101] To date, three fluorine-18 labeled tracers are FDA- and EMA-approved for clinical PET imaging of AD patients: [102] the fluorinated PiB-analog [^{18}F]flutemetamol [103] and the stilbene-based [^{18}F]florbetaben [104] and [^{18}F]florbetapir [105] (Figure 8). Complementary research has been pursuing the *in vivo* imaging of tau aggregates, leading to the FDA approval of [^{18}F]flortaucipir for the detection of tau pathology in AD patients. [106]

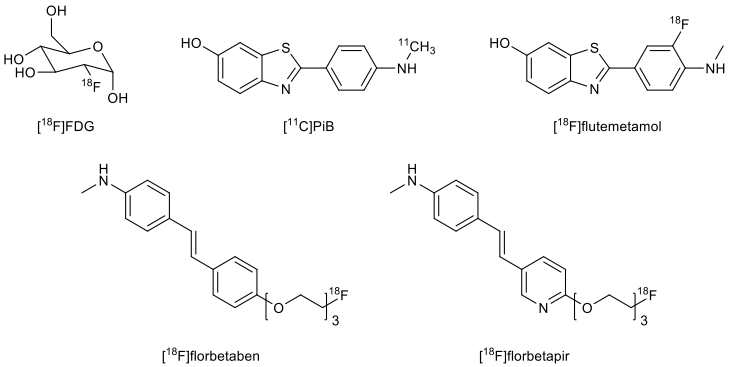

Figure 8. Structure of PET tracers commonly employed in clinical and/or preclinical neuroimaging.

Prompted by the successes discussed above, multiple studies have directed their efforts into the development of an αSYN PET tracer, but none of the proposed scaffolds has been able to reach clinical application yet.

2.4 The clinical need for an αSYN PET tracer

Neurodegenerative diseases represent an increasingly significant burden in a progressively older global population. An incidence of 108 to 212 per 100,000 new cases per year in 65+ aged persons was estimated in North America with univocal regard to PD, the most recurrent synucleinopathy and second most widespread age-related neurodegenerative disorder after AD. [107] Therefore, it is critical for the contemporary society to improve the current approach to diagnosis, monitoring, treatment and general understanding of this disease.

The clinical diagnosis of PD generally relies on fully recognizable motor symptoms. However, the synuclein-related pathogenesis anticipates them by several years. The International Parkinson and Movement Disorder Society (MDS) Task Force classified the disease expression into three progressive stages: preclinical PD, where neurodegenerative synucleinopathy is developing but no symptoms are observed; prodromal PD, which shows early non-motor (NMS) and motor symptoms; and clinical PD, with clearly defined motor symptoms. [108] At the prodromal stage, diagnosis can only be probabilistic, and defined as probable (> 80%) or possible (30% to 80%). A clear diagnosis is only produced in the clinical phase, although a definite examination is so far exclusively achievable by autopsy. [108, 109]

As illustrated by the Braak staging progression, [10] the brain regions involved in the olfactory function are the first to be affected by neurodegeneration. Hyposmia, together with sleep disorders,

depression and constipation can precede clinical symptoms by several years and therefore is considered as a possible biomarker for prodromal PD. [110, 111] The potential of rapid-eye-movement sleep behavior disorder (RBD) has been evaluated as well, as it exhibits a latency of more than 15 years and up to 50 years before the clinical manifestation of synucleinopathies. [112] Nevertheless, no reliable biomarkers are currently available for diagnosing αSYN pathology at the preclinical stage.

2.4.1 Currently employed imaging targets

Multiple different targets are currently employed for the *in vivo* detection and monitoring of prodromal and clinical synucleinopathies. [113, 114] The most commonly used PET tracers investigate dysfunctions of the dopaminergic system, responsible for rigidity and bradykinesia. For instance, this approach involves the imaging of dopamine transporters (DAT) with [^{11}C]methylphenidate [115] or [^{18}F]FE-PE2I, [116] vesicular monoamine transporter 2 (VMAT2) with [^{11}C]DTBZ, [117] dopamine turnover with [^{18}F]FDOPA, [118] D2 receptors with [^{11}C]raclopride. [119] The serotonergic function is analyzed as well, as it was proved to have a critical role in apathy, anxiety, depression, [120] and resting tremor. [121] Serotonin transporters (SERT) are typically evaluated with [^{11}C]DASB, [122] along with the 5-HT$_{1A}$ receptor, e.g. with its antagonist [^{11}C]WAY 100635. [121] Recently, the development of the synaptic vesicle glycoprotein 2A (SV2A) ligand, [^{11}C]UCB-J, added to the framework the imaging of synaptic density, which is consistently impaired in neurodegenerative diseases. [123] Furthermore, MRI techniques can detect αSYN-induced structural changes in different areas of the brain. [124] Although a combination of these approaches may be able to afford a reliable diagnosis, multiple scans can be necessary to reach

an accurate interpretation, [125, 126] which is not ideal for the patients' well-being, their radiation dose and the general costs. Also, by targeting the outcome of neurodegeneration and not its cause, none of these methods allows for a timely and definitive diagnosis as they lack in αSYN target specificity.

2.4.2 αSYN-targeted therapies and available biomarkers

To date, no therapy is available which yields full recovery from αSYN-related neurodegeneration. Current strategies solely aim at easing the severity of symptoms.

The conventional approach for treatment of PD relies on pharmacological dopamine replacement, typically with L-DOPA, often in combination with dopamine agonists, monoamine oxidase B inhibitors or catechol-O-methyl transferase inhibitors. [127] Other strategies have been developed which employ anticholinergics or amantadine but, like the dopamine-associated treatments, they exclusively focus on motor symptoms, whereas NMS are mostly addressed with symptom-specific drugs (e.g. antidepressants or anti-constipation drugs). [127] Furthermore, although in some cases effective against NMS, dopaminergic therapies are often implicated in worsening this group of symptoms. [128]

All the strategies discussed above only act at a symptomatic level, with no improvement on the actual neurodegeneration. In the past decade, several studies have focused on the development of αSYN-targeted new therapies, aiming at tackling different stages of the aggregation pathway (Figure 9). [47] Promising approaches involve: the development of small interfering RNA (siRNA) targeting αSYN messenger RNA (mRNA) to reduce its expression, [129] the increase of lysosomal and/or autophagic protein degradation, [130, 131] the suppression of post-translational modifications, [132] the decrease of

oligomers and fibrils aggregation, the obstruction of misfolded αSYN propagation, [133] the active or passive immunization with administration of vaccines or antibodies against the targeted protein respectively. [134, 135] Some small molecules have already reached clinical evaluation, [136] such as the aggregation inhibitors anle138b [137-139] (further discussed in paragraph 3.2), ENT-01 [140] and mannitol, [141] and memantine, an *N*-methyl-D-aspartate (NMDA) receptor antagonist reducing cell-to-cell αSYN transmission. [142] The progressive expansion of this field demands the establishment of a reliable biomarker for αSYN pathology as an imperative requirement: a generally validated non-invasive technique is needed to properly evaluate the effectiveness of treatments. Furthermore, in order to accurately select the patient population participating the clinical trials, it is imperative to be able to assess their condition in a systematic manner. Finally, for an αSYN-targeted therapy to be successful, it must be implemented before an excessive widening of neurodegeneration takes place.

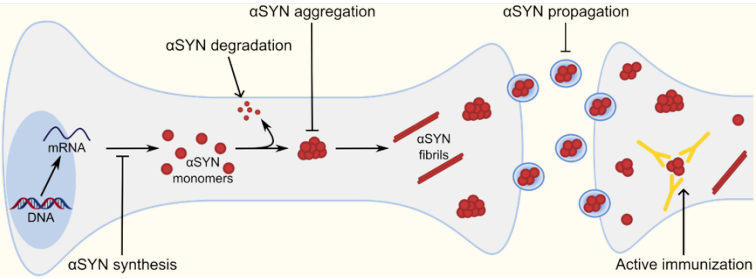

Figure 9. The multiple pathways that can be exploited in αSYN targeted therapeutic strategies. Figure generated via Inkscape 1.2.1 in reference to [47].

Recent research focused on the establishment of techniques detecting αSYN peripheral concentration as a fluid biomarker for synucleinopathies. [143] However, plasma and serum have exhibited

general inconsistency across the studies reported to date, [144] along with salivary levels displaying a non-significant divergence between PD patients and healthy controls. [145] More robust data is found in the analysis of αSYN concentration in the cerebrospinal fluid (CSF) [146] but it requires the more invasive procedure of a lumbar puncture. Slightly less invasive but still impractical, skin biopsies were examined as well, demonstrating an encouraging diagnostic accuracy. [147] Nevertheless, none of these strategies is yet fully validated for the diagnosis of synucleinopathies, nor has proved valuable for the assessment of disease progression. Furthermore, the abovementioned techniques cannot provide information on the spatial distribution of αSYN aggregates in the brain, which may prove necessary for therapy guidance.

2.4.3 Different strategies for the development of a PET tracer

On the grounds of the observations discussed so far, extensive work has been directed towards the establishment of a successful αSYN-targeted radiotracer, in order to adopt the non-invasive and quantitative *in vivo* imaging technique of PET as diagnostic and monitoring strategy. Because of the critical clinical and scientific need for such innovation, the Michael J. Fox Foundation announced a $2 million prize for the first team to successfully overcome the challenge. [148]

A considerable amount of research has focused on the development of small-molecule ligands binding to αSYN fibrils and will be discussed in more detail in paragraph 3.2. Simultaneously, a parallel approach was explored, with the implementation of both direct and pre-targeted antibody-based neuroimaging. [149-151] Antibodies offer the tremendous benefit of high target specificity, but raise greater challenges than small molecules with respect to their

pharmacokinetics, particularly their ability to sufficiently cross the blood-brain barrier (BBB) and clear from non-target tissues and blood pool. Bispecific antibodies adapted for transferrin receptor-mediated transcytosis over the BBB have been developed to overcome this limitation but several other obstacles complicate their clinical translation, such as receptor transport capacity, receptor inter-species differences, and radioisotope choice. [149] Attempts to image αSYN fibrils *in vivo* with antibody-based PET have so far proved unsuccessful: although sufficient brain concentrations were achieved, the permeation of an additional barrier to reach the intracellular target still hampered its detection. [152] To date, small-molecule ligands still remain the most promising path towards the development of a successful αSYN PET tracer.

3 Development of an αSYN PET tracer: current status and challenges

3.1 Requirements for a successful αSYN PET tracer and related challenges

The establishment of imaging agents for the *in vivo* detection of neurodegeneration is typically characterized by the limitation of BBB crossing. Multiple studies have attempted the definition of criteria predicting the ability of compounds to afford a suitable brain-uptake. Grading systems such as the BBB score [153] and the CNS MPO (Central Nervous System Multiparameter Optimization) [154] consider physicochemical parameters like molecular weight, number of aromatic rings and heavy atoms, number of hydrogen bond acceptors and donors, calculated logP, pK_a, and topological polar surface area (TPSA), to estimate the overall pharmacokinetic properties of the compound. Although not unambiguously differentiative, the predictive potential of these algorithms can be beneficial to the selection of the favorable structural properties throughout scaffold optimization. However, the targeting of αSYN fibrils raises several additional challenges.

As opposed to the widely spread Aβ plaques in AD, αSYN aggregates are considerably less abundant, with a 10-fold or more lower density. [85] Furthermore, they are typically located intracellularly and therefore increase the number of layers the tracer has to cross in order to reach the desired target. [155] Finally, αSYN fibrils are usually co-existing with the other age-related aggregates from the misfolded proteins Aβ and tau, whose secondary structure organizes in β-sheets as well. [2] Altogether, these factors set the requirement for an exceptionally high

affinity to αSYN and selectivity over Aβ and tau as a critical prerequisite for putative tracers.

In addition to these challenges, the structural variability of the fibrils further hampers the development of a suitable ligand. Li *et al*. recently performed cryo-EM studies that revealed two main αSYN fibril polymorphs and defined them as “rod” and “twister”. Both described polymorphs displayed two β-sheet protofilaments, bound together by a bent β-arch section but intersecting at different residue ranges (pre-NAC and NAC region, respectively). [64] Solid-state NMR (ssNMR) identified a single protofilament instead, which appeared similar to the protofilament kernel that “rod” and “twister” polymorphs share. [64, 156] Additional cryo-EM studies by Guerrero-Ferreira *et al*. recognized two other polymorphs, [60] therefore raising a concern for the extreme inconsistency of the fibrillation process, that proved highly variable with only minor changes in the experimental conditions. All discussed polymorphs are illustrated in Figure 10.

Further target diversification originated from the work of Van der Perren *et al*., showing that a disease-specific fingerprint can be identified in αSYN strains derived from PD, MSA or DLB patients, as they exhibit different shape and pathological behavior. [157]

In silico docking studies paired with competition binding assays revealed multiple binding sites are present in the targeted fibrils. Solely focusing on the single-polymorph model generated via ssNMR, [156] Hsieh *et al*. found three separate binding sites and observed different classes of putative ligands preferentially interacting with one of them. [158] As this study slightly predates the characterization of the multiple polymorphs, it is reasonable to speculate even more binding sites may exist.

Finally, one additional challenge hinders the establishment of a suitable αSYN ligand: the discrepancies among the assays employed for the evaluation of the compounds. Fibril binding assays are necessary for the preliminary screening of large libraries but, as discussed above, their conformational variability is a source of unreliability and leads to a poor reproducibility of the results. Assessment of binding affinity on *post-mortem* human brain tissue from PD and MSA patients is typically the most reliable assay, although it faces the limitations of supply shortage and pathology co-localization. [159]

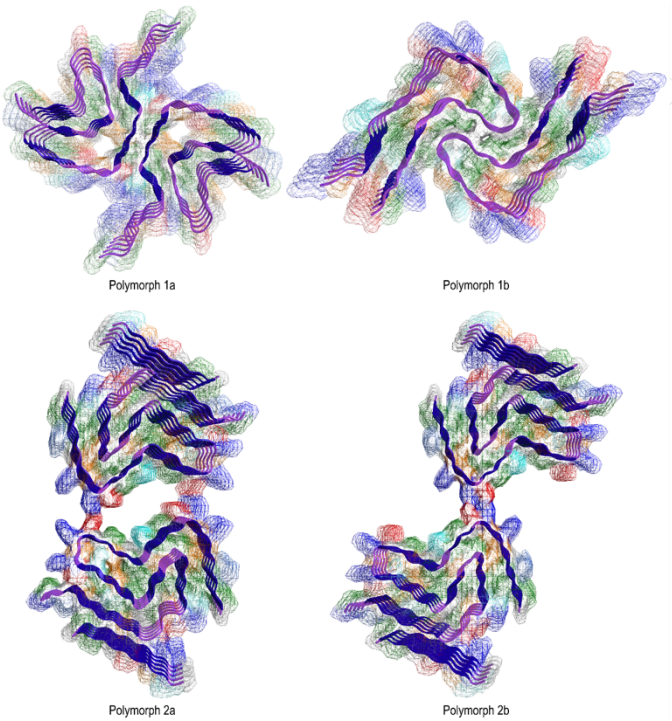

Figure 10. Different αSYN fibril polymorphs identified by cry-EM studies. PDB ID: 6H6B (1a – rod polymorph), [62] 6CU8 (1b – twister polymorph), [64] 6SSX (2a), 6SST (2b).[60] Structures visualized by Chem3D 20.1, PerkinElmer Informatics.

3.1.1 Multiple parameters to describe binding affinity

An accurate comparison on the various scaffolds presented in the literature is hampered by the use of different parameters to describe their binding affinity.

Fibril binding assays can either investigate the direct binding of a radioligand to the target or the displacement of a radiolabeled compound of choice by multiple putative ligands. Saturation binding assays employ several concentrations of the radioligand to determine the receptor density (B_{max}, Figure 11) as well as its dissociation constant (K_d, Figure 11), which is defined by the ligand concentration at which it binds to half its binding sites ($B_{max}/2$). [160] These assays generally adopt compounds labeled with long-lived radioisotopes like tritium of iodine-125. When such radiolabeling procedure is not available or a large library of compounds is under evaluation, a single concentration of the radioligand of choice is selected and competed for multiple concentration of the novel non-radioactive ligands. Competition assays describe the binding affinity via the IC_{50}, i.e. the concentration of the competitor displacing 50% of the radioligand (Figure 11). When the K_d of the latter has been previously determined, the inhibitor constant (K_i) is calculated according to equation (1) to afford a normalized value, describing the competitor affinity in a radioligand-concentration-independent manner. [160]

$$K_i = \frac{IC_{50}}{1 + \frac{[ligand]}{K_d}} \quad (1)$$

As previously discussed, αSYN fibrils bear multiple distinct binding site. Therefore, when designing a competition-based *in vitro* investigation, the selected radioligand is critical for the outcome of the study: a high-affinity ligand may display little or no competition when evaluated in

comparison with a radioligand that interacts with a different binding site.

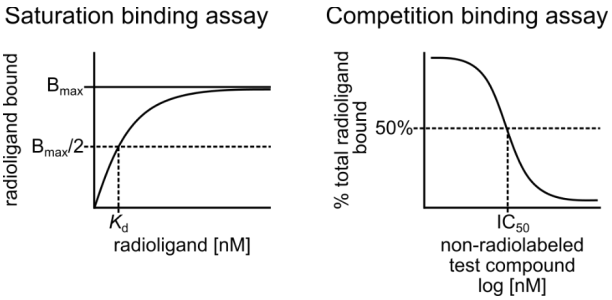

Figure 11. Schematic illustration of saturation and competition binding assays and the identification of the parameters describing binding affinity. Figure adapted from [160].

Depending on radioligand availability and structure similarity, different parameters can be found across the literature to present novel potential αSYN ligands, thus introducing an additional variable. Overall, affinity values lower than 10 nM are generally sought after in the development of suitable ligands. [161] In the investigation of novel Aβ PET tracers, Mathis *et al*. estimated that $K_d < 20$ nM were desirable. As conventionally a B_{max}/K_d ratio ≥ 10 is considered favorable for a putative PET tracer, a radioligand with $K_d \approx 200$ nM would satisfactorily detect Aβ plaques in AD patients. By accounting for the lower binding site concentration in the early stages of the disease, they suggested one less order of magnitude would generate attractive compounds. [100] As the previously discussed challenges make the detection of αSYN fibrils more challenging compared to Aβ plaques, affinities in the pM range may be required for the optimal radioligand.

3.2 The most promising scaffolds: their advantages and limitations

Despite the several challenges, in the past decade many efforts have been devoted to finding a scaffold fulfilling all requirements to function as an αSYN PET tracer. [2] Although a thorough review of all the available classes is beyond the scope of this thesis, some promising results are worth mentioning to better frame the work hereafter presented.

In the early stages of this investigation, encouraging evidence was found within the library of phenothiazine-based analogs developed by Yu *et al*. [161] *In vitro* screening via ThT competition binding assays identified SIL5 and SIL26 (Figure 12) as lead compounds, [161] when competing against the 3-iodoallyl-analog [^{125}I]SIL23, favorable αSYN affinity values were observed for both ($K_{i\ SIL5}$ = 66.2 nM, $K_{i\ SIL26}$ = 15.5 nM) and moderate selectivity over Aβ ($K_{i\ SIL26}$ = 103 nM) and tau ($K_{i\ SIL26}$ = 125 nM) was displayed by the latter. [162] *Ex vivo* studies in rats and *in vivo* studies in non-human primates highlighted favorable pharmacokinetics in healthy subjects, with suitable brain-uptake and rapid clearance for both [^{11}C]SIL5 and [^{18}F]SIL26. [163] [^{125}I]SIL23 only showed moderate affinity to human PD brain homogenates (119 nM ≤ K_d ≤ 168 nM), [162] proving further optimization was needed, but these preliminary results appeared overall promising. However, prior to the research discussed in this thesis, no additional phenothiazine-based αSYN ligands had been published.

The assessment of αSYN binding on the benzoxazole-derived Aβ tracer [^{18}F]BF-227 revealed a desirable K_d of 9.6 nM. [164] Shortly after, BF-227 (Figure 12) detected αSYN pathology in *post-mortem* PD and MSA tissue and its carbon-11 labeled equivalent showed slightly increased uptake in the affected brain regions in MSA patients. [165]

These findings prompted the development of the novel benzoxazole derivatives 2FBox and 4FBox (Figure 12). *In vitro* saturation assays displayed high affinity to αSYN fibrils (K_d = 3.3 ± 2.8 nM) and moderate selectivity over Aβ (K_d = 145.3 ± 114.5 nM) for the *ortho*-fluorinated compound, whereas opposite results arose for its *para*-substituted analog. *In vitro* autoradiography in *post-mortem* human brain slices exhibited no binding to either αSYN nor Aβ pathology as no signal was detected in PD, MSA, nor AD tissue. Overall, these findings appeared unreliable, as [^{18}F]BF-227 showed no αSYN- or Aβ-binding as well. [166]

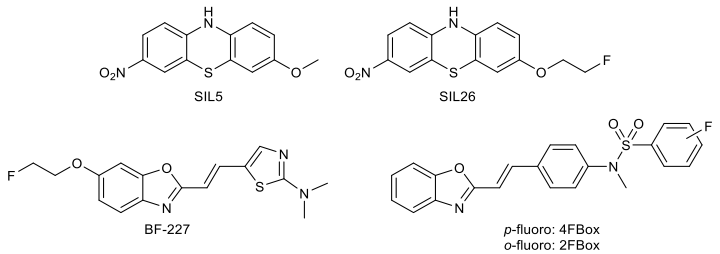

Figure 12. Structure of phenothiazine- and benzoxazole-based αSYN ligands. [161, 163, 164, 166]

Similarly to the benzoxazoles, the combination of a phenyl ring with a heteroatom-bearing five-membered ring has provided multiple valuable candidates across the recent literature. Chu *et al*. synthesized a group of indolinone- and indolinone-diene-derivatives (Figure 13) and observed satisfactory affinities, although only minor selectivity over Aβ and tau appeared. [167] Lengyel-Zhand *et al*. reported four benzofuranone-based fluorescent probes with high affinity to αSYN fibrils (up to K_i = 1.18 nM for Tg-52, Figure 13) but for most of them αSYN/Aβ selectivity was not assessed. [168]

Frequently occurring scaffolds, that are part of this class as well, are benzothiazoles. The putative tau tracer PBB3 and the fluorescent

probes PP-BTA-3 to -5 (Figure 13) all exhibited binding to αSYN pathology, despite their lack of selectivity. [169, 170] The development of the PBB3-analog C05-01 (Figure 13) improved affinity (αSYN fibrils: K_d = 24 nM, brain homogenates: K_i = 3.5 nM) but did not remove binding to Aβ and tau. [171] Instead, an encouraging αSYN/Aβ selectivity was displayed by the 2-styrylbenzothiazole RB1 (Figure 13), designed by Gaur *et al*., which will be further discussed in paragraph 4.2. [172]

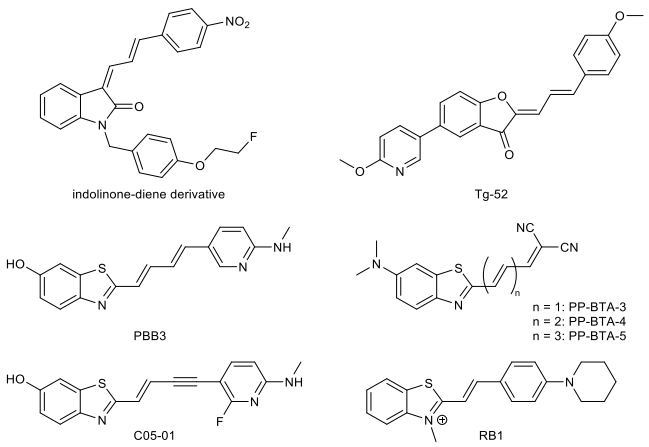

Figure 13. Structure of indolinone-, benzofuranone-, and benzothiazole-based αSYN ligands. [167-172]

A noteworthy scaffold is the diarylbisthiazole (DABTA). The DABTA-derivatives recently investigated by Uzuegbunam *et al*. (Figure 14) showed remarkably high affinities (0.1 nM ≤ K_i ≤ 1.2 nM), Aβ/αSYN K_i-ratio ≥ 200 and tau/αSYN K_i-ratio ≥ 1000 when tested in competition with the pan-amyloid ligand [^{3}H]DCVJ. Selected compounds exhibited satisfactory brain-uptake and clearance. These results overall appear promising, but they currently rely solely on fibril binding assays: no data on pathology animal models nor on human brain tissue has yet validated the potential of DABTAs. [173]

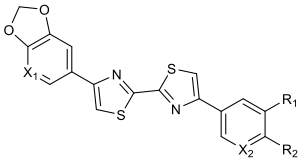

DABTA-d_2: X_1 = CH, X_2 = CH, R_1 = F, R_2 = OCH_3
DABTA-d_4: X_1 = N, X_2 = CH, R_1 = F, R_2 = OCH_3
DABTA-d_6: X_1 = CH, X_2 = N, R_1 = H, R_2 = F
DABTA-d_8: X_1 = N, X_2 = N, R_1 = H, R_2 = F

Figure 14. Structure of DABTA compounds. [173]

Structurally similar to this class are 3,5-diphenylpyrazoles (DPP). Via a systematic high-throughput screening combined with structure-activity relationship (SAR) studies, Wagner *et al.* identified the lead compound anle138b (Figure 15) from a DPP library of αSYN fibrils aggregation inhibitors (%inhibition $_{anle138b}$ = 77%) and pointed out it specifically binds to pathological αSYN oligomers (K_d = 190 ± 120 nM in concentration dependent fluorescence measurements). [174, 175] While anle138b is currently being evaluated in phase 1 clinical trials assessing its therapeutic potential, [137-139] additional derivatives have been developed to produce DPP-based carbon-11 labeled PET tracers. [^{11}C]anle253b (Figure 15) exhibited a favorable affinity to αSYN (IC_{50} = 1.6 nM) [176] and its pyridine-incorporating analog [^{11}C]MODAG-001 (Figure 15) showed improved *in vivo* pharmacokinetics as a result of decreased lipophilicity, alongside with an outstanding K_d of 0.6 ± 0.1 nM. [177] Although their selectivity over Aβ ($K_{d\ MODAG-001}$ = 20 ± 10 nM) and tau ($K_{d\ MODAG-001}$ = 19 ± 6.4 nM) may not be sufficient for clinical application, to date DPP represent one of the most promising classes of potential αSYN PET tracers.

The scaffolds discussed above generally displayed favorable affinities but lacked satisfactory selectivities. The first to overcome this challenge were Kaide *et al*. with the chalcone analogs PHNP-3 and FHCL-2 (Figure 15). [178, 179] Chalcone derivatives were firstly investigated by Ono *et al*. who observed encouraging αSYN binding but poor selectivity and low uptake in the brain of healthy mice. [180]

The Aβ/αSYN and tau/αSYN K_i-ratios were widened in the chalcone analogs developed by Hsieh *et al*. [181] but no insights on their pharmacokinetics or their binding to *post-mortem* human brain tissue were provided. The replacement of a dimethylamino *para*-substitution with a nitro group eliminated Aβ and tau binding in all evaluated compounds, as highlighted both by fibril binding assays and fluorescence staining of human brain sections. [178] PHNP-3, the most promising candidate standing out within the library (K_d = 6.9 ± 2.3 nM), exhibited insufficient brain-uptake in wt mice. Its less lipophilic derivative FHCL-2 achieved a significantly improved brain-uptake, but further structural optimization is still required to enhance brain clearance and potentially afford a suitable candidate for clinical evaluation. [179]

To date, two αSYN PET tracers are under investigation in first-in-human clinical trials in PD and MSA patients: [^{18}F]ACI-12589, developed by the Swiss company AC Immune SA [182, 183] and [^{18}F]SPAL-T-06, designed by Matsuoka *et al*. [184] However, only little results have been disclosed so far and their chemical structures are solely available in patents [185, 186] but are not explicitly indicated in peer-reviewed publications. Availability of additional data will be needed in order to more comprehensively frame these scaffolds within the αSYN ligands currently known.

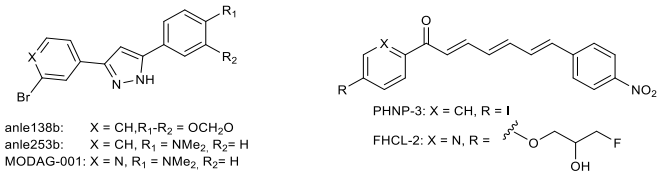

Figure 15. Structure of DPP- and chalcone-based αSYN ligands. [174, 177-179]

4 Aims of the study

This research focused on the development of novel compounds and the assessment of their binding properties, with the ultimate aim of establishing a clinically successful αSYN PET tracer. Parent compounds were selected from the previously discussed literature and two libraries were designed with the purpose of evaluating their SAR and improving their biological profile. These projects were carried out in the framework of a more comprehensive αSYN-targeted research as part of the European Union's Horizon 2020-funded consortium "PET-AlphaSy" (Marie Skłodowska-Curie grant agreement n° 813528).

The work hereafter discussed has been published as:

1. Di Nanni *et al*., The structural combination of SIL and MODAG scaffolds fails to enhance binding to α-synuclein but reveals promising affinity to amyloid β, *Molecules*, **2023**, 28, 4001, https://doi.org/10.3390/molecules28104001. [3]
2. Di Nanni *et al*., A fluorescent probe as a lead compound for a selective α-synuclein PET tracer: development of a library of 2-styrylbenzothiazoles and biological evaluation of [^{18}F]PFSB and [^{18}F]MFSB, *ACS Omega*, **2023**, 8, 31450–31467, https://doi.org/10.1021/acsomega.3c04292. [4]
3. Di Nanni *et al*., 2-styrylbenzothiazole derivatives as α-synuclein binding compounds, EU patent application 5402P670EP. [187]

The figures, schemes and tables displayed in the following chapters are adapted from these publications.

4.1 Aim 1: design and development of a library of diarylpyrazoles

Phenothiazines and DPP stand out as promising classes among the αSYN ligands investigated so far, as illustrated in the previous paragraph. [161-163, 176, 177] When evaluating its affinity to the multiple putative binding sites on αSYN fibrils (site 2 Y39-S42-T44, site 9 G86-F94-K96, site 3/13 K43-K45-V48-H50), Hsieh *et al*. found SIL26 preferentially interacts with the positively charged site 3/13. [158] None of the DPP analogs was included in this investigation, but [^{3}H]MODAG-001 showed effective displacement when competing with SIL26 in fibril binding assays. [177] As these results suggested the two compounds bind to overlapping sections of the same site, we hypothesized higher affinity would occur for a ligand involving a larger portion of the site and therefore releasing additional free energy upon binding (Figure 16).

This study aimed at merging these two established scaffolds to produce novel αSYN ligands by applying the technique of rational drug design by molecular hybridization. [3]

In medicinal chemistry, the combination of two structures with favorable properties is a widespread strategy to design enhanced scaffolds. Higher affinity and selectivity, improved pharmacokinetics and pharmacodynamics or reduced toxicity can be achieved by conjugation via a linker, fusion and merging of two promising ligands; [188, 189] or an integrated activity towards multiple targets can be implemented through this approach. [190, 191]

By combination of the SIL and the MODAG scaffolds, this research focused on the development of novel diarylpyrazole- (DAP) based compounds that would exhibit suitable affinity and selectivity for the establishment of an αSYN PET tracer (Figure 16). [3]

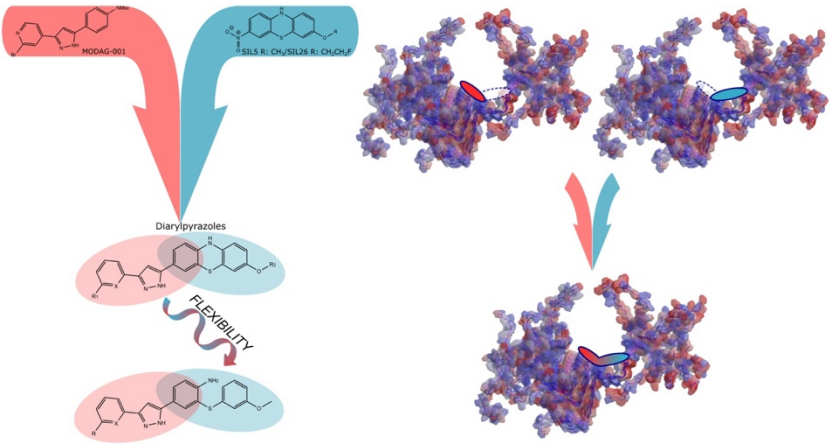

Figure 16. The development of DAP hybrid compounds by combination of the promising αSYN ligands MODAG-001 and SIL5/SIL26 as an attempt to achieve interaction with a larger portion of the binding site. αSYN structure described by solid-state NMR [156] (PDB ID: 2N0A) was visualized by Chem3D 20.1, PerkinElmer Informatics. Figure adapted from [3].

4.2 Aim 2: design and development of a library of 2-styrylbenzothiazoles

By focusing on the enhancement of both fluorescence and binding properties, Gaur *et al*. developed the fluorescent probes RB1 and RB2 as 2-styrylbenzothiazole derivatives of ThT. [172]

To date, ThT is still the gold-standard tool for the visualization of amyloid fibrils. However, as it is not selective for αSYN nor for amyloid fibrils in general, this probe is not suitable for imaging in living cells due to heavy background signal. On these grounds, Gaur *et al*. implemented structural modifications such as the elongation of the π-conjugation system and increase of rotational degree of freedom to enhance fluorescence features. Also, they replaced the dimethylamino group with superior electron-donating moieties, namely piperidine and piperazine, to improve the binding affinity. [172]

Fibril titration assays pointed out a considerably higher affinity to αSYN for RB1 than for its analog RB2 ($K_{d\ RB1}$ = 30 ± 10 nM, $K_{d\ RB2}$ = 4400 ± 500 nM). Furthermore, RB1 proved successful in selectively imaging αSYN fibrils in living SH-SY5Y and HeLa cells pre-incubated with sonicated fibrils, [172] therefore standing out among αSYN ligands as a promising tracer candidate.

By designing a library of derivatives based on the 2-(4-amino-1yl)styrylbenzothiazole scaffold (Figure 17), this study focused on the development of a selective αSYN PET tracer. [4]

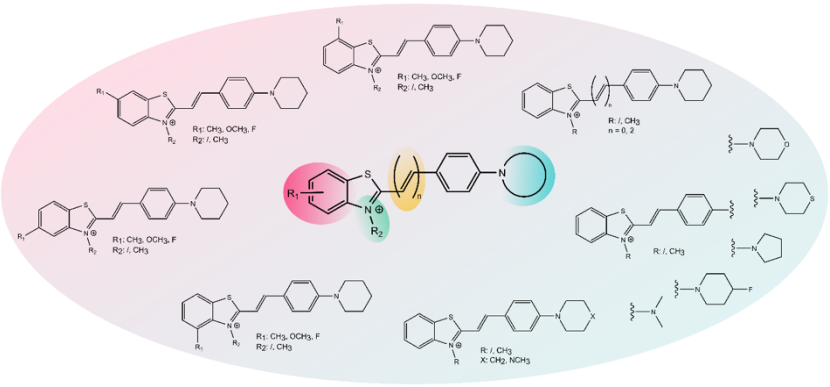

Figure 17. Development of a library of 2-styrylbenzothiazoles. Figure adapted from [4].

Experimental section

The methods presented in the experimental section are also described in [3, 4].

1. Chemistry

1.1 General materials and methods

All chemicals were purchased from Sigma Aldrich (St. Louis, MO, USA), abcr GmbH (Karlsruhe, Germany), or Carl Roth (Karlsruhe, Germany) and used without any further purification.

Reaction progress was monitored by thin-layer chromatography (TLC) on 0.20 mm Polygram SIL G/UV_{254} (silica gel 60) TLC plates (Macherey-Nagel, Düren, Germany) with the chosen eluent mixture and/or analytical HPLC-MS (quadrupole 6120 series ESI detector, Agilent, Santa Clara, CA, USA) equipped with a Luna 5µm C18 (2) 100 Å 50 x 2 mm column (Phenomenex, Torrance, CA, USA) [gradient: 0 – 7.60 min (0% to 100% B), 7.60 – 8.80 (100% B), 8.80 – 9.30 min (100% to 0% B), 9.30 – 13.0 min (0% B); solvent A: 0.1% formic acid in H2O; solvent B: MeCN; 0.4 mL/min] or with a Zorbax Eclipse XBD-C18 50 x 4.6 mm column (Agilent, Santa Clara, CA, USA) [gradient: 0 – 6 min (0% to 100% B); solvent A: H_2O:MeCN:formic acid 95:5:0.1 v/v%; solvent B: 0.1% formic acid in MeCN; 1 mL/min].

Purification was performed through automated flash chromatography on an Isolera 4 system (Biotage, Uppsala, Sweden) or a CombiFlash NextGen 300+ (Teledyne ISCO, Lincoln, NE, USA).

^{1}H and ^{13}C NMR spectra were acquired on an Avance III AV 600 (^{1}H: 600.13 MHz; ^{13}C: 150.61 MHz) spectrometer or an Avance II AV 400 (^{1}H: 400 MHz; ^{13}C: 101 MHz; ^{19}F: 376 MHz) spectrometer (Bruker

Biospin, Ettlingen, Germany). All chemical shifts (δ) are reported as parts per million (ppm) and referenced to residual solvent peaks ($CDCl_3$: δ_H = 7.26, δ_C = 77.16; DMSO-d_6: δ_H = 2.50, δ_C = 39.52). ^{1}H NMR spectra of all final compounds and radiolabeling precursors are displayed in the Appendix.

1.2 Synthesis of a library of diarylpyrazoles

1-(3-Methoxy-7-nitro-10H-phenothiazin-10-yl)ethan-1-one (1)

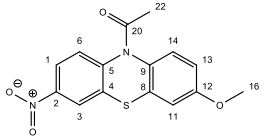

The three-step synthesis was carried out according to the literature procedure [161], starting from 2-amino-6-methoxybenzo[d]thiazole and 1-chloro-2,4-dinitrobenzene. The product was afforded as an orange solid (13.1 g, 58%), with all analytical data corresponding to the published data. R_f: 0.43 (PE/EtOAc 1:1). ^{1}H NMR (600 MHz, DMSO-d_6) δ 8.39 (d, *J* = 2.6 Hz, 1H, H3), 8.21 (dd, *J* = 8.8, 2.6 Hz, 1H, H1), 7.82 (d, *J* = 8.8 Hz, 1H, H6), 7.58 (d, *J* = 8.8 Hz, 1H, H14), 7.17 (d, *J* = 2.8 Hz, 1H, H11), 6.99 (dd, *J* = 8.8, 2.8 Hz, 1H, H13), 3.79 (s, 3H, H16), 2.16 (s, 3H, H22). ^{13}C NMR (151 MHz, DMSO-d_6) δ 168.6 (C20), 158.0 (C12), 145.3 (C1), 144.5 (C3), 133.7 (C5), 132.2 (C9), 130.4 (C14), 128.2 (C4), 128.0 (C8), 122.8 (C6), 122.3 (C2), 114.1 (C13), 112.5 (C11), 55.7 (C16), 22.7 (C22). HPLC-MS (ESI): m/z calculated for $C_{15}H_{12}N_2O_4S$ 316.05; $[M+H]^+$ found 317.10.

1-(3-Amino-7-methoxy-10H-phenothiazin-10-yl)ethan-1-one (2)

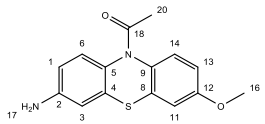

To a solution of **1** (13.1 g, 41.4 mmol) in MeCN/H_2O 10:1 v/v (260 mL, 26.0 mL) was added $NiCl_2 \cdot 6H_2O$ (1.97 g, 8.28 mmol) and the mixture was stirred at room temperature for 5 min. $NaBH_4$ (6.26 g, 165 mmol) was then added in portions, and the reaction was stirred at room temperature for a further 15 min. The reaction mixture was diluted with water and extracted with DCM. The organic phase was washed with water, dried over $MgSO_4$, and evaporated to afford the product as a brown solid (11.0 g, 93%). R_f: 0.20 (PE/EtOAc 1:1). ^{1}H NMR (600 MHz, DMSO-d_6) δ 7.42 (d, J = 8.8 Hz, 1H, H14), 7.19 (d, J = 8.5 Hz, 1H, H6), 7.05 (d, J = 2.8 Hz, 1H, H11), 6.89 (dd, J = 8.8, 2.8 Hz, 1H, H13), 6.66 (d, J = 2.4 Hz, 1H, H3), 6.53 (dd, J = 8.5, 2.4 Hz, 1H, H1), 5.30 (s, 2H, H17), 3.76 (s, 3H, H16), 2.04 (s, 3H, H20). ^{13}C NMR (151 MHz, DMSO-d_6) δ 168.9 (C18), 157.2 (C12), 147.4 (C2), 132.4 (C9), 127.8 (C5), 127.8 (C14), 127.4 (C6), 127.3 (C4), 127.3 (C8), 112.8 (C13), 112.5 (C1), 112.0 (C11), 111.4 (C3), 55.5 (C16), 22.4 (C20). HPLC-MS (ESI): m/z calculated for $C_{15}H_{14}N_2O_2S$ 286.08; $[M+H]^+$ found 287.10.

1-(3-Bromo-7-methoxy-10H-phenothiazin-10-yl)ethan-1-one (3)

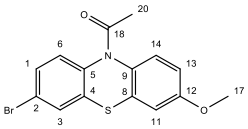

A solution of **2** (3.00 g, 10.5 mmol) in MeCN (1.00 L) was cooled to 0 °C under an argon atmosphere, and $CuBr_2$ (3.51 g, 15.7 mmol) was added. *t*-BuONO (2.08 mL, 15.7 mmol) was added dropwise at 0 °C, and the mixture was stirred at room temperature for 3 h. The reaction was quenched with H_3NSO_3 aq. 48.5 M (1.00 L) and extracted four times with EtOAc. The organic phase was dried over $MgSO_4$, evaporated under reduced pressure, and purified by flash chromatography (PE/EtOAc 5% to 45% B) to afford the product as a pink solid (1.07 g, 29%). R_f: 0.51 (PE/EtOAc 1:1). ^{1}H NMR (600 MHz,

DMSO-d_6) δ 7.79 (d, *J* = 2.2 Hz, 1H, H3), 7.56 (dd, *J* = 8.5, 2.2 Hz, 1H, H1), 7.52 (d, *J* = 8.5 Hz, 2H, H6-H14), 7.13 (d, *J* = 2.8 Hz, 1H, H11), 6.96 (dd, *J* = 8.8, 2.8 Hz, 1H, H13), 3.78 (s, 3H, H17), 2.10 (s, 3H, H20). ^{13}C NMR (151 MHz, DMSO-d_6) δ 168.6 (C18), 157.7 (C12), 138.3 (1), 138.3 (C3), 134.4 (C5), 131.2 (C9), 129.9 (C6), 129.9 (C14), 129.0 (C4), 128.0 (C8), 119.0 (C2), 113.7 (C13), 112.4 (C11), 55.7 (C17), 22.6 (C20). HPLC-MS (ESI): m/z calculated for $C_{15}H_{12}BrNO_2S$ 348.98; $[M+H]^+$ found 349.95, 351.90.

1-(3-Bromo-7-hydroxy-10H-phenothiazin-10-yl)ethan-1-one (4)

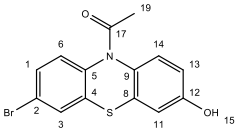

A solution of **3** (1.05 g, 3.01 mmol) in DCM (45.0 mL) was cooled to -78 °C under an argon atmosphere, and BBr_3 1 M in DCM (10.5 mL) was added. The reaction was stirred overnight at room temperature. The crude was poured into water and extracted with DCM. The organic phase was dried over $MgSO_4$, evaporated, and further purified by flash chromatography (PE/EtOAc 8% to 66% B) to afford the product as a pink solid (632 mg, 63%). R_f: 0.37 (PE/EtOAc 1:1). ^{1}H NMR (600 MHz, DMSO-d_6) δ 9.90 (s, 1H, H15), 7.77 (dd, *J* = 2.1, 1.1 Hz, 1H, H3), 7.54 (dd, *J* = 8.3, 2.1 Hz, 1H, H1), 7.50 (t, *J* = 8.3 Hz, 1H, H6), 7.40 (d, *J* = 8.7 Hz, 1H, H14), 6.89 (d, *J* = 2.7 Hz, 1H, H11), 6.78 (dd, *J* = 8.7, 2.7 Hz, 1H, H13), 2.09 (s, 3H, H19).^{13}C NMR (151 MHz, DMSO-d_6) δ 168.7 (C17), 156.1 (C12), 138.5 (C1), 138.4 (C3), 134.5 (C5), 132.4 (C9), 129.8 (C6), 129.8 (C14), 129.1 (C4), 128.0 (C8), 118.9 (C2), 114.6 (C13), 113.8 (C11), 22.6 (C19). HPLC-MS (ESI): m/z calculated for $C_{14}H_{10}BrNO_2S$ 334.96; $[M+H]^+$ found 336.15, 337.95.

1-(3-Bromo-7-(2-fluoroethoxy)-10H-phenothiazin-10-yl)ethan-1-one (5)

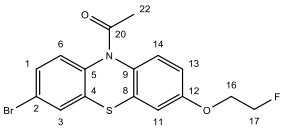

A solution of **4** (365 mg, 0.98 mmol) in dry DMF (24.0 mL) was cooled to 0 °C under an argon atmosphere and a NaH 60% dispersion in mineral oil (58.6 mg, 1.47 mmol) was added. The mixture was stirred at 0 °C for 15 min. 1-Bromo-2-fluoroethane (0.11 mL, 1.47 mmol) was added dropwise and the reaction was stirred overnight at room temperature. The reaction mixture was poured into water (220 mL) and extracted with EtOAc. The organic phase was dried over $MgSO_4$, evaporated under reduced pressure, and purified by flash chromatography (PE/EtOAc 8% to 66% B) to afford the product as a pink solid (301 mg, 91%). R_f: 0.18 (PE/EtOAc 2:1). ^{1}H NMR (600 MHz, DMSO-d_6) δ 7.79 (d, J = 2.1 Hz, 1H, H3), 7.56 (dd, J = 8.4, 2.1 Hz, 1H, H1), 7.55 – 7.47 (m, 2H, H6-H14), 7.18 (d, J = 2.8 Hz, 1H, H11), 7.00 (dd, J = 8.8, 2.8 Hz, 1H, H13), 4.73 (dt, J = 47.9, 3.9 Hz, 2H, H17), 4.27 (dq, J = 30.4, 4.4 Hz, 2H, H16), 2.10 (s, 3H, H22). ^{13}C NMR (151 MHz, DMSO-d_6) δ 168.6 (C20), 156.6 (C12), 138.3 (C1), 138.3 (C3), 131.5 (C5), 130.0 (C9), 130.0 (C6), 129.9 (C14), 129.0 (C4), 128.1 (C8), 119.0 (C2), 114.2 (C13), 113.0 (C11), 82.0 (d, $J_{C\text{-}F}$ = 166.6 Hz, C17), 67.6 (d, $J_{C\text{-}F}$ = 18.9 Hz, C16), 22.6 (C22). HPLC-MS (ESI): m/z calculated for $C_{16}H_{13}BrFNO_2S$ 380.98; $[M+H]^+$ found 382.05, 384.00.

4-Bromo-2-iodoaniline (7)

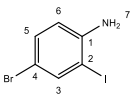

NH_4OAc 0.1% in MeOH (1.50 mL) was added to a solution of aniline (1.50 mL, 16.4 mmol) in MeCN (75.0 mL). *N*-bromosuccinimide (2.92 g, 16.4 mmol) was added in portions and the mixture was stirred at room temperature for 15 min. HPLC-MS confirmed that the mono-substitution of the aniline was achieved. *N*-iodosuccinimide (4.07 g, 18.1 mmol) was added in portions and the mixture was stirred at room temperature for 30 min. The solvent was concentrated under a vacuum and the crude was poured into water and extracted with EtOAc. The organic phase was dried over $MgSO_4$, evaporated under reduced pressure, and purified by flash chromatography (PE/EtOAc 10% to 20% B) to afford the product (1.98 g, 40%). R_f: 0.64 (PE/EtOAc 1:1). ^1H NMR (600 MHz, DMSO-d_6) δ 7.65 (d, J = 2.3 Hz, 1H, H3), 7.21 (dd, J = 8.6, 2.3 Hz, 1H, H5), 6.70 (d, J = 8.6 Hz, 1H, H6), 5.37 (s, 2H, H7). ^{13}C NMR (151 MHz, DMSO-d_6) δ 148.1 (C1), 139.3 (C3), 131.5 (C5), 115.5 (C6), 106.6 (C4), 83.4 (C2). HPLC-MS (ESI): m/z calculated for C_6H_5BrIN 296.87; found $[M+H]^+$ 297.90, 299.85.

4-Bromo-2-((3-methoxyphenyl)thio)aniline (8)

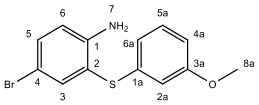

3-Methoxythiophenol (0.81 mL, 6.54 mmol) and potassium carbonate (1.09 g, 7.85 mmol) were added to a solution of **7** (1.95 g, 6.54 mmol) in NMP (20.0 mL) under argon atmosphere. CuI (62.3 mg, 5% mol) was added and the mixture was stirred overnight at 100 °C. The reaction mixture was poured into water and extracted with EtOAc. The organic phase was dried over $MgSO_4$, evaporated under reduced pressure, and purified by flash chromatography (PE/EtOAc 1% to 15% B) to afford the product (748 mg, 37%). R_f: 0.44 (PE/EtOAc 5:1). ^1H NMR (600 MHz, DMSO-d_6) δ 7.42 (d, J = 2.4 Hz, 1H, H3), 7.30 (dd, J

= 8.6, 2.4 Hz, 1H, H5), 7.20 (t, *J* = 8.3 Hz, 1H, H5a), 6.78 (d, *J* = 8.6 Hz, 1H, H6), 6.75 (ddd, *J* = 8.3, 2.4, 1.0 Hz, 1H, H6a), 6.66 – 6.62 (m, 2H, H2a-H4a), 5.59 (s, 2H, H7), 3.69 (s, 3H, H8a). ^{13}C NMR (151 MHz, DMSO-*d*$_6$) δ 159.7 (C3a), 149.6 (C1), 137.9 (C3), 137.1 (C1a), 133.5 (C5), 130.1 (C6a), 119.0 (C4a), 116.7 (C6), 114.1 (C2), 112.6 (C5a), 111.2 (C2a), 105.9 (C4), 55.1 (C8a). HPLC-MS (ESI): m/z calculated for $C_{13}H_{12}BrNOS$ 308.98; $[M+H]^+$ found 309.90, 312.00.

N-(4-bromo-2-((3-methoxyphenyl)thio)phenyl)acetamide (9)

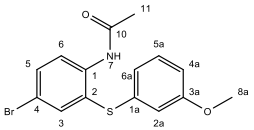

Pyridine (3.5 mL) was added to a solution of **8** (735 mg, 2.37 mmol) in acetic anhydride (20.0 mL), and the mixture was stirred at room temperature for 3 h. The reaction mixture was poured into water and extracted with EtOAc. The organic phase was dried over $MgSO_4$, evaporated under reduced pressure, and purified by flash chromatography (PE/EtOAc 1% to 20% B) to afford the product (708 mg, 85%). R_f: 0.28 (PE/EtOAc 5:1). ^{1}H NMR (600 MHz, DMSO-*d*$_6$) δ 9.43 (d, *J* = 22.9 Hz, 1H, H7), 7.56 (d, *J* = 8.6 Hz, 1H, H6), 7.49 (dd, *J* = 8.6, 2.4 Hz, 1H, H5), 7.35 (d, *J* = 2.4 Hz, 1H, H3), 7.31 (t, *J* = 8.2 Hz, 1H, H5a), 6.94 – 6.89 (m, 1H, H6a), 6.85 (d, *J* = 8.6 Hz, 1H, H4a), 6.85 (s, 1H, H2a), 3.73 (s, 3H, H8a), 2.00 (s, 3H, H11). ^{13}C NMR (151 MHz, DMSO-*d*$_6$) δ 168.6 (C10), 159.8 (C3a), 137.0 (C1a), 134.8 (C1), 133.9 (C3), 130.9 (C5a), 130.9 (C5), 130.5 (C6a), 127.3 (C2), 122.8 (C6), 117.3 (C4), 116.1 (C4a), 113.5 (C2a), 55.2 (C8a), 23.1 (C11). HPLC-MS (ESI): m/z calculated for $C_{15}H_{14}BrNO_2S$ 350.99; $[M+H]^+$ found 352.05, 354.00.

1-(Tetrahydro-2H-pyran-2-yl)-pyrazole (11)

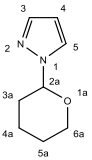

To a solution of 1*H*-pyrazole (1.40 g, 21.0 mmol) in 3,4-dihydro-2H-pyran (2.57 mL, 27.3 mmol), TFA (0.50 mL, 6.21 mmol) was added. The mixture was refluxed for 45 min. The reaction mixture was diluted in water and extracted with EtOAc. The organic phase was dried over $MgSO_4$, evaporated under reduced pressure, and purified by flash chromatography (PE/EtOAc 8% to 65% B) to afford the product as a colorless oil. (2.97 g, 93%). R_f: 0.48 (PE/EtOAc 2:1). ^{1}H NMR (600 MHz, DMSO-d_6) δ 7.84 (dd, *J* = 2.4, 0.7 Hz, 1H, H5), 7.47 (dd, *J* = 1.7, 0.7 Hz, 1H, H3), 6.29 (dd, *J* = 2.4, 1.7 Hz, 1H, H4), 5.40 (dd, *J* = 10.0, 2.5 Hz, 1H, H2a), 3.91 (dtd, *J* = 11.5, 3.8, 1.9 Hz, 1H, H6a), 3.67 – 3.57 (m, 1H, H6a), 2.15 – 2.02 (m, 1H, H3a), 1.97 – 1.86 (m, 2H, H3a-H4a), 1.71 – 1.62 (m, 1H, H4a), 1.57 – 1.50 (m, 2H, H5a). ^{13}C NMR (151 MHz, DMSO-d_6) δ 138.7 (C3), 128.6 (C5), 105.7 (C4), 86.7 (C2a), 66.8 (C6a), 30.0 (C3a), 24.7 (C5a), 22.1 (C4a). HPLC-MS (ESI): m/z calculated for $C_8H_{12}N_2O$ 152.09; $[M+H]^+$ found 153.15.

3-Bromo-1-(tetrahydro-2H-pyran-2-yl)-pyrazole (12)

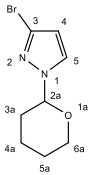

A solution of **11** (2.97 g, 152 mmol) in THF (22.0 mL) was cooled to -78 °C under argon atmosphere. A solution of *n*-BuLi 2.5 M in hexane (10.1 mL, 25.3 mmol) was added dropwise. Bromine (1.30 mL, 25.3 mmol) was added dropwise, and the mixture was stirred for 1 h. The

reaction mixture was poured into water and extracted with EtOAc. The organic phase was dried over $MgSO_4$, evaporated under reduced pressure, and heated at 150 °C for a few seconds to allow conversion into the thermodynamically more stable 3-bromo regioisomer. It was purified by flash chromatography (PE/EtOAc 6% to 20% B) to afford the product as a light yellow oil (1.84 g, 41%). R_f: 0.33 (PE/EtOAc 2:1). ^{1}H NMR (600 MHz, DMSO-d_6) δ 7.89 (d, J = 2.5 Hz, 1H, H5), 6.43 (d, J = 2.4 Hz, 1H, H4), 5.37 (dd, J = 9.9, 2.4 Hz, 1H, H2a), 3.91 (dtd, J = 11.5, 4.0, 1.8 Hz, 1H, H6a), 3.66 – 3.56 (m, 1H, H6a), 2.10 – 2.00 (m, 1H, H3a), 1.96 – 1.85 (m, 2H, H3a-H4a), 1.70 – 1.59 (m, 1H, H4a), 1.56 – 1.49 (m, 2H, H5a). ^{13}C NMR (151 MHz, DMSO-d_6) δ 131.8 (C5), 125.0 (C3), 108.5 (C4), 86.8 (C2a), 66.8 (C6a), 29.4 (3a), 24.5 (C5a), 21.8 (C4a). HPLC-MS (ESI): m/z calculated for $C_3H_3BrN_2$ (THP cleaved by acidic HPLC conditions) 145.95; $[M+H]^+$ found 147.00, 148.95.

1-(Tetrahydro-2H-pyran-2-yl)-3-(tributylstannyl)-pyrazole (13)

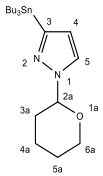

To a solution of **12** (500 mg, 2.16 mmol) in toluene (6.00 mL), bis(tributyltin) (1.31 mL, 2.60 mmol) and $Pd(PPh_3)_4$ (250 mg, 0.22 mmol) were added under an argon atmosphere. The mixture was stirred overnight at 100 °C. The reaction mixture was diluted in water and extracted with EtOAc. The organic phase was dried over $MgSO_4$, evaporated under reduced pressure, and purified by flash chromatography (PE/EtOAc 6% to 12% B) to afford the product as a colorless oil (359 mg, 38%). R_f: 0.46 (PE/EtOAc 9:1). ^{1}H NMR (600

MHz, DMSO-d_6) δ 7.86 (d, J = 2.3 Hz, 1H, H5), 6.32 (d, J = 2.2 Hz, 1H, H4), 5.45 (dd, J = 9.9, 2.6 Hz, 1H, H2a), 3.90 (dtd, J = 11.5, 3.8, 1.8 Hz, 1H, H6a), 3.67 – 3.56 (m, 1H, H6a), 2.07 (dddd, J = 12.9, 12.1, 9.8, 4.0 Hz, 1H, H3a), 1.95 (dtd, J = 13.3, 4.0, 1.8 Hz, 1H, H4a), 1.89 (dq, J = 12.9, 3.6 Hz, 1H, H3a), 1.72 – 1.64 (m, 1H, H4a), 1.65 – 1.55 (m, 2H, H5a), 1.55 – 1.51 (m, 6H, $SnBu_3$), 1.29 (h, J = 7.8, 7.2 Hz, 6H, $SnBu_3$), 1.01 (t, J = 7.9 Hz, 6H, $SnBu_3$), 0.85 (t, J = 7.3 Hz, 9H, $SnBu_3$). ^{13}C NMR (151 MHz, DMSO-d_6) δ 150.2 (C3), 128.1 (C5), 113.7 (C4), 86.4 (2a), 66.7 (C6a), 30.1 (C3a), 28.5 ($SnBu_3$), 26.6 ($SnBu_3$), 24.7 (C5a), 22.1 (C4a), 13.5 ($SnBu_3$), 9.4 ($SnBu_3$). HPLC-MS (ESI): m/z calculated for $C_{20}H_{38}N_2OSn$ 442.20; $[M+H]^+$ found 443.25.

General procedure A

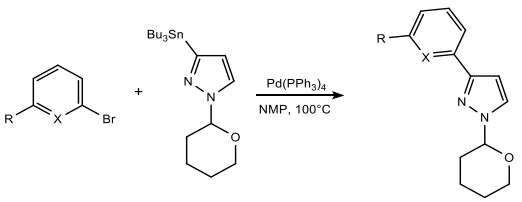

To a solution of **13** (1.13 mmol) and the selected aryl bromide (2.27 mmol) in NMP (3.50 mL) under argon atmosphere, was added $Pd(PPh_3)_4$ (5% mol). The mixture was stirred overnight at 100 °C. The crude product mixture was diluted in water and extracted with EtOAc. The organic phase was dried over $MgSO_4$, evaporated under reduced pressure, and purified by flash chromatography (PE/EtOAc).

3-Phenyl-1-(tetrahydro-2H-pyran-2-yl)-pyrazole (14a)

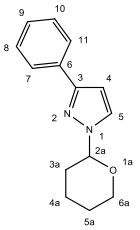

The synthesis was carried out according to general procedure A (149 mg, 58%). R_f: 0.51 (PE/EtOAc 3:1). ^{1}H NMR (600 MHz, DMSO-d_6) δ 7.92 (d, *J* = 2.5 Hz, 1H, H5), 7.81 (dd, *J* = 8.2, 1.3 Hz, 2H, H7-H11), 7.40 (t, *J* = 7.7 Hz, 2H, H8-H10), 7.30 (tt, *J* = 7.4, 1.2 Hz, 1H, H9), 6.77 (d, *J* = 2.4 Hz, 1H, H4), 5.43 (dd, *J* = 10.1, 2.3 Hz, 1H, H2a), 3.95 (dtd, *J* = 13.1, 4.1, 1.8 Hz, 1H, H6a), 3.69 – 3.60 (m, 1H, H6a), 2.19 – 2.09 (m, 1H, H3a), 1.98 – 1.90 (m, 2H, H3a-H4a), 1.74 – 1.65 (m, 1H, H4a), 1.64 – 1.57 (m, 2H, H5a). ^{13}C NMR (151 MHz, DMSO-d_6) δ 150.0 (C3), 133.2 (C6), 130.3 (C9), 128.6 (C7-C11), 127.6 (C5), 125.2 (C8-C10), 103.1 (C4), 86.9 (C2a), 66.9 (C6a), 29.9 (C3a), 24.6 (5a), 22.1 (4a). HPLC-MS (ESI): m/z calculated for $C_9H_8N_2$ 144.07 and $C_{14}H_{16}N_2O$ 228.13; $[M+H]^+$ found 145.20, 229.20.

2-(1-(Tetrahydro-2H-pyran-2-yl)-1H-pyrazol-3-yl)pyridine (14b)

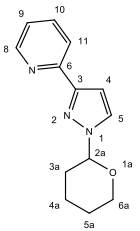

The synthesis was carried out according to general procedure A (171 mg, 66%). R_f: 0.23 (PE/EtOAc 1:1). ^{1}H NMR (600 MHz, DMSO-d_6) δ 8.57 (ddd, *J* = 4.8, 1.8, 1.0 Hz, 1H, H8), 7.96 (t, *J* = 2.4 Hz, 1H, H5), 7.94 (dq, *J* = 7.9, 1.2 Hz, 1H, H10)), 7.82 (td, *J* = 7.7, 1.8 Hz, 1H, H11),

7.34 – 7.28 (m, 1H, H9), 6.86 (t, *J* = 2.2 Hz, 1H, H4), 5.46 (dt, *J* = 10.1, 2.1 Hz, 1H, H2a), 3.95 (dtd, *J* = 13.4, 4.2, 1.8 Hz, 1H, H6a), 3.69 – 3.62 (m, 1H, H6a), 2.19 – 2.10 (m, 1H, H3a), 1.98 – 1.92 (m, 2H, H3a-H4a), 1.74 – 1.63 (m, 1H, H4a), 1.58 – 1.51 (m, 2H, H5a). ^{13}C NMR (151 MHz, DMSO-*d*$_6$) δ 151.7 (C6), 150.9 (C3), 149.3 (C8), 136.8 (C10), 130.5 (C5), 122.7 (C11), 119.3 (C9), 104.4 (C4), 87.0 (C2a), 66.9 (C6a), 29.8 (C3a), 24.6 (C5a), 22.0 (C4a). HPLC-MS (ESI): m/z calculated for $C_8H_7N_3$ 145.06 and $C_{13}H_{15}N_3O$ 229.12; $[M+H]^+$ found 146.10, 230.10.

3-(3-Fluorophenyl)-1-(tetrahydro-2H-pyran-2-yl)-pyrazole (14c)

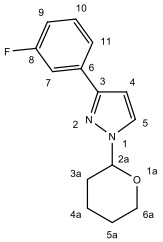

The synthesis was carried out according to general procedure A (386 mg, 69%). R_f: 0.61 (PE/EtOAc 2:1). ^{1}H NMR (600 MHz, DMSO-*d*$_6$) δ 7.94 (d, *J* = 2.5 Hz, 1H, H5), 7.66 (dt, *J* = 7.7, 1.2 Hz, 1H, H7), 7.59 (ddd, *J* = 10.6, 2.7, 1.6 Hz, 1H, H9), 7.44 (td, *J* = 8.0, 6.2 Hz, 1H, H10), 7.12 (tdd, *J* = 9.2, 2.7, 0.9 Hz, 1H, H11), 6.83 (d, *J* = 2.5 Hz, 1H, H4), 5.45 (dd, *J* = 10.1, 2.4 Hz, 1H, H2a), 3.95 (dtd, *J* = 11.5, 3.8, 1.8 Hz, 1H, H6a), 3.69 – 3.62 (m, 1H, H6a), 2.19 – 2.08 (m, 1H, H3a), 2.00 – 1.92 (m, 2H, H3a-H4a), 1.75 – 1.64 (m, 1H, H4a), 1.56 (tt, *J* = 7.8, 3.8 Hz, 2H, H5a). ^{13}C NMR (151 MHz, DMSO-*d*$_6$) δ 162.5 (d, $J_{C\text{-}F}$ = 242.7 Hz, C8), 148.8 (d, $J_{C\text{-}F}$ = 3.0 Hz, C3), 135.6 (d, $J_{C\text{-}F}$ = 8.3 Hz, C6), 130.5 (d, $J_{C\text{-}F}$ = 8.6 Hz, C10), 130.4 (C5), 121.1 (d, $J_{C\text{-}F}$ = 2.8 Hz, C11), 114.1 (d, $J_{C\text{-}F}$ = 21.2 Hz, C7), 111.6 (d, $J_{C\text{-}F}$ = 22.4 Hz, C9), 103.5 (C4), 86.8 (C2a), 66.7 (C6a), 29.7 (C3a), 24.5 (C5a), 21.9 (C4a). HPLC-MS (ESI):

m/z calculated for $C_9H_7FN_2$ 162.06 and $C_{14}H_{15}FN_2O$ 246.12; $[M+H]^+$ found 163.05, 247.20.

General procedure B

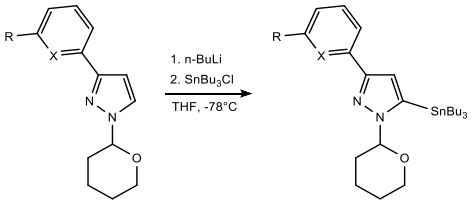

A solution of the selected 3-aryl-1-(tetrahydro-2H-pyran-2-yl)-pyrazole (0.63 mmol) in THF (2.50 mL) was cooled to -78 °C under a positive pressure of argon. A solution of *n*-BuLi 2.5 M in hexane (0.76 mmol) was added dropwise, after which the mixture was stirred for 15 min. $SnBu_3Cl$ (0.76 mmol) was added dropwise, and the resulting mixture was stirred for 1 h, allowing it to reach room temperature. The reaction mixture was poured into water and extracted with EtOAc. The organic phase was dried over $MgSO_4$, evaporated under reduced pressure, and purified by flash chromatography (PE/EtOAc).

3-Phenyl-1-(tetrahydro-2H-pyran-2-yl)-5-(tributylstannyl)-pyrazole (15a)

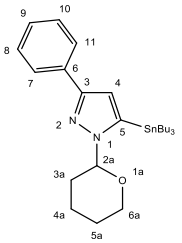

The synthesis was carried out according to general procedure B (298 mg, 91%). R_f: 0.74 (PE/EtOAc 5:1). ^{1}H NMR (600 MHz, DMSO-d_6) δ 7.80 (dd, *J* = 8.3, 1.2 Hz, 2H, H7-H11), 7.38 (t, *J* = 7.7 Hz, 2H, H8-

H10), 7.27 (tt, *J* = 7.4, 1.3 Hz, 1H, H9), 6.74 (t, *J* = 3.9 Hz, 1H, H4), 5.31 – 5.22 (m, 1H, H2a), 3.95 (dtd, *J* = 10.8, 3.6, 1.8 Hz, 1H, H6a), 3.68 – 3.58 (m, 1H, H6a), 2.12 – 2.04 (m, 2H, H3a), 2.03 – 1.95 (m, 1H, H4a), 1.72 – 1.64 (m, 1H, H4a), 1.64 – 1.56 (m, 2H, H5a), 1.56 – 1.47 (m, 6H, $SnBu_3$), 1.31 (h, *J* = 7.3 Hz, 6H, $SnBu_3$), 1.14 – 1.08 (m, 6H, $SnBu_3$), 0.89 – 0.85 (m, 9H, $SnBu_3$). ^{13}C NMR (151 MHz, DMSO-d_6) δ 149.8 (C3), 142.5 (C5), 133.5 (C6), 128.5 (C7-C11), 127.3 (C9), 125.2 (C8-C10), 112.1 (C4), 88.1 (C2a), 66.9 (C6a), 30.7 (C3a), 28.5 ($SnBu_3$), 26.6 ($SnBu_3$), 24.6 (C5a), 21.8 (C4a), 13.5 ($SnBu_3$), 10.3 ($SnBu_3$). HPLC-MS (ESI): m/z calculated for $C_{26}H_{42}N_2OSn$ 518.23; $[M+H]^+$ found 519.00.

2-(1-(Tetrahydro-2H-pyran-2-yl)-5-(tributylstannyl)-1H-pyrazol-3-yl)pyridine (15b)

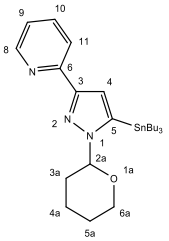

The synthesis was carried out according to general procedure B (245 mg, 68%). R_f: 0.25 (PE/EtOAc 5:1). ^1H NMR (600 MHz, DMSO-d_6) δ 8.56 (ddd, *J* = 4.8, 1.8, 0.9 Hz, 1H, H8), 7.90 (dt, *J* = 8.0, 1.1 Hz, 1H, H10), 7.80 (td, *J* = 7.7, 1.8 Hz, 1H, H11), 7.28 (ddd, *J* = 7.5, 4.8, 1.2 Hz, 1H, H9), 6.88 (t, *J* = 4.0 Hz, 1H, H4), 5.34 – 5.27 (m, 1H, H2a), 3.96 (dtd, *J* = 10.8, 4.2, 1.8 Hz, 1H, H6a), 3.69 – 3.60 (m, 1H, H6a), 2.09 (ddd, *J* = 11.0, 8.6, 4.2 Hz, 2H, H3a), 2.02 – 1.97 (m, 1H, H4a), 1.75 – 1.65 (m, 1H, H4a), 1.60 – 1.56 (m, 2H, H5a), 1.56 – 1.48 (m, 6H, $SnBu_3$), 1.31 (h, *J* = 7.3 Hz, 6H, $SnBu_3$), 1.14 – 1.08 (m, 6H, $SnBu_3$), 0.86 (t, *J* = 7.3 Hz, 9H, $SnBu_3$). ^{13}C NMR (151 MHz, DMSO-

d$_6$) δ 152.0 (C6), 150.6 (C3), 149.2 (C8), 142.7 (C5), 136.7 (C10), 122.4 (C11), 119.4 (C9), 113.4 (C4), 88.2 (C2a), 66.9 (C6a), 30.7 (C3a), 28.5 ($SnBu_3$), 26.6 ($SnBu_3$), 24.6 (C5a), 21.7 (C4a), 13.5 ($SnBu_3$), 10.4 ($SnBu_3$). HPLC-MS (ESI): m/z calculated for $C_{25}H_{41}N_3OSn$ 519.23; $[M+H]^+$ found 520.35.

3-(3-Fluorophenyl)-1-(tetrahydro-2H-pyran-2-yl)-5-(tributylstannyl)-pyrazole (15c)

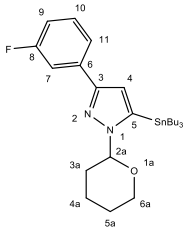

The synthesis was carried out according to general procedure B (516 mg, 63%). R_f: 0.74 (PE/EtOAc 5:1). ^{1}H NMR (600 MHz, DMSO-*d*$_6$) δ 7.65 (dt, *J* = 7.7, 1.2 Hz, 1H, H7), 7.59 (ddd, *J* = 10.5, 2.7, 1.5 Hz, 1H, H9), 7.42 (td, *J* = 8.0, 6.2 Hz, 1H, H10), 7.09 (tdd, *J* = 9.1, 2.6, 0.9 Hz, 1H, H11), 6.82 (t, *J* = 4.1 Hz, 1H, H4), 5.30 – 5.23 (m, 1H, H2a), 3.94 (dtd, *J* = 11.2, 3.9, 1.8 Hz, 1H, H6a), 3.67 – 3.58 (m, 1H, H6a), 2.10 – 2.04 (m, 2H, H3a), 1.97 (dtd, *J* = 13.2, 4.0, 1.6 Hz, 1H, H4a), 1.72 – 1.64 (m, 1H, H4a), 1.59 – 1.55 (m, 2H, H5a), 1.56 – 1.47 (m, 6H, $SnBu_3$), 1.30 (h, *J* = 7.3 Hz, 6H, $SnBu_3$), 1.13 – 1.07 (m, 6H, $SnBu_3$), 0.86 (t, *J* = 7.3 Hz, 9H, $SnBu_3$). ^{13}C NMR (151 MHz, DMSO-*d*$_6$) δ 162.6 (d, $J_{C\text{-}F}$ = 242.3 Hz, C8), 148.8 (d, $J_{C\text{-}F}$ = 2.7 Hz, C3), 142.9 (C5), 136.0 (d, $J_{C\text{-}F}$ = 8.3 Hz, C6), 130.6 (d, $J_{C\text{-}F}$ = 8.5 Hz, C10), 121.3 (d, $J_{C\text{-}F}$ = 2.7 Hz, C11), 113.9 (d, $J_{C\text{-}F}$ = 20.9 Hz, C7), 112.6 (C4), 111.7 (d, $J_{C\text{-}F}$ = 22.5 Hz, C9), 88.2 (C2a), 66.9 (C6a), 30.7 (C3a), 28.5 ($SnBu_3$), 26.6 ($SnBu_3$), 24.6 (C5a), 21.7 (C4a), 13.5 ($SnBu_3$), 10.3 ($SnBu_3$). HPLC-

MS (ESI): m/z calculated for $C_{21}H_{33}FN_2Sn$ (THP cleaved by acidic HPLC conditions) 452.16; $[M+NH_4]^+$ found 470.40.

General procedure C

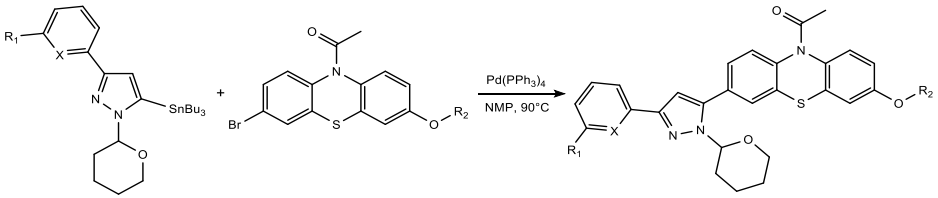

To a solution of the selected 3-aryl-1-(tetrahydro-2H-pyran-2-yl)-5-(tributylstannyl)-pyrazole (0.56 mmol) and the selected 3-bromo-7-OR_2-*N*-acetylphenothiazine (0.73 mmol) in NMP (8.50 mL) was added $Pd(PPh_3)_4$ (5% mol) under an argon atmosphere. The mixture was stirred overnight at 90 °C. The reaction mixture was diluted with water and extracted with EtOAc. The organic phase was dried over $MgSO_4$, evaporated under reduced pressure, and purified by flash chromatography (PE/EtOAc).

1-(3-Methoxy-7-(3-phenyl-1-(tetrahydro-2H-pyran-2-yl)-1H-pyrazol-5-yl)-10H-phenothiazin-10-yl)ethan-1-one (16a)

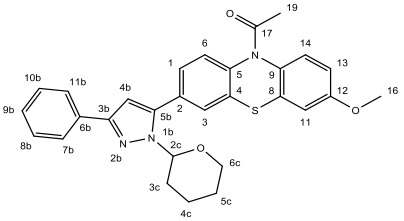

The synthesis was carried out according to general procedure C (149 mg, 53%). R_f: 0.35 (PE/EtOAc 1:1). ^{1}H NMR (600 MHz, DMSO-d_6) δ 7.87 (d, *J* = 7.3 Hz, 2H, H7b-H11b), 7.75 (d, *J* = 7.6 Hz, 2H, H1-H3), 7.60 (d, *J* = 8.1 Hz, 1H, H6), 7.57 (d, *J* = 8.8 Hz, 1H, H14), 7.43 (t, *J* = 7.7 Hz, 2H, H8b-H10b), 7.33 (t, *J* = 7.4 Hz, 1H, H9b), 7.17 (d, *J* = 2.8

Hz, 1H, H11), 7.02 (s, 1H, H4b), 6.97 (dd, *J* = 8.8, 2.8 Hz, 1H, H13), 5.29 (d, *J* = 9.6 Hz, 1H, H2c), 4.03 (d, *J* = 7.3 Hz, 1H, H6c), 3.79 (s, 3H, H19), 3.59 (t, *J* = 11.3 Hz, 1H, H6c), 2.50 – 2.43 (m, 1H, H3c), 2.17 (s, 3H, H17), 1.97 (s, 1H, H4c), 1.85 (d, *J* = 13.0 Hz, 1H, H3c), 1.66 – 1.57 (m, 2H, H5c), 1.55 – 1.50 (m, 1H, H4c). ^{13}C NMR (151 MHz, DMSO-*d*$_6$) δ 168.6 (C17), 157.7 (C12), 149.6 (C3b), 143.7 (C5b), 139.3 (C6b), 133.0 (C5), 132.8 (C9b), 132.5 (C9), 131.2 (C3), 128.7 (C7b-C11b), 128.1 (C14), 128.0 (C6), 127.9 (C1), 127.7 (C2), 127.4 (C4), 127.1 (C8), 125.3 (C8b-C10b), 113.6 (C13), 112.4 (C11), 104.4 (C4b), 83.8 (C2c), 66.5 (C6c), 55.7 (C16), 29.0 (C3c), 24.5 (C5c), 22.7 (C19), 22.0 (C4c). HPLC-MS (ESI): m/z calculated for $C_{24}H_{19}N_3O_2S$ (THP cleaved by acidic HPLC conditions) 413.12; $[M+H]^+$ found 414.15.

1-(3-Methoxy-7-(3-(pyridin-2-yl)-1-(tetrahydro-2H-pyran-2-yl)-1H-pyrazol-5-yl)-10H-phenothiazin-10-yl)ethan-1-one (16b)

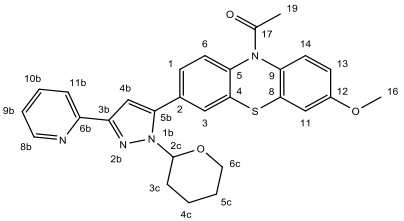

The synthesis was carried out according to general procedure C (43.0 mg, 30%). R_f: 0.18 (PE/EtOAc 1:3). ^{1}H NMR (600 MHz, DMSO-*d*$_6$) δ 8.60 (dt, *J* = 4.8, 1.4 Hz, 1H, H8b), 8.00 (dd, *J* = 7.7, 1.2 Hz, 1H, H10b), 7.86 (td, *J* = 7.7, 1.9 Hz, 1H, H11b), 7.77 (s, 1H, H3), 7.75 (d, *J* = 8.3 Hz, 1H, H1), 7.63 – 7.60 (m, 1H, H6), 7.57 (d, *J* = 8.9 Hz, 1H, H14), 7.34 (ddd, *J* = 7.5, 4.8, 1.2 Hz, 1H, H9b), 7.18 (d, *J* = 2.9 Hz, 1H, H11), 7.08 (s, 1H, H4b), 6.97 (dd, *J* = 8.9, 2.9 Hz, 1H, H13), 5.32 (dd, *J* = 11.6, 2.3 Hz, 1H, H2c), 4.08 – 4.01 (m, 1H, H6c), 3.79 (s, 3H, H16), 3.65 – 3.56 (m, 1H, H6c), 2.49 – 2.40 (m, 1H, H3c), 2.17 (s, 3H, H19),

2.05 – 1.95 (m, 1H, H4c), 1.87 (d, *J* = 12.8 Hz, 1H, H3c), 1.66 – 1.58 (m, 2H, H5c), 1.56 – 1.51 (m, 1H, H4c). ^{13}C NMR (151 MHz, DMSO-*d*$_6$) δ 168.6 (C17), 157.7 (C12), 151.4 (C6b), 150.4 (C3b), 149.3 (C8b), 143.8 (C5b), 139.4 (C5), 137.0 (C9), 136.9 (C10b), 131.2 (C3), 128.8 (C14), 128.7 (C6), 128.0 (C1), 127.7 (C2), 127.5 (C4), 127.2 (C8), 123.0 (C11b), 119.4 (C9b), 113.6 (C13), 112.4 (C11), 105.3 (C4b), 83.9 (C2c), 66.5 (C6c), 55.7 (C16), 29.0 (C3c), 24.5 (C5c), 22.7 (C19), 22.0 (C4c). HPLC-MS (ESI): m/z calculated for $C_{23}H_{18}N_4O_2S$ (THP cleaved by acidic HPLC conditions) 414.12; $[M+H]^+$ found 415.05.

1-(3-(3-(3-Fluorophenyl)-1-(tetrahydro-2H-pyran-2-yl)-1H-pyrazol-5-yl)-7-methoxy-10H-phenothiazin-10-yl)ethan-1-one (16c)

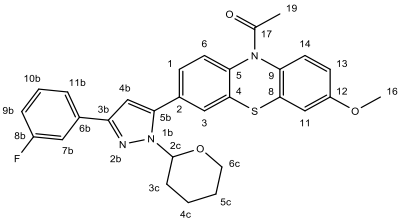

The synthesis was carried out according to general procedure C (134 mg, 56%). R_f: 0.37 (PE/EtOAc 1:1). ^{1}H NMR (600 MHz, DMSO-*d*$_6$) δ 7.80 – 7.73 (m, 2H, H1-H3), 7.72 (dd, *J* = 7.8, 1.2 Hz, 1H, H9b), 7.65 (dt, *J* = 10.5, 2.0 Hz, 1H, H7b), 7.63 – 7.58 (m, 1H, H6), 7.57 (d, *J* = 9.0 Hz, 1H, H14), 7.48 (dq, *J* = 8.2, 1.8 Hz, 1H, H10b), 7.20 – 7.14 (m, 2H, H11-H11b), 7.11 (s, 1H, H4b), 6.98 (dt, *J* = 8.9, 2.6 Hz, 1H, H13), 5.30 (t, *J* = 6.4 Hz, 1H, H2c), 4.03 (dt, *J* = 9.9, 3.5 Hz, 1H, H6c), 3.79 (s, 3H, H16), 3.60 (s, 1H, H6c), 2.46 (t, *J* = 11.3 Hz, 1H, H3c), 2.17 (s, 3H, H19), 1.98 – 1.93 (m, 1H, H4c), 1.89 – 1.81 (m, 1H, H3c), 1.62 (h, *J* = 11.6 Hz, 2H, H5c), 1.53 (d, *J* = 12.2 Hz, 1H, H4c). ^{13}C NMR (151 MHz, DMSO-*d*$_6$) δ 168.7 (C17), 162.6 (d, $J_{C\text{-}F}$ = 242.6 Hz, 8b), 157.7 (C12), 148.5 (d, $J_{C\text{-}F}$ = 2.3 Hz, C3b), 144.0 (C5b), 139.4 (C5), 135.3 (d,

$J_{C\text{-}F}$ = 8.4 Hz, C6b), 132.6 (C9), 131.2 (C3), 130.8 (d, $J_{C\text{-}F}$ = 8.3 Hz, 10b), 128.1 (C14), 128.0 (C6), 128.0 (C1), 127.7 (C2), 127.4 (C4), 127.2 (C8), 121.3 (d, $J_{C\text{-}F}$ = 1.8 Hz, C11b), 114.6 (d, $J_{C\text{-}F}$ = 21.0 Hz, C7b), 113.7 (C13), 112.4 (C11), 111.8 (d, $J_{C\text{-}F}$ = 22.7 Hz, C9b), 104.8 (C4b), 83.9 (C2c), 66.6 (C6c), 55.7 (C16), 29.0 (C3b), 24.5 (C5c), 22.7 (C19), 22.0 (C4c). HPLC-MS (ESI): m/z calculated for $C_{24}H_{18}FN_3O_2S$ (THP cleaved by acidic HPLC conditions) 431.11; $[M+H]^+$ found 432.15.

1-(3-(2-Fluoroethoxy)-7-(3-phenyl-1H-pyrazol-5-yl)-10H-phenothiazin-10-yl)ethan-1-one (17a)

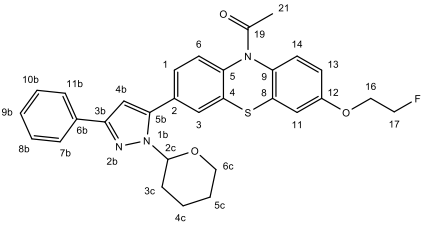

The synthesis was carried out according to general procedure C (51.0 mg, 20%). R_f: 0.28 (PE/EtOAc 1:2). ^{1}H NMR (600 MHz, DMSO-d_6) δ 7.86 (dt, *J* = 7.0, 1.2 Hz, 2H, H7b-H11b), 7.76 (br s, 2H, H1-H3), 7.61 (d, *J* = 9.0 Hz, 1H, H6), 7.58 (d, *J* = 8.8 Hz, 1H, H14), 7.43 (t, *J* = 7.7 Hz, 2H, H8b-H10b), 7.34 (tt, *J* = 7.4, 1.2 Hz, 1H, H9b), 7.23 (d, *J* = 2.8 Hz, 1H, H11), 7.03 (s, 1H, H4b), 7.02 (dd, *J* = 8.8, 2.8 Hz, 1H, H13), 5.29 (d, *J* = 9.6 Hz, 1H, H2c), 4.74 (dt, *J* = 47.8, 3.9 Hz, 2H, H17), 4.29 (d, *J* = 31.7 Hz, 2H, H16), 4.03 (dp, *J* = 11.3, 2.1 Hz, 1H, H6c), 3.60 (br s, 1H, H6c), 2.49 – 2.43 (m, 1H, H3c), 2.17 (s, 3H, H21), 2.01 – 1.95 (m, 1H, H4c), 1.85 (d, *J* = 12.9 Hz, 1H, H3c), 1.67 – 1.57 (m, 2H, H5c), 1.56 – 1.50 (m, 1H, H4c). ^{13}C NMR (151 MHz, DMSO-d_6) δ 168.7 (C19), 156.6 (C12), 149.6 (C3b), 143.7 (C5b), 139.2 (C6b), 133.0 (C5), 132.9 (C9b), 132.5 (C9), 131.5 (C3), 128.7 (C7b-C11b), 128.2 (C14),

128.1 (C6), 127.9 (C1), 127.7 (C2), 127.4 (C4), 127.2 (C8), 125.3 (C8b-C10b), 114.2 (C13), 113.1 (C11), 104.4 (C4b), 83.9 (C2c), 82.0 (d, J_{C-F} = 166.6 Hz, C17), 67.6 (d, J_{C-F} = 18.8 Hz, C16), 66.5 (C6c), 29.1 (C3c), 24.5 (C5c), 22.7 (C21), 22.1 (C4c). HPLC-MS (ESI): m/z calculated for $C_{25}H_{20}FN_3O_2S$ (THP cleaved by acidic HPLC conditions) 445.13; $[M+H]^+$ found 446.10.

1-(3-(2-Fluoroethoxy)-7-(3-(pyridin-2-yl)-1-(tetrahydro-2H-pyran-2-yl)-1H-pyrazol-5-yl)-10H-phenothiazin-10-yl)ethan-1-one (17b)

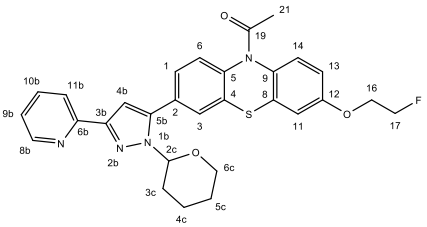

The synthesis was carried out according to general procedure C (66.0 mg, 29%). R_f: 0.23 (PE/EtOAc 1:5). ^{1}H NMR (600 MHz, DMSO-d_6) δ 8.61 (ddd, *J* = 4.9, 1.8, 1.0 Hz, 1H, H8b), 8.00 (dt, *J* = 7.9, 1.1 Hz, 1H, H10b), 7.86 (td, *J* = 7.7, 1.8 Hz, 1H, H11b), 7.78 (s, 1H, H3), 7.75 (d, *J* = 8.1 Hz, 1H, H1), 7.63 (d, *J* = 8.0 Hz, 1H, H6), 7.58 (d, *J* = 8.8 Hz, 1H, H14), 7.35 (ddd, *J* = 7.5, 4.8, 1.2 Hz, 1H, H9b), 7.23 (d, *J* = 2.8 Hz, 1H, H11), 7.08 (s, 1H, H4b), 7.02 (dd, *J* = 8.8, 2.8 Hz, 1H, H13), 5.32 (d, *J* = 9.6 Hz, 1H, H2c), 4.74 (dt, *J* = 47.8, 3.9 Hz, 2H, H17), 4.29 (d, *J* = 29.9 Hz, 2H, H16), 4.04 (d, *J* = 11.4 Hz, 1H, H6c), 3.61 (s, 1H, H6c), 2.49 – 2.43 (m, 1H, H3c), 2.17 (s, 3H, H21), 1.98 (br s, 1H, H4c), 1.85 (br s, 1H, H3c), 1.68 – 1.57 (m, 2H, H5c), 1.56 – 1.52 (m, 1H, H4c).^{13}C NMR (151 MHz, DMSO-d_6) δ 168.7 (C19), 156.6 (C12), 151.4 (C6b), 150.4 (C3b), 149.3 (C8b), 143.8 (C5b), 139.3 (C5), 139.3 (C9), 136.9 (C10b), 131.5 (C3), 128.8 (C14), 128.7 (C6), 128.1 (C1), 128.0 (C2), 127.7 (C4), 127.3 (C8), 123.0 (C11b), 119.5 (C9b), 114.2 (C13), 113.1

(C11), 105.3 (C4b), 83.9 (C2c), 82.0 (d, $J_{C\text{-}F}$ = 166.8 Hz, C17), 67.6 (d, $J_{C\text{-}F}$ = 18.8 Hz, C16), 66.6 (C6c), 29.0 (C3c), 24.5 (C5c), 22.7 (C21), 22.0 (C4c). HPLC-MS (ESI): m/z calculated for $C_{24}H_{19}FN_4O_2S$ (THP cleaved by acidic HPLC conditions) 446.12; $[M+H]^+$ found 447.15.

1-(3-(2-Fluoroethoxy)-7-(3-(3-fluorophenyl)-1H-pyrazol-5-yl)-10H-phenothiazin-10-yl)ethan-1-one (17c)

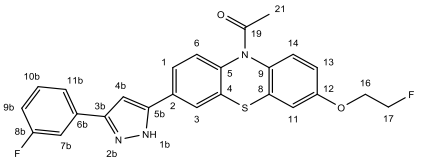

The synthesis was carried out according to general procedure C (109 mg, 43%). R_f: 0.31 (PE/EtOAc 1:2). ^{1}H NMR (600 MHz, DMSO-d_6) δ 13.55 (d, J = 10.2 Hz, 1H, H1b), 7.99 (d, J = 1.8 Hz, 1H, H3), 7.84 (dd, J = 39.6, 6.3 Hz, 1H, H1), 7.73 – 7.66 (m, 2H, H7b-H9b), 7.66 – 7.60 (m, 2H, H6-H10), 7.57 – 7.51 (m, 2H, H14-H11b), 7.36 (s, 1H, H4b), 7.21 (s, 1H, H11), 7.00 (dd, J = 9.3, 2.6 Hz, 1H, H13), 4.74 (dt, J = 47.8, 3.9 Hz, 2H, H17), 4.29 (dt, J = 29.8, 5.0 Hz, 2H, H16), 2.15 (s, 3H, H21). ^{13}C NMR (151 MHz, DMSO-d_6) δ 169.2 (C19), 163.7 (d, $J_{C\text{-}F}$ = 243.3 Hz, C8b), 157.0 (C12), 150.8 (d, $J_{C\text{-}F}$ = 13.8 Hz, C3b), 142.9 (C5b), 133.5 (C5), 132.8 (C9), 132.5 (C4), 132.5 (C8), 132.0 (d, $J_{C\text{-}F}$ = 9.9 Hz, C6b), 131.6 (C3), 129.2 (d, $J_{C\text{-}F}$ = 11.7 Hz, C10b), 128.6 (C14), 128.6 (C6), 124.5 (C2), 124.4 (C1), 121.6 (C11b), 115.3 (d, $J_{C\text{-}F}$ = 13.6 Hz, C7b), 114.5 (C13), 113.5 (C11), 112.2 (d, $J_{C\text{-}F}$ = 8.9 Hz, C9b), 101.3 (C4b), 82.5 (d, $J_{C\text{-}F}$ = 166.7 Hz, C17), 68.1 (d, $J_{C\text{-}F}$ = 18.9 Hz, C16), 23.1 (C21). HPLC-MS (ESI): m/z calculated for $C_{25}H_{19}F_2N_3O_2S$ 463.12; $[M+H]^+$ found 464.40.

General procedure D

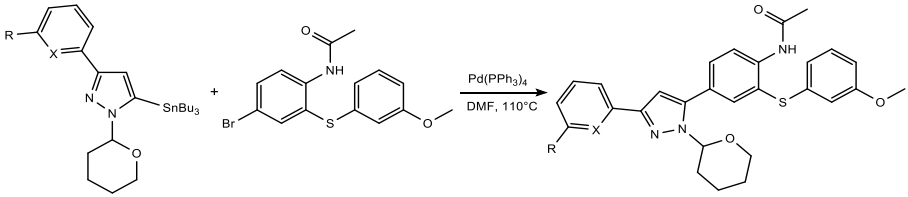

To a solution of the selected 3-aryl-1-(tetrahydro-2H-pyran-2-yl)-5-(tributylstannyl)-pyrazole (0.31 mmol) and **9** (0.40 mmol) in DMF (5.00 mL) was added $Pd(PPh_3)_4$ (10% mol), under an argon atmosphere. The mixture was stirred overnight at 110 °C. The crude was diluted with water and extracted with EtOAc. The organic phase was dried over $MgSO_4$, evaporated under reduced pressure, and purified by flash chromatography (PE/EtOAc).

N-(2-((3-methoxyphenyl)thio)-4-(3-phenyl-1-(tetrahydro-2H-pyran-2-yl)-1H-pyrazol-5-yl)phenyl)acetamide (18a)

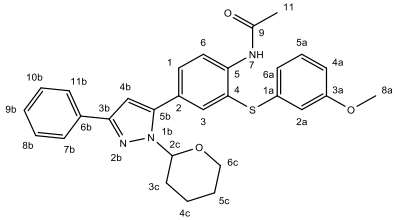

The synthesis was carried out according to general procedure D (45.0 mg, 29%). R_f: 0.56 (PE/EtOAc 1:1). ^{1}H NMR (600 MHz, DMSO-d_6) δ 9.55 (s, 1H, H7), 7.88 – 7.82 (m, 3H, H6-H7b-H11b), 7.61 – 7.55 (m, 2H, H3-H5), 7.42 (t, *J* = 7.7 Hz, 2H, H8b-H10b), 7.33 (tt, *J* = 7.4, 1.1 Hz, 1H, H9b), 7.29 (t, *J* = 8.0 Hz, 1H, H5a), 6.93 (s, 1H, H4b), 6.88 – 6.84 (m, 2H, H4a-H6a), 6.82 (t, *J* = 2.1 Hz, 1H, H2a), 5.11 (dd, *J* = 10.0, 2.5 Hz, 1H, H2c), 3.85 – 3.80 (m, 1H, H6c), 3.71 (s, 3H, H8a), 3.19 (td, *J* = 11.3, 2.6 Hz, 1H, H6c), 2.42 (tdd, *J* = 13.5, 9.9, 4.2 Hz, 1H, H3c),

2.06 (s, 3H, H11), 1.97 – 1.92 (m, 1H, H4c), 1.82 – 1.76 (m, 1H, H3c), 1.55 – 1.48 (m, 2H, H5c), 1.45 – 1.40 (m, 1H, H4c). ^{13}C NMR (151 MHz, DMSO-d_6) δ 168.7 (C9), 159.8 (3a), 149.6 (C3b), 143.8 (C5b), 138.9 (6b), 137.4 (C1a), 136.3 (C1), 133.0 (C3), 132.8 (C9b), 130.4 (C5a), 129.0 (C6a), 128.5 (C7b-C11b), 127.7 (C5), 126.9 (C4), 125.3 (C2), 125.2 (C8b-C10b), 121.9 (C6), 115.3 (C4a), 112.6 (C2a), 103.8 (C4b), 83.8 (C2c), 66.3 (C6c), 55.1 (C8a), 29.0 (C3c), 24.4 (C5c), 23.3 (C11), 22.0 (C4c). HPLC-MS (ESI): m/z calculated for $C_{24}H_{21}N_3O_2S$ (THP cleaved by acidic HPLC conditions) 415.14; $[M+H]^+$ found 416.25.

N-(2-((3-methoxyphenyl)thio)-4-(3-(pyridin-2-yl)-1-(tetrahydro-2H-pyran-2-yl)-1H-pyrazol-5-yl)phenyl)acetamide (18b)

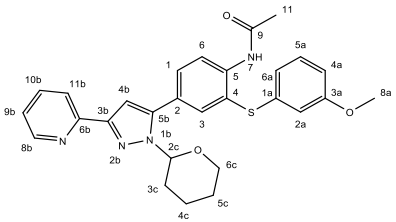

The synthesis was carried out according to general procedure D (65.0 mg, 21%). R_f: 0.17 (PE/EtOAc 1:1). ^{1}H NMR (600 MHz, DMSO-d_6) δ 9.63 (s, 1H, H7), 8.59 (dt, *J* = 4.8, 1.9, 0.9 Hz, 1H, H8b), 7.97 (d, *J* = 7.9 Hz, 1H, H10b), 7.84 (td, *J* = 7.9, 1.9 Hz, 1H, H11b), 7.82 (d, *J* = 8.3 Hz, 1H, H6), 7.58 (dd, *J* = 8.3, 2.2 Hz, 1H, H5), 7.56 (d, *J* = 2.2 Hz, 1H, H3), 7.33 (ddd, *J* = 7.5, 4.8, 1.2 Hz, 1H, H9b), 7.29 (t, *J* = 8.0 Hz, 1H, H5a), 6.98 (s, 1H, H4b), 6.88 – 6.84 (m, 3H, H2a-H4a-H6a), 5.12 (dd, *J* = 10.0, 2.4 Hz, 1H, H2c), 3.82 (dt, *J* = 12.1, 4.2 Hz, 1H, H6c), 3.71 (s, 3H, H8a), 3.16 (td, *J* = 11.4, 2.5 Hz, 1H, H6c), 2.46 – 2.40 (m, 1H, H3c), 2.06 (s, 3H, H11), 1.93 (dd, *J* = 10.1, 3.7 Hz, 1H, H4c), 1.80 (dd, *J* = 13.7, 3.1 Hz, 1H, H3c), 1.60 (p, *J* = 7.7 Hz, 2H, H5c), 1.51 (dd, *J* =

10.1, 2.7 Hz, 1H, H4c). ^{13}C NMR (151 MHz, DMSO-d_6) δ 168.8 (C9), 159.9 (C3a), 151.4 (C6b), 150.4 (C3b), 149.3 (C8b), 144.0 (C5b), 138.8 (C1a), 136.9 (C10b), 136.3 (C1), 131.4 (C3), 130.5 (C5a), 129.0 (C6a), 128.8 (C5), 128.7 (C4), 125.6 (C2), 123.0 (C11b), 122.3 (C6), 119.4 (C9b), 115.6 (C4a), 112.7 (C2a), 104.8 (C4b), 84.0 (C2c), 66.5 (C6c), 55.2 (C8a), 29.0 (C3c), 24.4 (C5c), 23.3 (C11), 22.1 (C4c). HPLC-MS (ESI): m/z calculated for $C_{23}H_{20}N_4O_2S$ (THP cleaved by acidic HPLC conditions) 416.13; $[M+H]^+$ found 417.15.

N-(4-(3-(3-fluorophenyl)-1-(tetrahydro-2H-pyran-2-yl)-1H-pyrazol-5-yl)-2-((3-methoxyphenyl)thio)phenyl)acetamide (18c)

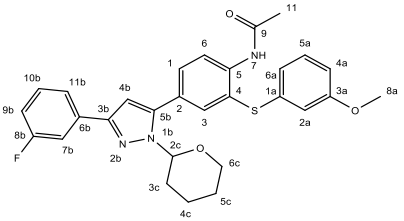

The synthesis was carried out according to general procedure D (29.0 mg, 15%). R_f: 0.55 (PE/EtOAc 1:1). ^{1}H NMR (600 MHz, DMSO-d_6) δ 9.55 (s, 1H), 7.87 (d, J = 8.3 Hz, 1H), 7.69 (dt, J = 7.8, 1.2 Hz, 1H), 7.62 (ddd, J = 10.4, 2.7, 1.5 Hz, 1H), 7.59 (d, J = 2.0 Hz, 1H), 7.57 (dd, J = 8.3, 2.1 Hz, 1H), 7.46 (td, J = 8.0, 6.1 Hz, 1H), 7.28 (t, J = 8.0 Hz, 1H), 7.15 (tdd, J = 9.0, 2.6, 0.9 Hz, 1H), 7.01 (s, 1H), 6.87 – 6.84 (m, 2H), 6.82 (t, J = 2.1 Hz, 1H), 5.12 (dd, J = 10.0, 2.4 Hz, 1H), 3.84 – 3.80 (m, 1H), 3.71 (s, 3H), 3.19 (td, J = 11.3, 2.5 Hz, 1H), 2.42 (qd, J = 9.9, 6.6 Hz, 1H), 2.06 (s, 3H), 1.96 – 1.93 (m, 1H), 1.79 (dd, J = 13.0, 3.5 Hz, 1H), 1.55 – 1.49 (m, 2H), 1.44 – 1.40 (m, 1H). ^{13}C NMR (151 MHz, DMSO-d_6) δ 168.7 (C9), 162.5 (d, $J_{C\text{-}F}$ = 242.8 Hz, C8b), 159.8 (C3a), 148.4 (d, $J_{C\text{-}F}$ = 2.9 Hz, C3b), 144.0 (C5b), 139.0 (C1a), 136.3 (C1), 135.3 (d, $J_{C\text{-}F}$ = 8.2 Hz, C6b), 133.0 (C3), 130.6 (d, $J_{C\text{-}F}$ = 8.4 Hz,

C10b), 130.4 (C5a), 129.0 (C6a), 126.7 (C5), 125.3 (C4), 124.5 (C2), 121.9 (C6), 121.2 (d, $J_{C\text{-}F}$ = 2.3 Hz, C11b), 115.3 (C4a), 114.4 (d, $J_{C\text{-}F}$ = 21.4 Hz, C7b), 112.6 (C2a), 111.7 (d, $J_{C\text{-}F}$ = 22.5 Hz, C9b), 104.3 (C4b), 83.9 (C2c), 66.4 (C6c), 55.1 (C8a), 28.9 (C3c), 24.3 (C5c), 23.3 (C11), 22.0 (C4c). HPLC-MS (ESI): m/z calculated for $C_{24}H_{20}FN_3O_2S$ (THP cleaved by acidic HPLC conditions) 433.13; $[M+H]^+$ found 434.10.

General procedure E

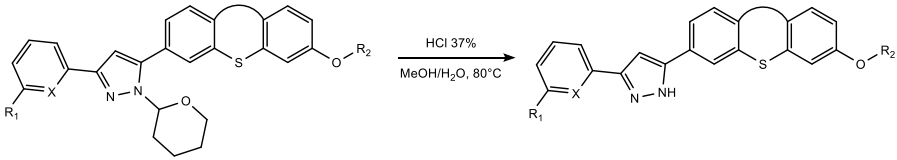

To a suspension of the selected protected DAP compound (0.26 mmol) in MeOH/H_2O 1:1 v/v (13.0 mL, 13.0 mL), HCl 37% (1.30 mL) was added, and the reaction was stirred at 80 °C for 6 h. The mixture was poured into water, neutralized with NaOH aq. 18 M, and extracted with EtOAc. The organic phase was dried over $MgSO_4$, evaporated under reduced pressure, and purified by flash chromatography (PE/EtOAc or DCM/MeOH).

3-Methoxy-7-(3-phenyl-1H-pyrazol-5-yl)-10H-phenothiazine (DAP1a)

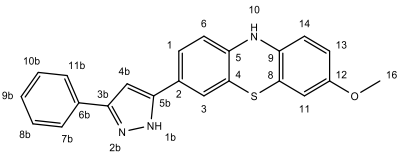

The synthesis was carried out according to general procedure E (43.0 mg, 44%). R_f: 0.55 (PE/EtOAc 1:3). ^{1}H NMR (600 MHz, DMSO-d_6) δ 13.16 (d, J = 71.1 Hz, 1H, H1b), 8.52 (d, J = 59.0 Hz, 1H, H10), 7.81 (dd, J = 38.5, 7.2 Hz, 2H, H7b-H11b), 7.51 – 7.37 (m, 4H, H3-H8b-

H9b-H10b), 7.32 (d, *J* = 27.8 Hz, 1H, H1), 7.03 (d, *J* = 13.3 Hz, 1H, H4b), 6.72 (d, *J* = 8.2 Hz, 1H, H6), 6.66 (d, *J* = 8.4 Hz, 1H, H14), 6.62 (dd, *J* = 11.3, 2.3 Hz, 1H, H13), 6.61 (d, *J* = 7.6 Hz, 1H, H11), 3.67 (s, 3H, H16). ^{13}C NMR (151 MHz, DMSO-*d*$_6$) δ 154.7 (C12), 151.1 (C3b), 142.8 (5b), 142.3 (C6b), 134.8 (C5), 133.7 (C9), 129.0 (C9b), 128.6 (C3), 127.3 (C1), 125.0 (C8b-C10b), 124.6 (C2), 122.7 (C7b-11b), 117.0 (C4), 116.3 (C8), 115.2 (C6), 114.2 (C13), 113.2 (C14), 111.6 (C11), 98.5 (C4b), 55.4 (C16). HPLC-MS (ESI): m/z calculated for $C_{22}H_{17}N_3OS$ 371.11; $[M+H]^+$ found 372.15.

3-Methoxy-7-(3-(pyridin-2-yl)-1H-pyrazol-5-yl)-10H-phenothiazine (DAP1b)

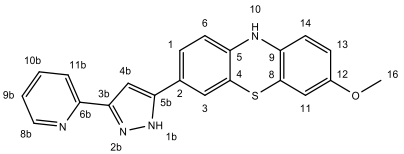

The synthesis was carried out according to general procedure E (9.00 mg, 34%). R_f: 0.35 (PE/EtOAc 1:5). ^{1}H NMR (600 MHz, DMSO-*d*$_6$) δ 13.32 (d, *J* = 117.9 Hz, 1H, H1b), 8.60 (s, 1H, H8b), 8.52 (d, *J* = 53.3 Hz, 1H, H10), 7.93 (d, *J* = 44.3 Hz, 1H, H10b), 7.84 (s, 1H, H11b), 7.53 – 7.28 (m, 3H, H1-H3-H4b), 7.16 (d, *J* = 69.4 Hz, 1H, H9b), 6.70 (d, *J* = 8.2 Hz, 1H, H6), 6.68 – 6.45 (m, 3H, H11-H13-H14), 3.67 (s, 3H, H16). ^{13}C NMR (151 MHz, DMSO-*d*$_6$) δ 154.7 (C12), 149.8 (C6b), 149.4 (C3b), 149.3 (C8b), 139.7 (C5b), 137.2 (C10b), 134.9 (C5), 134.0 (C9), 129.4 (C3), 124.7 (C2), 122.7 (C1), 122.6 (C11b), 119.3 (C9b), 117.2 (C4), 117.1 (C8), 115.1 (C6), 114.3 (C13), 113.2 (C14), 111.6 (C11), 99.9 (C4b), 55.4 (C16). HPLC-MS (ESI): m/z calculated for $C_{21}H_{16}N_4OS$ 372.10; $[M+H]^+$ found 373.05.

3-(3-(3-Fluorophenyl)-1H-pyrazol-5-yl)-7-methoxy-10H-phenothiazine (DAP1c)

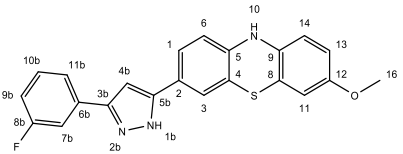

The synthesis was carried out according to general procedure E (26.0 mg, 29%). R_f: 0.34 (PE/EtOAc 1:1). ^{1}H NMR (600 MHz, DMSO-d_6) δ 13.24 (d, J = 50.7 Hz, 1H, H1b), 8.61 (d, J = 62.1 Hz, 1H, H10), 7.66 (br s, 1H, H7b), 7.62 (d, J = 10.4 Hz, 1H, H9b), 7.44 (d, J = 31.7 Hz, 2H, H10b-H1), 7.38 (s, 1H, H3), 7.13 (br s, 1H, H11b), 7.11 (s, 1H, H4b), 6.72 (d, J = 8.2 Hz, 1H, H6), 6.65 (d, J = 8.5 Hz, 1H, H14), 6.62 (dd, J = 8.8, 2.3 Hz, 1H, H13), 6.60 (d, J = 2.7 Hz, 1H, H11), 3.67 (s, 3H, H16). ^{13}C NMR (151 MHz, DMSO-d_6) δ 162.6 (d, $J_{C\text{-}F}$ = 242.7 Hz, C8b), 154.7 (C12), 150.3 (C3b), 142.9 (5b), 142.4 (C6b), 134.8 (C5), 133.4 (C9), 131.0 (C3), 130.7 (d, $J_{C\text{-}F}$ = 8.9 Hz, C10b), 124.6 (C2), 122.8 (C1), 121.1 (C11b), 117.0 (C4), 116.3 (C8), 115.2 (C6), 114.3 (C13), 114.0 (d, $J_{C\text{-}F}$ = 23.7 Hz, C7b), 113.2 (C14), 111.6 (C11), 111.5 (C9b), 99.0 (C4b), 55.4 (C16). HPLC-MS (ESI): m/z calculated for $C_{22}H_{16}FN_3OS$ 389.10; $[M+H]^+$ found 390.15.

3-(2-Fluoroethoxy)-7-(3-phenyl-1H-pyrazol-5-yl)-10H-phenothiazine (DAP2a)

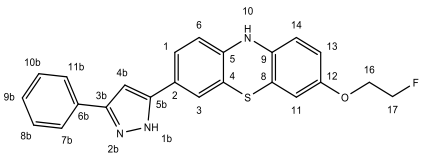

The synthesis was carried out according to general procedure E (14.0 mg, 40%). R_f: 0.50 (PE/EtOAc 1:2). ^{1}H NMR (600 MHz, DMSO-d_6) δ 13.10 (s, 1H, H1b), 8.56 (s, 1H, H10), 7.80 (d, J = 7.6 Hz, 2H, H7b-

H11b), 7.49 – 7.36 (m, 4H, H1-H3-H8b-H10b), 7.32 (t, *J* = 7.6 Hz, 1H, H9b), 7.03 (s, 1H, H4b), 6.80 – 6.56 (m, 4H, H6-H11-H13-H14), 4.68 (dt, *J* = 47.7, 3.9 Hz, 2H, H17), 4.13 (d, *J* = 30.2 Hz, 2H, H16). ^{13}C NMR (151 MHz, DMSO-*d*$_6$) δ 153.5 (C12), 146.9 (C3b), 143.1 (C5b), 142.1 (C6b), 135.4 (C5), 132.1 (C9), 128.8 (C9b), 127.7 (C3), 127.6 (C1), 125.0 (C8b-C10b), 124.6 (C2), 122.8 (C7b-C11b), 117.2 (C4), 116.2 (C8), 115.2 (C6), 114.3 (C13), 114.1 (C14), 112.5 (C11), 98.7 (C4b), 82.2 (d, $J_{C\text{-}F}$ = 166.8 Hz, C17), 67.6 (d, $J_{C\text{-}F}$ = 18.8 Hz, C16). HPLC-MS (ESI): m/z calculated for $C_{23}H_{18}FN_3OS$ 403.12; $[M+Na]^+$ found 446.10.

3-(2-Fluoroethoxy)-7-(3-(pyridin-2-yl)-1H-pyrazol-5-yl)-10H-phenothiazine (DAP2b)

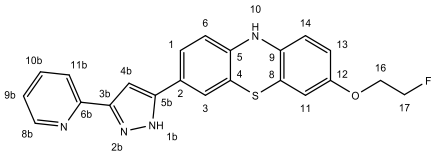

The synthesis was carried out according to general procedure E (12.0 mg, 26%). R$_f$: 0.44 (PE/EtOAc 1:5). ^{1}H NMR (600 MHz, DMSO-*d6*) δ 13.33 (d, *J* = 118.9 Hz, 1H, H1b), 8.61 (d, *J* = 18.9 Hz, 1H, H8b), 8.54 (d, *J* = 49.4 Hz, 1H, H10), 7.93 (dt, *J* = 47.1, 7.7 Hz, 1H, H10b), 7.83 (t, *J* = 7.7 Hz, 1H, H11b), 7.65 – 7.27 (m, 3H, H9b-H1-H3), 7.16 (d, *J* = 76.3 Hz, 1H, H4b), 6.68 (d, *J* = 38.2 Hz, 4H, H6-H11-H13-H14), 4.68 (d, *J* = 47.9 Hz, 2H, H17), 4.14 (d, *J* = 30.1 Hz, 2H, H16). ^{13}C NMR (151 MHz, DMSO-*d*$_6$) δ 153.5 (d, $J_{C\text{-}F}$ = 24.5 Hz, C12), 152.1 (d, $J_{C\text{-}F}$ = 28.5 Hz, C6b), 150.6 (C3b), 149.3 (d, $J_{C\text{-}F}$ = 38.2 Hz, C8b), 142.3 (C5b), 137.0 (d, $J_{C\text{-}F}$ = 97.0 Hz, C10b), 135.6 (C5), 135.2 (C9), 127.1 (C3), 124.7 (d, $J_{C\text{-}F}$ = 45.7 Hz, C2), 122.9 (C1), 122.7 (d, $J_{C\text{-}F}$ = 12.8 Hz, C11b), 119.5 (d, $J_{C\text{-}F}$ = 114.6 Hz, C9b), 117.2 (d, $J_{C\text{-}F}$ = 34.0 Hz, C4), 116.1 (d, $J_{C\text{-}F}$ = 62.7 Hz, C8), 115.2 (C6), 114.3 (C13), 114.1 (C14), 112.5 (C11), 99.9 (d, $J_{C\text{-}F}$ = 65.7 Hz, C4b), 82.2 (d, $J_{C\text{-}F}$ = 167.0 Hz,

C17), 67.5 (d, $J_{C\text{-}F}$ = 19.2 Hz, C16). HPLC-MS (ESI): m/z calculated for $C_{22}H_{17}FN_4OS$ 404.11; $[M+H]^+$ found 405.15.

3-(2-Fluoroethoxy)-7-(3-(3-fluorophenyl)-1H-pyrazol-5-yl)-10H-phenothiazine (DAP2c)

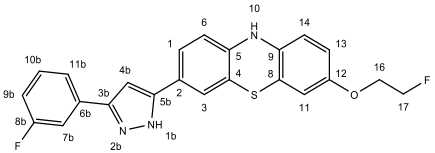

The synthesis was carried out according to general procedure E (11.0 mg, 13%). R_f: 0.57 (PE/EtOAc 1:2). ^{1}H NMR (600 MHz, DMSO-d_6) δ 13.25 (d, J = 59.9 Hz, 1H, H1b), 8.56 (d, J = 52.0 Hz, 1H, H10), 7.67 (br s, 1H, H7b), 7.61 (d, J = 10.5 Hz, 1H, H9b), 7.56 – 7.39 (m, 2H, H1-H10b), 7.38 (s, 1H, H3), 7.22 – 7.05 (m, 2H, H4b-H11b), 6.71 (d, J = 8.2 Hz, 1H, H6), 6.65 (s, 3H, H11-H13-H14), 4.68 (dt, J = 48.0, 3.8 Hz, 2H, H17), 4.13 (dt, J = 30.3, 3.8 Hz, 2H, H16). ^{13}C NMR (151 MHz, DMSO-d_6) δ 162.6 (d, $J_{C\text{-}F}$ = 242.5 Hz, C8b), 153.6 (C12), 150.1 (C3b), 143.1 (C5b), 140.4 (C6b), 135.2 (C5), 134.6 (C9), 131.7 (C3), 130.7 (d, $J_{C\text{-}F}$ = 18.8 Hz, C10b), 124.7 (C2), 122.8 (C1), 121.1 (C11b), 117.3 (C4), 117.1 (C8), 115.2 (C6), 114.3 (C13), 114.2 (d, $J_{C\text{-}F}$ = 7.0 Hz, C7b), 114.1 (C14), 112.5 (C11), 111.5 (d, $J_{C\text{-}F}$ = 11.9 Hz, C9b), 99.0 (C4b), 82.2 (d, $J_{C\text{-}F}$ = 166.4 Hz, C17), 67.5 (d, $J_{C\text{-}F}$ = 19.1 Hz, C16). HPLC-MS (ESI): m/z calculated for $C_{23}H_{17}F_2N_3OS$ 421.11; $[M+MeCN+2H]^+$ found 464.10.

2-((3-Methoxyphenyl)thio)-4-(3-phenyl-1H-pyrazol-5-yl)aniline (DAP3a)

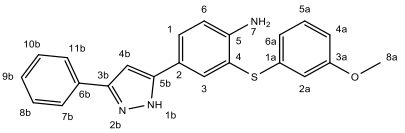

The synthesis was carried out according to general procedure E (23.0 mg, 81%). R_f: 0.42 (PE/EtOAc 1:1). ^{1}H NMR (600 MHz, DMSO-d_6) δ 13.02 (s, 1H, H1b), 7.84 (d, *J* = 2.1 Hz, 1H, H3), 7.81 (d, *J* = 7.7 Hz, 2H, H7b-H11b), 7.66 (d, *J* = 8.4 Hz, 1H, H5), 7.42 (t, *J* = 7.6 Hz, 2H, H8b-H10b), 7.31 (t, *J* = 7.4 Hz, 1H, H9b), 7.20 (t, *J* = 8.0 Hz, 1H, H5a), 6.99 (s, 1H, H4b), 6.90 (d, *J* = 8.4 Hz, 1H, H6), 6.73 (ddd, *J* = 8.0, 2.1, 0.9 Hz, 1H, H6a), 6.68 (dt, *J* = 8.0, 2.1, 0.9 Hz, 1H, H4a), 6.66 (t, *J* = 2.1 Hz, 1H, H2a), 5.57 (s, 2H, H7), 3.69 (s, 3H, H8a).^{13}C NMR (151 MHz, DMSO-d_6) δ 159.6 (C3a), 150.1 (C3b), 150.0 (C1), 143.2 (C5b), 137.9 (C6b), 137.8 (C1a), 133.7 (C3), 129.9 (C7b-C11b), 128.6 (C9b), 128.5 (C5a), 128.3 (C5), 127.4 (C4), 125.0 (C8b-C10b), 118.5 (C6a), 115.0 (C4a), 112.1 (C2a), 112.0 (C2), 110.8 (C6), 98.1 (C4b), 55.0 (C8a). HPLC-MS (ESI): m/z calculated for $C_{22}H_{19}N_3OS$ 373.12; $[M+H]^+$ found 374.10.

2-((3-Methoxyphenyl)thio)-4-(3-(pyridin-2-yl)-1H-pyrazol-5-yl)aniline (DAP3b)

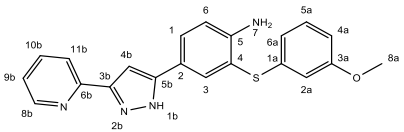

The synthesis was carried out according to general procedure E (21.0 mg, 47%). R_f: 0.42 (PE/EtOAc 1:4). ^{1}H NMR (600 MHz, DMSO-d_6) δ 13.27 (d, *J* = 84.4 Hz, 1H), 8.59 (d, *J* = 4.9 Hz, 1H), 7.92 (s, 1H), 7.85 (d, *J* = 2.0 Hz, 2H), 7.69 (d, *J* = 6.1 Hz, 1H), 7.31 (br s, 1H), 7.20 (t, *J* = 8.0 Hz, 1H), 7.10 (d, *J* = 8.1 Hz, 1H), 6.90 (d, *J* = 8.4 Hz, 1H), 6.73 (dd, *J* = 8.4, 2.3 Hz, 1H), 6.70 – 6.62 (m, 2H), 5.65 (br s, 2H), 3.68 (s, 3H).^{13}C NMR (151 MHz, DMSO-d6) δ 159.7 (C3a), 152.1 (C6b), 150.3 (C3b), 149.2 (C8b), 148.9 (C1), 141.9 (C5b), 138.0 (C1a), 136.8 (C10b), 133.7 (C3), 130.0 (C5a), 128.6 (C5), 128.5 (C4), 122.6 (C11b),

119.2 (C9b), 118.6 (C6a), 115.1 (C4a), 112.2 (C2a), 111.9 (C2), 110.8 (C6), 99.2 (C4b), 55.1 (C8a). HPLC-MS (ESI): m/z calculated for $C_{21}H_{18}N_4OS$ 374.12; $[M+H]^+$ found 375.15.

4-(3-(3-Fluorophenyl)-1H-pyrazol-5-yl)-2-((3-methoxyphenyl)thio)aniline (DAP3c)

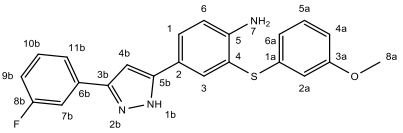

The synthesis was carried out according to general procedure E (16.0 mg, 68%). R_f: 0.45 (PE/EtOAc 1:1). ^{1}H NMR (600 MHz, DMSO-d_6) δ 13.10 (s, 1H, H1b), 7.84 (d, J = 2.0 Hz, 1H, H3), 7.66 (t, J = 8.8 Hz, 2H, H9b-H5), 7.62 (dt, J = 10.6, 2.0 Hz, 1H, H7b), 7.46 (q, J = 7.0, 6.6 Hz, 1H, H10b), 7.20 (t, J = 8.2 Hz, 1H, H5a), 7.12 (t, J = 9.7 Hz, 1H, H11b), 7.07 (s, 1H, H4b), 6.91 (d, J = 8.4 Hz, 1H, H6), 6.73 (dd, J = 8.2, 2.4 Hz, 1H, H6a), 6.68 (dt, J = 8.2, 2.1, 1.0 Hz, 1H, H4a), 6.66 (t, J = 2.1 Hz, 1H, H2a), 5.61 (br s, 2H, H7), 3.69 (s, 3H, H8a).^{13}C NMR (151 MHz, DMSO-d_6) δ 162.5 (d, $J_{C\text{-}F}$ = 242.7 Hz, C8b), 159.7 (C3a), 152.6 (C1), 150.2 (d, $J_{C\text{-}F}$ = 14.8 Hz, C3b), 143.7 (C5b), 137.8 (C1a), 135.1 (d, $J_{C\text{-}F}$ = 2.1 Hz, C6b), 133.8 (C3), 130.6 (d, $J_{C\text{-}F}$ = 5.3 Hz, C10b), 130.1 (C4), 129.9 (C5a), 128.3 (C5), 121.0 (d, $J_{C\text{-}F}$ = 1.8 Hz, C11b), 118.5 (C6a), 115.1 (C4a), 112.1 (C2a), 112.0 (C7b), 111.5 (d, $J_{C\text{-}F}$ = 23.1 Hz, C9b), 111.4 (C2), 110.8 (C6), 97.2 (C4b), 55.0 (C8a). HPLC-MS (ESI): m/z calculated for $C_{22}H_{18}FN_3OS$ 391.12; $[M+H]^+$ found 392.10.

1.3 Synthesis of a library of 2-styrylbenzothiazoles

General procedure F

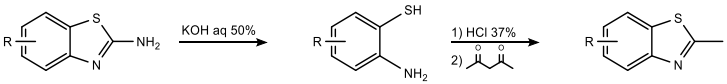

A suspension of the selected 2-aminobenzothiazole (7.36 mmol) in KOH aq 50% (28.0 mL) was refluxed for 18 h to 42 h. The mixture was acidified by addition of HCl 37% (20.0 mL). Color changed and precipitate formed. 2,4-pentanedione (11.04 mmol) was added and the reaction was stirred at room temperature for 90 min. The mixture was extracted with EtOAc. The organic phase was dried over $MgSO_4$, evaporated under reduced pressure, and purified by flash chromatography (Hept/EtOAc).

General procedure G

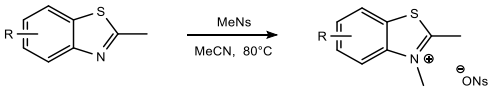

To a solution of the selected 2-methylbenzothiazole (0.63 mmol) in MeCN (2.00 mL) was added methyl nosylate (1.26 mmol). The mixture was stirred overnight at 80 °C. The precipitate was filtered under vacuum, washed with EtOAc and/or triturated in Et_2O.

General procedure H

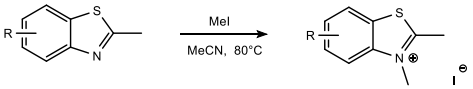

To a solution of the selected 2-methylbenzothiazole (8.24 mmol) in MeCN (25.0 mL) was added methyl iodide (16.5 mmol). The mixture was stirred overnight at 80 °C. The precipitate was filtered under vacuum, washed with EtOAc and/or triturated in Et_2O.

2,4-Dimethylbenzo[d]thiazole (19a)

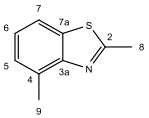

The synthesis was carried out according to general procedure F, additionally adding ethylen glycol (0.5 mL/mmol) to the mixture (393 mg, 33%). R_f: 0.41 (Hept/EtOAc 4:1). ^{1}H NMR (400 MHz, DMSO-d_6) δ 7.82 (pd, J = 3.6, 0.6 Hz, 1H, H5), 7.28 (s, 1H, H7), 7.27 – 7.25 (m, 1H, H6), 2.80 (s, 3H, 2-Me), 2.63 (s, 3H, 4-Me). ^{13}C NMR (101 MHz, DMSO-d_6) δ 165.6 (C2), 152.2 (C3a), 134.9 (C4), 131.4 (C7a), 126.4 (C5), 124.6 (C6), 119.2 (C7), 19.8 (2-Me), 18.1 (4-Me). HPLC-MS (ESI): m/z calculated for C_9H_9NS 163.05; $[M+H]^+$ found 164.06.

2,3,4-Trimethylbenzo[d]thiazol-3-ium 4-nitrobenzenesulfonate (19b)

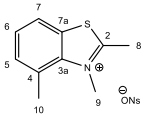

The synthesis was carried out according to general procedure G (248 mg, 67%). R_f: 0.29 (DCM/MeOH 9:1). ^{1}H NMR (400 MHz, DMSO-d_6) δ 8.30 – 8.22 (m, 1H, H5), 8.19 (d, J = 8.4 Hz, 2H, Ns), 7.82 (d, J = 8.3 Hz, 2H, Ns), 7.64 (d, J = 2.1 Hz, 1H, H6), 7.62 (s, 1H, H7), 4.36 (s, 3H, N-Me), 3.13 (s, 3H, 2-Me), 2.93 (s, 3H, 4-Me). ^{13}C NMR (151 MHz, DMSO-d_6) δ 176.6 (C2), 154.2 (Ns), 147.3 (Ns), 140.6 (C3a), 132.8 (C7a), 129.5 (C4), 128.3 (C5), 127.7 (C7), 126.9 (Ns), 123.4 (Ns), 122.4 (C6), 39.9 (N-Me), 20.4 (4-Me), 17.6 (2-Me). HPLC-MS (ESI): m/z calculated for $C_{10}H_{12}NS^+$ 178.07; $[M]^+$ found 178.07.

4-Methoxy-2-methylbenzo[d]thiazole (20a)

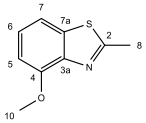

The synthesis was carried out according to general procedure F (223 mg, 20%). R_f: 0.09 (Hept/EtOAc 4:1). ^{1}H NMR (400 MHz, DMSO-d_6) δ

7.55 (dd, *J* = 8.0, 1.0 Hz, 1H, H5), 7.32 (t, *J* = 8.0 Hz, 1H, H6), 7.01 (dd, *J* = 8.0, 1.0 Hz, 1H, H7), 3.93 (s, 3H, 4-OMe), 2.77 (s, 3H, 2-Me). ^{13}C NMR (101 MHz, DMSO-d_6) δ 164.7 (C2), 152.6 (C4), 142.8 (C3a), 136.7 (C7a), 125.7 (C6), 113.6 (C7), 107.4 (C5), 55.7 (4-OMe), 19.7 (2-Me). HPLC-MS (ESI): m/z calculated for C_9H_9NOS 179.04; $[M+H]^+$ found 180.00.

4-Methoxy-2,3-dimethylbenzo[d]thiazol-3-ium iodide (20b)

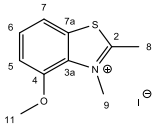

The synthesis was carried out according to general procedure H (35 mg, 20%). R_f: 0.34 (DCM/MeOH 9:1). ^{1}H NMR (600 MHz, DMSO-d_6) δ 7.93 (dd, *J* = 8.2, 0.9 Hz, 1H, H5), 7.70 (t, *J* = 8.2 Hz, 1H, H6), 7.45 (dd, *J* = 8.2, 0.9 Hz, 1H, H7), 4.35 (s, 3H, 4-OMe), 4.05 (s, 3H, N-Me), 3.09 (s, 3H, 2-Me). ^{13}C NMR (151 MHz, DMSO-d_6) δ 176.4 (C2), 150.4 (C4), 131.5 (C7a), 131.1 (C3a), 129.5 (C6), 116.4 (C7), 112.1 (C5), 57.5 (C4-OMe), 40.6 (N-Me), 17.6 (2-Me). HPLC-MS (ESI): m/z calculated for $C_{10}H_{12}NOS^+$ 194.06; $[M]^+$ found 194.10.

4-Fluoro-2-methylbenzo[d]thiazole (21a)

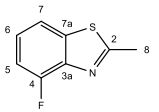

The synthesis was carried out according to general procedure F (431 mg, 36%). R_f: 0.35 (Hept/EtOAc 4:1). ^{1}H NMR (400 MHz, DMSO-d_6) δ 7.86 (dd, *J* = 8.1, 1.1 Hz, 1H, H7), 7.41 (td, *J* = 8.1, 4.9 Hz, 1H, H6), 7.31 (ddd, *J* = 11.0, 8.1, 1.1 Hz, 1H, H5), 2.82 (s, 3H, 2-Me). ^{13}C NMR (101 MHz, DMSO-d_6) δ 168.2 (C2), 154.4 (d, $J_{C\text{-}F}$ = 252.9 Hz, C4), 141.2 (d, $J_{C\text{-}F}$ = 13.3 Hz, C3a), 138.1 (d, $J_{C\text{-}F}$ = 3.8 Hz, C7a), 125.7 (d,

$J_{C\text{-}F}$ = 7.1 Hz, C6), 118.1 (d, $J_{C\text{-}F}$ = 4.1 Hz, C7), 111.7 (d, $J_{C\text{-}F}$ = 17.9 Hz. C5), 19.7 (2-Me). ^{19}F NMR (376 MHz, DMSO-d_6) δ -123.34. HPLC-MS (ESI): m/z calculated for C_8H_6FNS 167.02; $[M+2H]^+$ found 169.12.

4-Fluoro-2,3-dimethylbenzo[d]thiazol-3-ium 4-nitrobenzenesulfonate (21b)

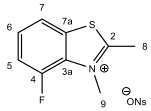

The synthesis was carried out according to general procedure G (188 mg, 78%). R_f: 0.32 (DCM/MeOH 9:1). ^{1}H NMR (400 MHz, DMSO-d_6) δ 8.28 – 8.20 (m, 1H, H7), 8.18 (d, J = 8.4 Hz, 2H, Ns), 7.86 – 7.75 (m, 4H, H5-H6-Ns), 4.29 (d, J = 2.7 Hz, 3H, N-Me), 3.16 (s, 3H, 2-Me). ^{13}C NMR (101 MHz, DMSO-d_6) δ 178.6 (C2), 154.3 (Ns), 150.8 (d, $J_{C\text{-}F}$ = 253.2 Hz, C4), 147.2 (Ns), 131.3 (C7a), 130.3 (d, $J_{C\text{-}F}$ = 10.7 Hz, C3a), 129.1 (d, $J_{C\text{-}F}$ = 7.5 Hz, C6), 126.9 (Ns), 123.3 (Ns), 120.8 (d, $J_{C\text{-}F}$ = 4.6 Hz, C7), 116.0 (d, $J_{C\text{-}F}$ = 19.1 Hz, C5), 39.2 (N-Me), 17.0 (2-Me). ^{19}F NMR (376 MHz, DMSO-d_6) δ -125.33. HPLC-MS (ESI): m/z calculated for $C_9H_9FNS^+$ 182.04; $[M]^+$ found 182.06.

2,3,5-Trimethylbenzo[d]thiazol-3-ium iodide (22b)

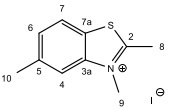

The synthesis was carried out according to general procedure H from the commercially available 2,5-dimethylbenzothiazole (**22a**, 460 mg, 61%). R_f: 0.32 (DCM/MeOH 9:1). ^{1}H NMR (400 MHz, DMSO-d_6) δ 8.29 (d, J = 8.4 Hz, 1H, H7), 8.14 (d, J = 1.5 Hz, 1H, H4), 7.64 (dd, J = 8.4, 1.5 Hz, 1H, H6), 4.17 (s, 3H, N-Me), 3.15 (s, 3H, 2-Me), 2.57 (s, 3H, 5-Me). ^{13}C NMR (101 MHz, DMSO-d_6) δ 176.8 (C2), 141.8 (C5), 139.8 (C3a), 129.5 (C6), 125.8 (C7a), 123.9 (C7), 116.4 (C4), 36.0 (N-Me),

21.1 (5-Me), 17.0 (2-Me). HPLC-MS (ESI): m/z calculated for $C_{10}H_{12}NS^+$ 178.07; $[M]^+$ found 178.08.

5-Methoxy-2-methylbenzo[d]thiazole (23a)

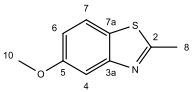

To a solution of 2-methyl-5-benzothiazolol (500 mg, 3.03 mmol) in DMF (8.50 mL) was added K_2CO_3 (836 mg, 6.05 mmol). The mixture was stirred at room temperature for 10 min. Methyl iodide (283 µL, 4.54 mmol) was added dropwise and the reaction was stirred at room temperature for 1 h. The mixture was diluted with water and extracted with EtOAc. The organic phase was dried over $MgSO_4$, evaporated under reduced pressure and used without any further purification (477 mg, 88%). R_f: 0.16 (Hept/EtOAc 4:1). ^{1}H NMR (400 MHz, DMSO-d_6) δ 7.87 (d, J = 8.8 Hz, 1H, H7), 7.45 (d, J = 2.5 Hz, 1H, H4), 7.02 (dd, J = 8.8, 2.5 Hz, 1H, H6), 3.83 (s, 3H, 5-OMe), 2.76 (s, 3H, 2-Me). ^{13}C NMR (101 MHz, DMSO-d_6) δ 168.0 (C2), 158.4 (C5), 154.3 (C3a), 126.8 (C7a), 122.2 (C7), 114.1 (C6), 105.1 (C4), 55.4 (5-OMe), 19.8 (2-Me). HPLC-MS (ESI): m/z calculated for C_9H_9NOS 179.04; $[M+H]^+$ found 180.05.

5-Methoxy-2,3-dimethylbenzo[d]thiazol-3-ium iodide (23b)

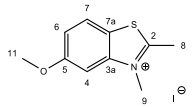

The synthesis was carried out according to general procedure H (204 mg, 54%). R_f: 0.40 (DCM/MeOH 9:1). ^{1}H NMR (400 MHz, DMSO-d_6) δ 8.29 (d, J = 9.0 Hz, 1H, H7), 7.78 (d, J = 2.4 Hz, 1H, H4), 7.42 (dd, J = 9.0, 2.4 Hz, 1H, H6), 4.17 (s, 3H, N-Me), 3.97 (s, 3H, 5-OMe), 3.13 (s, 3H, 2-Me). ^{13}C NMR (101 MHz, DMSO-d_6) δ 177.0 (C2), 160.6 (C5),

143.1 (C3a), 125.1 (C7), 120.4 (C7a), 117.7 (C6), 100.0 (C4), 56.4 (5-OMe), 36.2 (N-Me), 17.1 (2-Me). HPLC-MS (ESI): m/z calculated for $C_{10}H_{12}NOS^+$ 194.06; $[M]^+$ found 194.07.

5-Fluoro-2,3-dimethylbenzo[d]thiazol-3-ium iodide (24b)

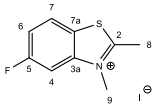

The synthesis was carried out according to general procedure H from commercially available 5-fluoro-2-methylbenzothiazole (**24a**, 168 mg, 23%). R_f: 0.32 (DCM/MeOH 9:1). ^{1}H NMR (400 MHz, DMSO-d_6) δ 8.48 (dd, J = 9.1, 5.1 Hz, 1H, H7), 8.34 (dd, J = 9.5, 2.5 Hz, 1H, H4), 7.74 (td, J = 9.0, 2.4 Hz, 1H, H6), 4.17 (s, 3H, N-Me), 3.17 (s, 3H, 2-Me). ^{13}C NMR (101 MHz, DMSO-d_6) δ 179.5 (C2), 162.3 (d, $J_{C\text{-}F}$ = 246.7 Hz, C5), 142.7 (d, $J_{C\text{-}F}$ = 12.8 Hz, C3a), 126.5 (d, $J_{C\text{-}F}$ = 10.1 Hz, C7), 124.7 (d, $J_{C\text{-}F}$ = 2.1 Hz, C7a), 116.8 (d, $J_{C\text{-}F}$ = 25.0 Hz, C6), 104.2 (d, $J_{C\text{-}F}$ = 28.8 Hz, C4), 36.4 (N-Me), 17.3 (2-Me). ^{19}F NMR (376 MHz, DMSO-d_6) δ -110.17. HPLC-MS (ESI): m/z calculated for $C_9H_9FNS^+$ 182.04; $[M]^+$ found 182.05.

2,6-Dimethylbenzo[d]thiazole (25a)

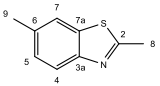

The synthesis was carried out according to general procedure F (1.50 g, 60%). R_f: 0.37 (Hept/EtOAc 3:1). ^{1}H NMR (400 MHz, DMSO-d_6) δ 7.80 (p, J = 0.8 Hz, 1H, H7), 7.77 (d, J = 8.3 Hz, 1H, H4), 7.27 (dd, J = 8.2, 1.6 Hz, 1H, H5), 2.76 (s, 3H, 2-Me), 2.42 (s, 3H, 6-Me). ^{13}C NMR (101 MHz, DMSO-d_6) δ 165.6 (C2), 151.1 (C3a), 135.3 (C7a), 134.2 (C6), 127.3 (C7), 121.5 (C4), 121.4 (C5), 20.9 (6-Me), 19.6 (2-Me).

HPLC-MS (ESI): m/z calculated for C_9H_9NS 163.05; $[M+H]^+$ found 164.06.

2,3,6-Trimethylbenzo[d]thiazol-3-ium iodide (25b)

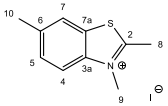

The synthesis was carried out according to general procedure H (378 mg, 50%). R_f: 0.28 (DCM/MeOH 9:1). ^{1}H NMR (400 MHz, DMSO-d_6) δ 8.21 (t, *J* = 1.2 Hz, 1H, H7), 8.18 (d, *J* = 8.7 Hz, 1H, H4), 7.72 (dd, *J* = 8.7, 1.7 Hz, 1H, H5), 4.17 (s, 3H, N-Me), 3.14 (s, 3H, 2-Me), 2.53 (s, 3H, 6-Me). ^{13}C NMR (101 MHz, DMSO-d_6) δ 176.0 (C2), 139.8 (C6), 138.4 (C3a), 130.5 (C5), 128.7 (C7a), 123.7 (C7), 116.3 (C4), 36.1 (N-Me), 21.0 (6-Me), 17.0 (2-Me). HPLC-MS (ESI): m/z calculated for $C_{10}H_{12}NS^+$ 178.07; $[M]^+$ found 178.07.

6-Methoxy-2-methylbenzo[d]thiazole (26a)

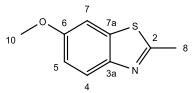

The synthesis was carried out according to general procedure F (1.34 g, 61%). R_f: 0.29 (Hept/EtOAc 3:1). ^{1}H NMR (400 MHz, DMSO-d_6) δ 7.78 (d, *J* = 8.9 Hz, 1H, H4), 7.59 (d, *J* = 2.6 Hz, 1H, H7), 7.05 (dd, *J* = 8.9, 2.6 Hz, 1H, H), 3.81 (s, 3H, 6-OMe), 2.73 (s, 3H, 2-Me). ^{13}C NMR (101 MHz, DMSO-d_6) δ 164.0 (C2), 156.9 (C6), 147.3 (C3a), 136.5 (C7a), 122.3 (C4), 114.9 (C5), 104.7 (C7), 55.6 (6-OMe), 19.5 (2-Me). HPLC-MS (ESI): m/z calculated for C_9H_9NOS 179.04; $[M+H]^+$ found 180.04.

6-Methoxy-2,3-dimethylbenzo[d]thiazol-3-ium iodide (26b)

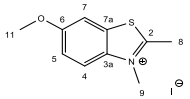

The synthesis was carried out according to general procedure H (410 mg, 57%). R_f: 0.15 (DCM/MeOH 9:1). ^{1}H NMR (400 MHz, DMSO-d_6) δ 8.18 (d, J = 9.3 Hz, 1H, H4), 8.00 (d, J = 2.6 Hz, 1H, H7), 7.47 (dd, J = 9.3, 2.6 Hz, 1H, H5), 4.16 (s, 3H, N-Me), 3.90 (s, 3H, 6-OMe), 3.11 (s, 3H, 2-Me). ^{13}C NMR (101 MHz, DMSO-d_6) δ 174.3 (C2), 159.0 (C6), 135.8 (C3a), 130.4 (C7a), 118.4 (C4), 117.6 (C5), 106.6 (C7), 56.2 (6-OMe), 36.2 (N-Me), 16.9 (2-Me). HPLC-MS (ESI): m/z calculated for $C_{10}H_{12}NOS^+$ 194.06; $[M]^+$ found 194.06.

6-Fluoro-2-methylbenzo[d]thiazole (27a)

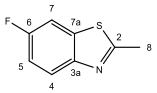

2-Amino-5-fluorobenzenethiol (300 mg, 2.09 mmol) and 2,4-pentanedione (323 µL, 3.14 mmol) were dissolved in MeCN (1 mL) and p-toluenesulfonic acid (18.0 mg, 0.10 mmol) was added. The mixture was stirred overnight at room temperature. It was diluted with water and extracted with EtOAc. The organic phase was dried over $MgSO_4$, evaporated under reduced pressure, and purified by flash chromatography (Hept/EtOAc 0% to 20% B) to afford the product (257 mg, 73%). R_f: 0.29 (Hept/EtOAc 5:1). ^{1}H NMR (400 MHz, DMSO-d_6) δ 7.94 (dd, J = 8.2, 2.1 Hz, 1H, H4), 7.91 (dd, J = 8.3, 4.3 Hz, 1H, H7), 7.33 (td, J = 9.1, 2.7 Hz, 1H, H5), 2.78 (s, 3H, 2-Me). ^{13}C NMR (101 MHz, DMSO-d_6) δ 167.1 (d, $J_{C\text{-}F}$ = 3.2 Hz, C2), 159.4 (d, $J_{C\text{-}F}$ = 241.7 Hz, C6), 149.7 (C3a), 136.4 (d, $J_{C\text{-}F}$ = 11.7 Hz, C7a), 123.0 (d, $J_{C\text{-}F}$ = 9.5 Hz, C4), 114.3 (d, $J_{C\text{-}F}$ = 24.8 Hz, C7), 108.3 (d, $J_{C\text{-}F}$ = 27.1 Hz, C5),

19.7 (2-Me). ^{19}F NMR (376 MHz, DMSO-d_6) δ -117.24. HPLC-MS (ESI): m/z calculated for C_8H_6FNS 167.02; $[M+H]^+$ found 168.04.

6-Fluoro-2,3-dimethylbenzo[d]thiazol-3-ium iodide (27b)

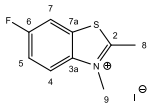

The synthesis was carried out according to general procedure H (73.6 mg, 24%). R_f: 0.17 (DCM/MeOH 9:1). ^{1}H NMR (600 MHz, DMSO-d_6) δ 8.36 (dd, J = 9.1, 4.3 Hz, 1H, H4), 8.32 (dd, J = 8.3, 2.7 Hz, 1H, H7), 7.84 (td, J = 9.1, 2.7 Hz, 1H, H5), 4.19 (s, 3H, N-Me), 3.15 (s, 3H, 2-Me). ^{13}C NMR (151 MHz, DMSO-d_6) δ 177.8 (d, $J_{C\text{-}F}$ = 2.5 Hz, C2), 160.7 (d, $J_{C\text{-}F}$ = 247.2 Hz, C6), 138.5 (C3a), 130.3 (d, $J_{C\text{-}F}$ = 12.2 Hz, C7a), 118.8 (d, $J_{C\text{-}F}$ = 9.6 Hz, C4), 117.9 (d, $J_{C\text{-}F}$ = 25.7 Hz, C7), 110.9 (d, $J_{C\text{-}F}$ = 28.6 Hz, C5), 36.5 (N-Me), 17.2 (2-Me). ^{19}F NMR (376 MHz, DMSO-d_6) δ -111.66. HPLC-MS (ESI): m/z calculated for $C_9H_9FNS^+$ 182.04; $[M]^+$ found 182.06.

1-Methyl-3-nitro-2-thiocyanatobenzene (28.1)

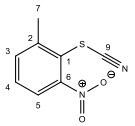

To a suspension of 2-methyl-6-nitroaniline (1.20 g, 7.89 mmol) in water (27.0 mL) cooled to 0 °C, HCl 37% (12.0 mL) was added. Sodium nitrite (653 mg, 9.46 mmol) was dissolved in water (5.00 mL) and added dropwise. After stirring for 5 min at 0 °C, a solution of potassium thiocyanate (2.30 g, 23.7 mmol) and iron (III) chloride (640 mg, 3.94 mmol) in water (9.00 mL) was added dropwise. The mixture was stirred at room temperature for 5 h. It was diluted with water and extracted with EtOAc. The organic phase was dried over $MgSO_4$, evaporated and used without any further purification (quant.). R_f: 0.54 (Hept/EtOAc

1:1). ^{1}H NMR (400 MHz, DMSO-d_6) δ 7.96 (d, J = 7.0 Hz, 1H, H4), 7.82 (d, J = 6.9 Hz, 1H, H6), 7.73 (t, J = 7.3 Hz, 1H, H5), 2.66 (s, 3H, Me). ^{13}C NMR (101 MHz, DMSO-d_6) δ 152.9 (C1), 144.5 (C3), 135.4 (C6), 132.1 (C2), 123.1 (C5), 117.0 (C4), 110.5 (C9), 21.1 (Me).

2,7-Dimethylbenzo[d]thiazole (28a)

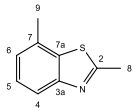

To a solution of **28.1** (2.55 g, 13.1 mmol) in EtOH/H_2O 1:1 v/v (45 mL, 45 mL), Na_2S (2.05 g, 26.3 mmol) was added in portions under argon atmosphere. The mixture was heated at 65 °C for 3 h and then extracted with EtOAc. The organic phase was dried over $MgSO_4$, evaporated under reduced pressure, and purified by flash chromatography (DCM/MeOH 0% to 2% B). The collected residue was dissolved in MeCN (1 mL) and 2,4-pentanedione (0.06 mL, 0.60 mmol) and p-toluenesulfonic acid (3.00 mg, 0.02 mmol) were added. The mixture was stirred at room temperature for 3 h. It was diluted with water and extracted with EtOAc. The organic phase was dried over $MgSO_4$, evaporated, and purified by flash chromatography (PE/EtOAc 0% to 20% B) to afford the product (17.0 mg, 1%). R_f: 0.26 (PE/EtOAc 4:1). ^{1}H NMR (400 MHz, $CDCl_3$) δ 7.79 (d, J = 8.1 Hz, 1H, H4), 7.36 (t, J = 7.7 Hz, 1H, H5), 7.15 (dt, J = 7.4, 1.0 Hz, 1H, H6), 2.85 (s, 3H, 2-Me), 2.54 (s, 3H, 7-Me). ^{13}C NMR (151 MHz, $CDCl_3$) δ 166.7 (C2), 153.2 (C3a), 136.2 (C7a), 131.7 (C7), 126.3 (C4), 125.1 (C5), 119.9 (C6), 21.6 (2-Me), 20.3 (7-Me). HPLC-MS (ESI): m/z calculated for C_9H_9NS 163.05; $[M+H]^+$ found 164.10.

2,3,7-Trimethylbenzo[d]thiazol-3-ium iodide (28b)

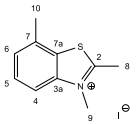

The synthesis was carried out according to general procedure H (12.0 mg, 40%). R_f: 0.35 (DCM/MeOH 9:1). ^{1}H NMR (600 MHz, DMSO-d_6) δ 8.15 (d, *J* = 8.5 Hz, 1H, H4), 7.83 (dd, *J* = 8.5, 7.5 Hz, 1H, H5), 7.66 (dt, *J* = 7.5, 1.0 Hz, 1H, H6), 4.21 (s, 3H, N-Me), 3.20 (s, 3H, 2-Me), 2.66 (s, 3H, 7-Me). ^{13}C NMR (151 MHz, DMSO-d_6) δ 176.2 (C2), 147.0 (C3a), 136.7 (C7a), 133.5 (C7), 129.7 (C5), 128.5 (C6), 114.5 (C4), 36.6 (N-Me), 19.3 (2-Me), 17.2 (7-Me). HPLC-MS (ESI): m/z calculated for $C_{10}H_{12}NS^+$ 178.07; $[M]^+$ found 178.05.

2-Methoxy-6-nitroaniline (29.1)

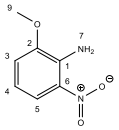

To a solution of 2-amino-3-nitrophenol (4.18 g, 27.1 mmol) in MeCN (47.0 mL) was added K_2CO_3 (3.75 g, 27.1 mmol). Methyl iodide (1.86 mL, 29.8 mmol) was added dropwise and the mixture was stirred at room temperature for 22 h. It was diluted with water and extracted with EtOAc. The organic phase was dried over $MgSO_4$, evaporated under reduced pressure, and purified by flash chromatography (Hept/EtOAc 0% to 20% B) to afford the product as an orange solid (2.63 g, 58%). R_f: 0.39 (Hept/EtOAc 2:1). ^{1}H NMR (400 MHz, $CDCl_3$) δ 7.73 (dd, *J* = 8.9, 1.3 Hz, 1H, H5), 6.88 (dd, *J* = 7.8, 1.3 Hz, 1H, H3), 6.61 (dd, *J* = 8.9, 7.8 Hz, 1H, H4), 6.42 (s, 2H, H7), 3.92 (s, 3H, O-Me). ^{13}C NMR (101 MHz, $CDCl_3$) δ 148.3 (C2), 137.2 (C6), 131.8 (C1), 117.5 (C5), 114.7 (C3), 113.5 (C4), 56.4 (O-Me). HPLC-MS (ESI): m/z calculated for $C_7H_8N_2O_3$ 168.05; $[M+H]^+$ found 169.06.

1-Methoxy-3-nitro-2-thiocyanatobenzene (29.2)

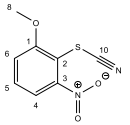

The synthesis was carried out following the same procedure as **28.1** (quant.). R_f: 0.21 (PE/EtOAc 3:1). ^{1}H NMR (600 MHz, DMSO-d_6) δ 7.82 – 7.70 (m, 2H, H4-H5), 7.64 (dd, *J* = 8.2, 4.2 Hz, 1H, H6), 4.07 (s, 3H, O-Me). ^{13}C NMR (151 MHz, DMSO-d_6) δ 158.8 (C1), 132.9 (C3), 124.5 (C10), 117.7 (C4), 117.3 (C6), 109.9 (C5), 106.6 (C2), 57.5 (O-Me).

7-Methoxy-2-methylbenzo[d]thiazole (29a)

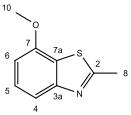

The synthesis was carried out following the same procedure as **28a** (49.0 mg, 2%). R_f: 0.27 (PE/EtOAc 4:1). ^{1}H NMR (600 MHz, DMSO-d_6) δ 6.79 (t, *J* = 8.0 Hz, 1H, H5), 6.26 (dd, *J* = 8.3, 0.9 Hz, 1H, H4), 6.21 (dd, *J* = 7.8, 0.9 Hz, 1H, H6), 3.70 (s, 3H, 7-OMe), 2.11 (s, 3H, 2-Me). ^{13}C NMR (151 MHz, DMSO-d_6) δ 206.2 (C2), 153.5 (C7), 147.4 (C3a), 126.2 (C5), 111.1 (C7a), 102.8 (C6), 101.5 (C4), 55.3 (7-OMe), 30.9 (2-Me). HPLC-MS (ESI): m/z calculated for C_9H_9NOS 179.04; $[M+H]^+$ found 180.00.

7-Methoxy-2,3-dimethylbenzo[d]thiazol-3-ium iodide (29b)

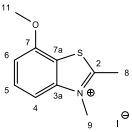

The synthesis was carried out according to general procedure H (39.0 mg, 52%). R_f: 38 (DCM/MeOH 9:1). ^{1}H NMR (600 MHz, DMSO-d_6) δ 7.88 (s, 2H, H4-H5), 7.41 (s, 1H, H6), 4.20 (s, 3H, N-Me), 4.07 (s, 3H,

7-OMe), 3.20 (s, 3H, 2-Me). ^{13}C NMR (151 MHz, DMSO-d_6) δ 176.9 (C2), 153.8 (C7), 142.9 (C3a), 131.4 (C5), 117.0 (C4), 109.1 (C6), 109.1 (C7a), 57.0 (7-OMe), 36.9 (N-Me), 17.6 (2-Me). HPLC-MS (ESI): m/z calculated for $C_{10}H_{12}NOS^+$ 194.06; $[M]^+$ found 194.10.

N-(2-bromo-3-fluorophenyl)acetamide (30.1)

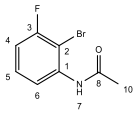

To a solution of 2-bromo-3-fluoroaniline (1.55 g, 8.16 mmol) in acetic anhydride (38.5 mL) was added pyridine (6.5 mL, 81.6 mmol). The mixture was stirred at room temperature for 3 h. It was poured into water and extracted with EtOAc. The organic phase was dried over $MgSO_4$, evaporated and used without any further purification (1.75 g, 93%). R_f: 0.18 (PE/EtOAc 4:1). ^{1}H NMR (600 MHz, DMSO-d_6) δ 9.58 (s, 1H, H7), 7.47 (dt, J = 8.1, 1.3 Hz, 1H, H6), 7.39 (td, J = 8.2, 6.2 Hz, 1H, H5), 7.18 (td, J = 8.5, 1.5 Hz, 1H, H4), 2.10 (s, 3H, H10). ^{13}C NMR (151 MHz, DMSO-d_6) δ 168.7 (C8), 158.8 (d, $J_{C\text{-}F}$ = 243.7 Hz, C3), 138.5 (C1), 128.7 (d, $J_{C\text{-}F}$ = 9.2 Hz, C5), 122.4 (C6), 112.7 (d, $J_{C\text{-}F}$ = 22.2 Hz, C4), 105.0 (d, $J_{C\text{-}F}$ = 24.1 Hz, C2), 23.3 (C10). HPLC-MS (ESI): m/z calculated for C_8H_7BrFNO 230.97; $[M+H]^+$ found 232.05, 234.00.

N-(2-bromo-3-fluorophenyl)ethanethioamide (30.2)

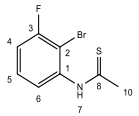

To a solution of **30.1** (1.40 g, 6.03 mmol) in THF (12 mL), Lawesson's reagent (1.71 g, 4.22 mmol) was added under argon atmosphere. The mixture was stirred overnight at room temperature and the precipitate was filtered. The filtrate was collected and further purified by flash

chromatography (PE/EtOAc 5% to 80% B) to afford the product as an orange oil (1.04 g, 69%). R_f: 0.72 (PE/EtOAc 1:1). ^{1}H NMR (600 MHz, DMSO-d_6) δ 11.54 (s, 1H, H7), 7.47 (td, J = 8.2, 6.1 Hz, 1H, H5), 7.35 (td, J = 8.5, 1.4 Hz, 1H, H4), 7.25 (dt, J = 8.0, 1.4 Hz, 1H, H4), 2.62 (s, 3H, H10). ^{13}C NMR (151 MHz, DMSO-d_6) δ 202.4 (C8), 159.1 (d, $J_{C\text{-}F}$ = 244.9 Hz, C3), 140.5 (d, $J_{C\text{-}F}$ = 1.9 Hz, C1), 129.1 (d, $J_{C\text{-}F}$ = 9.3 Hz, C5), 125.7 (d, $J_{C\text{-}F}$ = 3.1 Hz,C6), 115.3 (d, $J_{C\text{-}F}$ = 22.4 Hz,C4), 108.5 (d, $J_{C\text{-}F}$ = 21.4 Hz, C2), 33.2 (C10). HPLC-MS (ESI): m/z calculated for C_8H_7BrFNS 246.95; $[M+H]^+$ found 247.95, 249.90.

7-Fluoro-2-methylbenzo[d]thiazole (30a)

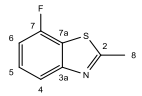

To a solution of **30.2** (810 mg, 3.26 mmol) in 1,4-dioxane (12 mL), Cs_2CO_3 (1.60 g, 4.90 mmol) and $Pd(PPh_3)_4$ (189 mg, 0.16 mmol) were added under argon atmosphere. The mixture was stirred overnight at 80 °C. It was diluted with water and extracted with EtOAc. The organic phase was dried over $MgSO_4$, evaporated under reduced pressure, and purified by flash chromatography (PE/EtOAc 1% to 15% B) to afford the product (314 mg, 58%). R_f: 0.53 (PE/EtOAc 3:1). ^{1}H NMR (600 MHz, DMSO-d_6) δ 7.78 (d, J = 8.1 Hz, 1H, H4), 7.51 (td, J = 8.1, 5.7 Hz, 1H, H5), 7.29 (ddd, J = 9.4, 8.2, 1.1 Hz, 1H, H6), 2.83 (s, 3H, 2-Me).^{13}C NMR (151 MHz, DMSO-d_6) δ 168.0 (C2), 156.2 (d, $J_{C\text{-}F}$ = 246.6 Hz, C7), 155.9 (d, $J_{C\text{-}F}$ = 2.6 Hz, C3a), 127.4 (d, $J_{C\text{-}F}$ = 7.6 Hz, C5), 121.9 (d, $J_{C\text{-}F}$ = 16.7 Hz, C7a), 118.3 (d, $J_{C\text{-}F}$ = 3.4 Hz, C4), 110.4 (d, $J_{C\text{-}F}$ = 18.7 Hz, C6), 19.7 (2-Me). HPLC-MS (ESI): m/z calculated for C_8H_6FNS 167.02; $[M+H]^+$ found 168.00.

7-Fluoro-2,3-dimethylbenzo[d]thiazol-3-ium iodide (30b)

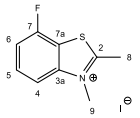

The synthesis was carried out according to general procedure H (47.0 mg, 25%). R_f: 0.19 (DCM/MeOH 9:1). ^{1}H NMR (600 MHz, DMSO-d_6) δ 8.21 (d, J = 8.5 Hz, 1H, H4), 7.97 (q, J = 7.5 Hz, 1H, H5), 7.78 (t, J = 8.9 Hz, 1H, H6), 4.24 (s, 3H, N-Me), 3.23 (s, 3H, 2-Me). ^{13}C NMR (151 MHz, DMSO-d_6) δ 178.4 (C2), 155.8 (d, J = 250.7 Hz, C7), 143.9 (d, J = 5.6 Hz, C3a), 131.5 (d, $J_{C\text{-}F}$ = 8.1 Hz, C5), 116.4 (d, $J_{C\text{-}F}$ = 23.4 Hz, C7a), 114.1 (d, $J_{C\text{-}F}$ = 17.8 Hz, C6), 113.6 (d, $J_{C\text{-}F}$ = 3.5 Hz, C4), 37.1 (N-Me), 17.6 (2-Me). HPLC-MS (ESI): m/z calculated for $C_9H_9FNS^+$ 182.04; $[M]^+$ found 182.10.

2-Methylbenzo[d]thiazole (31a)

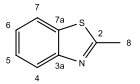

p-Toluenesulfonic acid (402 mg, 2.34 mmol) was added to a mixture of 2-aminobenzenethiol (5.00 mL, 46.7 mmol) and 2,4-pentanedione (7.20 mL, 70.1 mmol) and stirred overnight. The mixture was diluted with water and extracted with EtOAc. The organic phase was dried over $MgSO_4$, evaporated under reduced pressure, and purified by flash chromatography (Hept/EtOAc 0% to 20% B) to afford the product as an orange oil (5.74 g, 82%). R_f: 0.23 (Hept/EtOAc 5:1). ^{1}H NMR (400 MHz, DMSO-d_6) δ 8.02 (dt, J = 8.0, 1.0 Hz, 1H, H7), 7.91 (dt, J = 8.2, 0.9 Hz, 1H, H4), 7.47 (ddd, J = 8.2, 7.2, 1.4 Hz, 1H, H5), 7.38 (ddd, J = 8.3, 7.3, 1.3 Hz, 1H, H6), 2.79 (s, 3H, 2-Me). ^{13}C NMR (101 MHz, DMSO-d_6) δ 166.8 (C2), 153.0 (C3a), 135.2 (C7a), 125.9 (C7), 124.7 (C4), 121.9 (C5-C6), 19.7 (2-Me). HPLC-MS (ESI): m/z calculated for C_8H_7NS 149.03; $[M+H]^+$ found 150.06.

2,3-Dimethylbenzo[d]thiazol-3-ium iodide (31b)

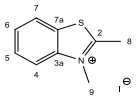

The synthesis was carried out according to general procedure H to afford a pink solid (1.21 g, 50%). R_f: 0.18 (DCM/MeOH 9:1). ^{1}H NMR (400 MHz, DMSO-d_6) δ 8.44 (dd, *J* = 8.1, 1.2 Hz, 1H, H4), 8.29 (d, *J* = 8.4 Hz, 1H, H7), 7.90 (ddd, *J* = 8.5, 7.3, 1.3 Hz, 1H, H5), 7.81 (ddd, *J* = 8.3, 7.2, 1.1 Hz, 1H, H6), 4.21 (s, 3H, N-Me), 3.18 (s, 3H, 2-Me). ^{13}C NMR (101 MHz, DMSO-d_6) δ 177.2 (C2), 141.6 (C3a), 129.2 (C7), 128.7 (C7a), 128.0 (C6), 124.5 (C5), 116.7 (C4), 36.2 (N-Me), 17.1 (2-Me). HPLC-MS (ESI): m/z calculated for $C_9H_{10}NS^+$ 164.05; $[M]^+$ found 164.35.

General procedure I

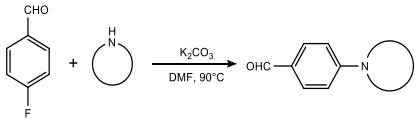

A mixture of 4-fluorobenzaldehyde (46.6 mmol) and the selected secondary amine (39.6 mmol) was diluted with DMF (25.0 mL). K_2CO_3 (58.3 mmol) was added and the reaction was stirred overnight at 90 °C. The mixture was diluted with water and extracted with EtOAc. The organic phase was dried over $MgSO_4$, evaporated under reduced pressure, and purified by flash chromatography (Hept/EtOAc).

4-(Piperidin-1-yl)benzaldehyde (32)

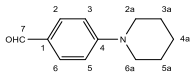

The synthesis was carried out according to general procedure I to afford a white solid (6.45 g, 86%). R_f: 0.18 (Hept/EtOAc 5:1). ^{1}H NMR (400 MHz, DMSO-d_6) δ 9.68 (s, 1H, H7), 7.67 (dt, *J* = 9.8, 2.9 Hz, 2H,

H2-H6), 7.00 (dt, *J* = 9.0, 2.7 Hz, 2H, H3-H5), 3.41 (dd, *J* = 6.6, 3.9 Hz, 4H, H2a-H6a), 1.64 – 1.52 (m, 6H, H3a-H4a-H5a). ^{13}C NMR (101 MHz, DMSO-d_6) δ 189.9 (C7), 154.6 (C4), 131.6 (C2-C6), 125.4 (C1), 113.0 (C3-C5), 47.6 (C2a-C6a), 24.8 (C3a-C5a), 23.9 (C4a). HPLC-MS (ESI): m/z calculated for $C_{12}H_{15}NO$ 189.12; $[M+H]^+$ found 190.13.

4-Morpholinobenzaldehyde (33)

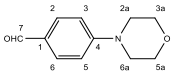

The synthesis was carried out according to general procedure I (1.77 g, 58%). R_f: 0.19 (Hept/EtOAc 3:1). ^{1}H NMR (600 MHz, DMSO-d_6) δ 9.74 (s, 1H, H7), 7.73 (dt, *J* = 9.0, 2.8 Hz, 2H, H2-H6), 7.06 (dt, *J* = 8.9, 2.6 Hz, 2H, H3-H5), 3.78 – 3.69 (m, 4H, H3a-H5a), 3.38 – 3.32 (m, 4H, H2a-H6a). ^{13}C NMR (151 MHz, DMSO-d_6) δ 190.4 (C7), 154.9 (C4), 131.4 (C2-C6), 126.7 (C1), 113.2 (C3-C5), 65.8 (C3a-C5a), 46.6 (C2a-C6a). HPLC-MS (ESI): m/z calculated for $C_{11}H_{13}NO_2$ 191.09; $[M+H]^+$ found 192.10.

4-Thiomorpholinobenzaldehyde (34)

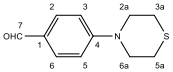

The synthesis was carried out according to general procedure I (73.5 mg, 11%). R_f: 0.22 (Hept/EtOAc 5:1). ^{1}H NMR (600 MHz, DMSO-d_6) δ 9.70 (s, 1H, H7), 7.71 (dd, *J* = 9.0, 2.8 Hz, 2H, H2-H6), 7.13 – 6.89 (m, 2H, H3-H5), 3.93 – 3.69 (m, 4H, H2a-H6a), 2.75 – 2.55 (m, 4H, H3a-H5a). ^{13}C NMR (151 MHz, DMSO-d_6) δ 190.1 (C7), 153.3 (C4), 131.7 (C2-C6), 125.8 (C1), 113.4 (C3-C5), 49.4 (C2a-C6a), 24.8 (C3a-C5a). HPLC-MS (ESI): m/z calculated for $C_{11}H_{13}NOS$ 207.07; $[M+H]^+$ found 208.09.

4-(Pyrrolidin-1-yl)benzaldehyde (35)

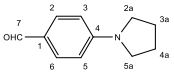

The synthesis was carried out according to general procedure I (381 mg, 46%). R_f: 0.37 (Hept/EtOAc 3:1). ^{1}H NMR (400 MHz, DMSO-d_6) δ 9.64 (s, 1H, H7), 7.67 (dt, J = 8.8, 2.7 Hz, 2H, H2-H6), 6.63 (dt, J = 8.8, 2.6 Hz, 2H, H3-H5), 3.38 – 3.30 (m, 4H, H2a-H5a), 1.98 – 1.93 (m, 4H, H3a-H4a).^{13}C 1NMR (101 MHz, DMSO-d_6) δ 189.6 (C7), 151.6 (C4), 131.7 (C2-C6), 124.2 (C1), 111.2 (C3-C5), 47.3 (C2a-C5a), 24.9 (C3a-C4a). HPLC-MS (ESI): m/z calculated for $C_{11}H_{13}NO$ 175.10; $[M+H]^+$ found 176.11.

4-(4-Fluoropiperidin-1-yl)benzaldehyde (36)

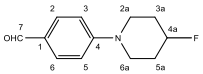

The synthesis was carried out according to general procedure I (293 mg, 59%). R_f: 0.21 (Hept/EtOAc 3:1). ^{1}H NMR (400 MHz, DMSO-d_6) δ 9.71 (s, 1H, H7), 7.70 (dt, J = 8.9, 2.5 Hz, 2H, H2-H6), 7.07 (dt, J = 8.9, 2.5 Hz, 2H, H3-H5), 4.90 (dtt, J = 48.9, 7.1, 3.6 Hz, 1H, H4a), 3.71 – 3.55 (m, 2H, H2a-H6a), 3.41 (ddd, J = 13.5, 7.4, 3.9 Hz, 2H, H2a-H6a), 1.94 (dddd, J = 24.9, 12.0, 8.1, 3.8 Hz, 2H, H3a-H5a), 1.84 – 1.62 (m, 2H, H3a-H5a). ^{13}C NMR (101 MHz, DMSO-d6) δ 190.6 (C7), 154.5 (C4), 132.1 (C2-C6), 126.5 (C1), 113.8 (C3-C5), 88.8 (d, $J_{C\text{-}F}$ = 169.5 Hz, C4a), 43.7 (d, $J_{C\text{-}F}$ = 6.6 Hz, C2a-C6a), 30.8 (d, $J_{C\text{-}F}$ = 19.3 Hz, C3a-C5a). ^{19}F NMR (376 MHz, DMSO-d_6) δ -177.3. HPLC-MS (ESI): m/z calculated for $C_{12}H_{14}FNO$ 207.11; $[M+H]^+$ found 208.11.

4-(Dimethylamino)benzaldehyde (37)

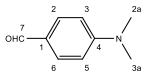

The synthesis was carried out according to general procedure I (346 mg, 41%). R_f: 0.33 (Hept/EtOAc 3:1). ^{1}H NMR (400 MHz, DMSO-d_6) δ 9.67 (s, 1H, H7), 7.68 (dt, J = 9.1, 2.7 Hz, 2H, H2-H6), 6.79 (dt, J = 8.9, 2.8 Hz, 2H, H3-H5), 3.04 (s, 6H, H2a-H3a). ^{13}C NMR (101 MHz, DMSO-d_6) δ 190.3 (C7), 154.7 (C4), 132.0 (C2-C6), 125.0 (C1), 111.5 (C3-C5), 40.1 (C2a-C3a). HPLC-MS (ESI): m/z calculated for $C_9H_{11}NO$ 149.08; $[M+H]^+$ found 150.09.

4-(4-Methylpiperazin-1-yl)benzaldehyde (38)

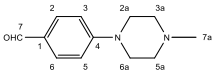

The synthesis was carried out according to general procedure I (408 mg, 50%). R_f: 0.08 (DCM/MeOH 2%). ^{1}H NMR (400 MHz, DMSO-d_6) δ 9.71 (s, 1H, H7), 7.70 (dt, J = 9.0, 2.8 Hz, 2H, H2-H6), 7.04 (dt, J = 9.0, 2.5 Hz, 2H, H3-H5), 3.37 (dd, J = 6.4, 3.8 Hz, 4H, H2a-H6a), 2.42 (dd, J = 6.6, 3.6 Hz, 4H, H3a-H5a), 2.21 (s, 3H, H7a). ^{13}C NMR (101 MHz, DMSO-d_6) δ 190.2 (C7), 154.7 (C4), 131.4 (C2-C6), 126.2 (C1), 113.3 (C3-C5), 54.2 (C3a-C5a), 46.3 (C2a-C6a), 45.7 (C7a). HPLC-MS (ESI): m/z calculated for $C_{12}H_{16}N_2O$ 204.13; $[M+H]^+$ found 205.14.

2-(4-Bromophenyl)benzo[d]thiazole (39)

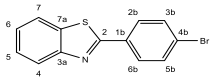

A solution of 2-aminobenzenethiol (750 mg, 5.99 mmol) and 4-bromobenzaldehyde (1.11 g, 5.99 mmol) in DMSO (6.00 mL) was heated at 140 °C for 75 min. The mixture was diluted with water and extracted with EtOAc. The organic phase was dried over $MgSO_4$, evaporated under reduced pressure, and recrystallized from Et_2O to afford the product as a white solid (569 mg, 33%). R_f: 0.70 (PE/EtOAc 5:1). ^{1}H NMR (600 MHz, DMSO-d_6) δ 8.16 (dt, J = 8.2, 0.8 Hz, 1H, H4),

8.07 (dt, *J* = 8.0, 0.8 Hz, 1H, H7), 8.03 (dt, *J* = 8.5, 2.5 Hz, 2H, H3b-H5b), 7.77 (dt, *J* = 8.5, 2.5 Hz, 2H, H2b-H6b), 7.56 (ddd, *J* = 8.2, 7.2, 1.3 Hz, 1H, H5), 7.48 (ddd, *J* = 8.2, 7.2, 1.2 Hz, 1H, H6). ^{13}C NMR (151 MHz, DMSO-d_6) δ 166.1 (C2), 153.5 (C3a), 134.5 (C7a), 132.4 (C3b-C5b), 132.0 (C1b), 129.0 (C2b-C6b), 126.8 (C4), 125.8 (C7), 124.9 (C4b), 123.0 (C5), 122.4 (C6). HPLC-MS (ESI): m/z calculated for $C_{13}H_8BrNS$ 288.96; $[M+H]^+$ found 289.95, 291.90.

3-(4-(Piperidin-1-yl)phenyl)acrylaldehyde (40)

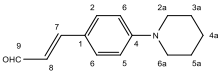

A solution of **32** (800 mg, 4.23 mmol) in H_2SO_4 96% (3 mL) was cooled to 0 °C and acetaldehyde (0.71 mL, 12.7 mmol) was added dropwise. The mixture was stirred for 1 h at 0 °C. It was poured into water, neutralized with NaOH aq 18 M and extracted with EtOAc. The organic phase was dried over $MgSO_4$, evaporated under reduced pressure, and purified by flash chromatography (PE/EtOAc 5% to 10% B) to afford the product (390 mg, 43%). R_f: 0.51 (PE/EtOAc 3:1). ^{1}H NMR (600 MHz, DMSO-d_6) δ 9.54 (d, *J* = 7.9 Hz, 1H, H9), 7.59 – 7.52 (m, 3H, H2-H6-H7), 6.95 (dt, *J* = 8.9, 3.1 Hz, 2H, H3-H5), 6.60 (dd, *J* = 15.6, 7.9 Hz, 1H, H8), 3.34 (d, *J* = 5.4 Hz, 4H, H2a-H6a), 1.60 – 1.56 (m, 6H, H3a-H4a-H5a). ^{13}C NMR (151 MHz, DMSO-d6) δ 193.7 (C9), 153.9 (C7), 152.9 (C4), 130.6 (C2-C6), 124.0 (C8), 122.7 (C1), 114.1 (C3-C5), 47.9 (C2a-C6a), 24.9 (C3a-C5a), 24.0 (C4a). HPLC-MS (ESI): m/z calculated for $C_{14}H_{17}NO$ 215.13; $[M+H]^+$ found 216.15.

3-(4-(Pyrrolidin-1-yl)phenyl)acrylaldehyde (41)

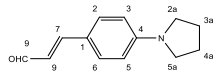

The synthesis was carried out following the same procedure as **40** (513 mg, 64%). R_f: 0.32 (PE/EtOAc 4:1). ^{1}H NMR (600 MHz, DMSO-d_6) δ

9.51 (d, *J* = 8.0 Hz, 1H, H9), 7.58 – 7.51 (m, 3H, H2-H6-H7), 6.59 – 6.53 (m, 3H, H3-H5-H8), 3.32 – 3.28 (m, 4H, H2a-H5a), 2.00 – 1.92 (m, 4H, H3a-H4a). ^{13}C NMR (151 MHz, DMSO-d_6) δ 193.3 (C9), 154.5 (C7), 149.7 (C4), 130.8 (C2-C6), 122.7 (C8), 120.8 (C1), 111.7 (C3-C5), 47.3 (C2a-C5a), 24.9 (C3a-C4a). HPLC-MS (ESI): m/z calculated for $C_{13}H_{15}NO$ 201.12; $[M+H]^+$ found 202.20.

General procedure J

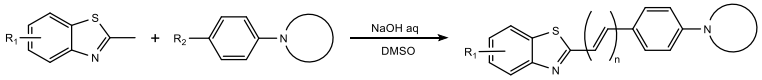

To a solution of the selected 2-methylbenzothiazole (6.70 mmol) and the selected 4-aminobenzaldehyde or 4-aminocinnamaldehyde (7.37 mmol) in DMSO (6.50 mL), NaOH aq. 18 M (6.50 mL) was slowly added. The mixture was stirred at room temperature for 2 h to 24 h. A yellow precipitate was formed. The mixture was diluted with water and complete precipitation was allowed. The precipitate was filtered under vacuum to afford a yellow solid which was recrystallized from EtOAc.

General procedure K

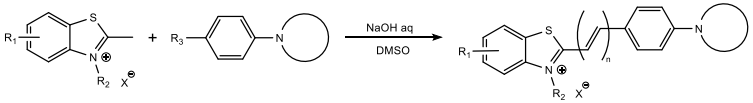

According to the literature procedure, [172] a solution of the selected 2,3-dimethylbenzothiazolium salt (0.86 mmol) and the selected 4-aminobenzaldehyde or 4-aminocinnamaldehyde (1.83 mmol) in EtOH (7.00 mL) was refluxed overnight. The color turned to red/purple. The precipitate was filtered under vacuum and washed with EtOAc to afford a dark solid which was recrystallized from EtOH and/or Et_2O.

4-Methyl-2-(4-(piperidin-1-yl)styryl)benzo[d]thiazole (42a)

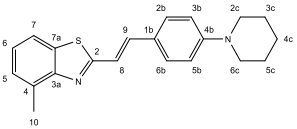

The synthesis was carried out according to general procedure J (46 mg, 60%). R_f: 0.48 (Hept/EtOAc 3:1). ^{1}H NMR (600 MHz, $CDCl_3$) δ 7.69 – 7.63 (m, 1H, H5), 7.47 (d, *J* = 8.8 Hz, 2H, H2b-H6b), 7.39 (d, *J* = 16.1 Hz, 1H, H9), 7.30 (d, *J* = 16.1 Hz, 1H, H8), 7.25 – 7.20 (m, 2H, H6-H7), 6.91 (d, *J* = 8.7 Hz, 2H, H3b-H5b), 3.28 (t, *J* = 5.6 Hz, 4H, H2c-H6c), 2.75 (s, 3H, 4-Me), 1.70 (p, *J* = 5.6 Hz, 4H, H3c-H5c), 1.66 – 1.60 (m, 2H, H4c). ^{13}C NMR (151 MHz, $CDCl_3$) δ 167.1 (C2), 153.5 (C3a), 152.6 (C4b), 137.9 (C9), 134.1 (C4), 132.7 (C7), 128.8 (C2b-C6b), 126.8 (C5), 125.6 (C8), 125.0 (C6), 119.0 (C7), 118.9 (C1b), 115.5 (C3b-C5b), 49.6 (C2c-C6c), 25.7 (C3c-C5c), 24.5 (C4c), 18.7 (4-Me). HPLC-MS (ESI): m/z calculated for $C_{21}H_{22}N_2S$ 334.15; $[M+H]^+$ found 335.25.

3,4-Dimethyl-2-(4-(piperidin-1-yl)styryl)benzo[d]thiazol-3-ium 4-nitrobenzenesulfonate (42b)

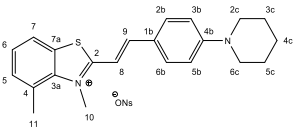

The synthesis was carried out according to general procedure K (119 mg, 59%). R_f: 0.19 (DCM/MeOH 5%). ^{1}H NMR (400 MHz, DMSO-d_6) δ 8.19 (d, *J* = 8.3 Hz, 2H, Ns), 8.12 (br s, 1H, H5), 8.01 (d, *J* = 15.3 Hz, 1H, H8), 7.89 (d, *J* = 8.5 Hz, 2H, H2b-H6b), 7.83 (d, *J* = 8.2 Hz, 2H, Ns), 7.66 (d, *J* = 15.3 Hz, 1H, H9), 7.54 (br s, 2H, H6-H7), 7.04 (d, *J* = 8.7 Hz, 2H, H3b-H5b), 4.43 (s, 3H, N-Me), 3.49 (s, 4H, H2c-H6c), 2.91 (s, 3H, 4-Me), 1.61 (s, 6H, H3c-H4c-H5c). ^{13}C NMR (101 MHz, DMSO-d_6) δ 171.5 (C2), 154.4 (C3a), 153.5 (C4b), 149.6 (Ns), 147.2 (Ns),

140.9 (C9), 132.8 (C2b-C6b), 132.7 (C7a), 127.7 (C5), 127.7 (C4), 127.3 (C7), 126.9 (Ns), 123.3 (Ns), 122.3 (C1b), 121.7 (C6), 113.5 (C3b-C5b), 107.0 (C8), 47.6 (C2c-C6c), 40.0 (N-Me), 25.0 (C3c-C5c), 23.9 (C4c), 20.9 (4-Me). HPLC-MS (ESI): m/z calculated for $C_{22}H_{25}N_2S^+$ 349.17; $[M]^+$ found 349.16.

4-Methoxy-2-(4-(piperidin-1-yl)styryl)benzo[d]thiazole (43a)

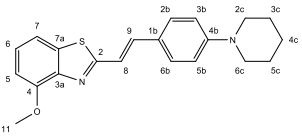

The synthesis was carried out according to general procedure J (10 mg, 5%). R_f: 0.18 (Hept/EtOAc 3:1). ^{1}H NMR (600 MHz, $CDCl_3$) δ 7.45 (dt, *J* = 8.7, 2.9 Hz, 2H, H2b-H6b), 7.41 (dd, *J* = 8.0, 0.9 Hz, 1H, H5), 7.38 (d, *J* = 16.1 Hz, 1H, H9), 7.31 (d, *J* = 16.1 Hz, 1H, H8), 7.28 (t, *J* = 8.0 Hz, 1H, H6), 6.91 (dd, *J* = 8.8, 2.7 Hz, 2H, H3b-H5b), 6.88 (dd, *J* = 8.0, 0.9 Hz, 1H, H7), 4.05 (s, 3H, 4-OMe), 3.27 (t, *J* = 5.6 Hz, 4H, H2c-H6c), 1.70 (p, *J* = 5.6 Hz, 4H, H3c-H5c), 1.65 – 1.60 (m, 2H, H4c). ^{13}C NMR (151 MHz, $CDCl_3$) δ 166.9 (C2), 153.3 (C4), 152.6 (C4b), 144.2 (C3a), 137.7 (C9), 135.8 (C7a), 128.8 (C2b-C6b), 126.0 (C6), 125.6 (C8), 119.0 (C1b), 115.5 (C3b-C5b), 113.6 (C7), 106.7 (C5), 56.0 (4-OMe), 49.6 (C2c-C6c), 25.7 (C3c-C5c), 24.5 (C4c). HPLC-MS (ESI): m/z calculated for $C_{21}H_{22}N_2OS$ 350.15; $[M+H]^+$ found 351.13.

4-Methoxy-3-methyl-2-(4-(piperidin-1-yl)styryl)benzo[d]thiazol-3-ium iodide (43b)

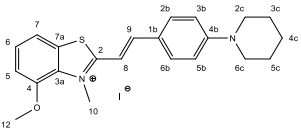

The synthesis was carried out according to general procedure K (46 mg, quant.). R_f: 0.24 (DCM/MeOH 5%). ^{1}H NMR (600 MHz, DMSO-d_6)

δ 7.97 (d, *J* = 15.3 Hz, 1H, H8), 7.87 (d, *J* = 8.6 Hz, 2H, H2b-H6b), 7.83 (d, *J* = 8.1 Hz, 1H, H5), 7.66 – 7.52 (m, 2H, H6-H9), 7.37 (d, *J* = 8.2 Hz, 1H, H7), 7.04 (d, *J* = 8.6 Hz, 2H, H3b-H5b), 4.43 (s, 3H, N-Me), 4.04 (s, 3H, 4-OMe), 3.49 (t, *J* = 5.3 Hz, 4H, H2c-H6c), 1.77 – 1.51 (m, 6H, H3c-H4c-H5c). ^{13}C NMR (151 MHz, DMSO-*d*$_6$) δ 170.7 (C2), 153.5 (C4b), 149.7 (C4), 149.3 (C9), 132.7 (C2b-C6b), 131.1 (C3a), 128.7 (C7a), 128.6 (C6), 122.3 (C1b), 115.5 (C7), 113.5 (C3b-C5b), 111.7 (C5), 106.9 (C8), 56.9 (4-OMe), 47.5 (Cc2c-C6c), 39.3 (N-Me), 25.1 (C3c-C5c), 23.9 (C4c). HPLC-MS (ESI): m/z calculated for $C_{22}H_{25}N_2OS^+$ 365.17; $[M]^+$ found 365.25.

4-Fluoro-2-(4-(piperidin-1-yl)styryl)benzo[d]thiazole (44a)

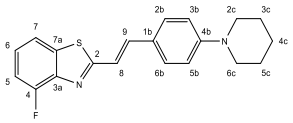

The synthesis was carried out according to general procedure J (187 mg, 56%). R_f: 0.43 (Hept/EtOAc 3:1). ^{1}H NMR (400 MHz, $CDCl_3$) δ 7.58 (dd, *J* = 8.0, 1.0 Hz, 1H, H7), 7.51 – 7.40 (m, 3H, H2b-H6b-H9), 7.30 – 7.24 (m, 2H, H6-H8), 7.14 (ddd, *J* = 10.5, 8.2, 1.0 Hz, 1H, H5), 6.91 (dt, *J* = 8.8, 8.8, 2.7 Hz, 1H, H3b-H5b), 3.34 – 3.22 (m, 4H, H2c-H6c), 1.76 – 1.66 (m, 4H, H3c-H5c), 1.66 – 1.59 (m, 2H, H4c). ^{13}C NMR (101 MHz, $CDCl_3$) δ 168.7 (C2), 155.6 (d, $J_{C\text{-}F}$ = 255.6 Hz, C4), 152.7 (C4b), 143.0 (d, $J_{C\text{-}F}$ = 13.4 Hz, C3a), 139.1 (C9), 136.9 (d, $J_{C\text{-}F}$ = 3.6 Hz, C7a), 129.0 (C2b-C6b), 125.6 (d, $J_{C\text{-}F}$ = 7.0 Hz, C6), 125.1 (C8), 118.1 (C1b), 117.2 (d, $J_{C\text{-}F}$ = 4.3 Hz, C7), 115.3 (C3b-C5b), 112.0 (d, $J_{C\text{-}F}$ = 18.0 Hz, C5), 49.4 (C2c-C6c), 25.6 (C3c-C5c), 24.5 (C4c). ^{19}F NMR (376 MHz, $CDCl_3$) δ -122.8. HPLC-MS (ESI): m/z calculated for $C_{20}H_{19}FN_2S$ 338.13; $[M+H]^+$ found 339.10.

4-Fluoro-3-methyl-2-(4-(piperidin-1-yl)styryl)benzo[d]thiazol-3-ium 4-nitrobenzenesulfonate (44b)

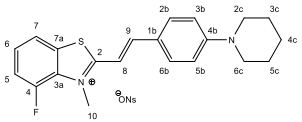

The synthesis was carried out according to general procedure K (165 mg, 76%). R_f: 0.12 (DCM/MeOH 5%). ^{1}H NMR (400 MHz, DMSO-d_6) δ 8.19 (d, J = 8.3 Hz, 2H, Ns), 8.14 – 8.09 (m, 1H, H5), 8.06 (d, J = 15.3 Hz, 1H, H8), 7.91 (d, J = 8.6 Hz, 2H, H2b-H6b), 7.83 (d, J = 8.4 Hz, 2H, Ns), 7.73 – 7.57 (m, 3H, H6-H7-H9), 7.04 (d, J = 8.7 Hz, 2H, H3b-H5b), 4.33 (d, J = 2.3 Hz, 3H, N-Me), 3.52 (t, J = 5.1 Hz, 4H, H2c-H6c), 1.79 – 1.49 (m, 6H, H3c-H4c-H5c). ^{13}C NMR (101 MHz, DMSO-d_6) δ 172.1 (C2), 154.4 (C4b), 153.7 (Ns), 151.0 (Ns), 150.5 (d, $J_{C\text{-}F}$ = 252.0 Hz, C4), 147.2 (C9), 133.3 (C2b-C6b), 130.5 (d, $J_{C\text{-}F}$ = 9.8 Hz, C3a), 129.3 (C7a), 128.3 (d, $J_{C\text{-}F}$ = 8.0 Hz, C6), 126.9 (Ns), 123.3 (Ns), 122.2 (C1b), 120.1 (d, $J_{C\text{-}F}$ = 4.0 Hz, C7), 115.9 (d, $J_{C\text{-}F}$ = 20.2 Hz, C5), 113.4 (C3b-C5b), 106.0 (C8), 47.5 (C2c-C6c), 38.3 (d, $J_{C\text{-}F}$ = 11.1 Hz, N-Me), 25.1 (C3c-C5c), 23.9 (C4c). ^{19}F NMR (376 MHz, DMSO-d_6) δ -125.2. HPLC-MS (ESI): m/z calculated for $C_{21}H_{22}FN_2S^+$ 353.15; $[M]^+$ found 353.13.

5-Methyl-2-(4-(piperidin-1-yl)styryl)benzo[d]thiazole (45a)

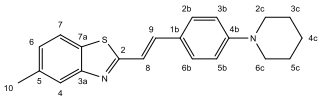

The synthesis was carried out according to general procedure J (100 mg, 43%). R_f: 0.44 (Hept/EtOAc 3:1). ^{1}H NMR (400 MHz, $CDCl_3$) δ 7.75 (s, 1H, H4), 7.69 (d, J = 8.1 Hz, 1H, H7), 7.46 (d, J = 8.6 Hz, 2H, H2b-H6b), 7.42 (d, J = 16.1 Hz, 1H, H9), 7.21 (d, J = 16.1 Hz, 1H, H8), 7.16 (dd, J = 8.1, 1.6 Hz, 1H, H6), 6.91 (d, J = 8.6 Hz, 2H, H3b-H5b), 3.28

(t, *J* = 5.5 Hz, 4H, H2c-H6c), 2.49 (s, 3H, 5-Me), 1.70 (p, *J* = 5.5 Hz, 4H, H3c-H5c), 1.64 (d, *J* = 5.8 Hz, 4H, H4c). ^{13}C NMR (101 MHz, $CDCl_3$) δ 168.3 (C2), 154.5 (C3a), 152.6 (C4b), 137.8 (C9), 136.3 (C5), 131.2 (C7a), 128.9 (C2b-C6b), 126.6 (C7), 125.5 (C8), 122.8 (C4), 121.0 (C6), 118.6 (C1b), 115.5 (C3b-C5b), 49.6 (C2c-C6c), 25.7 (C3c-C5c), 24.5 (C4c), 21.6 (C5-Me). HPLC-MS (ESI): m/z calculated for $C_{21}H_{22}N_2S$ 334.15; $[M+H]^+$ found 335.14.

3,5-Dimethyl-2-(4-(piperidin-1-yl)styryl)benzo[d]thiazol-3-ium iodide (45b)

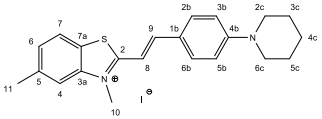

The synthesis was carried out according to general procedure K (278 mg, 99%). R_f: 0.21 (DCM/MeOH 5%). ^{1}H NMR (400 MHz, DMSO-d_6) δ 8.17 (d, *J* = 8.3 Hz, 1H, H7), 8.01 (d, *J* = 15.4 Hz, 1H, H8), 7.96 (br s, 1H, H4), 7.88 (d, *J* = 8.8 Hz, 2H, H2b-H6b), 7.63 (d, *J* = 15.4 Hz, 1H, H9), 7.53 (dd, *J* = 8.3, 1.5 Hz, 1H, H6), 7.04 (d, *J* = 8.8 Hz, 2H, H3b-H5b), 4.21 (s, 3H, N-Me), 3.49 (t, *J* = 5.2 Hz, 4H, H2c-H6c), 2.54 (s, 3H, 5-Me), 1.71 – 1.50 (m, 6H, H3c-H4c-H5c). ^{13}C NMR (101 MHz, DMSO-d_6) δ 171.3 (C2), 153.5 (C4b), 149.2 (C9), 142.2 (C5), 139.3 (C3a), 132.7 (C2b-C6b), 128.8 (C6), 123.9 (C7a), 123.3 (C7), 122.3 (C1b), 115.9 (C4), 113.4 (C3b-C5b), 107.0 (C8), 47.5 (C2c-C6c), 35.6 (N-Me), 25.1 (C3c-C5c), 23.9 (C4c), 21.1 (5-Me). HPLC-MS (ESI): m/z calculated for $C_{22}H_{25}N_2S^+$ 349.17; $[M]^+$ found 349.15.

5-Methoxy-2-(4-(piperidin-1-yl)styryl)benzo[d]thiazole (46a)

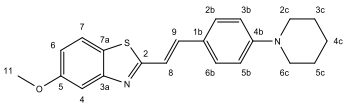

The synthesis was carried out according to general procedure J (170 mg, 58%). R_f: 0.29 (Hept/EtOAc 3:1). ^{1}H NMR (400 MHz, $CDCl_3$) δ 7.67 (d, *J* = 8.7 Hz, 1H, H7), 7.51 – 7.40 (m, 4H, H2b-H6b-H6-H9), 7.18 (d, *J* = 16.1 Hz, 1H, H8), 6.98 (dd, *J* = 8.7, 2.5 Hz, 1H, H6), 6.91 (dt, *J* = 8.8, 2.9 Hz, 2H, H3b-H5b), 3.89 (s, 3H, 5-OMe), 3.35 – 3.21 (m, 4H, H2c-H6c), 1.77 – 1.65 (m, 4H, H3c-H5c), 1.62 (ddd, *J* = 7.7, 5.9, 3.4 Hz, 2H, H4c). ^{13}C NMR (101 MHz, $CDCl_3$) δ 169.3 (C2), 159.2 (C5), 155.4 (C3a), 152.6 (C4b), 137.6 (C9), 128.9 (C2b-C6b), 126.2 (C7a), 125.5 (C8), 121.7 (C7), 118.3 (C1b), 115.4 (C3b-C5b), 115.0 (C6), 105.3 (C4), 55.7 (5-OMe), 49.5 (C2c-C6c), 25.7 (C3c-C5c), 24.5 (C4c). HPLC-MS (ESI): m/z calculated for $C_{21}H_{22}N_2OS$ 350.15; $[M+H]^+$ found 351.30.

5-Methoxy-3-methyl-2-(4-(piperidin-1-yl)styryl)benzo[d]thiazol-3-ium iodide (46b)

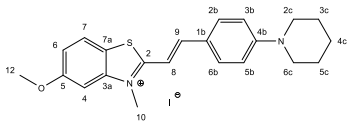

The synthesis was carried out according to general procedure K (222 mg, 97%). R_f: 0.19 (DCM/MeOH 5%). ^{1}H NMR (400 MHz, DMSO-d_6) δ 8.18 (d, *J* = 8.9 Hz, 1H, H7), 7.99 (d, *J* = 15.4 Hz, 1H, H8), 7.87 (d, *J* = 8.8 Hz, 2H, H2b-H6b), 7.63 (d, *J* = 2.3 Hz, 1H, H4), 7.62 (d, *J* = 15.4 Hz, 1H, H9), 7.32 (dd, *J* = 8.9, 2.3 Hz, 1H, H6), 7.04 (d, *J* = 8.8 Hz, 2H, H3b-H5b), 4.22 (s, 3H, N-Me), 3.94 (s, 3H, 5-Me), 3.48 (t, *J* = 5.2 Hz, 4H, H2c-H6c), 1.73 – 1.51 (m, 6H, H3c-H4c-H5c). ^{13}C NMR (101 MHz, DMSO-d_6) δ 171.9 (C2), 160.5 (C5), 153.4 (C4b), 148.6 (C3a), 143.4 (C9), 132.6 (C2b-C6b), 124.5 (C7a), 122.3 (C1b), 118.5 (C7), 116.6 (C6), 113.5 (C3b-H5b), 107.2 (C8), 99.9 (C4), 56.3 (5-OMe), 47.5 (C2c-C6c), 35.7 (N-Me), 25.0 (C3c-C5c), 23.9 (C4c). HPLC-MS (ESI): m/z calculated for $C_{22}H_{25}N_2OS^+$ 365.17; $[M]^+$ found 365.40.

5-Fluoro-2-(4-(piperidin-1-yl)styryl)benzo[d]thiazole (47a)

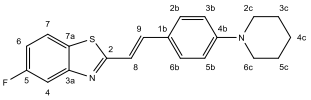

The synthesis was carried out according to general procedure J (402 mg, 99%). R_f: 0.45 (Hept/EtOAc 3:1). ^{1}H NMR (400 MHz, $CDCl_3$) δ 7.73 (dd, *J* = 8.8, 5.1 Hz, 1H, H7), 7.62 (dd, *J* = 9.6, 2.5 Hz, 1H, H4), 7.51 – 7.41 (m, 3H, H2b-H6b-H9), 7.19 (d, *J* = 16.1 Hz, 1H, H8), 7.09 (td, *J* = 8.8, 2.5 Hz, 1H, H6), 6.91 (dt, *J* = 8.9, 3.0 Hz, 2H, H3b-H5b), 3.35 – 3.23 (m, 4H, H2c-H6c), 1.78 – 1.66 (m, 4H, H3c-H5c), 1.66 – 1.58 (m, 2H, H4c). ^{13}C NMR (101 MHz, $CDCl_3$) δ 170.6 (C2), 162.1 (d, $J_{C\text{-}F}$ = 242.8 Hz, C5), 155.1 (d, $J_{C\text{-}F}$ = 12.1 Hz, C3a), 152.7 (C4b), 138.6 (C9), 129.7 (d, $J_{C\text{-}F}$ = 1.9 Hz, 7a), 129.1 (C2b-C6b), 125.1 (C8), 122.1 (d, $J_{C\text{-}F}$ = 9.9 Hz, C7), 118.0 (C1b), 115.3 (C3b-C5b), 113.4 (d, $J_{C\text{-}F}$ = 25.0 Hz, C6), 108.8 (d, $J_{C\text{-}F}$ = 23.6 Hz, C4), 49.4 (C2c-C6c), 25.7 (C3c-C5c), 24.5 (C4c). ^{19}F NMR (376 MHz, $CDCl_3$) δ -116.3. HPLC-MS (ESI): m/z calculated for $C_{20}H_{19}FN_2S$ 338.13; $[M+H]^+$ found 339.12.

5-Fluoro-3-methyl-2-(4-(piperidin-1-yl)styryl)benzo[d]thiazol-3-ium iodide (47b)

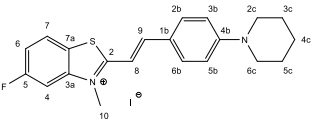

The synthesis was carried out according to general procedure K (175 mg, quant.). R_f: 0.19 (DCM/MeOH 5%). ^{1}H NMR (400 MHz, DMSO-d_6) δ 8.34 (dd, *J* = 9.0, 5.1 Hz, 1H, H7), 8.12 (dd, *J* = 9.7, 2.4 Hz, 1H, H4), 8.06 (d, *J* = 15.3 Hz, 1H, H8), 7.89 (d, *J* = 8.9 Hz, 2H, H2b-H6b), 7.64 – 7.55 (m, 2H, H6-H9), 7.04 (d, *J* = 8.9 Hz, 2H, H3b-H5b), 4.19 (s, 3H, N-Me), 3.51 (t, *J* = 5.2 Hz, 4H, H2c-H6c), 1.71 – 1.54 (m, 6H, H3c-H4c-H5c). ^{13}C NMR (101 MHz, DMSO-d_6) δ 173.7 (C2), 162.8 (d, $J_{C\text{-}F}$ =

245.4 Hz, C5), 154.2 (C4b), 150.5 (C9), 143.7 (d, $J_{C\text{-}F}$ = 12.6 Hz, C3a), 133.6 (C2b-C6b), 126.1 (d, $J_{C\text{-}F}$ = 10.0 Hz, C7a), 123.1 (d, $J_{C\text{-}F}$ = 2.1 Hz, C7), 122.7 (C1b), 116.1 (d, $J_{C\text{-}F}$ = 24.6 Hz, C6), 113.9 (C3b-C5b), 107.2 (C8), 104.0 (d, $J_{C\text{-}F}$ = 28.9 Hz, C4), 48.0 (C2c-C6c), 36.3 (N-Me), 25.6 (C3c-C5c), 24.4 (C4c). ^{19}F NMR (376 MHz, DMSO-d_6) δ -111.1. HPLC-MS (ESI): m/z calculated for $C_{21}H_{22}FN_2S^+$ 353.15; $[M]^+$ found 353.14.

6-Methyl-2-(4-(piperidin-1-yl)styryl)benzo[d]thiazole (48a)

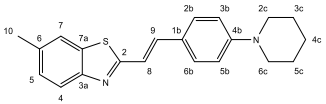

The synthesis was carried out according to general procedure J (132 mg, 26%). R_f: 0.31 (Hept/EtOAc 3:1). ^{1}H NMR (400 MHz, $CDCl_3$) δ 7.89 (d, J = 8.3 Hz, 1H, H4), 7.69 (d, J = 1.7 Hz, 1H, H7), 7.53 (dt, J = 8.8, 2.6 Hz, 1H, H2b-H6b), 7.47 (d, J = 16.1 Hz, 1H, H9), 7.35 – 7.28 (m, 2H, H5-H8), 6.99 (d, J = 8.4 Hz, 2H, H3b-H5b), 3.47 – 3.23 (m, 4H, 2c-H6c), 2.55 (s, 3H, 6-Me), 1.78 (p, J = 5.7 Hz, 4H, H3c-H5c), 1.73 – 1.62 (m, 3H, H4c). ^{13}C NMR (151 MHz, $CDCl_3$) δ 167.1 (C2), 152.6 (C3a), 152.2 (C4b), 137.6 (C9), 135.2 (C6), 134.5 (C7a), 128.8 (C2b-C6b), 127.8 (C7), 125.6 (C8), 122.2 (C5), 121.3 (C4), 118.6 (C1b), 115.5 (C3b-C5b), 49.6 (C2c-C6c), 25.7 (C3c-C5c), 24.5 (C4c), 21.7 (6-Me). HPLC-MS (ESI): m/z calculated for $C_{21}H_{22}N_2S$ 334.15; $[M+H]^+$ found 335.14.

3,6-Dimethyl-2-(4-(piperidin-1-yl)styryl)benzo[d]thiazol-3-ium iodide (48b)

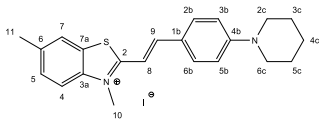

The synthesis was carried out according to general procedure K (273 mg, 97%). R_f: 0.27 (DCM/MeOH 5%). ^{1}H NMR (600 MHz, DMSO-d_6) δ 8.10 (s, 1H, H7), 8.01 (d, *J* = 15.3 Hz, 2H, H8), 8.00 (d, *J* = 8.6 Hz, 1H, H4), 7.87 (d, *J* = 8.8 Hz, 2H, H2b-H6b), 7.62 (d, *J* = 15.3 Hz, 1H, H9), 7.61 (dd, *J* = 8.6, 1.6 Hz, 1H, H5), 7.04 (d, *J* = 8.8 Hz, 2H, H3b-H5b), 4.22 (s, 3H, N-Me), 3.49 (t, *J* = 5.2 Hz, 4H, H2c-H6c), 2.51 (s, 1H, 6-Me), 1.70 – 1.62 (m, 2H, H4c), 1.62 – 1.56 (m, 4H, H3c-H5c). ^{13}C NMR (151 MHz, DMSO-d_6) δ 170.5 (C2), 153.5 (C4b), 149.1 (C9), 140.1 (C6), 137.9 (C3a), 132.7 (C2b-C6b), 130.1 (C7a), 126.9 (C5), 123.3 (C7), 122.3 (C1b), 115.7 (C4), 113.5 (C3b-C5b), 107.0 (C8), 47.5 (C2c-C6c), 35.6 (N-Me), 25.1 (C3c-C5c), 23.9 (C4c), 20.9 (6-Me). HPLC-MS (ESI): m/z calculated for $C_{22}H_{25}N_2S^+$ 349.17; $[M]^+$ found 349.16.

6-Methoxy-2-(4-(piperidin-1-yl)styryl)benzo[d]thiazole (49a)

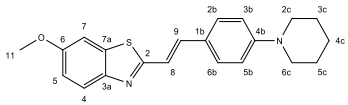

The synthesis was carried out according to general procedure J (95 mg, 19%). R_f: 0.22 (Hept/EtOAc 3:1). ^{1}H NMR (400 MHz, $CDCl_3$) δ 7.83 (d, *J* = 8.9 Hz, 1H, H4), 7.45 (d, *J* = 8.4 Hz, 2H, H2b-H6b), 7.34 (d, *J* = 16.1 Hz, 1H, H9), 7.29 (d, *J* = 2.6 Hz, 1H, H7), 7.19 (d, *J* = 16.1 Hz, 1H, H8), 7.04 (dd, *J* = 8.9, 2.6 Hz, 1H, H5), 6.91 (d, *J* = 8.4 Hz, 2H, H3b-H5b), 3.88 (s, 3H, 6-OMe), 3.27 (t, *J* = 5.4 Hz, 4H, H2c-H6c), 1.70 (p, *J* = 5.6 Hz, 4H, H3c-H5c), 1.62 (q, *J* = 6.5 Hz, 2H, H4c). ^{13}C NMR (151 MHz, $CDCl_3$) δ 165.8 (C2), 157.8 (C6), 152.5 (C4b), 148.7 (C3a), 137.1 (C9), 135.7 (C7a), 128.7 (C2b-C6b), 125.6 (C8), 123.2 (C4), 118.6 (C1b), 115.5 (C3b-C5b), 115.4 (C5), 104.4 (C7), 56.0 (6-OMe), 49.6 (C2c-C6c), 25.7 (C3c-C5c), 24.5 (C4c). HPLC-MS (ESI): m/z calculated for $C_{21}H_{22}N_2OS$ 350.15; $[M+H]^+$ found 351.14.

6-Methoxy-3-methyl-2-(4-(piperidin-1-yl)styryl)benzo[d]thiazol-3-ium iodide (49b)

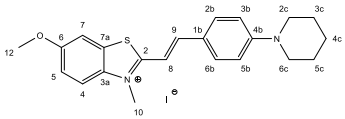

The synthesis was carried out according to general procedure K (89 mg, 32%). R_f: 0.18 (DCM/MeOH 5%). ^{1}H NMR (400 MHz, DMSO-d_6) δ 8.02 (d, J = 9.2 Hz, 1H, H4), 7.99 – 7.91 (m, 2H, H7-H8), 7.86 (d, J = 8.5 Hz, 2H, H2b-H6b), 7.60 (d, J = 15.4 Hz, 1H, H9), 7.38 (d, J = 9.2 Hz, 1H, H5), 7.03 (d, J = 8.6 Hz, 2H, H3b-H5b), 4.21 (s, 3H, N-Me), 3.90 (s, 3H, 6-OMe), 3.57 – 3.44 (m, 4H, H2c-H6c), 1.82 – 1.47 (m, 6H, H3c-H4c-H5c). ^{13}C NMR (101 MHz, DMSO-d_6) δ 169.2 (C2), 158.9 (C6), 153.4 (C4b), 148.3 (C9), 136.1 (C3a), 132.4 (C2b-C6b), 128.7 (C7a), 122.4 (C1b), 117.6 (C4), 117.0 (C5), 113.5 (C3b-C5b), 107.3 (C8), 106.7 (C7), 56.2 (6-OMe), 47.5 (C2c-C6c), 35.8 (N-Me), 25.0 (C3c-C5c), 23.9 (C4c). HPLC-MS (ESI): m/z calculated for $C_{22}H_{25}N_2OS^+$ 365.17; $[M]^+$ found 365.14.

6-Fluoro-2-(4-(piperidin-1-yl)styryl)benzo[d]thiazole (50a – PFSB)

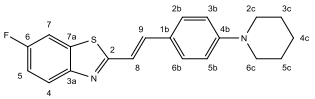

The synthesis was carried out according to general procedure J (34 mg, 24%). R_f: 0.38 (Hept/EtOAc 3:1). ^{1}H NMR (400 MHz, $CDCl_3$) δ 7.87 (dd, J = 8.9, 4.8 Hz, 1H, H4), 7.50 (dd, J = 8.2, 2.6 Hz, 1H, H7), 7.46 (d, J = 8.4 Hz, 2H, H2b-H6b), 7.39 (d, J = 16.1 Hz, 1H, H9), 7.23 – 7.12 (m, 2H, H5-H8), 6.91 (d, J = 8.6 Hz, 2H, H3b-H5b), 3.28 (t, J = 5.3 Hz, 4H, H2c-H6c), 1.86 – 1.66 (m, 4H, H3c-H5c), 1.67 – 1.57 (m, 2H, H4c). ^{13}C NMR (101 MHz, $CDCl_3$) δ 167.9 (d, $J_{C\text{-}F}$ = 3.3 Hz, C2), 160.5 (d, $J_{C\text{-}F}$ = 245.1 Hz, C6), 152.7 (C4b), 150.8 (d, $J_{C\text{-}F}$ = 1.7 Hz, C3a), 138.3

(C9), 135.3 (d, $J_{C\text{-}F}$ = 11.0 Hz, C7a), 128.9 (C2b-C6b), 125.2 (C8), 123.4 (d, $J_{C\text{-}F}$ = 9.4 Hz, C4), 118.1 (C1b), 115.4 (C3b-C5b), 114.7 (d, $J_{C\text{-}F}$ = 24.6 Hz, C7), 107.8 (d, $J_{C\text{-}F}$ = 26.8 Hz, C5), 49.5 (C2c-C6c), 25.7 (C3c-C5c), 24.5 (C4c). ^{19}F NMR (376 MHz, $CDCl_3$) δ -116.4. HPLC-MS (ESI): m/z calculated for $C_{20}H_{19}FN_2S$ 338.13; $[M+H]^+$ found 339.12.

6-Fluoro-3-methyl-2-(4-(piperidin-1-yl)styryl)benzo[d]thiazol-3-ium iodide (50b)

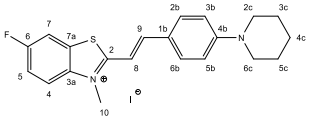

The synthesis was carried out according to general procedure K (96 mg, 88%). R_f: 0.16 (DCM/MeOH 5%). ^{1}H NMR (400 MHz, DMSO-d_6) δ 8.25 (dd, J = 8.3, 2.7 Hz, 1H, H7), 8.15 (dd, J = 9.1, 4.3 Hz, 1H, H4), 8.04 (d, J = 15.3 Hz, 1H, H8), 7.89 (d, J = 8.8 Hz, 2H, H2b-H6b), 7.70 (td, J = 9.1, 2.7 Hz, 1H, H5), 7.62 (d, J = 15.3 Hz, 1H, H9), 7.04 (d, J = 8.8 Hz, 2H, H3b-H5b), 4.22 (s, 3H, N-Me), 3.50 (t, J = 5.2 Hz, 4H, H2c-H6c), 1.70 – 1.51 (m, 6H, H3c-H4c-H5c). ^{13}C NMR (101 MHz, DMSO-d_6) δ 172.1 (d, $J_{C\text{-}F}$ = 1.6 Hz, C2), 161.0 (d, $J_{C\text{-}F}$ = 246.6 Hz, C6), 154.1 (C4b), 150.4 (C9), 139.3 (C3a), 133.4 (C2b-C6b), 129.0 (d, $J_{C\text{-}F}$ = 12.0 Hz, C7a), 122.7 (C1b), 118.2 (d, $J_{C\text{-}F}$ = 9.5 Hz, C4), 117.6 (d, $J_{C\text{-}F}$ = 25.6 Hz, C7), 113.9 (C3b-C5b), 111.1 (d, $J_{C\text{-}F}$ = 28.8 Hz, C5), 107.3 (C8), 48.0 (C2c-C6c), 36.4 (N-Me), 25.6 (C3c-C5c), 24.4 (C4c). ^{19}F NMR (376 MHz, DMSO-d_6) δ -112.6. HPLC-MS (ESI): m/z calculated for $C_{21}H_{22}FN_2S^+$ 353.15; $[M]^+$ found 353.13.

7-Methyl-2-(4-(piperidin-1-yl)styryl)benzo[d]thiazole (51a)

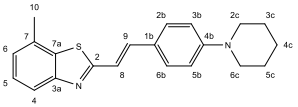

The synthesis was carried out according to general procedure J (28 mg, 43%). R_f: 0.40 (Hept/EtOAc 3:1). ^{1}H NMR (400 MHz, $CDCl_3$) δ 7.79 (d, *J* = 8.1 Hz, 1H, H4), 7.54 – 7.40 (m, 3H, H2b-H6b-H9), 7.36 (t, *J* = 7.7 Hz, 1H, H5), 7.23 (d, *J* = 16.1 Hz, 1H, H8), 7.13 (d, *J* = 7.3 Hz, 1H, H6), 6.91 (d, *J* = 8.4 Hz, 2H, H3b-H5b), 3.28 (t, *J* = 5.3 Hz, 4H, H2c-H6c), 2.56 (s, 3H, 7-Me), 1.70 (p, *J* = 5.4 Hz, 4H, H3c-H5c), 1.65 – 1.62 (m, 2H, H4c). ^{13}C NMR (101 MHz, $CDCl_3$) δ 167.7 (C2), 154.0 (C3a), 152.5 (C4b), 138.0 (C9), 134.7 (C7a), 131.6 (C7), 128.9 (C2b-C6b), 126.4 (C4), 125.6 (C8), 125.3 (C5), 120.1 (C6), 118.6 (C1b), 115.6 (C3b-C5b), 49.7 (C2c-C6c), 25.6 (C3c-C5c), 24.5 (C4c), 21.6 (7-Me). HPLC-MS (ESI): m/z calculated for $C_{21}H_{22}N_2S$ 334.15; $[M+H]^+$ found 335.15.

3,7-Dimethyl-2-(4-(piperidin-1-yl)styryl)benzo[d]thiazol-3-ium iodide (51b)

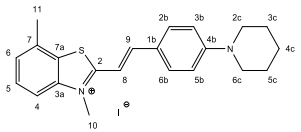

The synthesis was carried out according to general procedure K (11 mg, 64%). R_f: 0.19 (DCM/MeOH 5%). ^{1}H NMR (600 MHz, DMSO-d_6) δ 8.13 (d, *J* = 15.3 Hz, 1H, H8), 7.95 (d, *J* = 8.4 Hz, 1H, H4), 7.88 (d, *J* = 8.8 Hz, 2H, H2b-H6b), 7.72 (dd, *J* = 8.4, 7.4 Hz, 1H, H5), 7.66 (d, *J* = 15.3 Hz, 1H, H9), 7.54 (d, *J* = 7.4 Hz, 1H, H6), 7.05 (d, *J* = 8.8 Hz, 2H, H3b-H5b), 4.24 (s, 3H, N-Me), 3.51 (t, *J* = 5.4 Hz, 4H, H2c-H6c), 2.60 (s, 3H, 7-Me), 1.70 – 1.62 (m, 2H, H4c), 1.62 – 1.55 (m, 4H, H3c-H5c). ^{13}C NMR (151 MHz, DMSO-d_6) δ 170.7 (C2), 153.6 (C4b), 150.1 (C3a), 141.8 (C9), 132.9 (C2b-C6b), 132.7 (C7), 129.3 (C7a), 127.9 (C5), 126.6 (C6), 122.3 (C1b), 113.7 (C4), 113.5 (C3b-C5b), 106.8 (C8), 47.5 (C2c-C6c), 35.9 (N-Me), 25.1 (C3c-C5c), 23.9 (C4c), 19.3 (7-Me).

HPLC-MS (ESI): m/z calculated for $C_{22}H_{25}N_2S^+$ 349.17; $[M]^+$ found 349.20.

7-Methoxy-2-(4-(piperidin-1-yl)styryl)benzo[d]thiazole (52a)

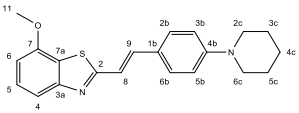

The synthesis was carried out according to general procedure J and purified by flash chromatography (PE/EtOAc 1% to 20% B) to afford the product as a yellow solid (25 mg, 13%). R_f: 0.41 (PE/EtOAc 4:1). ^{1}H NMR (600 MHz, $CDCl_3$) δ 7.60 (d, *J* = 8.1 Hz, 1H, H4), 7.52 – 7.45 (m, 3H, H2b-H6b-H9), 7.39 (t, *J* = 8.0 Hz, 1H, H5), 7.24 (d, *J* = 15.8 Hz, 1H, H8), 7.03 (s, 2H, H3b-H5b), 6.80 (d, *J* = 8.0 Hz, 1H, H6), 3.99 (s, 3H, 7-OMe), 3.30 (t, *J* = 5.5 Hz, 4H, H2c-H6c), 1.89 – 1.70 (m, 4H, H3c-H5c), 1.68 – 1.62 (m, 2H, H4c). ^{13}C NMR (151 MHz, $CDCl_3$) δ 168.4 (C2), 155.6 (C4b), 154.4 (C3a), 154.3 (C7), 137.6 (C9), 129.0 (C2b-C6b), 127.2 (C5), 126.8 (C8), 122.8 (C4), 119.2 (C1b), 116.0 (C7a), 115.5 (C3b-C5b), 105.3 (C6), 56.1 (7-OMe), 50.0 (C2c-C6c), 25.3 (C3c-C5c), 24.0 (C4c). HPLC-MS (ESI): m/z calculated for $C_{21}H_{22}N_2OS$ 350.15; $[M+H]^+$ found 351.15.

7-Methoxy-3-methyl-2-(4-(piperidin-1-yl)styryl)benzo[d]thiazol-3-ium iodide (52b)

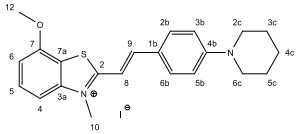

The synthesis was carried out according to general procedure K (21 mg, 46%). R_f: 0.21 (DCM/MeOH 5%). ^{1}H NMR (600 MHz, DMSO-d_6) δ 8.12 (d, *J* = 15.3 Hz, 1H, H8), 7.87 (d, *J* = 8.6 Hz, 2H, H2b-H6b), 7.75 (t, *J* = 8.2 Hz, 1H, H5), 7.69 (d, *J* = 8.5 Hz, 1H, H4), 7.63 (d, *J* = 15.3

Hz, 1H, H9), 7.31 (d, *J* = 8.1 Hz, 1H, H6), 7.05 (d, *J* = 8.6 Hz, 2H, H3b-H5b), 4.21 (s, 3H, N-Me), 4.06 (s, 3H, 7-Me), 3.46 – 3.42 (m, 4H, H2c-H6c), 1.69 – 1.54 (m, 6H, H3c-H4c-H5c). ^{13}C NMR (151 MHz, DMSO-*d*$_6$) δ 171.4 (C2), 153.6 (C7), 153.6 (C4b), 150.2 (C3a), 143.2 (C9), 133.0 (C2b-C6b), 130.8 (C5), 122.2 (C1b), 114.7 (C4), 113.4 (C3b-C5b), 108.7 (C7a), 108.4 (C6), 106.7 (C8), 56.9 (7-OMe), 47.5 (C2c-C6c), 36.0 (N-Me), 25.1 (C3c-C5c), 23.9 (C4c). HPLC-MS (ESI): m/z calculated $C_{22}H_{25}N_2OS^+$ 365.17; $[M]^+$ found 365.25.

7-Fluoro-2-(4-(piperidin-1-yl)styryl)benzo[d]thiazole (53a)

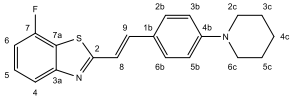

The synthesis was carried out according to general procedure J and purified by flash chromatography (PE/EtOAc 1% to 20% B) to afford the product as a yellow solid (119 mg, 72%). R_f: 0.49 (PE/EtOAc 4:1). ^{1}H NMR (600 MHz, $CDCl_3$) δ 7.75 (d, *J* = 8.1 Hz, 1H, H4), 7.50 – 7.45 (m, 3H, H2b-H6b-H9), 7.39 (td, *J* = 8.1, 5.4 Hz, 1H, H5), 7.21 (d, *J* = 16.1 Hz, 1H, H8), 7.05 (t, *J* = 8.6 Hz, 1H, H6), 6.98 – 6.90 (m, 2H, H3b-H5b), 3.29 (t, *J* = 5.5 Hz, 4H, H2c-H6c), 1.71 (br s, 4H, H3c-H5c), 1.65 – 1.60 (m, 2H, H4c). ^{13}C NMR (151 MHz, $CDCl_3$) δ 169.0 (C2), 157.1 (d, $J_{C\text{-}F}$ = 248.7 Hz, C7), 157.0 (d, $J_{C\text{-}F}$ = 2.7 Hz, C3a), 152.5 (C4b), 138.9 (C9), 129.1 (C2b-C6b), 127.1 (d, $J_{C\text{-}F}$ = 7.3 Hz, C5), 125.3 (C8), 121.3 (d, $J_{C\text{-}F}$ = 16.6 Hz, C7a), 118.4 (d, $J_{C\text{-}F}$ = 3.5 Hz, C4), 117.8 (C1b), 115.6 (C3b-C5b), 110.5 (d, $J_{C\text{-}F}$ = 18.9 Hz, C6), 49.7 (C2c-C6c), 25.5 (C3c-C5c), 24.3 (C4c). HPLC-MS (ESI): m/z calculated for $C_{20}H_{19}FN_2S$ 338.13; $[M+H]^+$ found 339.15.

7-Fluoro-3-methyl-2-(4-(piperidin-1-yl)styryl)benzo[d]thiazol-3-ium iodide (53b)

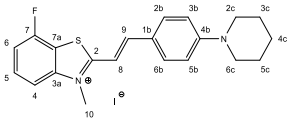

The synthesis was carried out according to general procedure K (42 mg, 69%). R_f: 0.19 (DCM/MeOH 5%). ^{1}H NMR (600 MHz, DMSO-d_6) δ 8.18 (d, J = 15.1 Hz, 1H, H8), 7.96 (d, J = 8.4 Hz, 1H, H4), 7.90 (d, J = 8.6 Hz, 2H, H2b-H6b), 7.83 (q, J = 8.0 Hz, 1H, H5), 7.69 – 7.57 (m, 2H, H6-H9), 7.06 (d, J = 8.6 Hz, 2H, H3b-H5b), 4.22 (s, 3H, N-Me), 3.54 (t, J = 5.4 Hz, 4H, H2c-H6c), 1.65 (q, J = 5.6 Hz, 2H, H4c), 1.63 – 1.53 (m, 4H, H3c-H5c). ^{13}C NMR (151 MHz, DMSO-d_6) δ 172.2 (C2), 156.3 (d, $J_{C\text{-}F}$ = 247.7 Hz, C7), 154.4 (C4b), 151.8 (C9), 144.9 (d, $J_{C\text{-}F}$ = 15.5 Hz, C3a), 134.1 (C2b-C6b), 131.4 (d, $J_{C\text{-}F}$ = 7.5 Hz, C5), 122.6 (C1b), 114.4 (d, $J_{C\text{-}F}$ = 23.1 Hz, C6), 113.9 (C3b-C5b), 113.0 (C4), 109.5 (C7a), 106.5 (C8), 48.0 (C2c-C6c), 36.7 (N-Me), 25.7 (C3c-C5c), 24.4 (C4c). HPLC-MS (ESI): m/z calculated for $C_{21}H_{22}FN_2S^+$ 353.15; $[M]^+$ found 353.10.

2-(4-(Piperidin-1-yl)phenyl)benzo[d]thiazole (54a)

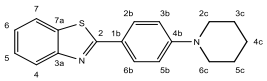

To a solution of **39** (140 mg, 0.48 mmol) in toluene (4.00 mL), $Pd(PPh_3)_4$ (28.0 mg, 0.02 mmol) and Cs_2CO_3 (140 mg, 0.72 mmol) were added under argon atmosphere. Piperidine (0.12 mL, 1.21 mmol) was diluted with toluene (1.00 mL) and slowly added. The mixture was refluxed for 5 h. It was diluted with water and extracted with EtOAc. The organic phase was dried over $MgSO_4$, evaporated under reduced pressure, and purified by flash chromatography (PE/EtOAc 1% to 10% B) to afford the product (14.0 mg, 10%). R_f: 0.50 (PE/EtOAc 5:1). ^{1}H

NMR (600 MHz, $CDCl_3$) δ 8.01 (d, *J* = 8.1 Hz, 1H, H7), 7.98 (d, *J* = 8.5 Hz, 2H, H2b-H6b), 7.85 (d, *J* = 7.9 Hz, 1H, H4), 7.47 – 7.42 (m, 1H, H5), 7.35 – 7.29 (m, 1H, H6), 7.02 (br s, 2H, H3b-H5b), 3.34 (t, *J* = 5.5 Hz, 4H, H2c-H6c), 1.77 – 1.74 (m, 4H, H3c-H5c), 1.65 (p, *J* = 5.7 Hz, 2H, H4c). ^{13}C NMR (151 MHz, $CDCl_3$) δ 166.2 (C2), 154.2 (C3a), 151.7 (C4b), 134.7 (C7a), 129.0 (C2b-C6b), 128.3 (C7), 126.3 (C4), 124.7 (C5), 122.7 (C6), 121.7 (C1b), 121.6 (C3b-C5b), 52.7 (C2c-C6c), 29.8 (C3c-C5c), 25.3 (C4c). HPLC-MS (ESI): m/z calculated for $C_{18}H_{18}N_2S$ 294.12; $[M+H]^+$ found 295.05.

3-Methyl-2-(4-(piperidin-1-yl)phenyl)benzo[d]thiazol-3-ium (54b)

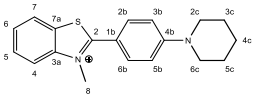

To a solution of **54a** (16.0 mg, 0.05 mmol) in chlorobenzene (1.50 mL) was added methyl nosylate (14.0 mg, 0.06 mmol). The mixture was stirred overnight at 80 °C. The precipitate was filtered under vacuum and triturated in Et_2O. The yellow solid was further purified by semipreparative HPLC (0.1% TFA in H_2O/MeCN 20% to 60% B in 15 min) to isolate the product from the aniline *N*-methylated byproduct (10.0 mg, 59%). R_f: 0.13 (DCM/MeOH 5%). ^1H NMR (600 MHz, DMSO-d_6) δ 8.40 (dd, *J* = 8.1, 1.2 Hz, 1H, H4), 8.25 (d, *J* = 8.4 Hz, 1H, H7), 7.89 (ddd, *J* = 8.5, 7.2, 1.2 Hz, 1H, H5), 7.81 (dt, *J* = 9.1, 3.2 Hz, 2H, H2b-H6b), 7.78 (ddd, *J* = 8.2, 7.2, 1.0 Hz, 1H, H6), 7.19 (dt, *J* = 9.1, 3.2 Hz, 2H, H3b-H5b), 4.25 (s, 3H, N-Me), 3.55 – 3.53 (m, 4H, H2c-H6c), 1.72 – 1.64 (m, 2H, H4c), 1.64 – 1.57 (m, 4H, H3c-H5c). ^{13}C NMR (151 MHz, DMSO-d_6) δ 173.4 (C2), 153.8 (C4b), 142.7 (C3a), 132.5 (C2b-C6b), 129.3 (C7a), 128.1 (C5), 127.7 (C7), 123.9 (C6), 116.9 (C4), 113.5 (C3b-C5b), 111.6 (C1b), 47.4 (C2c-C6c), 38.1 (N-Me), 24.9

(C3c-C5c), 23.8 (C4c). HPLC-MS (ESI): m/z calculated for $C_{19}H_{21}N_2S^+$ 309.14; $[M]^+$ found 309.15.

2-(4-(4-(Piperidin-1-yl)phenyl)buta-1,3-dien-1-yl)benzo[d]thiazole (55a)

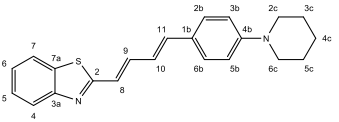

The synthesis was carried out according to general procedure J (32 mg, 17%). R_f: 0.48 (PE/EtOAc 4:1). ^{1}H NMR (600 MHz, $CDCl_3$) δ 7.90 (d, *J* = 8.1 Hz, 1H, H7), 7.78 (d, *J* = 8.0 Hz, 1H, H4), 7.39 (t, *J* = 7.7 Hz, 1H, H6), 7.33 (d, *J* = 8.3 Hz, 2H, H2b-H6b), 7.29 (t, *J* = 7.5 Hz, 2H, H5), 7.23 (d, *J* = 16.1 Hz, 1H, H11), 6.84 (d, *J* = 7.7 Hz, 2H, H3b-H5b), 6.83 – 6.66 (m, 3H, H8-H9-H10), 3.20 (t, *J* = 5.4 Hz, 4H, H2c-H6c), 1.64 (q, *J* = 5.8 Hz, 4H, H3c-H5c), 1.59 – 1.53 (m, 2H, H4c). ^{13}C NMR (151 MHz, $CDCl_3$) δ 167.6 (C2), 154.1 (C4b), 152.2 (C3a), 139.3 (C11), 138.3 (C9), 134.4 (C7a), 128.4 (C2b-C6b), 126.8 (C7), 126.3 (C1b), 125.1 (C4), 124.1 (C8), 123.4 (C10), 122.7 (C5), 121.5 (C6), 115.6 (C3b-C5b), 49.7 (C2c-C6c), 25.7 (C3c-C5c), 24.4 (C4c). HPLC-MS (ESI): m/z calculated for $C_{22}H_{22}N_2S$ 346.15; $[M+H]^+$ found 347.10.

3-Methyl-2-(4-(4-(piperidin-1-yl)phenyl)buta-1,3-dien-1-yl)benzo[d]thiazol-3-ium iodide (55b)

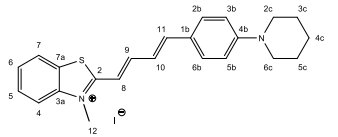

The synthesis was carried out according to general procedure K (109 mg, 87%). R_f: 0.16 (DCM/MeOH 5%). ^{1}H NMR (600 MHz, DMSO-d_6) δ 8.33 (d, *J* = 8.1 Hz, 1H, H4), 8.15 (d, *J* = 8.4 Hz, 1H, H7), 7.99 (dd, *J* = 14.6, 10.9 Hz, 1H, H9), 7.81 (ddd, *J* = 8.5, 7.2, 1.2 Hz, 1H, H5), 7.71

(ddd, *J* = 8.1, 7.3, 1.0 Hz, 1H, H6), 7.53 (d, *J* = 8.8 Hz, 2H, H2b-H6b), 7.43 (d, *J* = 15.1 Hz, 1H, H8), 7.35 (d, *J* = 14.6 Hz, 1H, H11), 7.21 (dd, *J* = 15.1, 10.9 Hz, 1H, H10), 7.00 (d, *J* = 8.8 Hz, 2H, H3b-H5b), 4.16 (s, 3H, N-Me), 3.39 (t, *J* = 5.1 Hz, 4H, H2c-H6c), 1.63 – 1.56 (m, 6H, H3c-H4c-H5c). ^{13}C NMR (151 MHz, DMSO-d_6) δ 170.6 (C2), 154.5 (C3a), 152.4 (C4b), 150.9 (C11), 147.4 (C10), 141.9 (C9), 130.4 (C2b-C6b), 129.1 (C7a), 127.8 (C5), 127.3 (C7), 124.0 (C6), 122.9 (C1b), 116.3 (C3b-C5b), 114.3 (C4), 112.9 (C8), 48.0 (C2c-C6c), 35.7 (N-Me), 25.0 (C3c-C5c), 24.0 (C4c). HPLC-MS (ESI): m/z calculated for $C_{23}H_{25}N_2S^+$ 361.17; $[M]^+$ found 361.20.

4-(4-(2-(Benzo[d]thiazol-2-yl)vinyl)phenyl)morpholine (56a)

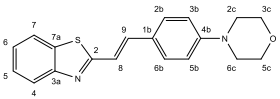

The synthesis was carried out according to general procedure J (47 mg, 59%). R_f: 0.21 (Hept/EtOAc 3:1). ^{1}H NMR (600 MHz, $CDCl_3$) δ 7.96 (d, *J* = 8.1 Hz, 1H, H7), 7.84 (d, *J* = 8.0 Hz, 1H, H4), 7.51 (d, *J* = 8.5 Hz, 2H, H2b-H6b), 7.46 (d, *J* = 16.1 Hz, 1H, H9), 7.45 (t, *J* = 7.4 Hz, 1H, H5), 7.35 (t, *J* = 7.6 Hz, 1H, H6), 7.26 (d, *J* = 16.1 Hz, 1H, H8), 6.91 (d, *J* = 8.5 Hz, 2H, H3b-H5b), 3.87 (t, *J* = 4.9 Hz, 4H, H3c-H5c), 3.25 (t, *J* = 4.8 Hz, 4H, H2c-H6c).^{13}C NMR (151 MHz, $CDCl_3$) δ 167.8 (C2), 154.1 (C3a), 152.1 (C4b), 137.7 (C9), 134.4 (C7a), 128.9 (C2b-C6b), 126.8 (C7), 126.3 (C8), 125.1 (C4), 122.8 (C5), 121.6 (C6), 119.2 (C1b), 115.2 (C3b-C5b), 66.9 (C3c-C5c), 48.5 (C2c-C6c). HPLC-MS (ESI): m/z calculated for $C_{19}H_{18}N_2OS$ 322.11; $[M+H]^+$ found 323.12.

3-Methyl-2-(4-morpholinostyryl)benzo[d]thiazol-3-ium iodide (56b)

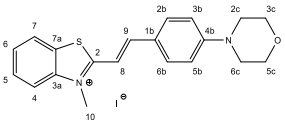

The synthesis was carried out according to general procedure K (52 mg, 69 %). R_f: 0.13 (DCM/MeOH 5%). ^{1}H NMR (600 MHz, DMSO-d_6) δ 8.34 (dd, *J* = 8.2, 1.2 Hz, 1H, H4), 8.14 (d, *J* = 8.3 Hz, 1H, H7), 8.10 (d, *J* = 15.4 Hz, 1H, H8), 7.95 (dt, *J* = 9.0, 2.9 Hz, 2H, H2b-H6b), 7.81 (ddd, *J* = 8.5, 7.2, 1.2 Hz, 1H, H5), 7.74 (d, *J* = 15.4 Hz, 1H, H9), 7.72 (ddd, *J* = 8.2, 7.2, 1.0 Hz, 1H, H6), 7.09 (dt, *J* = 9.0, 3.1 Hz, 2H, H3b-H5b), 4.27 (s, 3H, N-Me), 3.80 – 3.70 (m, 4H, H3c-H5c), 3.42 (dd, *J* = 5.7, 4.1 Hz, 4H, H2c-H6c). ^{13}C NMR (151 MHz, DMSO-d_6) δ 171.7 (C2), 153.8 (C4b), 149.5 (C3a), 142.0 (C9), 132.4 (C2b-C6b), 129.0 (C7a), 127.7 (C5), 127.1 (C7), 123.9 (C6), 123.5 (C1b), 116.2 (C4), 113.6 (C3b-C5b), 108.2 (C8), 65.8 (C3c-C5c), 46.5 (C2c-C6c), 35.8 (N-Me). HPLC-MS (ESI): m/z calculated for $C_{20}H_{21}N_2OS^+$ 337.14; $[M]^+$ found 337.14.

2-(4-Thiomorpholinostyryl)benzo[d]thiazole (57a)

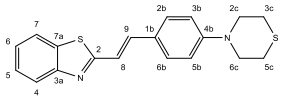

The synthesis was carried out according to general procedure J (6 mg, 11%). R_f: 0.39 (Hept/EtOAc 3:1). ^{1}H NMR (600 MHz, $CDCl_3$) δ 7.96 (d, *J* = 8.1 Hz, 1H, H7), 7.84 (d, *J* = 7.9 Hz, 1H, H4), 7.49 (d, *J* = 8.5 Hz, 2H, H2b-H6b), 7.47 – 7.42 (m, 2H, H5-H9), 7.35 (td, *J* = 8.0, 1.1 Hz, 1H, H6), 7.25 (d, *J* = 16.1 Hz, 1H, H8), 6.88 (d, *J* = 8.3 Hz, 2H, H3b-H5b), 3.77 – 3.67 (m, 4H, H2c-H6c), 2.74 (t, *J* = 5.1 Hz, 4H, H3c-H5c). ^{13}C NMR (151 MHz, $CDCl_3$) δ 167.9 (C2), 154.0 (C3a), 151.2 (C4b),

137.8 (C9), 134.3 (C7a), 129.1 (C2b-C6b), 126.4 (C7), 126.1 (C8), 125.1 (C4), 122.7 (C5), 121.6 (C6), 119.0 (C1b), 116.0 (C3b-C5b), 51.2 (C2c-C6c), 26.3 (C3c-C5c). HPLC-MS (ESI): m/z calculated for $C_{19}H_{18}N_2S_2$ 338.09; $[M+H]^+$ found 339.07.

3-Methyl-2-(4-thiomorpholinostyryl)benzo[d]thiazol-3-ium iodide (57b)

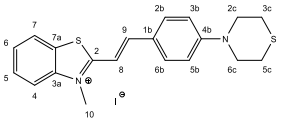

The synthesis was carried out according to general procedure K (33 mg, 65%). R_f: 0.13 (DCM/MeOH 5%). ^{1}H NMR (600 MHz, DMSO-d_6) δ 8.33 (dd, *J* = 8.1, 1.2 Hz, 1H, H4), 8.13 (d, *J* = 8.4 Hz, 1H, H7), 8.08 (d, *J* = 15.4 Hz, 1H, H8), 7.97 – 7.89 (m, 2H, H2b-H6b), 7.81 (ddd, *J* = 8.5, 7.2, 1.2 Hz, 1H, H5), 7.74 – 7.66 (m, 2H, H5), 7.07 (d, *J* = 9.0 Hz, 2H, H6-H9), 4.26 (s, 3H, N-Me), 3.94 – 3.84 (m, 4H, H2c-H6c), 2.72 – 2.63 (m, 4H, H3c-H5c). ^{13}C NMR (151 MHz, DMSO-d_6) δ 171.6 (C2), 152.3 (C4b), 149.5 (C3a), 142.0 (C9), 132.8 (C2b-C6b), 128.9 (C7a), 127.6 (C5), 127.0 (C7), 123.9 (C6), 122.7 (C1b), 116.1 (C4), 113.9 (C3b-C5b), 107.6 (C8), 49.5 (C2c-C6c), 35.7 (N-Me), 25.2 (C3c-C5c). HPLC-MS (ESI): m/z calculated for $C_{20}H_{21}N_2S_2^+$ 353.11; $[M]^+$ found 353.09.

2-(4-(Pyrrolidin-1-yl)styryl)benzo[d]thiazole (58a)

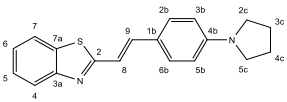

The synthesis was carried out according to general procedure J (15 mg, 15%). R_f: 0.50 (Hept/EtOAc 3:1). ^{1}H NMR (600 MHz, $CDCl_3$) δ 7.93 (d, *J* = 8.1 Hz, 1H, H7), 7.82 (d, *J* = 7.9 Hz, 1H, H4), 7.55 – 7.38 (m, 4H, H2b-H6b-H5-H9), 7.31 (t, *J* = 7.5 Hz, 1H, H6), 7.18 (d, *J* = 16.1 Hz,

1H, H8), 6.57 (d, *J* = 8.3 Hz, 2H, H3b-H5b), 3.35 (t, *J* = 6.1 Hz, 4H, H2c-H5c), 2.03 (hept, *J* = 3.4 Hz, 4H, H3c-H4c). ^{13}C NMR (151 MHz, $CDCl_3$) δ 168.6 (C2), 154.2 (C3a), 148.9 (C4b), 138.8 (C9), 134.2 (C7a), 129.2 (C2b-C6b), 126.2 (C7), 124.8 (C4), 122.8 (C8), 122.5 (C5), 121.5 (C6), 116.7 (C1b), 112.0 (C3b-Cb), 47.7 (C2c-C5c), 25.6 (C3c-C4c). HPLC-MS (ESI): m/z calculated for $C_{19}H_{18}N_2S$ 306.12; $[M+H]^+$ found 307.11.

3-Methyl-2-(4-(pyrrolidin-1-yl)styryl)benzo[d]thiazol-3-ium iodide (58b)

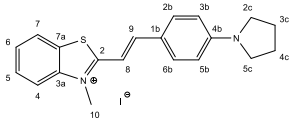

The synthesis was carried out according to general procedure K (118 mg, 96%). R_f: 0.16 (DCM/MeOH 5%). ^{1}H NMR (400 MHz, DMSO-d_6) δ 8.28 (d, *J* = 8.0 Hz, 1H, H4), 8.12 – 7.99 (m, 2H, H7-H8), 7.90 (d, *J* = 8.6 Hz, 2H, H2b-H6b), 7.77 (t, *J* = 7.6 Hz, 1H, H5), 7.67 (t, *J* = 7.6 Hz, 1H, H6), 7.58 (d, *J* = 15.2 Hz, 1H, H9), 6.69 (d, *J* = 8.6 Hz, 2H, H3b-H5b), 4.21 (s, 3H, N-Me), 3.43 – 3.35 (m, 4H, H2c-H5c), 2.00 (p, *J* = 3.2 Hz, 4H, H3c-H4c). ^{13}C NMR (101 MHz, DMSO-d_6) δ 171.1 (C2), 151.0 (C4b), 150.3 (C3a), 141.9 (C9), 133.1 (C2b-C6b), 128.8 (C7a), 127.3 (C5), 126.7 (C7), 123.7 (C6), 121.3 (C1b), 115.8 (C4), 112.4 (C3b-C5b), 105.6 (C8), 47.6 (C2c-C5c), 35.4 (N-Me), 24.8 (C3c-C4c). HPLC-MS (ESI): m/z calculated for $C_{20}H_{21}N_2S^+$ 321.14; $[M]^+$ found 321.14.

2-(4-(4-Fluoropiperidin-1-yl)styryl)benzo[d]thiazole (59a)

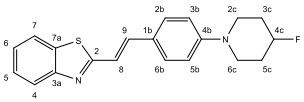

The synthesis was carried out according to general procedure J (84 mg, 57%). R_f: 0.23 (Hept/EtOAc 3:1). ^{1}H NMR (400 MHz, DMSO-d_6) δ 8.04 (dd, J = 7.9, 1.1 Hz, 1H, H7), 7.91 (d, J = 8.1 Hz, 1H, H4), 7.61 (d, J = 8.6 Hz, 2H, H2b-H6b), 7.54 (d, J = 16.1 Hz, 1H, H9), 7.48 (td, J = 7.2, 1.0 Hz, 1H, H5), 7.39 (td, J = 8.2, 0.9 Hz, 1H, H6), 7.36 (d, J = 16.1 Hz, 1H, H8), 7.00 (d, J = 8.4 Hz, 2H, H3b-H5b), 4.87 (dtt, J = 49.0, 7.3, 3.6 Hz, 1H, H4c), 3.58 – 3.42 (m, 2H, H2c-H6c), 3.27 (ddd, J = 12.6, 7.7, 3.8 Hz, 2H, H2c-H6c), 2.05 – 1.87 (m, 2H, H3c-H5c), 1.83 – 1.69 (m, 2H, H3c-H5c). ^{13}C NMR (101 MHz, DMSO-d_6) δ 167.7 (C2), 154.1 (C3a), 151.5 (C4b), 138.3 (C9), 134.2 (C7a), 129.6 (C2b-C6b), 126.8 (C7), 125.5 (C8), 125.3 (C4), 122.6 (C5), 122.5 (C6), 118.1 (C1b), 115.3 (C3b-C5b), 89.0 (d, $J_{C\text{-}F}$ = 169.4 Hz, C4c), 44.5 (d, $J_{C\text{-}F}$ = 6.9 Hz, C2c-C6c), 30.9 (d, J = 19.1 Hz, C3c-C5c). HPLC-MS (ESI): m/z calculated for $C_{20}H_{19}FN_2S$ 338.13; $[M+H]^+$ found 339.10.

2-(4-(4-Fluoropiperidin-1-yl)styryl)-3-methylbenzo[d]thiazol-3-ium iodide (59b)

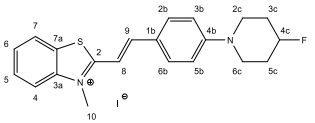

The synthesis was carried out according to general procedure K (143 mg, 87%). R_f: 0.19 (DCM/MeOH 5%). ^{1}H NMR (400 MHz, DMSO-d_6) δ 8.33 (dd, J = 8.1, 1.2 Hz, 1H, H4), 8.13 (d, J = 8.4 Hz, 1H, H7), 8.07 (d, J = 15.5 Hz, 1H, H8), 7.92 (d, J = 8.7 Hz, 2H, H2b-H6b), 7.80 (td, J = 8.1, 7.2, 1.3 Hz, 1H, H5), 7.75 – 7.64 (m, 2H, H6-H9), 7.11 (d, J = 8.7 Hz, 2H, H3b-H5b), 4.93 (dtt, J = 48.9, 7.1, 3.5 Hz, 1H, H4c), 4.26 (s, 3H, N-Me), 3.76 – 3.58 (m, 2H, H2c-H6c), 3.55 – 3.44 (m, 2H, H2c-H6c), 1.98 (dddd, J = 24.8, 16.1, 7.5, 3.6 Hz, 2H, H3c-H5c), 1.78 (dtt, J = 14.1, 7.2, 3.8 Hz, 2H, H3c-H5c). ^{13}C NMR (101 MHz, DMSO-d_6) δ 172.1 (C2), 153.5 (C4b), 150.0 (C3a), 142.4 (C9), 133.2 (C2b-C6b),

129.4 (C7a), 128.1 (C5), 127.5 (C7), 124.4 (C6), 123.3 (C1b), 116.6 (C4), 114.3 (C3b-C5b), 108.1 (C8), 88.7 (d, $J_{C\text{-}F}$ = 169.5 Hz, C4c), 43.6 (d, $J_{C\text{-}F}$ = 6.6 Hz, C2c-C6c), 36.2 (N-Me), 31.0 (d, $J_{C\text{-}F}$ = 19.4 Hz, C3c-C5c). ^{19}F NMR (376 MHz, DMSO-d_6) δ -177.5. HPLC-MS (ESI): m/z calculated for $C_{21}H_{22}FN_2S^+$ 353.15; $[M]^+$ found 353.14.

4-(2-(Benzo[d]thiazol-2-yl)vinyl)-N,N-dimethylaniline (60a)

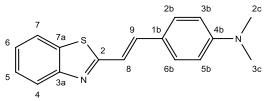

The synthesis was carried out according to general procedure J (58 mg, 34%). R_f: 0.40 (Hept/EtOAc 3:1). ^{1}H NMR (600 MHz, $CDCl_3$) δ 7.94 (dt, *J* = 8.0, 0.9 Hz, 1H, H7), 7.82 (dt, *J* = 7.7, 0.9 Hz, 1H, H4), 7.48 (dt, *J* = 8.8, 2.8 Hz, 2H, H2b-H6b), 7.45 (d, *J* = 16.1 Hz, 1H, H9), 7.43 (ddd, *J* = 8.3, 7.2, 1.2 Hz, 1H, H5), 7.32 (ddd, *J* = 8.2, 7.2, 1.2 Hz, 1H, H6), 7.21 (d, *J* = 16.1 Hz, 1H, H8), 6.72 (dt, *J* = 8.9, 2.9 Hz, 2H, H3b-H5b), 3.03 (s, 6H, H2c-H3c). ^{13}C NMR (151 MHz, $CDCl_3$) δ 168.4 (C2), 154.2 (C3a), 151.4 (C4b), 138.5 (C9), 134.3 (C7a), 129.1 (C2b-C6b), 126.2 (C7), 124.9 (C4), 123.5 (C8), 122.6 (C5), 121.5 (C6), 117.4 (C1b), 112.2 (C3b-C5b), 40.4 (C2c-C3c). HPLC-MS (ESI): m/z calculated for $C_{17}H_{16}N_2S$ 280.10; $[M+H]^+$ found 281.11.

2-(4-(Dimethylamino)styryl)-3-methylbenzo[d]thiazol-3-ium iodide (60b)

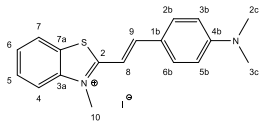

The synthesis was carried out according to general procedure K (125 mg, 90%). R_f: 0.14 (DCM/MeOH 5%). ^{1}H NMR (400 MHz, DMSO-d_6) δ 8.30 (dd, *J* = 8.1, 1.2 Hz, 1H, H4), 8.15 – 7.99 (m, 2H, H7-H8), 7.91 (d, *J* = 8.9 Hz, 2H, H2b-H6b), 7.78 (ddd, *J* = 8.5, 7.2, 1.2 Hz, 1H, H5), 7.72

– 7.65 (m, 1H, H6), 7.62 (d, *J* = 15.3 Hz, 1H, H9), 6.84 (d, *J* = 8.9 Hz, 2H, H3b-H5b), 4.23 (s, 3H, N-Me), 3.10 (s, 6H, H2c-H3c). ^{13}C NMR (101 MHz, DMSO-d_6) δ 171.3 (C2), 153.5 (C4b), 150.1 (C3a), 141.9 (C9), 132.8 (C2b-C6b), 128.8 (C7a), 127.4 (C5), 126.8 (C7), 123.8 (C6), 121.4 (C1b), 115.9 (C4), 111.9 (C3b-C5b), 106.2 (C8), 39.8 (C2c-C3c), 35.5 (N-Me). HPLC-MS (ESI): m/z calculated for $C_{18}H_{19}N_2S^+$ 295.13; $[M]^+$ found 295.11.

2-(4-(Piperidin-1-yl)styryl)benzo[d]thiazole (61)

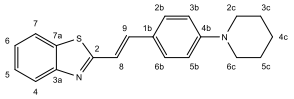

The synthesis was carried out according to general procedure J (1.14 g, 53%). R_f: 0.38 (Hept/EtOAc 3:1). ^{1}H NMR (400 MHz, $CDCl_3$) δ 7.95 (d, *J* = 8.1 Hz, 1H, H7), 7.83 (d, *J* = 7.9 Hz, 1H, H4), 7.53 – 7.39 (m, 4H, H2b-H6b-H5-H9), 7.33 (t, *J* = 7.6 Hz, 1H, H6), 7.23 (d, *J* = 16.2 Hz, 1H, H8), 6.91 (d, *J* = 8.5 Hz, 2H, H3b-H5b), 3.28 (t, *J* = 5.6 Hz, 4H, H2c-H6c), 1.70 (p, *J* = 5.6 Hz, 4H, H3c-H5c), 1.63 (q, *J* = 6.5, 5.6 Hz, 2H, H4c). ^{13}C NMR (101 MHz, $CDCl_3$) δ 168.1 (C2), 154.2 (C3a), 152.6 (C4b), 138.1 (C9), 134.3 (C7a), 128.9 (C2b-C6b), 126.3 (C7), 125.4 (C8), 125.0 (C4), 122.7 (C5), 121.5 (C6), 118.4 (C1b), 115.4 (C3b-C5b), 49.5 (C2c-C6c), 25.7 (C3c-C5c), 24.5 (C4c). HPLC-MS (ESI): m/z calculated for $C_{20}H_{20}N_2S$ 320.13; $[M+H]^+$ found 321.13.

3-Methyl-2-(4-(piperidin-1-yl)styryl)benzo[d]thiazol-3-ium iodide (RB1)

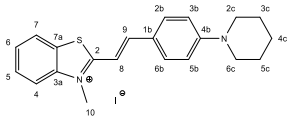

The synthesis was carried out according to general procedure K (322 mg, 81%). R_f: 0.17 (DCM/MeOH 5%). ^{1}H NMR (400 MHz, DMSO-d_6) δ

8.31 (dd, *J* = 8.2, 1.2 Hz, 1H, H4), 8.11 (d, *J* = 8.4 Hz, 1H, H7), 8.05 (d, *J* = 16.1 Hz, 1H, H8), 7.90 (d, *J* = 9.0 Hz, 2H, H2b-H6b), 7.79 (ddd, *J* = 8.5, 7.3, 1.3 Hz, 1H, H5), 7.73 – 7.62 (m, 2H, H6-H9), 7.05 (d, *J* = 8.7 Hz, 2H, H3b-H5b), 4.24 (s, 3H, N-Me), 3.50 (t, *J* = 5.1 Hz, 4H, H2c-H6c), 1.69 – 1.51 (m, 6H, H3c-H4c-H5c). ^{13}C NMR (101 MHz, DMSO-*d*$_6$) δ 171.9 (C2), 154.1 (C3a), 150.2 (C4b), 142.4 (C9), 133.4 (C2b-C6b), 129.4 (C7a), 128.0 (C5), 127.4 (C7), 124.3 (C6), 122.7 (C1b), 116.5 (C4), 113.9 (C3b-C5b), 107.4 (C8), 48.0 (C2c-C6c), 36.1 (N-Me), 25.6 (C3c-C5c), 24.4 (C4c). HPLC-MS (ESI): m/z calculated for $C_{21}H_{23}N_2S^+$ 335.16; $[M]^+$ found 335.17.

3-Methyl-2-(4-(4-methylpiperazin-1-yl)styryl)benzo[d]thiazol-3-ium iodide (RB2)

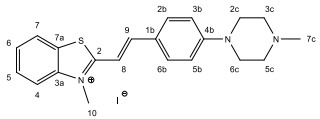

The synthesis was carried out according to general procedure K (159 mg, 97%). R_f: 0.19 (DCM/MeOH 5%). ^{1}H NMR (400 MHz, DMSO-*d*$_6$) δ 8.35 (d, *J* = 7.9 Hz, 1H, H4), 8.15 (d, *J* = 8.4 Hz, 1H, H7), 8.10 (d, *J* = 15.5 Hz, 1H, H8), 7.95 (d, *J* = 8.5 Hz, 2H, H2b-H6b), 7.82 (t, *J* = 7.9 Hz, 1H, H5), 7.75 (d, *J* = 15.5 Hz, 1H, H9), 7.72 (t, *J* = 7.7 Hz, 1H, H6), 7.11 (d, *J* = 8.5 Hz, 2H, H3b-H5b), 4.28 (s, 3H, N-Me), 3.56 (br s, 4H, H2c-H6c), 2.85 (br s, 4H, H3c-H5c), 2.53 (s, 3H, N-Me). ^{13}C NMR (101 MHz, DMSO-*d*$_6$) δ 171.7 (C2), 153.0 (C4b), 149.3 (C3a), 141.9 (C9), 132.4 (C2b-C6b), 129.0 (C7a), 127.7 (C5), 127.1 (C7), 123.9 (C6), 123.7 (C1b), 116.2 (C4), 114.0 (C3b-C5b), 108.4 (C8), 53.3 (C3c-C5c), 45.2 (C2c-C6c), 44.0 (N-Me), 35.9 (N-Me). HPLC-MS (ESI): m/z calculated for $C_{21}H_{24}N_3S^+$ 350.17; $[M+H]^+$ found 350.15.

6-Fluoro-2-(4-(4-(piperidin-1-yl)phenyl)buta-1,3-dien-1-yl)benzo[d]thiazole (62)

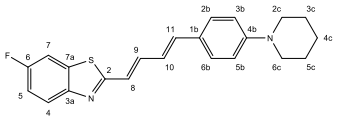

The synthesis was carried out according to general procedure J (37 mg, 28%). R_f: 0.47 (PE/EtOAc 4:1). ^{1}H NMR (600 MHz, $CDCl_3$) δ 7.90 (dd, *J* = 8.9, 4.8 Hz, 1H, H4), 7.52 (dd, *J* = 7.1, 1.6 Hz, 1H, H7), 7.40 (d, *J* = 8.3 Hz, 2H, H2b-H6b), 7.33 – 7.27 (m, 1H, H11), 7.19 (t, *J* = 8.7 Hz, 1H, H5), 6.92 (d, *J* = 8.3 Hz, 2H, H3b-H5b), 6.88 – 6.80 (m, 3H, H8-H9-H10), 3.27 (t, *J* = 5.4 Hz, 4H, H2c-H6c), 1.81 – 1.68 (m, 4H, H3c-H5c), 1.64 (p, *J* = 5.7 Hz, 2H, H4c). ^{13}C NMR (151 MHz, $CDCl_3$) δ 167.3 (C2), 160.5 (d, $J_{C\text{-}F}$ = 245.6 Hz, C6), 152.1 (C4b), 150.8 (d, $J_{C\text{-}F}$ = 1.5 Hz, C3a), 139.3 (C11), 138.4 (C9), 135.4 (d, $J_{C\text{-}F}$ = 11.2 Hz, C7a), 128.4 (C2b-C6b), 126.9 (C1b), 124.0 (C8), 123.5 (d, $J_{C\text{-}F}$ = 9.3 Hz, C4), 123.1 (C10), 115.7 (C3b-C5b), 114.8 (d, $J_{C\text{-}F}$ = 24.8 Hz, C7), 107.8 (d, $J_{C\text{-}F}$ = 27.0 Hz, C5), 49.8 (C2c-C6c), 25.6 (C3c-C5c), 24.4 (C4c). HPLC-MS (ESI): m/z calculated for $C_{22}H_{21}FN_2S$ 364.14; $[M+H]^+$ found 365.10.

6-Fluoro-2-(4-(4-(pyrrolidin-1-yl)phenyl)buta-1,3-dien-1-yl)benzo[d]thiazole (63)

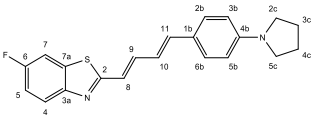

The synthesis was carried out according to general procedure J (24 mg, 36%). R_f: 0.51 (PE/EtOAc 4:1). ^{1}H NMR (600 MHz, $CDCl_3$) δ 7.92 – 7.77 (m, 1H, H4), 7.46 (d, *J* = 8.3 Hz, 1H, H7), 7.34 (d, *J* = 8.1 Hz, 2H, H2b-H6b), 7.25 – 7.20 (m, 1H, H11), 7.13 (t, *J* = 9.1 Hz, 1H, H5), 6.93 – 6.68 (m, 3H, H8-H9-H10), 6.52 (d, *J* = 8.8 Hz, 2H, H3b-H5b),

3.31 (s, 4H, H2c-H5c), 2.00 (s, 4H, H3c-H4c). ^{13}C NMR (151 MHz, $CDCl_3$) δ 167.7 (C2), 162.1 (d, $J_{C\text{-}F}$ = 239.1 Hz, H6), 150.5 (C3a), 148.3 (C4b), 140.1 (C11), 139.4 (C9), 137.2 (C7a), 128.8 (C2b-C6b), 127.8 (C1b), 123.3 (d, $J_{C\text{-}F}$ = 8.4 Hz, C4), 122.4 (C8), 121.9 (C10), 114.8 (d, $J_{C\text{-}F}$ = 24.0 Hz, C7), 112.1 (C3b-C5b), 107.8 (d, $J_{C\text{-}F}$ = 26.8 Hz, C5), 47.9 (C2c-C5c), 25.6 (C3c-C4c). HPLC-MS (ESI): m/z calculated for $C_{21}H_{19}FN_2S$ 350.13; $[M+H]^+$ found 351.15.

4-(4-(2-(6-Fluorobenzo[d]thiazol-2-yl)vinyl)phenyl)morpholine (64 – MFSB)

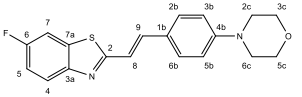

The synthesis was carried out according to general procedure J (21 mg, 69%). R_f: 0.18 (PE/EtOAc 4:1). ^{1}H NMR (600 MHz, $CDCl_3$) δ 7.90 (dd, *J* = 9.0, 4.8 Hz, 1H, H4), 7.58 – 7.47 (m, 3H, H2b-H6b), 7.43 (d, *J* = 16.0 Hz, 1H, H9), 7.24 (d, *J* = 16.0 Hz, 1H, H8), 7.19 (td, *J* = 8.9, 2.6 Hz, 1H, H5), 6.96 (d, *J* = 8.2 Hz, 2H, H3b-H5b), 3.90 (t, *J* = 4.6 Hz, 4H, H3c-H5c), 3.27 (t, *J* = 4.2 Hz, 4H, H2c-H6c). ^{13}C NMR (151 MHz, $CDCl_3$) δ 167.6 (C2), 160.6 (d, $J_{C\text{-}F}$ = 245.5 Hz, C6), 151.8 (C4b), 150.4 (C3a), 138.0 (C9), 135.2 (C7a), 129.0 (C2b-C6b), 127.0 (C8), 123.5 (d, $J_{C\text{-}F}$ = 9.0 Hz, C4), 118.9 (C1b), 115.4 (C3b-C5b), 115.0 (d, $J_{C\text{-}F}$ = 25.1 Hz, C7), 107.9 (d, $J_{C\text{-}F}$ = 27.1 Hz, C5), 66.7 (C3c-C5c), 48.7 (C2c-C6c). HPLC-MS (ESI): m/z calculated for $C_{19}H_{17}FN_2OS$ 340.10; $[M+H]^+$ found 341.10.

6-Bromo-2-(4-(piperidin-1-yl)styryl)benzo[d]thiazole (65)

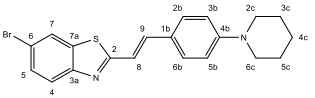

The synthesis was carried out according to general procedure J (2.80 g, 80%). R_f: 0.51 (PE/EtOAc 4:1). ^{1}H NMR (600 MHz, $CDCl_3$) δ 7.94 (s, 1H, H7), 7.78 (d, *J* = 8.6 Hz, 1H, H4), 7.52 (d, *J* = 8.6 Hz, 1H, H5), 7.46 (d, *J* = 8.3 Hz, 2H, H2b-H6b), 7.43 (d, *J* = 16.0 Hz, 1H, H9), 7.18 (d, *J* = 16.0 Hz, 1H, H8), 6.92 (br s, 2H, H3b-H5b), 3.29 (t, *J* = 5.4 Hz, 4H, H2c-H6c), 1.70 (br s, 4H, H3c-H5c), 1.63 (q, *J* = 5.7 Hz, 2H, H4c). ^{13}C NMR (151 MHz, $CDCl_3$) δ 168.6 (C2), 153.0 (C4b), 152.5 (C3a), 138.7 (C9), 136.0 (C7a), 129.7 (C5), 129.0 (C2b-C6b), 125.3 (C8), 124.0 (C7), 123.7 (C4), 118.4 (C1b), 117.9 (C6), 115.5 (C3b-C5b), 49.6 (C2c-C6c), 25.5 (C3c-C5c), 24.4 (C4c). HPLC-MS (ESI): m/z calculated for $C_{20}H_{19}BrN_2S$ 398.05; $[M+H]^+$ found 399.00, 400.95.

4-(4-(2-(6-Bromobenzo[d]thiazol-2-yl)vinyl)phenyl)morpholine (66)

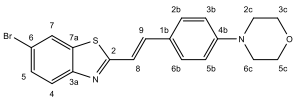

The synthesis was carried out according to general procedure J (639 mg, 73%). R_f: 0.15 (PE/EtOAc 4:1). ^{1}H NMR (600 MHz, $CDCl_3$) δ 7.97 (d, *J* = 1.9 Hz, 1H, H7), 7.82 (d, *J* = 8.6 Hz, 1H, H4), 7.55 (dd, *J* = 8.6, 1.9 Hz, 1H,H5), 7.53 (dt, *J* = 8.7, 2.0 Hz, 2H, H2b-H6b), 7.48 (d, *J* = 16.1 Hz, 1H, H9), 7.25 (d, *J* = 16.1 Hz, 1H, H8), 7.00 (d, *J* = 8.4 Hz, 2H, H3b-H5b), 3.92 (t, *J* = 4.8 Hz, 4H, H3c-H5c), 3.30 – 3.26 (m, 4H, H2c-H6c). ^{13}C NMR (151 MHz, $CDCl_3$) δ 168.3 (C2), 151.9 (C4b), 151.0 (C3a), 138.7 (C9), 135.6 (C7a), 130.1 (C5), 129.3 (C2b-C6b), 126.2 (C8), 124.2 (C7), 123.6 (C4), 118.9 (C1b), 118.7 (C6), 116.0 (C3b-C5b), 66.4 (C3c-C5c), 49.2 (C2c-C6c). HPLC-MS (ESI): m/z calculated for $C_{19}H_{17}BrN_2OS$ 400.02; $[M+H]^+$ found 400.95, 403.05.

2-(4-(Piperidin-1-yl)styryl)-6-(4,4,5,5-tetramethyl-1,3,2-dioxaborolan-2-yl)benzo[d]thiazole (67)

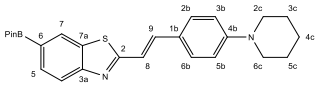

$Pd(dppf)Cl_2$ (303 mg, 0.40 mmol) was added to a solution of **65** (1.60 g, 4.01 mmol), potassium acetate (786 mg, 8.01 mmol), and bis(pinacolato)diboron (1.53 g, 6.01 mmol) in dry DMF (34.0 mL). The mixture was heated at 100 °C for 45 min. It was poured into water and extracted with EtOAc. The organic phase was dried over $MgSO_4$, evaporated under reduced pressure, and purified by flash chromatography (PE/EtOAc 5% to 20% B) to afford the product as a yellow solid (1.66 g, 93%). R_f: 0.35 (PE/EtOAc 6:1). ^{1}H NMR (600 MHz, $CDCl_3$) δ 8.31 (d, *J* = 1.1 Hz, 1H, H7), 7.93 (d, *J* = 8.1 Hz, 1H, H4), 7.87 (dd, *J* = 8.1, 1.1 Hz, 1H, H5), 7.49 – 7.44 (m, 3H, H2b-H6b-H9), 7.23 (d, *J* = 16.1 Hz, 1H, H8), 6.90 (d, *J* = 8.4 Hz, 2H, H3b-H5b), 3.29 – 3.23 (m, 4H, H2c-H6c), 1.68 (p, *J* = 5.5 Hz, 4H, H3c-H5c), 1.60 (q, *J* = 7.0, 6.4 Hz, 2H, H4c), 1.37 (s, 12H, BPin-Me). ^{13}C NMR (151 MHz, $CDCl_3$) δ 169.6 (C2), 156.1 (C4b), 152.4 (C3a), 138.5 (C9), 133.8 (C7a), 132.3 (C5), 129.0 (C6), 129.0 (C2b-C6b), 128.4 (C7), 125.4 (C8), 121.8 (C4), 118.4 (C1b), 115.4 (C3b-C5b), 84.1 (BPin), 49.5 (C2c-C6c), 25.5 (C3c-C5c), 25.0 (BPin-Me), 24.3 (C4c). HPLC-MS (ESI): m/z calculated for $C_{26}H_{31}BN_2O_2S$ 446.22; $[M+H]^+$ found 447.30.

4-(4-(2-(6-(4,4,5,5-Tetramethyl-1,3,2-dioxaborolan-2-yl)benzo[d]thiazol-2-yl)vinyl)phenyl)morpholine (68)

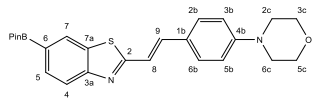

The synthesis was carried out following the same procedure as **67** (124 mg, 18%). R_f: 0.17 (PE/EtOAc 3:1). ^{1}H NMR (600 MHz, $CDCl_3$) δ 8.31

(d, *J* = 1.1 Hz, 1H, H7), 7.94 (d, *J* = 8.1 Hz, 1H, H4), 7.87 (dd, *J* = 8.1, 1.1 Hz, 1H, H5), 7.49 (d, *J* = 8.7 Hz, 2H, H2b-H6b), 7.48 (d, *J* = 16.1 Hz, 1H, H9), 7.26 (d, *J* = 16.1 Hz, 1H, H8), 6.89 (dt, *J* = 8.8, 2.9 Hz, 2H, H3b-H5b), 3.87 – 3.84 (m, 4H, H3c-H5c), 3.25 – 3.21 (m, 4H, H2c-H6c), 1.36 (s, 12H, BPin-Me). ^{13}C NMR (151 MHz, $CDCl_3$) δ 169.5 (C2), 155.6 (C3a), 152.0 (C4b), 138.5 (C9), 133.6 (C7a), 132.4 (C5), 130.7 (C6), 129.0 (C2b-C6b), 128.5 (C7), 126.6 (C8), 121.8 (C4), 118.8 (C1b), 115.1 (C3b-C5b), 84.2 (BPin), 66.7 (C3c-C5c), 48.3 (C2c-C6c), 25.0 (BPin-Me). HPLC-MS (ESI): m/z calculated for $C_{25}H_{29}BN_2O_3S$ 448.20; $[M+H]^+$ found 449.10.

2. Radiochemistry

2.1 Manual synthesis of [^{18}F]PFSB

[^{18}F]Fluoride was produced using a PETtrace 890 cyclotron (GE Healthcare, Uppsala, Sweden) and delivered as a target wash in water. It was trapped onto a Sep-Pak Plus Light QMA carb cartridge (previously conditioned with a sequence of: 10 mL of KOTf aq 90 mg/mL, 10 mL of air, 10 mL of H_2O, 10 mL of air), dried with argon (10 mL passed through the cartridge) and eluted with a solution of TBAOTf in MeOH (10 mg/1 mL) to afford [^{18}F]TBAF. The resulting solution was aliquoted in 4 reaction vials and the solvent was evaporated at 90 °C. A stock solution of $Cu(OTf)_2$ in DMA was prepared (100 mg/mL). Each reaction mixture was prepared by diluting 25.5 µL of the stock solution in the chosen amount of DMA (510 µL for a and b; 499 µL for c and d). *n*-BuOH (60.0 µL) and pyridine (4.90 µL, 60 µmol for a and b; 16.0 µL, 200 µmol for c and d) were added. The solution was added to the precursor **67** (9.00 mg, 20.2 µmol for a and c; 4.50 mg, 10.1 µmol for b and d). Entries a-d refer to the parameters optimization discussed in the Results, Table 7. Each mixture was sonicated, added to the corresponding reaction vial and heated at 120 °C for 20 min. The reaction was quenched with 1 mL HCl 0.1 M and neutralized with 1 mL NaOH 0.1 M. 500 µL MeCN were added to avoid product precipitation. Reaction performance was evaluated by radioTLC (PE/EtOAc 2:1) and radioHPLC. Analytical HPLC conditions and chromatograms are reported in the Results, Figure 22.

2.2 Automated synthesis of [^{18}F]PFSB and [^{18}F]MFSB

A Sep-Pak Plus Light QMA carb cartridge (conditioned with a sequence of: 10 mL of KOTf aq 90 mg/mL, 10 mL of air, 10 mL of H_2O,

10 mL of air), Sep-Pak Plus Light Alumin N cartridge (prepared with 5 mL of H_2O), a Sep-Pak Plus tC18 and a Sep-Pak Light C18 (conditioned with 10 mL of EtOH and 10 mL of H_2O each) were installed in their corresponding positions in an FxNPro module (GE Healthcare, Münster, Germany).

$Cu(OTf)_2$ (2.40 mg, 6.72 µmol) was dissolved in 535.7 µL of DMA and *n*-BuOH (60.0 µL) and pyridine (4.30 µL, 53.8 µmol) were added. The solution was added to the **PFSB** precursor **67** (4.00 mg, 8.96 µmol) or the **MFSB** precursor **68** (4.00 mg, 8.92 µmol) and sonicated to afford the corresponding reaction mixtures.

[^{18}F]Fluoride was produced by a PETtrace 890 cyclotron (GE Healthcare), delivered into the module, trapped onto the QMA cartridge, and eluted into the reactor with a solution of TBAOTf in MeOH (10 mg/1 mL). The solvent was evaporated at 90 °C. The reaction mixture was added to the reactor and it was heated to 120 °C for 20 min. It was diluted with 10 mL of MeCN/ammonium formate buffer (25 mM, pH 8) 1:1 v/v and trapped on a stack of Alox and tC18 cartridges. The desired product was eluted with MeCN (3.4 mL for [^{18}F]**PFSB**; 2.8 mL for [^{18}F]**MFSB**) into tube 2, which was equipped with 25 mM ammonium formate (1.6 mL for [^{18}F]**PFSB**; 2.2 mL for [^{18}F]**MFSB**), and the resulting mixture was injected into the semipreparative HPLC. The radiolabeled products were purified using the following conditions: Luna 5 µm C8 (2) 100 Å 250 x 10 mm column (Phenomenex, Torrance, CA, USA); 68% MeCN in 25 mM ammonium formate at pH 8 (retention time ≈ 17 min) for [^{18}F]**PFSB**; 55% MeCN in 25 mM ammonium formate at pH 8 (retention time ≈ 12 min) for [^{18}F]**MFSB**; 6 mL/min.

The product peak was recovered and diluted with water (55 mL). It was trapped onto a C18 cartridge. It was washed with water (5 mL), eluted

with EtOH (0.5 mL), formulated with PBS (4.5 mL) and transferred into the product vial. Quality control was performed on 100 µL of the final product via analytical HPLC (gradient conditions and chromatograms are reported in the Results, Figure 22).

2.3 Synthesis of tritium-labeled radioligands

[^{3}H]PiB and [^{3}H]MODAG-001 were radiolabeled by RC Tritec AG (Teufen, Switzerland) with radiochemical purities > 99% for both radioligands and molar activity (A_m) of 0.8 GBq/µmol and 2.9 GBq/µmol, respectively. The products were dissolved in EtOH and stored at -80 °C until use.

[^{3}H]SIL26 was synthesized by reacting its *N*-acetylated phenolic precursor with [^{3}H]2-fluoroethyl(p-tolyl)benzenesulfonate (1.7 GBq/µmol, RC Tritec AG, Figure 18) according to the procedure described in [3]. The product was obtained with A_m: 1.7 GBq/µmol, RCY: 30%, RCP > 98%.

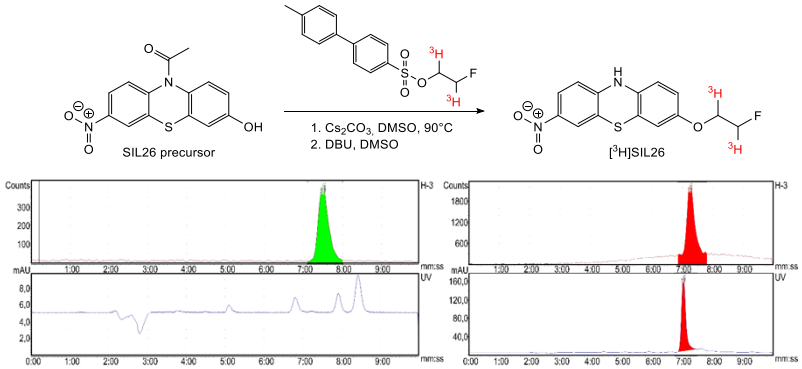

Figure 18. Reaction scheme for the tritium-labeling of SIL26 and radio-HPLC chromatograms of formulated [^{3}H]SIL26 (left) and co-injection with non-radioactive SIL26 (right). Analytical HPLC method: Luna 5 µm C18 (2) 100 Å 250 x 4.6 mm column, 50% MeCN in H_2O, 1 mL/min. Figure adapted from [3].

3. Biological evaluation

3.1 Calculation of BBB score and CNS MPO

All required properties (cLogP, TPSA, molecular weight, pKa, Table 1) were calculated via Chemicalize (ChemAxon, Budapest, Hungary) and entered into the calculation Excel tables provided in the literature. [153, 154]

*Table 1. Chemical properties required for the calculation of BBB score and CNS MPO for all non-ionic 2-styrylbenzothiazole-based compounds. N-morpholine derivatives **56a** and **64** (**MFSB**) exhibit the lowest cLogP and the highest CNS MPO within the library. BBB penetration was not investigated in DAP compounds. Table adapted from [4].*

#	cLogP	TPSA (A^2)	MW (g/mol)	pKa	Aromatic rings	Heavy atoms	Hydrogen bond acceptors	Hydrogen bond donors	BBB score	CNS MPO
42a	6.15	16.13	334.48	5.30	3	24	2	0	4.79	3.0
43a	5.48	25.36	350.48	5.30	3	25	3	0	4.90	3.3
44a	5.78	16.13	338.44	5.30	3	24	2	0	4.78	3.0
45a	6.15	16.13	334.48	5.31	3	24	2	0	4.79	3.0
46a	5.48	25.36	350.48	5.31	3	25	3	0	4.90	3.3
47a	5.78	16.13	338.44	5.30	3	24	2	0	4.78	3.0
48a	6.15	16.13	334.48	5.30	3	24	2	0	4.79	3.0
49a	5.48	25.36	350.48	5.30	3	25	3	0	4.90	3.3
50a (PFSB)	5.78	16.13	338.44	5.30	3	24	2	0	4.78	3.0
51a	6.15	16.13	334.48	5.31	3	24	2	0	4.79	3.0
52a	5.48	25.36	350.48	5.31	3	25	3	0	4.90	3.3
53a	5.78	16.13	338.44	5.30	3	24	2	0	4.78	3.0
54a	5.10	16.13	294.42	4.36	3	21	2	0	4.77	3.0
55a	6.16	16.13	346.49	5.37	3	25	2	0	4.76	3.0
56a	4.57	25.36	322.42	2.20	3	23	3	0	4.76	3.5
57a	5.15	16.13	338.49	3.50	3	23	2	0	4.62	3.0
58a	5.19	16.13	306.43	4.89	3	22	2	0	4.81	3.0
59a	5.00	16.13	338.44	4.44	3	24	2	0	4.68	3.0
60a	4.79	16.13	280.39	4.75	3	20	2	0	4.84	3.1
61	5.64	16.13	320.45	5.30	3	23	2	0	4.83	3.0
62	6.30	16.13	364.48	5.37	3	26	2	0	4.71	3.0
63	5.86	16.13	350.46	4.96	3	25	2	0	4.70	3.0
64 (MFSB)	4.71	25.36	340.42	2.26	3	24	3	0	4.73	3.4

3.2 Fibril binding assays

Saturation binding assays were performed on human recombinant αSYN and synthetic human $A\beta_{1-42}$ fibrils to determine K_d values of [^{3}H]SIL26, [^{3}H]MODAG-001 and [^{3}H]PiB. αSYN fibrils were diluted in PBS at 35 nM, 50 nM, and 180 nM respectively. Aβ fibrils were diluted at 1 µM for [^{3}H]SIL26 and [^{3}H]MODAG-001, and 2 µM for [^{3}H]PiB. They were incubated in 96-well plates (Ratiolab GmbH, Dreieich, Germany) with increasing concentrations of radioligand (up to 64 nM for [^{3}H]SIL26, up to 36 nM for [^{3}H]MODAG-001, and up to 56 nM for [^{3}H]PiB) in BSA buffer (30 mM Tris-HCl, 0.1% bovine serum albumin, 0.05% Tween20) to afford a total volume of 200 µL/well. Each tracer was incubated with the corresponding non-radioactive reference dissolved in DMSO (0.5 µM SIL26, 0.5 µM MODAG-001, 1.5 µM PiB) to calculate non-specific binding (NSB).

Competition binding assays against the tritium-labeled radioligands of choice were performed for the newly developed compounds from both libraries to determine their K_i values. A 1 mM stock solution in DMSO was prepared for each test compound. Increasing concentrations of the DAP hybrid compounds (0.06 – 2500 nM) competed against [^{3}H]SIL26 (7 nM for αSYN, 7 or 14 nM for $A\beta_{1-42}$) and 1 nM [^{3}H]MODAG-001 (for both αSYN and $A\beta_{1-42}$). Increasing concentrations of the 2-styrylbenzothiazole novel compounds (0.6 nM – 10 µM) competed against 6 nM [^{3}H]PiB and 1 nM [^{3}H]MODAG-001. The same fibrils concentrations as in the saturation binding assays were used.

The plates were shaked at 37 °C, 50 rpm for 2 h, filtered under vacuum and read-out as described in [177]. The detected signal was plotted against the increasing concentration values and data points were fitted via non-linear regression analysis in GraphPad Prism (GraphPad Software, Inc., Version 8.4.0, La Jolla, USA).

3.3 Autoradiography and immunohistochemistry

Post-mortem human brain slices with 10 µm thickness were provided by the Neurobiobank München (NBM, Munich, Germany) as described in Table 2. The use of the abovementioned samples in this study was approved by the ethics committee of the Faculty of Medicine, University of Tübingen (Ethics approval number: 813/2018BO2).

Table 2. Overview of the human brain tissues used in the autoradiography and IHC experiments. Table adapted from [4].

Cases	Region	Age at death (years)	Gender	PMI (hours)	LBD (Braak)	AD (Braak & Braak)	AD (Thal)	Pathology		
								αSYN	Aβ	pTau
MSA1	CB	64	F	52	0	I	1	+++	-	-
MSA2	CB	54	M	71	0	0-I	0	+++	-	-
Cerebellum ctrl	CB	66	F	27-39	0	I	3	-	-	-
PD	FC	79	F	26	6	IV	3	+++	++	+
AD	FC	70	M	24	0	VI	5	-	+++	+++
Frontal cortex ctrl	FC	64	F	39	0	0	0	-	-	-

The extent of pathology in each subject case was analyzed by Neurobiobank München and is indicated by the symbols "+" and "-". The number of "+" symbols indicates increasing pathology from low (+), moderate (++) to high (+++); "-" symbolizes the absence of pathology. Abbreviations: CB, cerebellum; Ctrl, control; F, female; FC, frontal cortex; M, male; PMI, postmortem interval; pTau, phospho-Tau.

After 1 h thawing and 25 min pre-incubation in BSA buffer at room temperature, the brain slices were incubated with 10 nM [^{18}F]**PFSB** or [^{18}F]**MFSB** for 1 h. For each sample, consecutive slices were incubated for 1 h with the corresponding non-radioactive compound (10 µM **PFSB** or **MFSB**) to determine NSB. All slices were washed in cold BSA buffer (3 x 10 min) and then dipped 3 times in cold deionized water. They were dried under an infrared lamp and exposed to a storage phosphor screen (Molecular Dynamics, Caesarea, Israel) for 18 h, which was then scanned in a phosphor imager (STORM 840, Molecular dynamics, Sunnyvale, CA, USA).

Four regions of interest (ROIs) were drawn in the relevant areas of each slice and one ROI was placed next to it for background

subtraction (ImageJ 1.8.0_172, National Institute of Health, Bethesda, MD, USA). [192] Specific binding (SB) was calculated as the difference of total binding – NSB.

Immunohistochemistry (IHC) was performed on the same slices, after storing them at -20 °C. They were fixed in 4.5% paraformaldehyde (PFA, SAV Liquid Production GmbH, Flintsbach am Inn, Germany) at room temperature for 20 min, washed in PBS (2 x 5 min), and incubated in the corresponding buffer (pre-heated – T > 90°C – sodium citrate buffer 10 mM pH 6 for 30 min at room temperature for αSYN pSer129; 97% formic acid for 10 min at room temperature for Aβ). The brain slices were washed, quenched for 20 min (1 mL quenching solution = 890 µL Tris-buffered saline (TBS), 100 µL MeOH, and 10 µL 30% H_2O_2), washed with TBS (2 x 5 min) and TBS-X (TBS supplemented with 0.1% Triton X-100 and 1% BSA) for 5 min. A mixture of TBS with 0.3% Triton X-100 and 10% normal goat serum was used for blocking (60 min, room temperature). The slices were incubated overnight at 4 °C with the primary antibody: anti-phosphorylated αSYN pSer129 monoclonal antibody (1:5000 in TBS-X, clone pSyn#64, 015-25191, Fujifilm Wako Chemicals, Neuss, Germany) was used for PD, MSA and control tissues; mouse anti-β-amyloid 17-24 antibody (1:6000 in TBS-X, clone 4G8, 800708, BioLegend, Amsterdam, The Netherlands) was used for AD tissue. [4] After washing with TBS-X (3 x 10 min) the brain slices were incubated with secondary antibody (EnVision+/HRP Dual Link Rabbit/Mouse, K406189-2, Agilent, Waldbronn, Germany) for 30 min at room temperature, washed in TBS-X (2 x 10 min) and TBS (1 x 10 min), and incubated with 3,3′-diaminobenzidine (1:50, Agilent, Waldbronn, Germany) for 10 min. They were washed with water (2 x 5 min), incubated in hematoxylin (Merck KGaA, Darmstadt, Germany) for 45 s

and then rinsed for 10 min with running tap water. The samples were washed in 70% EtOH (1 min), 95% EtOH (2 x 1 min), 100% EtOH (2 x 1 min) and xylene (2 x 2 min) and then mounted with Eukitt quick-hardening mounting medium (Fluka Analytical, Munich, Germany). The tissues thus prepared were scanned with NanoZoomer 2.0 HT (Hamamatsu Photonics K.K., Hamamatsu, Japan) at 40x magnification.

3.4 *In vivo* PET/MR imaging

The animal experiments were carried out in compliance to the European directives on the protection and use of laboratory animals (Council Directive 2010/63/UE) and the German animal welfare act and received approval from the local authorities (Regierungspräsidium Tübingen, R3/19G).

Healthy C57BL/6J female mice (20.3 ± 0.9 g; 9 weeks old) were purchased from Charles River Laboratories (Sulzbach, Germany) and maintained in our vivarium on a 12:12 hours light-dark cicle, at 22 °C with 40-60% humidity and were given free access to tap water and a standard diet.

1.5% isoflurane evaporated in 100% O_2 at 0.8 L/min was used to anesthetize the mice (n = 3). Their body temperature was kept at 37 °C via a feedback temperature control unit. One-hour dynamic acquisitions were performed on a microPET system (Inveon D-PET, Siemens, Knoxville, TN, USA) and divided into 39 time frames (12 × 5 s, 6 × 10 s, 6 × 30 s, 5 × 60 s and 10 × 300 s). The mice were injected intravenously with [^{18}F]**MFSB** (9.9 ± 0.6 MBq, A_m = 46.2 ± 2.5 GBq/µmol at time of injection) 5 s after the start of the PET acquisition. Attenuation correction was performed via a 13 min transmission measurement with a cobalt-57 point source. An anatomical MR scan

was acquired (7 Tesla MR scanner, ClinScan, Bruker Biospin, Ettlingen, Germany) by using a rat whole-body volume coil. A T2-weighted Turbo-RARE MRI sequence was employed (Paravision software 6.0.1, Bruker).

The PET data was reconstructed via the OSEM3D/SP-MAP reconstruction algorithm. It was co-registered to the MRI results and volumes of interest (VOIs) for each of the relevant organs were hand-drawn in PMOD (PMOD Technologies, Faellanden, Switzerland, Version 4.2) based on the MR data. VOIs of the brain regions were drawn based on the atlas provided by PMOD. The corresponding decay-corrected time-activity curves (TACs) were calculated for each VOI. Standardized uptake values (SUVs) were obtained as a ratio of the detected activity with the product of injected activity and weight: SUV = TAC (kBq/cc) / (inj. activity (kBq) * weight (g)).

Results

1. Design and development of a library of diarylpyrazoles

Fibril binding assays between the parent scaffolds demonstrated a reciprocal competition for αSYN fibrils, with SIL26 displacing [^{3}H]MODAG-001 with a K_i of 51.6 nM and MODAG-001 displacing [^{3}H]SIL26 with a K_i of 10.8 nM (Figure 19), corroborating the hypothesis of a shared binding site. With the aim of producing a novel compound with improved αSYN binding properties, two classes of DAP-based analogs were designed by combining the structures of the abovementioned parent scaffolds SIL and MODAG (Figure 16).

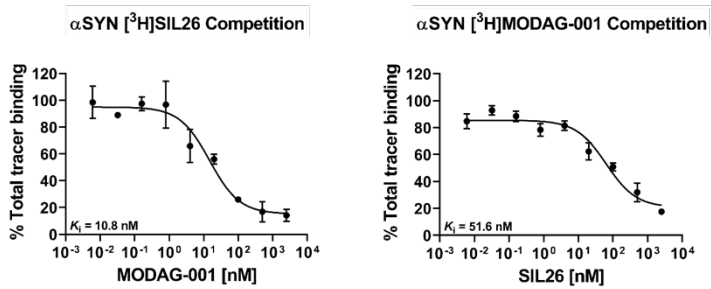

Figure 19. Competition between SIL26 and MODAG-001 for the binding to αSYN fibrils (three separate experiments per curve). K_i values were calculated based on the following K_d values: $K_{d\ SIL26}$ = 19.0 nM, $K_{d\ MODAG-001}$ = 4.4 nM. Figure adapted from [3].

3-Bromo-derivatives of SIL5 (**3**) and SIL6 (**5**) were produced via a $NiCl_2$-catalyzed NO_2-reduction into a primary amine followed by a bromination reaction, employing *t*-BuONO as nitrite source and $CuBr_2$ as bromine source (Scheme 1). [193, 194] $Pd(PPh_3)_4$-catalyzed cross-couplings of compounds **3** and **5** with diversely substituted *N*-THP-

protected 3-aryl stannylpyrazoles and the subsequent acidic deprotection of their products afforded a small library of novel DAP derivatives (Scheme 2, 3).

Competition binding assays against [^{3}H]SIL26 and [^{3}H]MODAG-001 were performed on human recombinant αSYN fibrils to assess their affinity and on synthetic $A\beta_{1-42}$ fibrils to investigate their potential αSYN/Aβ selectivity. The K_i values reported in Table 3 show a significant decrease in affinity to αSYN for all DAP hybrids compared to their parent scaffolds (mostly K_i > 400 nM). Interestingly, compounds **DAP1a-2c** exhibited an enhanced binding to Aβ, with K_i values in the range of 1 nM to 10 nM for most analogs (Table 3).

Table 3. Binding affinity of DAP hybrid compounds determined by [^{3}H]SIL26 and [^{3}H]MODAG-001 competition assays (mean K_i ± SEM, three data points). Table adapted from [3].

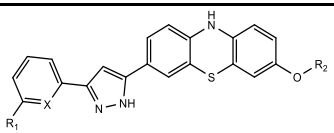

#	R_1	R_2	X	αSYN – K_i (nM)		Aβ – K_i (nM)	
				[^{3}H]SIL26	[^{3}H]MODAG-001	[^{3}H]SIL26	[^{3}H]MODAG-001
DAP1a	H	CH_3	CH	186.3 ± 144.9	289.3 ± 158.8	10.7[b]	10.5 ± 0.9
DAP1b	H	CH_3	N	90.1 ± 56.8	69.9 ± 14.9	7.6[b]	10.3 ± 0.8
DAP1c	F	CH_3	CH	> 400	> 400	1.0[b]	15.9 ± 2.4
DAP2a	H	CH_2CH_2F	CH	> 400	143.8 ± 49.5	25.8 ± 5.8[a]	7.7 ± 1.7
DAP2b	H	CH_2CH_2F	N	> 400	106.9 ± 31.4	65.8 ± 56.4[a]	12.2 ± 1.7
DAP2c	F	CH_2CH_2F	CH	> 400	212.2 ± 93.8	3.1 ± 2.1[a]	8.0 ± 1.3

[a] Two data points available. [b] Single data point available.

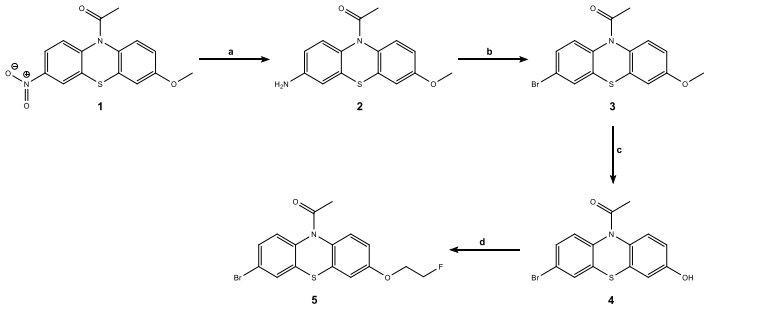

Scheme 1. Synthesis of phenothiazine-based building blocks: a) $NiCl_2 \cdot 6H_2O$, $NaBH_4$, $MeCN/H_2O$, r.t., 15 min; b) $CuBr_2$, t-BuONO, MeCN, 0 °C to r.t., 3 h; c) BBr_3 1 M in DCM, DCM, -78 °C to r.t., overnight; d) NaH, 1-bromo-2-fluoroethane, DMF, 0 °C to r.t., overnight; e) NH_4OAc 0.1% in MeOH, NBS, NIS, MeCN, r.t., 45 min; f) 3-methoxythiophenol, K_2CO_3, NMP, 100 °C, overnight; g) pyridine, acetic anhydride, r.t., 3 h. Scheme adapted from [3].

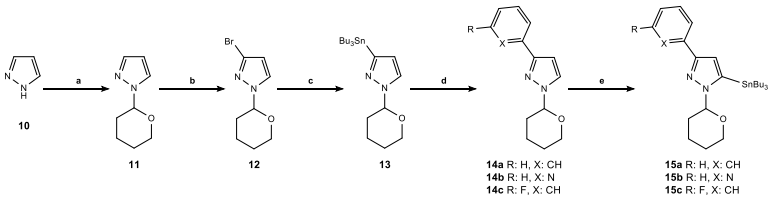

Scheme 2. Synthesis of pyrazole-based building blocks: a) DHP, TFA, reflux, 45 min; b) n-BuLi, Br_2, THF, -78 °C, 1 h; c) $(SnBu_3)_2$, $Pd(PPh_3)_4$, toluene, 100 °C, overnight; d) aryl bromide, $Pd(PPh_3)_4$, NMP, 100 °C, overnight; e) n-BuLi, $SnBuCl_3$, THF, -78 °C, 1 h. Scheme adapted from [3].

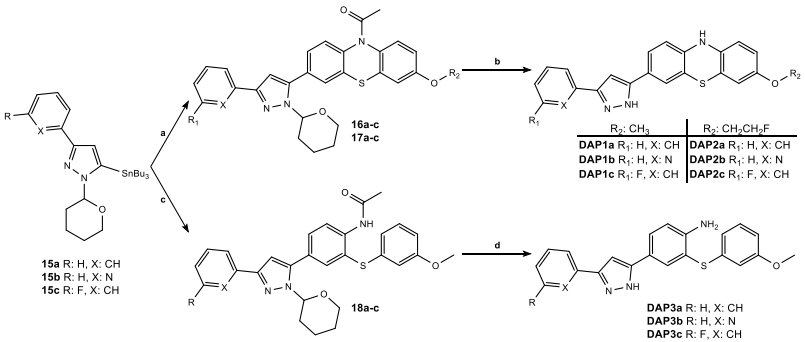

*Scheme 3. Synthesis of DAP hybrid compounds: a) **3** or **5**, $Pd(PPh_3)_4$, NMP, 90 °C, overnight; b) HCl 37%, MeOH/H_2O, 80 °C, 6 h; c) **9**, $Pd(PPh_3)_4$, DMF, 110 °C, overnight, d) HCl 37%, MeOH/H_2O, 80 °C, 6 h. Scheme adapted from [3].*

Based on the hypothesis that a successful interaction with the fibrils' binding site may be hampered by the constrained 3D conformation of the first set of DAP hybrid compounds, new analogs were designed with a focus on increasing their flexibility.

By adapting the NH_4OAc-catalyzed bromination strategy proposed by Das *et al*., [195] a sequential one-pot substitution of aniline employing *N*-bromosuccinimide and *N*-iodosuccinimide was performed to produce 2-iodo-4-bromoaniline (**7**, Scheme 1). The ring-opened analog (compound **9**) of the phenothiazine-based intermediate **3** was synthesized by further reaction with 3-methoxythiophenol and *N*-acetylation (Scheme 1). The previously established synthetic pathway was applied to generate a group of ring-open DAP hybrid compounds via $Pd(PPh_3)_4$-catalyzed cross-couplings followed by acidic deprotection (Scheme 3). As illustrated by the *in vitro* results reported in Table 4, αSYN fibril binding assays on **DAP3a-c** displayed a complete loss of competition against both tracers ([^{3}H]SIL26 and [^{3}H]MODAG-001). A significant decrease in affinity to $A\beta_{1\text{-}42}$ fibrils was detected as well.

Table 4. Binding affinity of ring-open DAP hybrid compounds determined by [^{3}H]SIL26 and [^{3}H]MODAG-001 competition assays (mean K_i ± SEM, three data points). Table adapted from [3].

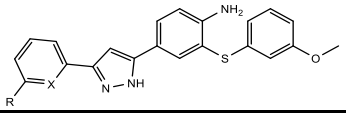

#	R_1	X	αSYN – K_i (nM)		Aβ – K_i (nM)	
			[^{3}H]SIL26	[^{3}H]MODAG-001	[^{3}H]SIL26	[^{3}H]MODAG-001
DAP3a	H	CH	no competition[a]	no competition	86.1[b]	> 400
DAP3b	H	N	no competition[a]	no competition	n.a.	> 400
DAP3c	F	CH	no competition[a]	no competition	n.a.	> 400

[a] Two data points available. [b] Single data point available.

2. Design and development of a library of 2-styrylbenzothiazoles

2.1 Synthesis of a 2-styrylbenzothiazol-based library and *in vitro* evaluation

Six sub-classes of 2-styrylbenzothiazole derivatives were designed to systematically introduce structural modifications on the parent scaffold and evaluate their impact on the affinity to αSYN fibrils (Figure 17). Three different substitutions (methyl-, methoxy-, fluoro-) were separately applied at the four available positions on the benzothiazole ring (compounds **42a-53b**). Analogs with a modified length of the π-system were developed as well, by removing the two carbon atoms connecting the two main moieties of the molecule (compounds **54a-b**) or including one additional double bond between them (compounds **55a-b**). Furthermore, derivatives with diverse groups substituting the anilinic nitrogen were synthesized (compounds **56a-60b**).

The fluorescent probe RB1, carrying a *N*-methylation on the benzothiazole ring, bears a permanent positive charge that would, as such, hinder its ability to cross the BBB. [196] Being brain-uptake an imperative feature for the *in vivo* imaging of neurodegeneration, each structural modification was also combined with non-methylated benzothiazoles.

Dedicated synthetic pathway were established for the variously substituted benzothiazoles (compounds **19a-31a**), depending on starting material availability. These intermediates were all *N*-methylated, employing methyl iodide or methyl nosylate, according to their reactivity (compounds **19b-31b**, Scheme 4). Diverse base-activated amine substitutions of 4-fluorobenzaldehyde afforded 4-

aminobenzaldehydes (compounds **32-38**), which were variously combined with the benzothiazole-moieties in condensation reactions producing 35 novel analogs, together with the parent scaffolds RB1 and RB2 (Scheme 4).

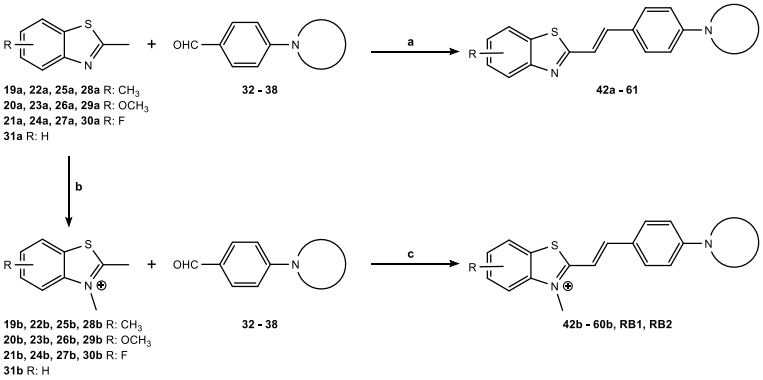

Scheme 4. General synthetic pathway for N-methylated and non-methylated 2-styrylbenzothiazoles: a) NaOH aq. 18 M, DMSO, r.t., 2 h to 24 h; b) MeI or MeONs, MeCN, 80 °C, overnight; c) EtOH, 80 °C, overnight. Scheme adapted from [4].

The analogs bearing alterations of the conjugated system length required dedicated synthetic pathways. 2-(4-bromophenyl)benzothiazole (**39**) underwent a $Pd(PPh_3)_4$ catalyzed amination and subsequent *N*-methylation to produce compounds **54a** and **54b** (Scheme 5). 4-piperidine benzaldehyde (**32**) and acetaldehyde under strongly acid conditions afforded 4-piperidine cinnamaldehyde (**40**), which generated the 1,3-butadiene derivatives **55a** and **55b** when coupled with the corresponding benzothiazole (Scheme 5).

In vitro screening of the compounds via [^{3}H]PiB competition assays on αSYN fibrils highlighted that binding affinity is significantly affected by structural modifications within the library (Table 5, 6), with substantial improvement in some analogs, displaying K_i values as low as 14.7 nM for the 6-methoxy derivative **49b**.

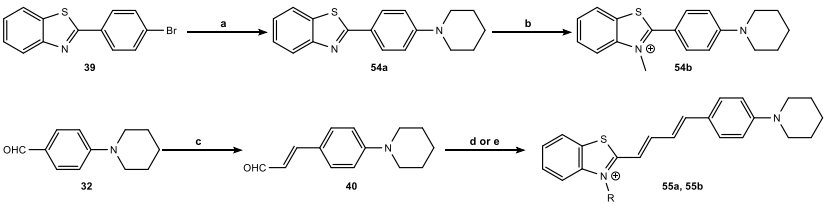

Scheme 5. Synthetic pathway for analogs with altered π-system length: a) $Pd(PPh_3)_4$, Cs_2CO_3, piperidine, toluene, 110 °C, 5 h; b) MeONs, chlorobenzene, 80 °C, overnight; c) H_2SO_4 conc., acetaldehyde, 0 °C, 1 h; d) ***31a****, DMSO, NaOH aq. 18 M, r.t., 3 h; e)* ***31b****, EtOH, 80 °C, overnight. Scheme adapted from [4].*

To suitably select the most promising compounds within the library, their binding properties were cross-matched with their predicted ability to afford brain-uptake. Two predictive parameters, BBB score and CNS MPO (Central Nervous System Multiparameter Optimization), were calculated according to the corresponding models available in the literature. [153, 154] All non-ionic analogs displayed values in the interval 4.62 – 4.90 for BBB score (range: 0 to 6) and 3.0 – 3.5 for CNS MPO (range: 0 to 5). As none of these predictive values stood out throughout the library (Table 5), they were not taken into account when selecting the lead compound.

The analogs with the most encouraging affinities to αSYN were further investigated in competition binding assays to Aβ fibrils. The lack of significant competition against the tritium-labeled tracer for all the tested compounds suggested the 2-styrylbenzothiazoles in this library may bear a notable αSYN/Aβ selectivity (Figure 20b, 21b).

Table 5. Binding affinity (mean K_i ± SEM, two data points) of non-methylated compounds determined by [^{3}H]PiB competition assays on αSYN fibrils and calculated values for BBB score and CNS MPO. Table adapted from [4].

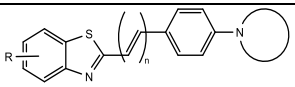

#	R	n	*N*-substitution	K_i (nM)	BBB score	CSN MPO
42a	4-CH_3	1	*N*-piperidine	134.8 ± 63.5	4.79	3.0
43a	4-OCH_3	1	*N*-piperidine	> 400	4.90	3.3
44a	4-F	1	*N*-piperidine	148.6 ± 38.0	4.78	3.0
45a	5-CH_3	1	*N*-piperidine	160.7 ± 72.7	4.79	3.0
46a	5-OCH_3	1	*N*-piperidine	158.1 ± 29.7	4.90	3.3
47a	5-F	1	*N*-piperidine	146 .8 ± 22.3	4.78	3.0
48a	6-CH_3	1	*N*-piperidine	223.9 ± 6.1	4.79	3.0
49a	6-OCH_3	1	*N*-piperidine	106.5 ± 3.6	4.90	3.3
50a (PFSB)	6-F	1	*N*-piperidine	25.4 ± 2.3[a]	4.78	3.0
51a	7-CH_3	1	*N*-piperidine	> 400	4.79	3.0
52a	7-OCH_3	1	*N*-piperidine	> 400	4.90	3.3
53a	7-F	1	*N*-piperidine	283.3[b]	4.78	3.0
54a	H	0	*N*-piperidine	73.3 ± 61.2	4.77	3.0
55a	H	2	*N*-piperidine	81.9 ± 15.6[a]	4.76	3.0
56a	H	1	*N*-morpholine	92.0 ± 30.3[a]	4.76	3.5
57a	H	1	*N*-thiomorpholine	138.9 ± 80.2	4.62	3.0
58a	H	1	*N*-pyrrolidine	73.4 ± 19.0[a]	4.81	3.0
59a	H	1	*N*-fluoropiperidine	99.8 ± 32.6[a]	4.68	3.0
60a	H	1	*N*-dimethylamine	> 400	4.84	3.1
61	H	1	*N*-piperidine	102.0 ± 68.5	4.83	3.0

[a] Three data points available. [b] Single data point available.

Table 6. Binding affinity (mean K_i ± SEM, two data points) of methylated compounds determined by [^{3}H]PiB competition assays on αSYN fibrils. Calculated BBB score and CNS MPO values are not displayed for this group of derivatives as their permanent charge would in any case hamper BBB penetration, making the prediction inapplicable. Table adapted from [4].

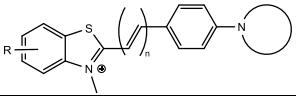

#	R	n	*N*-substitution	K_i (nM)
RB1	H	1	*N*-piperidine	> 400
RB2	H	1	*N*-(*N*-methyl)piperazine	> 400
42b	4-CH_3	1	*N*-piperidine	60.0 ± 23.9
43b	4-OCH_3	1	*N*-piperidine	52.6 ± 18.3
44b	4-F	1	*N*-piperidine	> 400
45b	5-CH_3	1	*N*-piperidine	72.2 ± 12.4
46b	5-OCH_3	1	*N*-piperidine	95.2 ± 67.7
47b	5-F	1	*N*-piperidine	351.7 ± 83.5
48b	6-CH_3	1	*N*-piperidine	20.3 ± 3.5
49b	6-OCH_3	1	*N*-piperidine	14.7 ± 5.1
50b	6-F	1	*N*-piperidine	189.5 ± 145.9
51b	7-CH_3	1	*N*-piperidine	147.6 ± 83.7
52b	7-OCH_3	1	*N*-piperidine	205.5 ± 28.2
53b	7-F	1	*N*-piperidine	> 400
54b	H	0	*N*-piperidine	> 400
55b	H	2	*N*-piperidine	19.9 ± 3.1
56b	H	1	*N*-morpholine	> 400
57b	H	1	*N*-thiomorpholine	> 400
58b	H	1	*N*-pyrrolidine	101.7 ± 43.0
59b	H	1	*N*-fluoropiperidine	> 400
60b	H	1	*N*-dimethylamine	> 400

2.2 Structural optimization

With the aim of further optimizing the binding to αSYN fibrils, the structural features which stood out for particularly favoring the affinity were combined to generate additional analogs. The 6-fluoro substitution of the benzothiazole-moiety was found to improve K_i values, together with providing a site for fluorine-18 labeling. Additional selected features were a longer π-system (n = 2) and the *N*-pyrrolidine substitution. The combination of these moieties afforded compounds **62** and **63** (Figure 20a). Although the selectivity over Aβ remained favorable (Figure 20b), a decreased affinity to αSYN fibrils ($K_{i\,\mathbf{62}}$ = 213.9 ± 121.5 nM, $K_{i\,\mathbf{63}}$ = 85.0 ± 41.0 nM) was detected in [^{3}H]PiB competition binding assays.

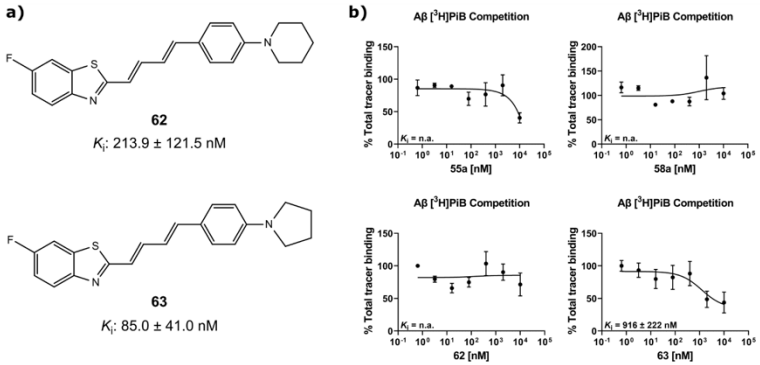

*Figure 20. a) Structure of compounds combining the selected promising features and their αSYN binding affinity (mean K_i ± SEM, three data points) determined by [^{3}H]PiB competition assays; b) competition binding assays on Aβ fibrils for compounds **55a**, **58a**, **62**, **63**. Figure adapted from [4].*

The structural optimization process also focused on the improvement of the pharmacokinetic profile. In fact, most compounds within the library exhibited a cLogP ≥ 5.5 (Table 1), raising a concern on their lipophilicity and therefore prompting us to develop a more hydrophilic derivative. For this purpose, the *N*-morpholine moiety was chosen due

to the comparable affinity displayed by compound **56a** as to its *N*-piperidine analog **61**, as well as the enhanced cLogP (4.57, Table 1) and CNS MPO (3.5, Table 1).

Within the first set of analogs, compound **50a** (**PFSB**) was selected for radiolabeling and further biological evaluation. Therefore, 4-morpholinebenzaldehyde (**33**) was reacted with the 6-fluorobenzothiazole (**27a**) to produce its analog **MFSB** (**64**, Figure 21a). Competition binding assays against [^{3}H]PiB showed affinity to αSYN fibrils was not only comparable to **PFSB** but enhanced by a 2.5 factor (K_i = 10.3 ± 4.7 nM). The incorporation of a different moiety did not affect αSYN/Aβ selectivity (Figure 21b).

In order to conduct a SAR evaluation of the full library and identify the most favorable structural features, all fibril binding assays were performed in competition with the benzothiazole-based radioligand [^{3}H]PiB. The use of a non-selective radioligand allowed for the investigation of the compounds interaction with both αSYN and Aβ fibrils. However, the study was lacking a less scaffold-related assessment of the binding affinity of the lead compounds. [^{3}H]MODAG-001, being the current gold-standard for αSYN preclinical imaging (K_d = 0.6 ± 0.1 nM), [177] was employed as the radiolabeled competitor. Both **PFSB** and **MFSB** displayed moderate to good competition for αSYN fibrils, with **MFSB** showing a 4.6-fold higher affinity ($K_{i\ \mathbf{PFSB}}$ = 142.1 ± 16.9 nM, $K_{i\ \mathbf{MFSB}}$ = 30.8 ± 10.5 nM, Figure 21c).

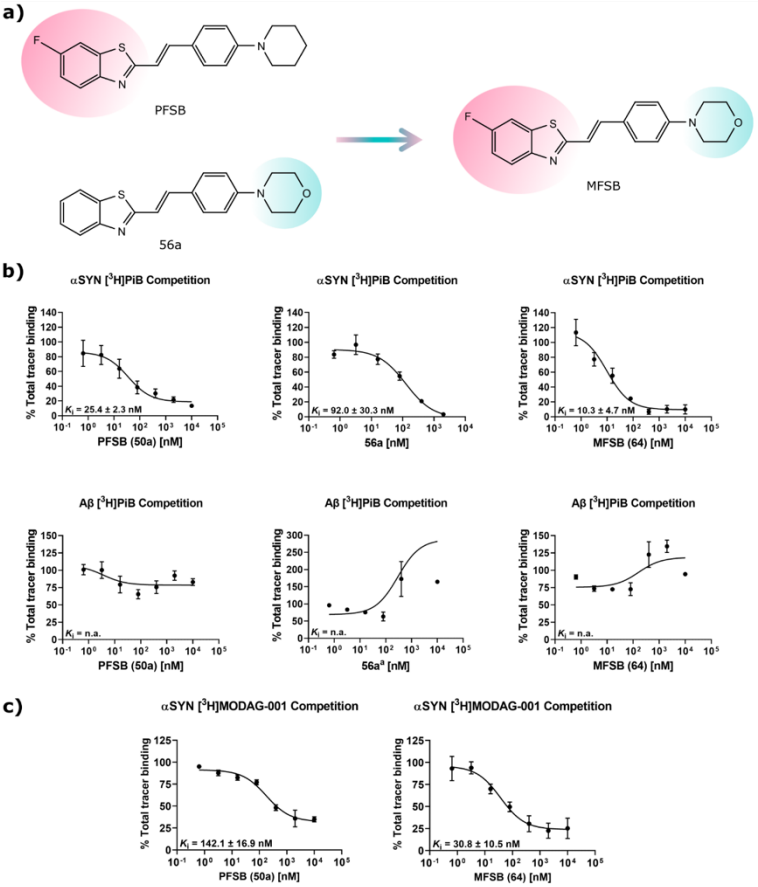

*Figure 21. a) Development of the less lipophilic analog **MFSB**; b) binding affinity of **PFSB**, **MFSB,** and **15a** to αSYN and Aβ fibrils determined by [^{3}H]PiB competition assays (three repetitions each, [a] two repetitions), c) competition of **PFSB** and **MFSB** with [^{3}H]MODAG-001 for αSYN binding. Figure adapted from [4].*

2.3 Radiolabeling of [^{18}F]PFSB and [^{18}F]MFSB

PFSB was selected from the first set of analogs as a lead compound to be radiolabeled and further investigated. The 6-bromo-derivative **65**, synthesized according to general procedure J (Scheme 4), underwent a Pd(dppf)Cl_2-catalyzed borylation to afford the pinacol boronate precursor **67** (Scheme 6). A CMRF procedure was established. Standard conditions were applied to manual radiolabeling experiments, aiming at the optimization of the amount of precursor and pyridine (Table 7), while employing a constant amount of $Cu(OTf)_2$, *n*-BuOH and DMA. Precursor load displayed no significant impact on the radiochemical conversion (RCC), hence a lower amount was preferred due to the compound's poor solubility. As the reaction efficiency was negatively affected by an increased pyridine concentration, the values from entry (b) were selected as a starting point for the automation process (precursor 10 µmol, pyridine 60 µmol, Table 7). The automated radiolabeling of [^{18}F]**PFSB** afforded the product with a radiochemical yield (RCY) of 5.8 ± 1.3% and A_m of 36.5 ± 8.5 GBq/µmol (n = 3).
The precursor synthesis (**66**) and automated radiolabeling of the *N*-morpholine analog [^{18}F]**MFSB** was carried out according to the same procedure (Scheme 6), to produce the tracer with RCY of 11.6 ± 2.9% and A_m of 41.2 ± 12.0 GBq/µmol (n = 3). Analytical results for both tracers are illustrated in Figure 22.

*Table 7. Optimization of CMRF of [^{18}F]**PFSB**: variation of the amount of precursor and pyridine and corresponding RCC. The amount of $Cu(OTf)_2$, n-BuOH and DMA remained constant in all experiments. Table adapted from [4].*

#	Precursor 67 (µmol)	Pyridine (µmol)	RCC (%)
a	20	60	7.6
b	10	60	7.0
c	20	200	2.4
d	10	200	4.0

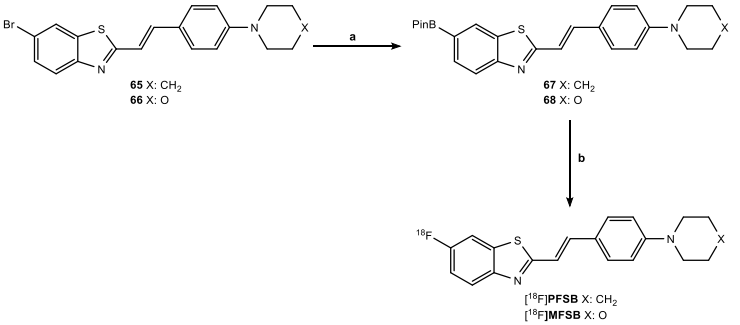

Scheme 6. General synthetic pathway for the synthesis of BPin precursors and fluorine-18 labeling: a) B_2Pin_2, KOAc, Pd(dppf)Cl_2, DMF, 100 °C, 45 min; b) Cu(OTf)$_2$, pyridine, [^{18}F]TBAF, n-BuOH 10% in DMA, 120 °C, 20 min. Scheme adapted from [4].

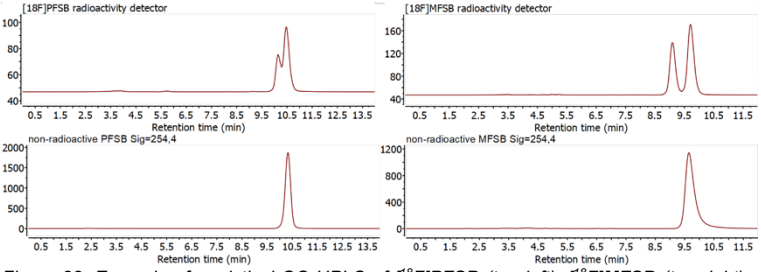

*Figure 22. Example of analytical QC HPLC of [^{18}F]**PFSB** (top left), [^{18}F]**MFSB** (top right) and their non-radioactive reference compounds (bottom left and right) using a Luna 5 µm C18 (2) 100 Å 250 x 4.6 mm column. Isocratic method: 88% MeCN in 25 mM ammonium formate at pH 8 for [^{18}F]**PFSB**; 72% MeCN in 25 mM ammonium formate at pH 8 for [^{18}F]**MFSB**; 1 mL/min. The ratio between the two peaks (retention time ≈ 10.1 - 10.5 min and 9.1 - 9.7 min, respectively) is dependent on the E/Z isomer ratio.*

2.4 *In vitro* autoradiography and *in vivo* PET imaging

To validate the binding profile observed in the fibril binding assays, the two radioligands [^{18}F]**PFSB** and [^{18}F]**MFSB** were parallelly evaluated in *in vitro* autoradiography experiments on human brain slices. The *N*-piperidine tracer clearly exhibited affinity to areas bearing αSYN pathology, showing high SB in MSA sections (Figure 23a), with a ratio

of 3.94 ± 0.30 in signal intensity when compared to the control section from the same brain area (Table 8, Figure 23b). Importantly, the experiment corroborated the desirable αSYN/Aβ selectivity, as no increased binding was reported in the regions of the AD sample where a dense presence of Aβ plaques was identified via IHC (AD/frontal cortex SB ratio: 1.06, Table 8). Despite the encouraging results, NSB to the white matter remained a pending issue in all sections (Figure 23a).

The evaluation of the less lipophilic [^{18}F]**MFSB** was expected to decrease NSB. Instead, the high binding to the white matter area hampered the accurate quantification of the disease/control SB ratios, resulting in only slightly intensified signal in synucleinopathies patients' sections (MSA and PD) compared to their corresponding controls (cerebellum and frontal cortex, respectively). Although hindered by NSB, the autoradiography experiment investigating [^{18}F]**MFSB** validated the selective αSYN binding of the novel 2-styrylbenzothiazoles as it confirmed the lack of Aβ binding in the grey matter of the AD section (Figure 23).

*Table 8. Quantitative analysis of in vitro autoradiography of [^{18}F]**PFSB** and [^{18}F]**MFSB**. Table adapted from [4].*

SB disease/SB control	[^{18}F]**PFSB**	[^{18}F]**MFSB**
MSA1/ctrl – cerebellum	3.73	1.20
MSA2/ctrl – cerebellum	4.15	1.27
PD/ctrl – frontal cortex	1.51	1.18
AD/ctrl – frontal cortex	1.06	1.03

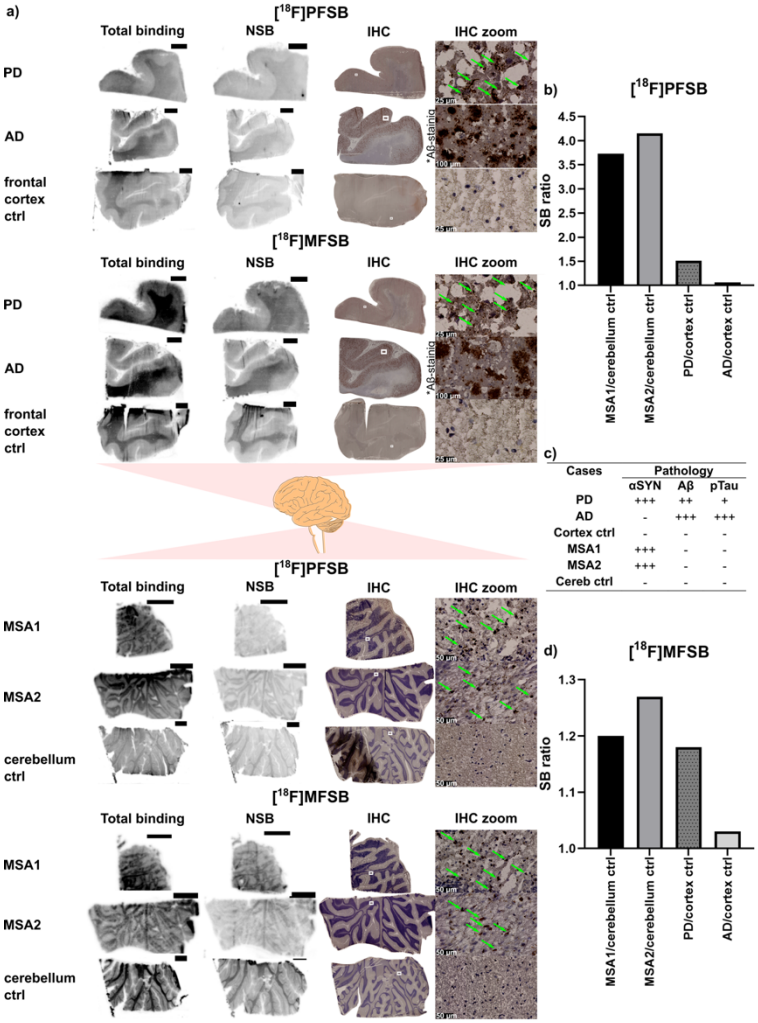

*Figure 23. In vitro autoradiography of [^{18}F]**PFSB** and [^{18}F]**MFSB** on human brain slices: a) total binding and non-specific binding on consecutive slices for each case and corresponding IHC with αSYN-staining (MSA, PD, and Ctrl tissues) and Aβ-staining (AD tissue); pathological aggregates are highlighted by arrows; scale bar in autoradiography samples: 0.5 cm; b) quantitative analysis of [^{18}F]**PFSB** via $SB_{disease}/SB_{ctrl}$ ratio; c) the extent of pathology in each subject case, indicated by the symbols "+" and "-"; the number of "+" symbols indicates increasing pathology from low (+), moderate (++) to high (+++); "-"*

*symbolizes the absence of pathology; d) quantitative analysis of [^{18}F]**MFSB** via $SB_{disease}/SB_{ctrl}$ ratio. Figure adapted from [4].*

In vivo experiments were carried out to evaluate the pharmacokinetic profile of the novel *N*-morpholine radioligand. Three healthy mice were injected with [^{18}F]**MFSB** and underwent 60 min dynamic PET scans with subsequent MRI. Although slow brain-uptake and unsatisfactory wash-out were observed, the tracer successfully crossed the BBB (Figure 24).

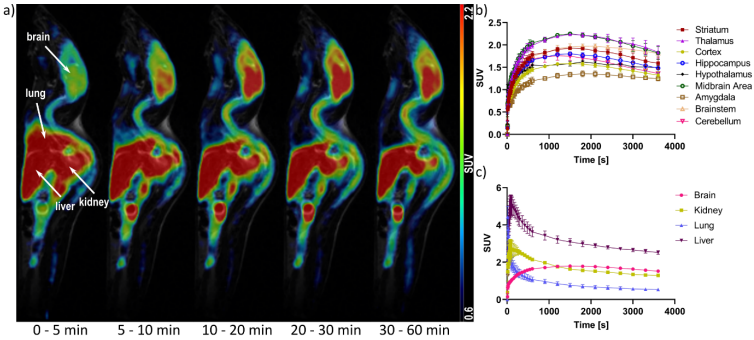

*Figure 24. In vivo evaluation of [^{18}F]**MFSB** pharmacokinetic profile: a) whole-body PET/MR sagittal images at different time points; b) TACs in brain regions; c) TACs of whole brain, kidney, lung, and liver. Figure adapted from [4].*

Discussion

1. Design and development of a library of diarylpyrazoles

The hypothesis that the application of the drug design approach of molecular hybridization to the SIL and MODAG scaffolds could result in enhanced binding properties was not validated by the *in vitro* findings from competition binding assays against [^{3}H]SIL26 and [^{3}H]MODAG-001. All analogs from the first set (**DAP1a-2c**) displayed significantly higher K_i values than both parent scaffolds, ranging from a 6-fold increase compared to SIL26 up to a 117- to 848-fold raise compared to MODAG-001. [162, 177]

In their SAR studies on the DPP library, Wagner *et al*. recognized a loss of the aggregation inhibitor activity when transferring the bromo-substitution from the *meta* to the *ortho* position. [174] This observation highlighted the relevance of a planar conformation in suitable αSYN ligands. These findings may justify the little affinity exhibited by DAP hybrids: when these relatively large compounds approach the binding site, the constrained structure of phenothiazines may hamper a successful interaction by interrupting the linearity of the two moieties bound to the pyrazole. Based on this hypothesis, an enhancement of structural flexibility was pursued.

The energy minimization of the 3D structure of **DAP1a** and **DAP3a** revealed a significant alteration of the molecules' most stable conformation (Figure 25). Furthermore, the replacement of an heteroaromatic amine with an aniline resulted in an electronic change as well. Overall, compounds **DAP3a-c** bear very different properties

than the previously investigated analogs. However, these modifications failed to improve their affinity to αSYN but instead impaired the binding.

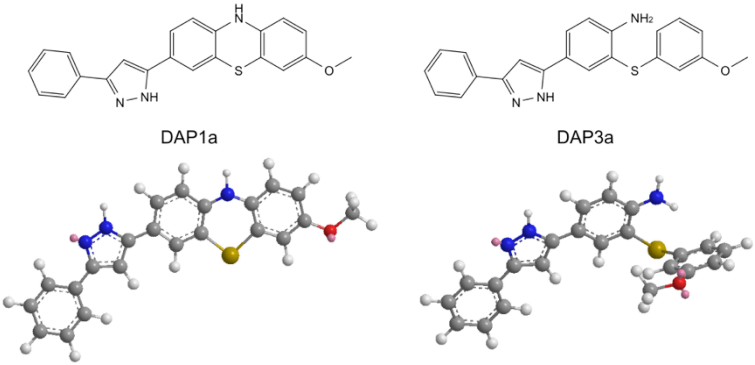

*Figure 25. Predicted 3D structure of **DAP1a** and **DAP3a** (MM2 energy minimization calculated by Chem3D 20.1, PerkinElmer Informatics). Figure adapted from [3].*

The *in vitro* evaluation of DAP hybrid compounds did not corroborate the hypothesis of a shared binding site for the SIL and the MODAG scaffolds, as suggested by their reciprocal displacement in competition binding assays observed both in this study (Figure 19) and the previous literature. [177] It can be speculated that the two classes of compounds interact with distinct binding sites partially overlapping with each other, resulting in the detected competition. This leads to the hypothesis that, to achieve a successful binding, a different molecular hybridization strategy should be pursued, such as a larger overlap of the parent scaffolds generating a smaller compound or the implementation of a linker connecting the two moieties.

Furthermore, due to starting material availability, a direct comparison with the MODAG-001 scaffold was not performed: it cannot be excluded that the *para*-localization of the pyridine-like nitrogen and a *meta*-bromo-substitution may produce significantly different results.

An additional concern involves the overall size of the DAP analogs. This interpretation was prompted by a recent ssNMR study

investigating the interaction of anle138b with αSYN fibrils where the most stable mode was described as the end-to-end filling of a tubular cavity. [197] The novel hybrid compounds may be too bulky to afford a successful binding.

As opposed to the original aim of this study, compounds **DAP1a-2c** displayed a favorable binding to Aβ fibrils, raising an interest for further evaluation in this regard. Aβ-targeting PET tracers with comparable or greater affinities are already established for clinical employment (flutemetamol: K_i = 0.74 ± 0.38 nM, florbetaben: K_i = 6.70 ± 0.30 nM, florbetapir: K_d = 3.72 ± 0.30 nM) [103-105] but DAPs may be attractive for their potential theranostic profile. Dao *et al*. developed a library of rhodamine-substituted phenothiazine-derivatives which proved capable of inhibiting the aggregation of $A\beta_{1-42}$ fibrils ($IC_{50\ 4a1}$ = 0.67 ± 0.02 μM) as well as inducing the disaggregation of preformed fibrils ($IC_{50\ 4a1}$ = 0.82 ± 0.10 μM). [198] The partial overlap of the DAP's overall structure with these fluorescent probes (Figure 26) leads to the hypothesis of a shared biological profile, suggesting DAPs may be relevant to the treatment of AD.

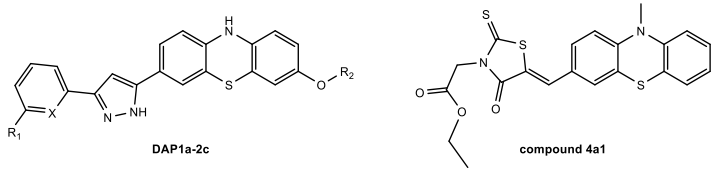

Figure 26. Comparison of the general structure of phenothiazine-based DAP hybrids with the structure of the theranostic compound 4a1 developed by Dao et al. [198]

The open-ring derivatives **DAP3a-c** exhibiting a drastic decrease in binding affinity to Aβ fibrils pointed out the critical impact of the 3D conformation in the design of new ligands aimed at differentiating among misfolded proteins.

2. Design and development of a library of 2-styrylbenzothiazoles

2.1 Synthesis of a 2-styrylbenzothiazol-based library and *in vitro* evaluation

Gaur *et al*. carried out the *in vitro* titration of RB1 and RB2 solutions with αSYN fibrils and assessed the subsequently increased fluorescence intensity, highlighting that RB1 selectively binds to αSYN. Instead, its *N*-methylpiperazine analog RB2 exhibited a two orders of magnitude reduction of the binding affinity. [172] Although [^{3}H]PiB competition binding assays detected only a moderate-to-low affinity, our results were overall consistent with the previous literature, being the RB1/RB2 ratio unvaried ($K_{i\text{-}RB1}$ = 480.8 nM, $K_{i\text{-}RB2}$ = 333.5 μM).

From the general evaluation of the binding properties of all compounds within the library, some SAR-based guidelines were identified. Structural modifications were found to unequally affect the interaction of ionic and non-ionic 2-styrylbenzothiazoles with αSYN fibrils. Methyl- and methoxy-substituents on the *N*-methylated benzothiazoles granted similar outcomes for each substitution position, whereas their corresponding fluoro-substituted derivatives afforded higher K_i values. A shorter π-system presented with a significantly decreased affinity (**54b**), while the insertion of an additional double bond enhanced it to a K_i < 20 nM (**55b**). A common trend observed in both *N*-methylated and non-ionic compounds identified 6-substituted benzothiazoles as the most favorable position for affinity, as opposed to their 7-substituted analogs affording the lowest binding.

In non-ionic analogs, alterations of the π-system length did not substantially impact the affinity. Furthermore, all groups replacing the

N-piperidine moiety (**56a-59a**), except for the *N*-dimethyl substitution (**60a**), afforded K_i values comparable to the parent scaffold **61**. These results were in agreement with the findings from a recent study on ThT-based fluorophores: Needham *et al*. applied a similar variety of *N*-substituting groups and detected an analogous trend within non-cationic compounds, along with the significant affinity reduction in their *N*-methylated analogs that 2-styrylbenzothiazoles displayed as well. [199]

The different impact structural modifications had on neutral and cationic analogs may be related to the configuration of their double bond. The former group appears as a mixture of E- and Z-isomers, whereas the latter, being provided by a different procedure, preferentially displays a Z configuration, as highlighted by the corresponding ^{1}H NOESY NMR spectra (Figure 27). Analogous alterations in binding affinity were identified by Chu *et al*. in the E/Z stereoisomers of their indolinone-derivatives. [167]

Based on the abovementioned SAR analysis, only non-ionic compounds were further pursued: the *N*-methylation impacts how coexisting structural modifications affect the binding but it does not induce an affinity improvement per se, while the permanent charge precludes BBB penetration. [196]

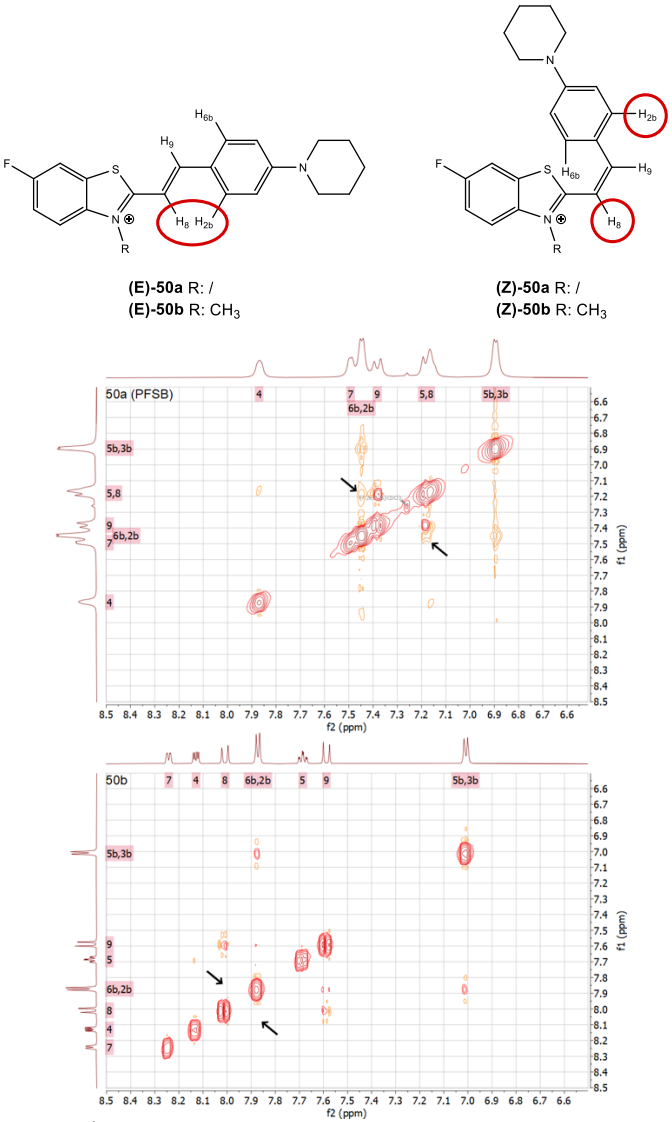

*Figure 27. 2D ^{1}H NOESY NMR spectra of **PFSB** (**50a**) and **50b**. In the top spectrum, a weak interaction between H_8 and $H_{2b}H_{6b}$ shows the sample is a mixture of (E)-**50a** and (Z)-**50a**. Such interaction is not detected in the second spectrum, highlighting (Z)-**50b** as the preferential configuration for the N-methylated compound. Figure adapted from [4].*

The BBB score and CNS MPO predicted values calculated for the neutral analogs were in all cases above a threshold of suitable properties, [153, 154] indicating they were expected to reach the brain. As no substantial divergence was identified among the derivatives, these parameters did not affect the selection of a lead compound.

Analogs **50a**, **55a**, **56a** and **58a** stood out as the most promising αSYN ligands. Their affinity to $A\beta_{1-42}$ fibrils was investigated and none of them showed significant competition against [^{3}H]PiB (Figure 20b, 21b). Consistent binding curves producing a mean K_i of 161.3 ± 4.7 nM for the competition between [^{3}H]PiB and its non-radioactive analog validated the reliability of the assay. These findings indicated 2-styrylbenzothiazole potentially carry a high αSYN/Aβ selectivity, prompting further validation of their properties by investigation of the direct interaction of radiolabeled compounds with human brain samples.

Mallesh *et al*. recently developed a set of benzothiazole-based fluorescent probes demonstrating modest affinity to Aβ and no αSYN binding. [200] Their extensive structure similarity with the compounds herein investigated (Figure 28) highlights once again the difficulty of discriminating among neurodegeneration-associated misfolded proteins.

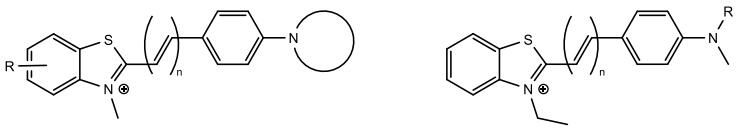

Figure 28. General structure of 2-styrylbenzothiazoles investigated in this study (left) and general structure of RM compounds exhibiting Aβ binding (RM-27 and RM-28, [200], right).

2.2 Structural optimization

The combination of favorable features into compounds **62** and **63** failed to afford enhanced binding properties and highlighted the irregularity of affinity fluctuations induced by structural alterations on the 2-styrylbenzothiazole scaffold. The replacement of a benzothiazole moiety with its 6-fluorosubstituted analog produced a significant K_i decrease for **PFSB** compared to its analog **61**, whereas it generated a ~ 3-fold reduction of affinity for the pair **55a**-**62**. Similarly, the combination of the *N*-pyrrolidine substitution with a 6-fluorobenzothiazole and a 1,3-butadiene moiety in compound **63** led to a minor affinity decrease compared to its parent compound **58a** but no substantial discrepancy from its non-fluorinated *N*-piperidine analog **55a** was observed. With a focus on the anilinic nitrogen substitution, the K_i values exhibited by analogs **62** and **63** aligned with the trend outlined both by the main library (Table 5, 6) and the previous literature: [199] *N*-pyrrolidine derivatives exhibit enhanced affinities compared to their corresponding analogs bearing diverse *N*-substitutions.

Several studies researching αSYN ligands found the incorporation of a 1,3-butadiene moiety into the π-system often favors the interaction. In the library developed by Chu *et al*., K_i values were consistently reduced by the replacement of indolinones with indolinone-dienes. [167] Similarly, binding affinities were gradually improved in the n = 1, 2, 3, 4 series of chalcone derivatives from Ono *et al*. [180] A possible explanation for this trend was provided by a study from Hsieh *et al*. highlighting the αSYN affinity of a group of ligands being enhanced consequently to a broadened intramolecular distance between hydrogen bond acceptors. [181] Nonetheless, while the distance between the nitrogen atoms in our scaffold does affect the K_i values

within our library, our results indicate that this factor alone does not afford improved binding affinities per se.

The structural optimization focusing on the pharmacokinetic properties afforded the *N*-morpholine analog **MFSB** which exhibited not only a considerably decreased lipophilicity but an enhanced affinity as well. The binding competition detected for both lead compounds, **PFSB** and **MFSB**, against the validated αSYN ligand [^{3}H]MODAG-001 corroborates the potential of 2-styrylbenzothiazoles as a promising scaffold with an attractive affinity and a notable αSYN/Aβ selectivity.

2.3 Radiolabeling of [^{18}F]PFSB and [^{18}F]MFSB

The radiofluorination of benzothiazole moieties is frequently addressed by the use of prosthetic groups, typically [^{18}F]fluoroethyl tosylate affording fluoroethoxy-substituted products. [201, 202] The first direct fluorine-18 labeling of benzothiazoles was reported by Lee *et al*., who described the synthesis of diaryliodonium salt precursors and their late-stage radiolabeling (Figure 29). However, this procedure involved the employment of highly unstable hydroxy(tosyloxy)iodoarenes for the precursor synthesis and required the use of a radical scavenger (2,2,6,6-tetramethylpiperidinyloxyl) as well as microwave irradiation to provide acceptable RCCs. [203]

The substrate scope investigation carried out by Taylor *et al*. revealed CMRF successfully affords [^{18}F]6-fluorobenzothiazoles, showing RCC values up to 36% within the tested compounds. [204] Prompted by this favorable results, the CMRF strategy was selected for the radiolabeling of [^{18}F]**PFSB** and [^{18}F]**MFSB**. The DoE-optimized conditions reported by Bowden *et al*. [96] were adopted as a starting point for the establishment of a radiosynthetic procedure.

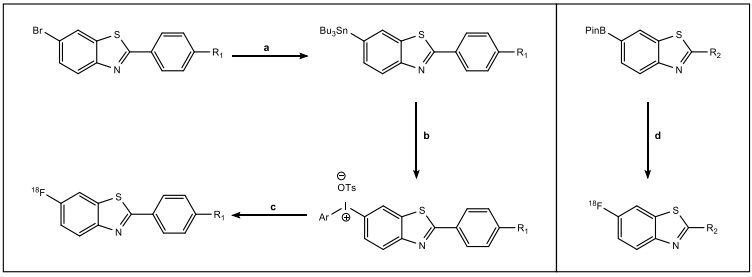

Figure 29. Comparison of the late-stage direct fluorine-18 labeling procedures described by Lee et al. (left) and Taylor et al. (right). [203, 204] Reaction conditions: a) Sn_2Bu_6, Pd(0), THF, 85 °C, 8 h; b) Koser's reagent, MeCN, r.t., 12 h; c) $nBu_4N[^{18}F]F$, MeCN, TEMPO, microwave (100 W), 6 min; d) $[^{18}F]KF/K_{222}$, $[Cu(OTf)_2(py)_4]$, DMF, 110 °C, 20 min.

The set up of an automated process pointed out radiochemical purity (RCP) issues, demanding for additional troubleshooting. The scarce solubility of the lipophilic [^{18}F]**PFSB** required the use of particularly high percentages of organic solvents throughout all transferring and purification steps, with a 75% MeCN in ammonium formate solution as preparative-HPLC eluent, which hampered a successful isolation of the final product. The replacement of a standard C18 reverse-phase HPLC column with a C8 column allowed for a decreased amount of MeCN (68%) without broadening the retention time, affording a more effective separation of polar impurities such as unreacted fluoride. Further SPE purification was implemented before the HPLC step, with a Sep-Pak Plus Light Alumin N cartridge aimed at trapping [^{18}F]F^- and a Sep-Pak Plus tC18 long-body cartridge providing a preliminary separation of potential byproducts. For the automated synthesis of [^{18}F]**PFSB** RCP was optimized up to 89.7 ± 1.5 (Figure 30).

The application of the same radiolabeling procedure to the less lipophilic [^{18}F]**MFSB** proved less critical: MeCN was reduced to 55% of the preparative-HPLC eluent mixture, allowing for a more efficient separation, with RCP values up to 99.3% (Figure 30).

Despite the room for improvement on RCP, RCC and overall RCY, the fluorine-18 labeling approach herein proposed provides a simple procedure which affords a sufficient amount of radioactive compound to be used for the desired experiments.

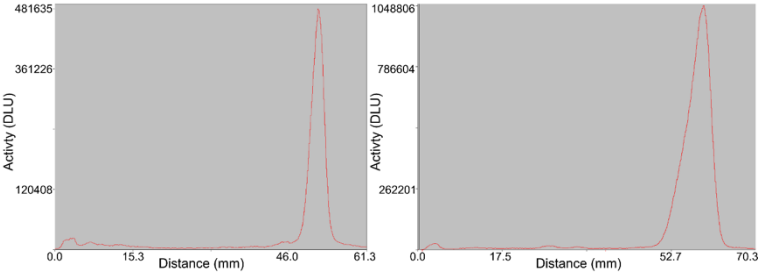

*Figure 30. Example of radioTLC of [^{18}F]**PFSB** (left, eluent: PE/EtOAc 2:1) and [^{18}F]**MFSB** (right, eluent: PE/EtOAc 1:1). Figure adapted from [4].*

2.4 *In vitro* autoradiography and *in vivo* PET imaging

The results from the *in vitro* evaluation of both radioligands [^{18}F]**PFSB** and [^{18}F]**MFSB** via autoradiography on human brain sections supported the binding profile preliminary outlined by fibril competition assays: both tracers successfully bound to MSA and PD tissue containing αSYN pathology, while showing no interaction with Aβ plaques. Despite the reduction of lipophilicity in the *N*-morpholine radioligand, NSB remained an unsolved issue, hindering the accurate quantification of pathology-associated signal in the experiment evaluating [^{18}F]**MFSB**. This limitation resulted in an unsatisfactory ratio between SB in pathological tissues and SB in their corresponding healthy controls.

Analytical HPLC on the produced tracers (Figure 22) highlighted they were both produced as an E/Z mixture of stereoisomers. The significance of the double bond configuration was previously discussed in paragraph 2.1 (Figure 27) with respect to its impact on the detected binding affinity: in the examination of these results it should be considered that the identification and isolation of the most favorable isomer could potentially improve SB.

The crucial result highlighted by the autoradiography experiment was the potential capability of both radioligands to differentiate between neurodegeneration-related misfolded proteins. Among the examined literature, 2-styrylbenzothiazoles are the only scaffold other than the chalcone-derivatives from Kaide *et al*. [178, 179] to show such selectivity. However, their structure additionally provides the grounds for extensive optimization aimed at a decreased NSB.

Despite the lipophilicity-associated limitations causing excessive NSB and deficient wash-out, [^{18}F]**MFSB** afforded encouraging results when injected into healthy mice. *In vivo* PET scans showed a moderate brain-

uptake, with the SUV reaching 1.58 in the frontal cortex and 1.76 in the cerebellum.

3. General conclusion

Prompted by the unmet scientific and clinical need for an αSYN PET tracer, the research described in this thesis focused on the design, development, and biological evaluation of novel αSYN ligands, with the aim of identifying a compound with suitable binding properties. Three noteworthy scaffolds were chosen from the recent literature and employed as parent compounds for the construction of two libraries.

The application of the rational drug design technique of molecular hybridization generated the set of DAP analogs from the combination of the SIL and MODAG scaffolds. Instead of an increased αSYN affinity, they exhibited a shift of selectivity towards Aβ fibril. Further studies investigating the AD-directed theranostic potential of DAP hybrid compounds may provide valuable insights in the field of neurodegenerative diseases. A different hybridization strategy may produce SIL-MODAG hybrids with more favorable αSYN binding properties.

As opposed the abovementioned findings, the synthesis and evaluation of a library of 2-styrylbenzothiazoles based on the fluorescent probe RB1 generated a series of analogs displaying favorable αSYN binding and a remarkable αSYN/Aβ selectivity, overcoming a major challenge typically hampering a clinically successful outcome for several studies. Although further structural optimization will be needed to improve the pharmacokinetic profile and reduce NSB, [^{18}F]**MFSB** exhibiting brain-uptake along with attractive properties lays the foundation for the potential establishment of a MFSB-based clinically successful αSYN PET tracer.

In this study, two different strategies were implemented to develop potential radioligands, suitable for the *in vivo* detection of our target.

Many additional approaches have been pursued in the recent literature, such as *in silico* ligand-based drug design. As αSYN fibrils are indeed a challenging target, any additional insights on the structural features favoring a selective binding will be valuable, but a combination of multiple strategies may be necessary in order to successfully identify an effective tracer.

Publications and patent applications

1. **Di Nanni, A.**; Saw, R. S.; Bowden, G. D.; Bidesi, N. S. R.; Bjerregaard-Andersen, K.; Korat, S.; Herth, M. M.; Pichler, B. J.; Herfert, K.; Maurer, A.; The structural combination of SIL and MODAG scaffolds fails to enhance binding to α-synuclein but reveals promising affinity to amyloid β. *Molecules* **2023**, 28, 4001, doi:10.3390/ molecules28104001.

2. **Di Nanni, A.**; Saw, R. S.; Battisti, U. M.; Bowden, G. D.; Boeckermann, A.; Bjerregaard-Andersen, K.; Pichler, B. J.; Herfert, K.; Herth, M. M.; Maurer, A.; A fluorescent probe as a lead compound for a selective α-synuclein PET tracer: development of a library of 2-styrylbenzothiazoles and biological evaluation of [^{18}F]PFSB and [^{18}F]MFSB. *ACS Omega* **2023**, 8, 31450–31467, doi:10.1021/acsomega.3c04292.

3. **Di Nanni, A.**; Saw, R. S.; Maurer, A.; Battisti, U. M.; Bowden, G. D.; Herfert, K.; Herth, M. M.; Pichler, B. J.; Boeckermann, A.; 2-styrylbenzothiazole derivatives as α-synuclein binding compounds, EU patent application 5402P670EP, **2023.**

4. Cotton, J.; Pichler, B. J.; Reche, F.; Zhou, B.; **Di Nanni, A.**; Kinzler, J.; Krüger, M.; New Senescence Tracer Generation, patent application 5402P665, **2023.**

5. Korat, S.; Bidesi, N. S. R.; Bonanno, F.; **Di Nanni, A.**; Hoàng, A. N. N.; Herfert, K.; Maurer, A.; Battisti, U. M.; Bowden, G. D.; Thonon, D.; Vugts, D., Windhorst, A. D.; Herth, M. M.; Alpha-Synuclein PET Tracer Development—An Overview about Current Efforts. *Pharmaceuticals* **2021**, 14 (9), 847, doi:10.3390/ph14090847.

References

1. Spillantini, M. G. *et al.*, Filamentous a-synuclein inclusions link multiple system atrophy with Parkinson's disease and dementia with Lewy bodies. *Neurosci Lett* **1998**, *251*, 205-208, doi:10.1016/s0304-3940(98)00504-7.

2. Korat, S. *et al.*, Alpha-Synuclein PET Tracer Development—An Overview about Current Efforts. *Pharmaceuticals* **2021**, *14* (9), 847, doi:10.3390/ph14090847.

3. Di Nanni, A. *et al.*, The structural combination of SIL and MODAG scaffolds fails to enhance binding to α-synuclein but reveals promising affinity to amyloid β. *Molecules* **2023**, *28*, 4001, doi:10.3390/molecules28104001.

4. Di Nanni, A. *et al.*, A fluorescent probe as a lead compound for a selective α-synuclein PET tracer: development of a library of 2-styrylbenzothiazoles and biological evaluation of [^{18}F]PFSB and [^{18}F]MFSB. *ACS Omega* **2023**, 8, 31450–31467, doi:10.1021/acsomega.3c04292.

5. Parkinson, J., An essay on the shaking palsy. *J Neuropsychiatry Clin Neurosci* **1817**, *14* (2), 223-236, doi:10.1176/jnp.14.2.223.

6. Greenfield, J.G. and Bosanquet, F.D., The brain-stem lesions in Parkinsonism. *J Neurol Neurosurg Psychiat* **1953**, *16*, 213-226, doi:10.1136/jnnp.16.4.213.

7. Gai, W. P. *et al.*, Ubiquitin-positive degenerating neurites in the brainstem in Parkinson's disease. *Brain* **1995**, *118*, 1447-1459, doi:10.1093/brain/118.6.1447.

8. Spillantini, M. G. *et al.*, α-Synuclein in Lewy bodies. *Nature* **1997**, *388*, 839-840, doi:10.1038/42166

9. Spillantini, M. G. *et al.*, α-Synuclein in filamentous inclusions of Lewy bodies from Parkinson's disease and dementia with Lewy bodies. *PNAS* **1998**, *95*, 6469–6473, doi:10.1073/pnas.95.11.6469.

10. Braak, H. *et al.*, Staging of brain pathology related to sporadic Parkinson's disease. *Neurobiol Aging* **2003**, *24*, 197–211, doi:10.1016/s0197-4580(02)00065-9.

11. Braak, H. *et al.*, Parkinson's disease: lesions in dorsal horn layer I, involvement of parasympathetic and sympathetic pre- and postganglionic neurons. *Acta Neuropathol* **2007**, *113* (4), 421-9, doi:10.1007/s00401-007-0193-x.

12. Del Tredici, K. and Braak, H., Spinal cord lesions in sporadic Parkinson's disease. *Acta Neuropathol* **2012**, *124* (5), 643-64, doi:10.1007/s00401-012-1028-y.

13. Dogra, N. *et al.*, The Gut-Brain Axis: Two Ways Signaling in Parkinson's Disease. *Cell Mol Neurobiol* **2022**, *42* (2), 315-332, doi:10.1007/s10571-021-01066-7.

14. Herva, M. E. and Spillantini, M. G., Parkinson's disease as a member of Prion-like disorders. *Virus Research* **2015**, *207*, 38–46, doi:10.1016/j.virusres.2014.10.016.

15. Li, J. Y. *et al.*, Lewy bodies in grafted neurons in subjects with Parkinson's disease suggest host-to-graft disease propagation. *Nat Med* **2008**, *14* (5), 501-3, doi:10.1038/nm1746.

16. Kordower, J. H. *et al.*, Lewy body-like pathology in long-term embryonic nigral transplants in Parkinson's disease. *Nat Med* **2008**, *14* (5), 504-6, doi:10.1038/nm1747.

17. Mendez, I. *et al.*, Dopamine neurons implanted into people with Parkinson's disease survive without pathology for 14 years. *Nat Med* **2008**, *14* (5), 507-9, doi:10.1038/nm1752.

18. Desplats, P.; *et al.*, Inclusion formation and neuronal cell death through neuron-to-neuron transmission of α-synuclein. *PNAS* **2009**, *106* (31), 13010-13015, doi:10.1073/pnas.0903691106.

19. Olanow, C. W. and Prusiner, S. B., Is Parkinson's disease a prion disorder? *PNAS* **2009**, *106* (31), 12571-12572, doi:10.1073/pnas.0906759106.

20. Emmanouilidou, E. *et al.*, Cell-produced alpha-synuclein is secreted in a calcium-dependent manner by exosomes and impacts neuronal survival. *J Neurosci* **2010**, *30* (20), 6838-51, doi:10.1523/JNEUROSCI.5699-09.2010.

21. Alvarez-Erviti, L. *et al.*, Lysosomal dysfunction increases exosome-mediated alpha-synuclein release and transmission. *Neurobiol Dis* **2011**, *42* (3), 360-7, doi:10.1016/j.nbd.2011.01.029.

22. Kosaka, K. *et al.*, Presenile Dementia with Alzheimer-, Pick- and Lewy-Body Changes. *Acta neuropath* **1976**, *36*, 221-233, doi:10.1007/BF00685366.

23. McKeith, I.G. *et al.*, Consensus guidelines for the clinical and pathologic diagnosis of dementia with Lewy bodies (DLB): Report of the consortium on DLB international workshop. *Neurology* **1996**, *47*, 1113-1124, doi:10.1212/wnl.47.5.1113.

24. McKeith, I.G. *et al.*, Diagnosis and management of dementia with Lewy bodies: Fourth consensus report of the DLB Consortium. *Neurology* **2017**, *89*, 88-100, doi:10.1212/WNL.0000000000004058.

25. Ince, P.G. *et al.*, Dementia with Lewy Bodies. A Distinct Non-Alzheimer Dementia Syndrome? *Brain Pathology* **1998**, *8*, 299-324, doi:10.1111/j.1750-3639.1998.tb00156.x.

26. Cummings, J. L., Intellectual Impairment in Parkinson's Disease: Clinical, Pathologic, and Biochemical Correlates. *J Geriatr Psychiatry Neurol* **1988**, *1*, 24-36, doi:10.1177/089198878800100106.

27. Aarsland, D. *et al.*, A systematic review of prevalence studies of dementia in Parkinson's disease. *Mov Disord* **2005**, *20* (10), 1255-63, doi:10.1002/mds.20527.

28. Adams, R.D. *et al.*, Striato-nigral degeneration. *J Neuropathol Exp Neurol* **1964**, *23*, 584-608.

29. Critchley, M. and Greenfield, J.G., Olivo-ponto-cerebellar atrophy. *Brain* **1948**, *71* (4), 344-64.

30. Shy, G.M. and Drager, G.A., A Neurological Syndrome Associated with Orthostatic Hypotension. *Arch Neurol* **1960**, *2*, 511-27, doi:10.1001/archneur.1960.03840110025004.

31. Papp, M. I. *et al.*, Glial cytoplasmic inclusions in the CNS of patients with multiple system atrophy (striatonigral degeneration, olivopontocerebellar atrophy and Shy-Drager syndrome). *J Neurol Sci* **1989**, *94*, 79-100, doi:10.1016/0022-510x(89)90219-0.

32. Murayama, S. *et al.*, Immunocytochemical and ultrastructural studies of neuronal and oligodendroglial cytoplasmic inclusions in multiple system atrophy. 2. Oligodendroglial cytoplasmic inclusions. *Acta Neuropath* **1992**, *84* (1), 32-8, doi:10.1007/BF00427212.

33. Arima, K. *et al.*, Immunocytochemical and ultrastructural studies of neuronal and oligodendroglial cytoplasmic inclusions in multiple system atrophy. 1.

Neuronal cytoplasmic inclusions. *Acta neuropath* **1992**, *83* (5), 453-60, doi:10.1007/BF00310020.

34. Kaji, S. *et al.*, Insights into the pathogenesis of multiple system atrophy: focus on glial cytoplasmic inclusions. *Transl Neurodegener* **2020**, *9*, 7, doi:10.1186/s40035-020-0185-5.

35. Ueda, K. *et al.*, Molecular cloning of cDNA encoding an unrecognized component of amyloid in Alzheimer disease. *PNAS* **1993**, *90* (23), 11282-11286, doi:10.1073/pnas.90.23.11282.

36. Tofaris, G. K. and Spillantini, M. G., Alpha-synuclein dysfunction in Lewy body diseases. *Mov Disord* **2005**, *20* (12), S37-44, doi:10.1002/mds.20538.

37. Jenco, J. M. *et al.*, Regulation of Phospholipase D2: Selective Inhibition of Mammalian Phospholipase D Isoenzymes by α- and β-Synucleins. *Biochemistry* **1998**, *37* (14), 4901–4909, doi:10.1021/bi972776r.

38. Barber, C. N. *et al.*, Phosphatidic acid-producing enzymes regulating the synaptic vesicle cycle: Role for PLD? *Adv Biol Regul* **2018**, *67*, 141-147, doi:10.1016/j.jbior.2017.09.009.

39. Varkey, J. *et al.*, Membrane curvature induction and tubulation are common features of synucleins and apolipoproteins. *J Biol Chem* **2010**, *285* (42), 32486-93, doi:10.1074/jbc.M110.139576.

40. Perez, R. G., A Role for α-Synuclein in the Regulation of Dopamine Biosynthesis. *J Neurosci* **2002**, *22* (8), 3090-9, doi:10.1523/JNEUROSCI.22-08-03090.2002.

41. Schaser, A. J. *et al.*, Alpha-synuclein is a DNA binding protein that modulates DNA repair with implications for Lewy body disorders. *Sci Rep* **2019**, *9* (1), 10919, doi:10.1038/s41598-019-47227-z.

42. Souza, J. M. *et al.*, Chaperone-like activity of synucleins. *FEBS Lett* **2000**, *474* (1), 116-9, doi:10.1016/s0014-5793(00)01563-5.

43. Kim, T. D. *et al.*, Structural and Functional Implications of C-Terminal Regions of α-Synuclein. *Biochemistry* **2002**, *41* (46), 13782-90, doi:10.1021/bi026284c.

44. Dev, K. K. *et al.*, Part II: alpha-synuclein and its molecular pathophysiological role in neurodegenerative disease. *Neuropharmacology* **2003**, *45* (1), 14-44, doi:10.1016/s0028-3908(03)00140-0.

45. George, J. M. *et al.*, Characterization of a Novel Protein Regulated during the Critical Period for Song Learning in the Zebra Finch. *Neuron* **1995**, *15* (2), 361-72, doi:10.1016/0896-6273(95)90040-3.

46. Kokhan, V. S. *et al.*, alpha-Synuclein knockout mice have cognitive impairments. *Behav Brain Res* **2012**, *231* (1), 226-30, doi:10.1016/j.bbr.2012.03.026.

47. Wong, Y. C. and Krainc, D., Alpha-synuclein toxicity in neurodegeneration: mechanism and therapeutic strategies. *Nat Med* **2017**, *23* (2), 1-13, doi:10.1038/nm.4269.

48. Alam, P. *et al.*, Alpha-synuclein oligomers and fibrils: a spectrum of species, a spectrum of toxicities. *J Neurochem* **2019**, *150* (5), 522-534, doi:10.1111/jnc.14808.

49. Zhang, J. *et al.*, The Roles of Post-translational Modifications on alpha-Synuclein in the Pathogenesis of Parkinson's Diseases. *Front Neurosci* **2019**, *13*, 381, doi:10.3389/fnins.2019.00381.

50. Giasson, B. L. *et al.*, Oxidative Damage Linked to Neurodegeneration by Selective α-Synuclein Nitration in Synucleinopathy Lesions. *Science* **2000**, *290*, 985-9, doi:10.1126/science.290.5493.985.

51. Hodara, R. *et al.*, Functional consequences of alpha-synuclein tyrosine nitration: diminished binding to lipid vesicles and increased fibril formation. *J Biol Chem* **2004**, *279* (46), 47746-53, doi:10.1074/jbc.M408906200.

52. Fujiwara, H. *et al.*, Alpha-Synuclein is phosphorylated in synucleinopathy lesions. *Nat Cell Biol* **2002**, *4* (2), 160-4, doi:10.1038/ncb748.

53. Tofaris, G. K. *et al.*, Alpha-synuclein metabolism and aggregation is linked to ubiquitin-independent degradation by the proteasome. *FEBS Lett* **2001**, *509* (1), 22-6, doi:10.1016/s0014-5793(01)03115-5.

54. McNaught, K. S. and Jenner, P., Proteasomal function is impaired in substantia nigra in Parkinson's disease. *Neurosci Lett* **2001**, *297* (3), 191-4, doi:10.1016/s0304-3940(00)01701-8.

55. Tofaris, G. K. *et al.*, Ubiquitination of alpha-synuclein in Lewy bodies is a pathological event not associated with impairment of proteasome function. *J Biol Chem* **2003**, *278* (45), 44405-11, doi:10.1074/jbc.M308041200.

56. Crowther, R. A. *et al.*, Synthetic filaments assembled from C-terminally truncated alpha-synuclein. *FEBS Lett* **1998**, *436* (3), 309-12, doi:10.1016/s0014-5793(98)01146-6.

57. Murray, I. V. J. *et al.*, Role of α-Synuclein Carboxy-Terminus on Fibril Formation in Vitro. *Biochemistry* **2003**, *42* (28), 8530–8540, doi:10.1021/bi027363r.

58. Biere, A. L. *et al.*, Parkinson's disease-associated alpha-synuclein is more fibrillogenic than beta- and gamma-synuclein and cannot cross-seed its homologs. *J Biol Chem* **2000**, *275* (44), 34574-9, doi:10.1074/jbc.M005514200.

59. Giasson, B. I. *et al.*, A hydrophobic stretch of 12 amino acid residues in the middle of alpha-synuclein is essential for filament assembly. *J Biol Chem* **2001**, *276* (4), 2380-6, doi:10.1074/jbc.M008919200.

60. Guerrero-Ferreira, R. *et al.*, Two new polymorphic structures of human full-length alpha-synuclein fibrils solved by cryo-electron microscopy. *Elife* **2019**, *8*, doi:10.7554/eLife.48907.

61. Xu, L. and Pu, J., Alpha-Synuclein in Parkinson's Disease: From Pathogenetic Dysfunction to Potential Clinical Application. *Parkinsons Dis* **2016**, *2016*, 1720621, doi:10.1155/2016/1720621.

62. Guerrero-Ferreira, R. *et al.*, Cryo-EM structure of alpha-synuclein fibrils. *Elife* **2018**, *7*, doi:10.7554/eLife.36402.

63. Li, Y. *et al.*, Amyloid fibril structure of alpha-synuclein determined by cryo-electron microscopy. *Cell Res* **2018**, *28* (9), 897-903, doi:10.1038/s41422-018-0075-x.

64. Li, B. *et al.*, Cryo-EM of full-length alpha-synuclein reveals fibril polymorphs with a common structural kernel. *Nat Commun* **2018**, *9* (1), 3609, doi:10.1038/s41467-018-05971-2.

65. Polymeropoulos, M. H. *et al.*, Mutation in the α-Synuclein Gene Identified in Families with Parkinson's Disease. *Science* **1997**, *276*, 2045-7, doi:10.1126/science.276.5321.2045.

66. Weinreb, P. H. *et al.*, NACP, A Protein Implicated in Alzheimer's Disease and Learning, Is Natively Unfolded. *Biochemistry* **1996**, *35* (43), 13709–13715, doi:10.1021/bi961799n.

67. Krüger, R. *et al.*, Ala30Pro mutation in the gene encoding a-synuclein in Parkinson's disease. *Nat Genet* **1998**, *18* (2), 106-8, doi:10.1038/ng0298-106.

68. Zarranz, J. J. *et al.*, The new mutation, E46K, of alpha-synuclein causes Parkinson and Lewy body dementia. *Ann Neurol* **2004**, *55* (2), 164-73, doi:10.1002/ana.10795.

69. Appel-Cresswell, S. *et al.*, Alpha-synuclein p.H50Q, a novel pathogenic mutation for Parkinson's disease. *Mov Disord* **2013**, *28* (6), 811-3, doi:10.1002/mds.25421.

70. Lesage, S. *et al.*, G51D alpha-synuclein mutation causes a novel parkinsonian-pyramidal syndrome. *Ann Neurol* **2013**, *73* (4), 459-71, doi:10.1002/ana.23894.

71. Pasanen, P. *et al.*, Novel alpha-synuclein mutation A53E associated with atypical multiple system atrophy and Parkinson's disease-type pathology. *Neurobiol Aging* **2014**, *35* (9), 2180 e1-5, doi:10.1016/j.neurobiolaging.2014.03.024.

72. Yoshino, H. *et al.*, Homozygous alpha-synuclein p.A53V in familial Parkinson's disease. *Neurobiol Aging* **2017**, *57*, 248 e7-248 e12, doi:10.1016/j.neurobiolaging.2017.05.022.

73. Chartier-Harlin, M. C. *et al.*, Alpha-synuclein locus duplication as a cause of familial Parkinson's disease. *Lancet* **2004**, *364* (9440), 1167-9, doi:10.1016/S0140-6736(04)17103-1.

74. Singleton, A. B. *et al.*, α-Synuclein Locus Triplication Causes Parkinson's Disease. *Science* **2003**, *302*, 841, doi:10.1126/science.1090278.

75. Plaas, M. *et al.*, Alpha-synuclein A30P point-mutation generates age-dependent nigrostriatal deficiencyin mice. *J Physiol Pharmacol* **2008**, *59* (2), 205-216.

76. Dawson, T. M. *et al.*, Genetic animal models of Parkinson's disease. *Neuron* **2010**, *66* (5), 646-61, doi:10.1016/j.neuron.2010.04.034.

77. Koprich, J. B. *et al.*, Animal models of alpha-synucleinopathy for Parkinson disease drug development. *Nat Rev Neurosci* **2017**, *18* (9), 515-529, doi:10.1038/nrn.2017.75.

78. Prince, M. *et al.*, The global prevalence of dementia: a systematic review and metaanalysis. *Alzheimers Dement* **2013**, *9* (1), 63-75 e2, doi:10.1016/j.jalz.2012.11.007.

79. Busche, M. A. and Hyman, B. T., Synergy between amyloid-beta and tau in Alzheimer's disease. *Nat Neurosci* **2020**, *23* (10), 1183-1193, doi:10.1038/s41593-020-0687-6.

80. Glenner, G. G. and Wong, C. W., Alzheimer's disease: initial report of the purificaiton and characterization od a novel cerebrovascular amyloid protein. *Biochem Biophys Res Commun* **1984**, *120* (3), 885-890.

81. Grundke-Iqbal, I. *et al.*, Abnormal phosphorylation of the microtubule-associated protein X (tau) in Alzheimer cytoskeletal pathology. *PNAS* **1986**, *83*, 4913-4917.

82. Nisbet, R. M. *et al.*, Tau aggregation and its interplay with amyloid-β. *Acta Neuropathol* **2014**, *129* (2), 207-220, doi:10.1007/s00401-014-1371-2.

83. Myers, W. G., Georg Charles de Hevesy: the father of Nuclear Medicine. *J Nucl Med* **1979**, *20* (6), 590-4.

84. Jadvar, H. and Parker, J. A., *Clinical PET and PET/CT*. Springer: 2005.

85. Mathis, C. A. *et al.*, Small-molecule PET Tracers for Imaging Proteinopathies. *Semin Nucl Med* **2017**, *47* (5), 553-575, doi:10.1053/j.semnuclmed.2017.06.003.

86. Miller, P. W. *et al.*, Synthesis of ^{11}C, ^{18}F, ^{15}O, and ^{13}N radiolabels for positron emission tomography. *Angew Chem Int Ed Engl* **2008**, *47* (47), 8998-9033, doi:10.1002/anie.200800222.

87. Preshlock, S. *et al.*, ^{18}F-Labeling of Arenes and Heteroarenes for Applications in Positron Emission Tomography. *Chem Rev* **2016**, *116* (2), 719-66, doi:10.1021/acs.chemrev.5b00493.

88. Coenen, H. H., *Fluorine-18 Labeling Methods: Features and Possibilities of Basic Reactions*. Springer: 2007.

89. Tredwell, M. *et al.*, A General Copper-Mediated Nucleophilic ^{18}F Fluorination of Arenes. *Angew Chem Int Ed* **2014**, *53* (30), 7751-7755, doi:10.1002/anie.201404436.

90. Ye, Y. *et al.*, $Cu(OTf)_2$-Mediated Fluorination of Aryltrifluoroborates with Potassium Fluoride. *JACS* **2013**, *135* (44), 16292-16295, doi:10.1021/ja408607r.

91. Mossine, A. V. *et al.*, Synthesis of [^{18}F]Arenes via the Copper-Mediated [^{18}F]Fluorination of Boronic Acids. *Org Lett* **2015**, *17* (23), 5780-3, doi:10.1021/acs.orglett.5b02875.

92. Mossine, A. V. *et al.*, Automated synthesis of PET radiotracers by copper-mediated ^{18}F-fluorination of organoborons: Importance of the order of addition and competing protodeborylation. *J Labelled Comp Radiopharm* **2018**, *61* (3), 228-236, doi:10.1002/jlcr.3583.

93. Mossine, A. V. *et al.*, Development of Customized [^{18}F]Fluoride Elution Techniques for the Enhancement of Copper-Mediated Late-Stage Radiofluorination. *Sci Rep* **2017**, *7* (1), 233, doi:10.1038/s41598-017-00110-1.

94. Bowden, G. D. *et al.*, A Design of experiments (Doe) Approach Accelerates the optimization of copper-Mediated ^{18}F-fluorination Reactions of Arylstannanes. *Sci Rep* **2019**, *9*, 11370, doi:10.1038/s41598-019-47846-6.

95. Bowden, G. D. *et al.*, Scalable ^{18}F processing conditions for copper-mediated radiofluorination chemistry facilitate DoE optimization studies and afford an improved synthesis of [^{18}F]olaparib. *Org Biomol Chem* **2021**, *19* (32), 6995-7000, doi:10.1039/d1ob00903f.

96. Bowden, G. D. *et al.*, DoE Optimization Empowers the Automated Preparation of Enantiomerically Pure [^{18}F]Talazoparib and its In Vivo Evaluation as a PARP Radiotracer. *J Med Chem* **2021**, *64* (21), 15690-15701, doi:10.1021/acs.jmedchem.1c00903.

97. Ido, T. *et al.*, Labeled 2-deoxy-D-glucose analogs. ^{18}F-labeled 2-deoxy-2-fluoro-D-glucose, 2-deoxy-2-fluoro-D-mannose and ^{14}C-2-deoxy-2-fluoro-D-glucose. *J Label Compd Radiopharm* **1978**, *14* (2), 175-183, doi:10.1002/jlcr.2580140204.

98. Hoffman, J. M. *et al.*, FDG PET Imaging in Patients with Pathologically Verified Dementia. *J Nucl Med* **2000**, *41* (11), 1920-8.

99. Rocher, A. B. *et al.*, Resting-state brain glucose utilization as measured by PET is directly related to regional synaptophysin levels: a study in baboons. *NeuroImage* **2003**, *20*, 1894–1898, doi:10.1016/S1053-8119(03)00419-1.

100. Mathis, C. A. *et al.*, Synthesis and Evaluation of ^{11}C-Labeled 6-Substituted 2-Arylbenzothiazoles as Amyloid Imaging Agents. *J Med Chem* **2003**, *46* (13), 2740–2754, doi:10.1021/jm030026b.

101. Klunk, W. E. *et al.*, Imaging brain amyloid in Alzheimer's disease with Pittsburgh Compound-B. *Ann Neurol* **2004**, *55* (3), 306-19, doi:10.1002/ana.20009.

102. Krishnadas, N. *et al.*, Advances in Brain Amyloid Imaging. *Semin Nucl Med* **2021**, *51* (3), 241-252, doi:10.1053/j.semnuclmed.2020.12.005.

103. Koole, M. *et al.*, Whole-body biodistribution and radiation dosimetry of ^{18}F-GE067: a radioligand for in vivo brain amyloid imaging. *J Nucl Med* **2009**, *50* (5), 818-22, doi:10.2967/jnumed.108.060756.

104. Zhang, W. *et al.*, F-18 Polyethyleneglycol stilbenes as PET imaging agents targeting Aβ aggregates in the brain. *Nucl Med Biol* **2005**, *32* (8), 799-809, doi:10.1016/j.nucmedbio.2005.06.001.

105. Choi, S. R. *et al.*, Preclinical Properties of ^{18}F-AV-45: A PET Agent for Aβ Plaques in the Brain. *J Nucl Med* **2009**, *50* (11), 1887-1894, doi:10.2967/jnumed.109.065284.

106. Jie, Cvml *et al.*, Tauvid: The First FDA-Approved PET Tracer for Imaging Tau Pathology in Alzheimer's Disease. *Pharmaceuticals* **2021**, *14* (2), doi:10.3390/ph14020110.

107. Willis, A. W. *et al.*, Incidence of Parkinson disease in North America. *NPJ Parkinsons Dis* **2022**, *8* (1), 170, doi:10.1038/s41531-022-00410-y.

108. Berg, D. *et al.*, Time to redefine PD? Introductory statement of the MDS Task Force on the definition of Parkinson's disease. *Mov Disord* **2014**, *29* (4), 454-62, doi:10.1002/mds.25844.

109. Berg, D. *et al.*, MDS research criteria for prodromal Parkinson's disease. *Mov Disord* **2015**, *30* (12), 1600-11, doi:10.1002/mds.26431.

110. Ponsen, M. M. *et al.*, Idiopathic hyposmia as a preclinical sign of Parkinson's disease. *Ann Neurol* **2004**, *56* (2), 173-81, doi:10.1002/ana.20160.

111. Bang, Y. *et al.*, Recent advances in the pathology of prodromal non-motor symptoms olfactory deficit and depression in Parkinson's disease: clues to early diagnosis and effective treatment. *Arch Pharm Res* **2021**, *44* (6), 588-604, doi:10.1007/s12272-021-01337-3.

112. Claassen, D. O. *et al.*, REM sleep behavior disorder preceding other aspects of synucleinopathies by up to half a century. *Neurology* **2010**, *75*, 494–499, doi:10.1212/WNL.0b013e3181ec7fac.

113. Brooks, D. J., Imaging Approaches to Parkinson Disease. *J Nucl Med* **2010**, *51* (4), 596-609, doi:10.2967/jnumed.108.059998.

114. Prange, S. *et al.*, Molecular Imaging in Parkinsonian Disorders-What's New and Hot? *Brain Sci* **2022**, *12* (9), doi:10.3390/brainsci12091146.

115. Volkow, N. D. *et al.*, A New PET Ligand for the Dopamine Transporter: Studies in the Human Brain. *J Nucl Med* **1995**, *36* (12), 2162-8.

116. Delva, A. *et al.*, Quantification and discriminative power of ^{18}F-FE-PE2I PET in patients with Parkinson's disease. *Eur J Nucl Med Mol Imaging* **2020**, *47* (8), 1913-1926, doi:10.1007/s00259-019-04587-y.

117. Koeppe, R. A. *et al.*, ^{11}C-DTBZ and ^{18}F-FDG PET Measures in Differentiating Dementias. *J Nucl Med* **2005**, *46* (6), 936-944.

118. Leeders, K. L. *et al.*, The Nigrostriatal Dopaminergic System Assessed In Vivo by Positron Emission Tomography in Healthy Volunteer Subjects and Patients With Parkinson's Disease. *Arch Neurol* **1990**, *47* (12), 1290-8, doi:10.1001/archneur.1990.00530120034007.

119. Volkow, N. D. *et al.*, Imaging endogenous dopamine competition with [^{11}C]raclopride in the human brain. *Synapse* **1994**, *16* (4), 255-62, doi:10.1002/syn.890160402.

120. Maillet, A. *et al.*, The prominent role of serotonergic degeneration in apathy, anxiety and depression in de novo Parkinson's disease. *Brain* **2016**, *139* (Pt 9), 2486-502, doi:10.1093/brain/aww162.

121. Doder, M. *et al.*, Tremor in Parkinson's disease and serotonergic dysfunction - An ^{11}C-WAY 100635 PET study. *Neurology* **2003**, *60* (4), 601-5, doi:10.1212/01.wnl.0000031424.51127.2b.

122. Politis, M. *et al.*, Staging of serotonergic dysfunction in Parkinson's disease: an in vivo ^{11}C-DASB PET study. *Neurobiol Dis* **2010**, *40* (1), 216-21, doi:10.1016/j.nbd.2010.05.028.

123. Carson, R. E. *et al.*, Imaging of Synaptic Density in Neurodegenerative Disorders. *J Nucl Med* **2022**, *63* (Suppl 1), 60S-67S, doi:10.2967/jnumed.121.263201.

124. Ryman, S. G. and Poston, K. L., MRI biomarkers of motor and non-motor symptoms in Parkinson's disease. *Parkinsonism Relat Disord* **2020**, *73*, 85-93, doi:10.1016/j.parkreldis.2019.10.002.

125. Ghaemi, M. *et al.*, Differentiating multiple system atrophy from Parkinson's disease: contribution of striatal and midbrain MRI volumetry and multi-tracer PET imaging. *J Neurol Neurosurg Psychiatry* **2002**, *73* (5), 517-23, doi:10.1136/jnnp.73.5.517.

126. Fu, J. F. *et al.*, Spatiotemporal patterns of putaminal dopamine processing in Parkinson's disease: A multi-tracer positron emission tomography study. *Neuroimage Clin* **2022**, *36*, 103246, doi:10.1016/j.nicl.2022.103246.

127. Church, F. C., Treatment Options for Motor and Non-Motor Symptoms of Parkinson's Disease. *Biomolecules* **2021**, *11* (4), doi:10.3390/biom11040612.

128. Schaeffer, E. and Berg, D., Dopaminergic Therapies for Non-motor Symptoms in Parkinson's Disease. *CNS Drugs* **2017**, *31* (7), 551-570, doi:10.1007/s40263-017-0450-z.

129. Cooper, J. M. *et al.*, Systemic exosomal siRNA delivery reduced alpha-synuclein aggregates in brains of transgenic mice. *Mov Disord* **2014**, *29* (12), 1476-85, doi:10.1002/mds.25978.

130. Lee, B. H. *et al.*, Enhancement of proteasome activity by a small-molecule inhibitor of USP14. *Nature* **2010**, *467* (7312), 179-84, doi:10.1038/nature09299.

131. Xilouri, M. *et al.*, Boosting chaperone-mediated autophagy in vivo mitigates alpha-synuclein-induced neurodegeneration. *Brain* **2013**, *136* (Pt 7), 2130-46, doi:10.1093/brain/awt131.

132. Dehay, B. *et al.*, Targeting α-synuclein for treatment of Parkinson's disease: mechanistic and therapeutic considerations. *Lancet Neurol* **2015**, *14*, 855–866, doi:10.1016/S1474-4422(15)00006-X.

133. Tran, H. T. *et al.*, α-Synuclein Immunotherapy Blocks Uptake and Templated Propagation of Misfolded α-Synuclein and Neurodegeneration. *Cell Reports* **2014**, *7* (6), 2054-2065, doi:10.1016/j.celrep.2014.05.033.

134. Schneeberger, A. *et al.*, Active immunization therapies for Parkinson's disease and multiple system atrophy. *Mov Disord* **2016**, *31* (2), 214-24, doi:10.1002/mds.26377.

135. Bergstrom, A. L. *et al.*, Development of Passive Immunotherapies for Synucleinopathies. *Mov Disord* **2016**, *31* (2), 203-13, doi:10.1002/mds.26481.

136. McFarthing, K. *et al.*, Parkinson's Disease Drug Therapies in the Clinical Trial Pipeline: 2020. *J Parkinsons Dis* **2020**, *10* (3), 757-774, doi:10.3233/JPD-202128.

137. Singh, N. A First-in-Human Study of Single and Multiple Doses of anle138b in Healthy Subjects. https://ClinicalTrials.gov/show/NCT04208152 (accessed Dec 2022).

138. Singh, N. and Evans, J. A Study to Assess the Safety, Tolerability, Pharmacokinetics and Pharmacodynamics of anle138b in Parkinson's Disease. https://ClinicalTrials.gov/show/NCT04685265 (accessed Dec 2022).

139. Singh, N. A Drug-Drug Interaction Study to Assess the CYP1A2 and CYP3A4 Interaction Potential of TEV-56286 (anle138b). https://ClinicalTrials.gov/show/NCT05532358 (accessed Dec 2022).

140. Camilleri, M. *et al.*, Oral ENT-01 Targets Enteric Neurons to Treat Constipation in Parkinson Disease : A Randomized Controlled Trial. *Ann Intern Med* **2022**, *175* (12), 1666-1674, doi:10.7326/M22-1438.

141. Shaltiel-Karyo, R. *et al.*, A blood-brain barrier (BBB) disrupter is also a potent alpha-synuclein (alpha-syn) aggregation inhibitor: a novel dual mechanism of mannitol for the treatment of Parkinson disease (PD). *J Biol Chem* **2013**, *288* (24), 17579-88, doi:10.1074/jbc.M112.434787.

142. Lee, J. *et al.*, Memantine exerts neuroprotective effects by modulating α-synuclein transmission in a parkinsonian model. *Exp Neurol* **2021**, *344*, 113810, doi:10.1016/j.expneurol.2021.113810.

143. Singer, W., Recent advances in establishing fluid biomarkers for the diagnosis and differentiation of alpha-synucleinopathies - a mini review. *Clin Auton Res* **2022**, *32* (4), 291-297, doi:10.1007/s10286-022-00882-1.

144. Zubelzu, M. *et al.*, Plasma and serum alpha-synuclein as a biomarker in Parkinson's disease: A meta-analysis. *Parkinsonism Relat Disord* **2022**, *99*, 107-115, doi:10.1016/j.parkreldis.2022.06.001.

145. Devic, I. *et al.*, Salivary alpha-synuclein and DJ-1: potential biomarkers for Parkinson's disease. *Brain* **2011**, *134* (Pt 7), e178, doi:10.1093/brain/awr015.

146. Poggiolini, I. *et al.*, Diagnostic value of cerebrospinal fluid alpha-synuclein seed quantification in synucleinopathies. *Brain* **2022**, *145* (2), 584-595, doi:10.1093/brain/awab431.

147. Donadio, V. *et al.*, In Vivo Diagnosis of Synucleinopathies: A Comparative Study of Skin Biopsy and RT-QuIC. *Neurology* **2021**, *96* (20), e2513-e2524, doi:10.1212/WNL.0000000000011935.

148. MJFF Alpha-Synuclein Imaging Prize. https://www.michaeljfox.org/news/alpha-synuclein-imaging-prize (accessed February 2023).

149. Sehlin, D. *et al.*, Engineered antibodies: new possibilities for brain PET? *Eur J Nucl Med Mol Imaging* **2019**, *46* (13), 2848-2858, doi:10.1007/s00259-019-04426-0.

150. Steen, E. J. L. *et al.*, Pretargeting in nuclear imaging and radionuclide therapy: Improving efficacy of theranostics and nanomedicines. *Biomaterials* **2018**, *179*, 209-245, doi:10.1016/j.biomaterials.2018.06.021.

151. Shalgunov, V. *et al.*, Pretargeted imaging beyond the blood–brain barrier. *RSC Medicinal Chemistry* **2023**, doi:10.1039/d2md00360k.

152. Roshanbin, S. *et al.*, In vivo imaging of alpha-synuclein with antibody-based PET. *Neuropharmacology* **2022**, *208*, 108985, doi:10.1016/j.neuropharm.2022.108985.

153. Gupta, M. *et al.*, The Blood–Brain Barrier (BBB) Score. *J Med Chem* **2019**, *62* (21), 9824-9836, doi:10.1021/acs.jmedchem.9b01220.

154. Wager, T. T. *et al.*, Moving beyond Rules: The Development of a Central Nervous System Multiparameter Optimization (CNS MPO) Approach To Enable Alignment of Druglike Properties. *ACS Chem Neurosci* **2010**, *1* (6), 435-449, doi:10.1021/cn100008c.

155. Miraglia, F. *et al.*, Subcellular localization of alpha-synuclein aggregates and their interaction with membranes. *Neural Regen Res* **2018**, *13* (7), 1136-1144, doi:10.4103/1673-5374.235013.

156. Tuttle, M. D. *et al.*, Solid-state NMR structure of a pathogenic fibril of full-length human alpha-synuclein. *Nat Struct Mol Biol* **2016**, *23* (5), 409-15, doi:10.1038/nsmb.3194.

157. Van der Perren, A. *et al.*, The structural differences between patient-derived alpha-synuclein strains dictate characteristics of Parkinson's disease, multiple system atrophy and dementia with Lewy bodies. *Acta Neuropathol* **2020**, *139* (6), 977-1000, doi:10.1007/s00401-020-02157-3.

158. Hsieh, C.-J. *et al.*, Alpha Synuclein Fibrils Contain Multiple Binding Sites for Small Molecules. *ACS Chem Neurosci* **2018**, *9*, 2521-2527, doi:10.1021/acschemneuro.8b00177.

159. Alzghool, O. M. *et al.*, Alpha-Synuclein Radiotracer Development and In Vivo Imaging: Recent Advancements and New Perspectives. *Mov Disord* **2022**, *37* (5), 936-948, doi:10.1002/mds.28984.

160. Hein, P. and Michel, M. C., Receptor and Binding Studies. In: Dhein, S., Mohr, F.W., Delmar, M. (eds) Practical Methods in Cardiovascular Research. 2005; pp 723-747.

161. Yu, L. *et al.*, Synthesis and in vitro evaluation of alpha-synuclein ligands. *Bioorg Med Chem* **2012**, *20* (15), 4625-34, doi:10.1016/j.bmc.2012.06.023.

162. Bagchi, D. P. *et al.*, Binding of the radioligand SIL23 to alpha-synuclein fibrils in Parkinson disease brain tissue establishes feasibility and screening approaches for developing a Parkinson disease imaging agent. *PLoS One* **2013**, *8* (2), e55031, doi:10.1371/journal.pone.0055031.

163. Zhang, X. *et al.*, Radiosynthesis and in Vivo Evaluation of Two PET Radioligands for Imaging alpha-Synuclein. *Appl Sci* **2014**, *4* (1), 66-78, doi:10.3390/app4010066.

164. Fodero-Tavoletti, M. T. *et al.*, In vitro characterisation of BF227 binding to α-synuclein/Lewy bodies. *Eur J Pharmacol* **2009**, *617* (1-3), 54-58, doi:10.1016/j.ejphar.2009.06.042.

165. Kikuchi, A. *et al.*, In vivo visualization of alpha-synuclein deposition by carbon-11-labelled 2-[2-(2-dimethylaminothiazol-5-yl)ethenyl]-6-[2-(fluoro)ethoxy]benzoxazole positron emission tomography in multiple system atrophy. *Brain* **2010**, *133* (Pt 6), 1772-8, doi:10.1093/brain/awq091.

166. Verdurand, M. *et al.*, In Silico, in Vitro, and in Vivo Evaluation of New Candidates for αSynuclein PET Imaging. *Mol Pharmaceutic* **2018**, *15*, 3153−3166, doi:10.1021/acs.molpharmaceut.8b00229.

167. Chu, W. *et al.*, Design, Synthesis, and Characterization of 3-(Benzylidene)indolin-2-one Derivatives as Ligands for alpha-Synuclein Fibrils. *J Med Chem* **2015**, *58* (15), 6002-17, doi:10.1021/acs.jmedchem.5b00571.

168. Lengyel-Zhand, Z. *et al.*, Synthesis and characterization of high affinity fluorogenic a-synuclein probes. *Chem Comm* **2020**, *56*, 3567-3570, doi:10.1039/C9CC09849F.

169. Koga, S. *et al.*, Fluorescence and autoradiographic evaluation of tau PET ligand PBB3 to alpha-synuclein pathology. *Mov Disord* **2017**, *32* (6), 884-892, doi:10.1002/mds.27013.

170. Watanabe, H. *et al.*, Novel Benzothiazole Derivatives as Fluorescent Probes for Detection of βAmyloid and αSynuclein Aggregates. *ACS Chem Neurosci* **2017**, *8* (8), 1656–1662, doi:10.1021/acschemneuro.6b00450.

171. Miranda-Azpiazu, P. *et al.*, Identification and in vitro characterization of C05-01, a PBB3 derivative with improved affinity for alpha-synuclein. *Brain Res* **2020**, *1749*, 147131, doi:10.1016/j.brainres.2020.147131.

172. Gaur, P. *et al.*, Fluorescent Probe for Selective Imaging of α-Synuclein Fibrils in Living Cells. *ACS Chem Neurosci* **2021**, *12* (8), 1293–1298, doi:10.1021/acschemneuro.1c00090.

173. Uzuegbunam, B. C. *et al.*, Toward Novel [^{18}F]Fluorine-Labeled Radiotracers for the Imaging of alpha-Synuclein Fibrils. *Front Aging Neurosci* **2022**, *14*, 830704, doi:10.3389/fnagi.2022.830704.

174. Wagner, J. *et al.*, Anle138b: a novel oligomer modulator for disease modifying therapy of neurodegenerative diseases such as prion and Parkinson's disease. *Acta Neuropathol* **2013**, *125*, 795-813, doi:10.1007/s00401-013-1114-9).

175. Deeg, A. A. *et al.*, Anle138b and related compounds are aggregation specific fluorescence markers and reveal high affinity binding to alpha-synuclein aggregates. *Biochim Biophys Acta* **2015**, *1850* (9), 1884-90, doi:10.1016/j.bbagen.2015.05.021.

176. Maurer, A. *et al.*, ^{11}C radiolabeling of anle253b: A putative PET tracer for Parkinson's disease that binds to alpha-synuclein fibrils in vitro and crosses the blood-brain barrier. *ChemMedChem* **2019**, *15* (5), 411-415, doi:10.1002/cmdc.201900689.

177. Kuebler, L. *et al.*, [^{11}C]MODAG-001—towards a PET tracer targeting α-synuclein aggregates. *EJNMMI* **2020**, *48*, 1759-1772, doi:10.1007/s00259-020-05133-x.

178. Kaide, S. *et al.*, Chalcone Analogue as New Candidate for Selective Detection of alpha-Synuclein Pathology. *ACS Chem Neurosci* **2022**, *13* (1), 16-26, doi:10.1021/acschemneuro.1c00441.

179. Kaide, S. *et al.*, Synthesis and Evaluation of ^{18}F-Labeled Chalcone Analogue for Detection of alpha-Synuclein Aggregates in the Brain Using the Mouse Model. *ACS Chem Neurosci* **2022**, *13* (20), 2982-2990, doi:10.1021/acschemneuro.2c00473.

180. Ono, M. *et al.*, Structure–activity relationships of radioiodinated diphenyl derivatives with different conjugated double bonds as ligands for a-synuclein aggregates. *RSC Advances* **2016**, *6*, 44305, doi:10.1039/C6RA02710E.

181. Hsieh, C. J. *et al.*, Chalcones and Five-Membered Heterocyclic Isosteres Bind to Alpha Synuclein Fibrils in Vitro. *ACS Omega* **2018**, *3* (4), 4486-4493, doi:10.1021/acsomega.7b01897.

182. Capotosti, F. *et al.*, The development of [^{18}F]ACI-12589, a high affinity and selective alpha-synuclein radiotracer, as a biomarker for Parkinson's disease and other synucleinopathies. *Alzheimer's & Dementia* **2021**, *17* (S5), doi:10.1002/alz.053943.

183. Capotosti, F. *et al.*, Discovery of [^{18}F]ACI-12589, a Novel and Promising PET-Tracer for Alpha-Synuclein. *Alzheimer's & Dementia* **2022**, *18* (S6), doi:10.1002/alz.064680.

184. Matsuoka, K. *et al.*, High-Contrast Imaging of alpha-Synuclein Pathologies in Living Patients with Multiple System Atrophy. *Mov Disord* **2022**, *37* (10), 2159-2161, doi:10.1002/mds.29186.

185. Molette, J., Novel compounds for diagnosis, WO 2021/224489 A1, **2021**.

186. Higuchi, M. *et al.*, Preparation of benzothiazole compound as α-synuclein aggregate binder, WO 2022/045093 A1, **2022**.

187. Di Nanni, A. *et al.*, 2-styrylbenzothiazole derivatives as α-synuclein binding compounds, EU Application 5402P670EP, **2023**.

188. Lazar, C. *et al.*, Drug Evolution Concept in Drug Design: 1. Hybridization Method. *J Med Chem* **2004**, *47*, 6973-6982, doi:10.1021/jm049637+.

189. Viegas-Junior, C. *et al.*, Molecular Hybridization: A Useful Tool in the Design of New Drug Prototypes. *Curr Med Chem* **2007**, *14*, 1829-1852, doi:10.2174/092986707781058805.

190. Morphy, R. *et al.*, From magic bullets to designed multiple ligands. *Drug Discov Today* **2004**, *9* (15), 641-651, doi:10.1016/s1359-6446(04)03163-0.

191. Morphy, R. and Rankovic, Z., Designed Multiple Ligands. An Emerging Drug Discovery Paradigm. *J Med Chem* **2005**, *48* (21), 6523–6543, doi:10.1021/jm058225d.

192. Schneider, C. A. *et al.*, NIH Image to ImageJ: 25 years of image analysis. *Nat Methods* **2012**, *9* (7), 671-5, doi:10.1038/nmeth.2089.

193. Setamdideh, D. and Khezri, B., Rapid and Efficient Reduction of Nitroarenes to Their Corresponding Amines with Promotion of $NaBH_4/NiCl_2{\cdot}6H2O$ System in Aqueous CH_3CN. *Chem Asian J* **2010**, *22* (7), 5575-5580.

194. Schäfer, G. *et al.*, Development of a Scalable Route for a Key Thiadiazole Building Block via Sequential Sandmeyer Bromination and Room-Temperature Suzuki–Miyaura Coupling. *Org Process Res Dev* **2020**, *24* (2), 228-234, doi:10.1021/acs.oprd.9b00495.

195. Das, B. *et al.*, A facile nuclear bromination of phenols and anilines using NBS in the presence of ammonium acetate as a catalyst. *J Mol Catal A Chem* **2007**, *267* (1-2), 30-33, doi:10.1016/j.molcata.2006.11.002.

196. Seelig, A., The Role of Size and Charge for Blood–Brain Barrier Permeation of Drugs and Fatty Acids. *J Mol Neurosci* **2007**, *33* (1), 32-41, doi:10.1007/s12031-007-0055-y.

197. Antonschmidt, Leif *et al.*, The clinical drug candidate anle138b binds in a cavity of lipidic α-synuclein fibrils. *Nature Comm* **2022**, *13* (1), 5385, doi:10.1038/s41467-022-32797-w.

198. Dao, P. *et al.*, Development of Phenothiazine-Based Theranostic Compounds That Act Both as Inhibitors of βAmyloid Aggregation and as Imaging Probes for Amyloid Plaques in Alzheimer's Disease. *ACS Chem Neurosci* **2017**, *2017* (8), 798-806, doi:10.1021/acschemneuro.6b00380.

199. Needham, L.-M. *et al.*, A Comparative Photophysical Study of Structural Modifications of Thioflavin T-Inspired Fluorophores. *J Phys Chem Lett* **2020**, *11* (19), 8406-8416, doi:10.1021/acs.jpclett.0c01549.

200. Mallesh, R. *et al.*, Design and Development of Benzothiazole-Based Fluorescent Probes for Selective Detection of Abeta Aggregates in Alzheimer's Disease. *ACS Chem Neurosci* **2022**, *13* (16), 2503-2516, doi:10.1021/acschemneuro.2c00361.

201. Zheng, Ming-Qiang *et al.*, Syntheses and evaluation of fluorinated benzothiazole anilines as potential tracers for β-amyloid plaques in Alzheimer's disease. *J Fluor Chem* **2008**, *129* (3), 210-216, doi:10.1016/j.jfluchem.2007.11.005.

202. Neumaier, B. *et al.*, Synthesis and evaluation of ^{18}F-fluoroethylated benzothiazole derivatives for in vivo imaging of amyloid plaques in Alzheimer's disease. *Appl Radiat Isot* **2010**, *68* (6), 1066-72, doi:10.1016/j.apradiso.2009.12.044.

203. Lee, B. C. *et al.*, Aromatic radiofluorination and biological evaluation of 2-aryl-6-[^{18}F]fluorobenzothiazoles as a potential positron emission tomography imaging probe for beta-amyloid plaques. *Bioorg Med Chem* **2011**, *19* (9), 2980-90, doi:10.1016/j.bmc.2011.03.029.

204. Taylor, N. J. *et al.*, Derisking the Cu-Mediated ^{18}F-Fluorination of Heterocyclic Positron Emission Tomography Radioligands. *JACS* **2017**, *139* (24), 8267-8276, doi:10.1021/jacs.7b03131.

Appendix

1. ^{1}H NMR spectra of the tested compounds

Figures are adapted from [3,4].

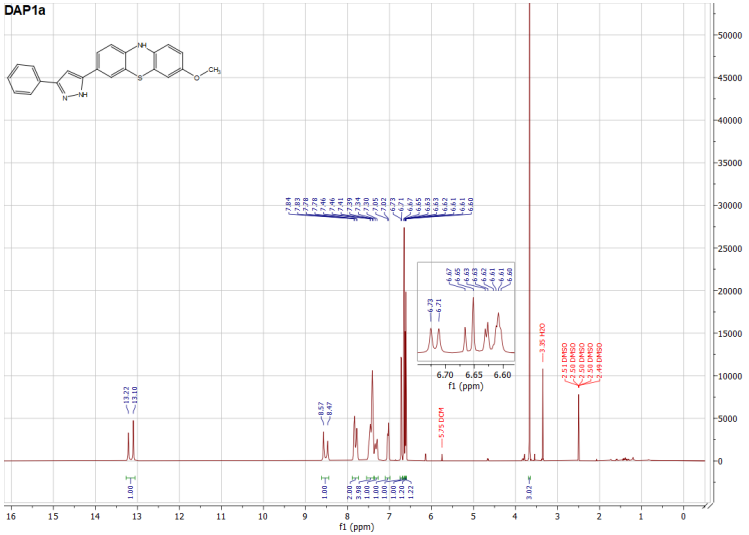

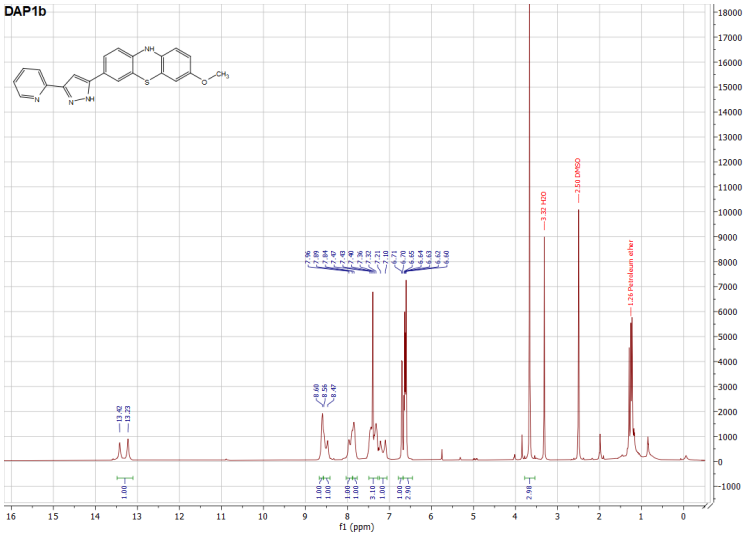

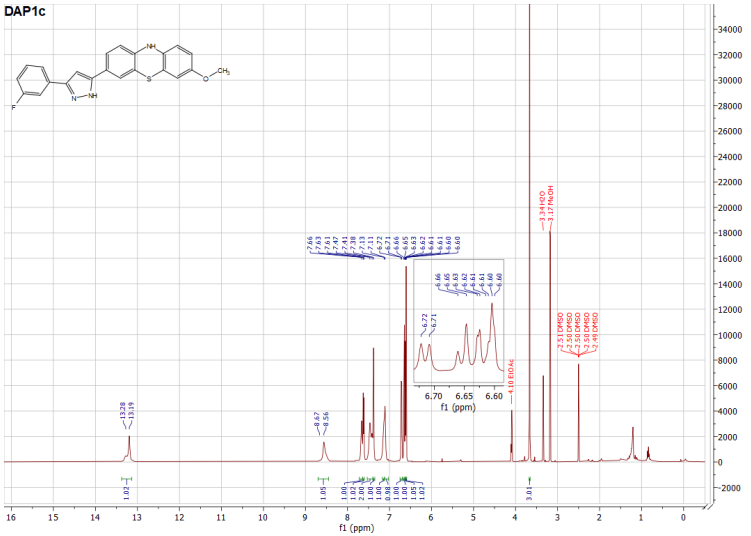
DAP1c
f1 (ppm)

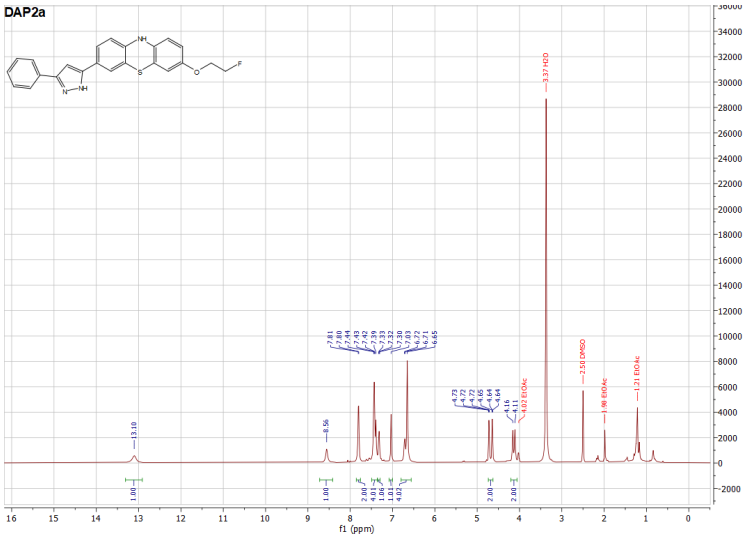
DAP2a
f1 (ppm)

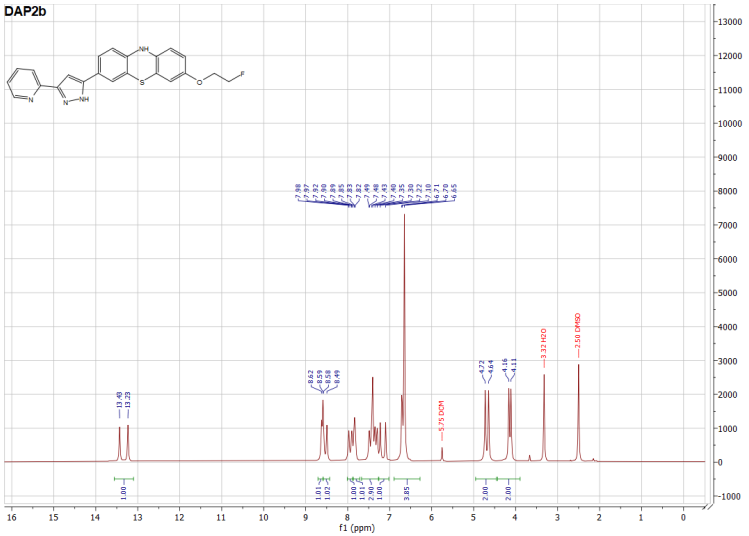
DAP2b
f1 (ppm)

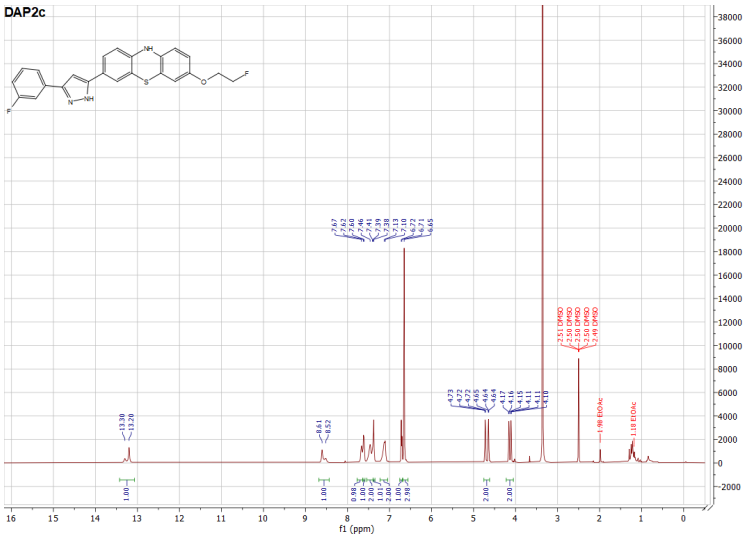
DAP2c
f1 (ppm)

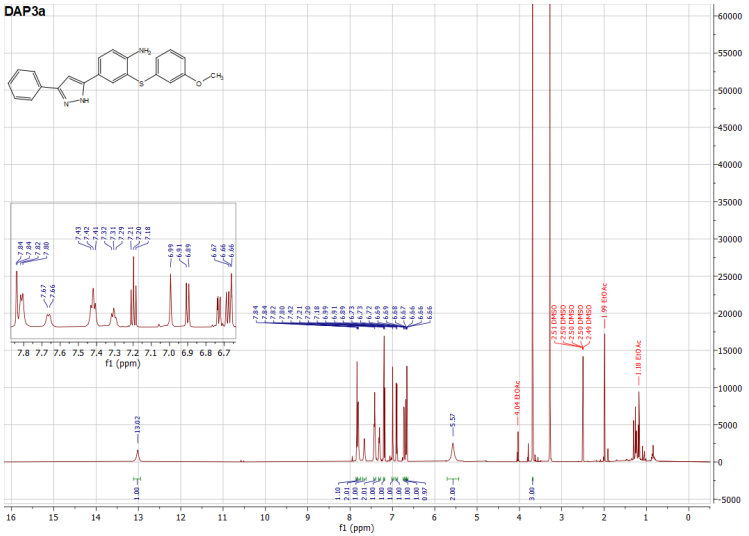
DAP3a
f1 (ppm)

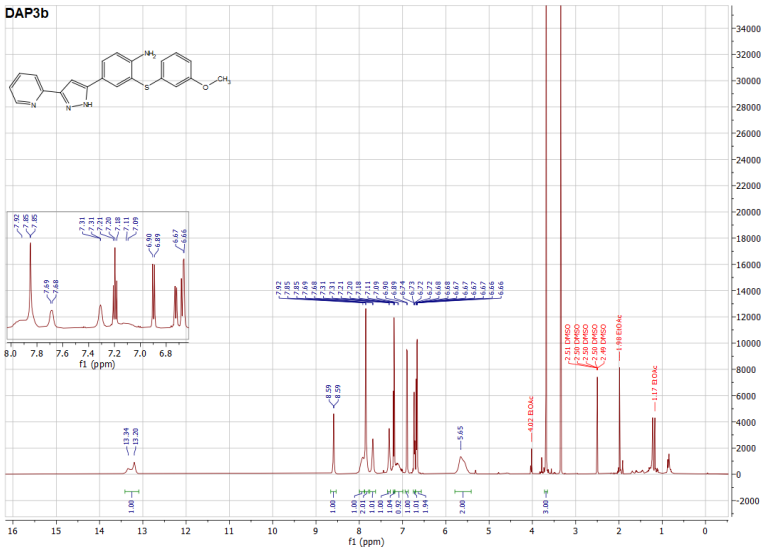
DAP3b
f1 (ppm)

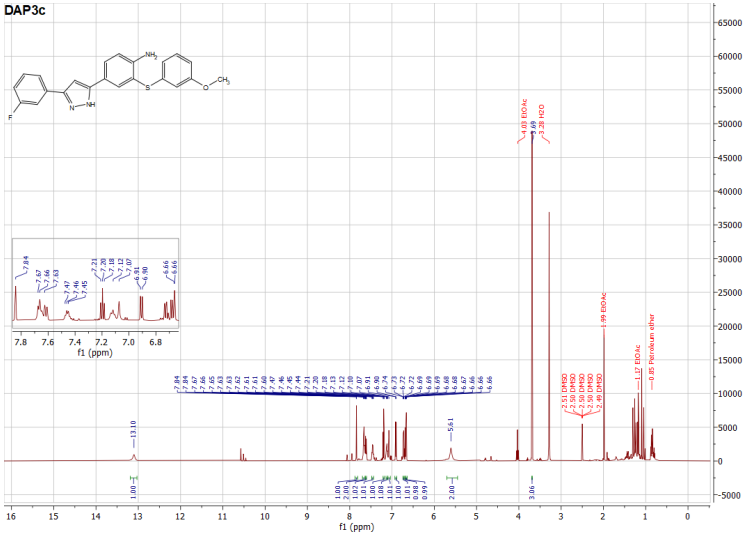
DAP3c
f1 (ppm)

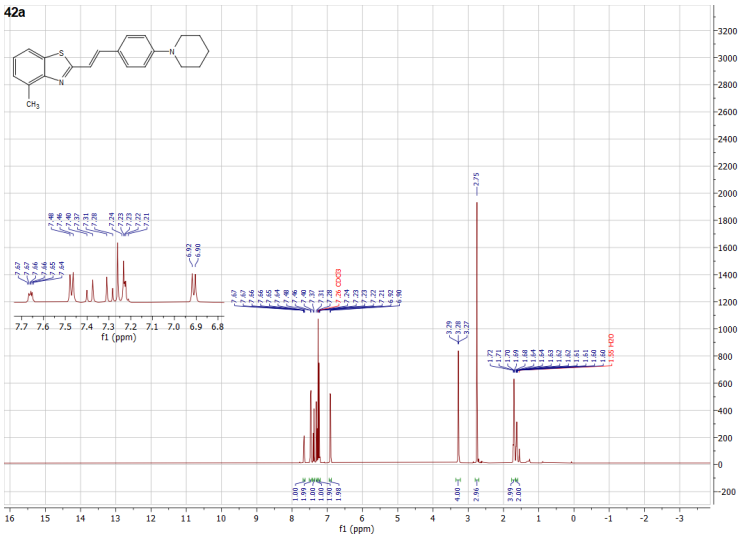
42a
f1 (ppm)

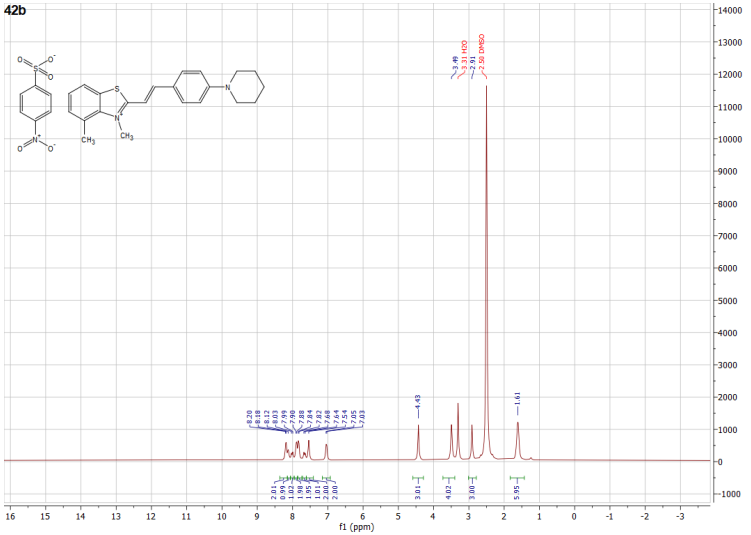
42b
f1 (ppm)

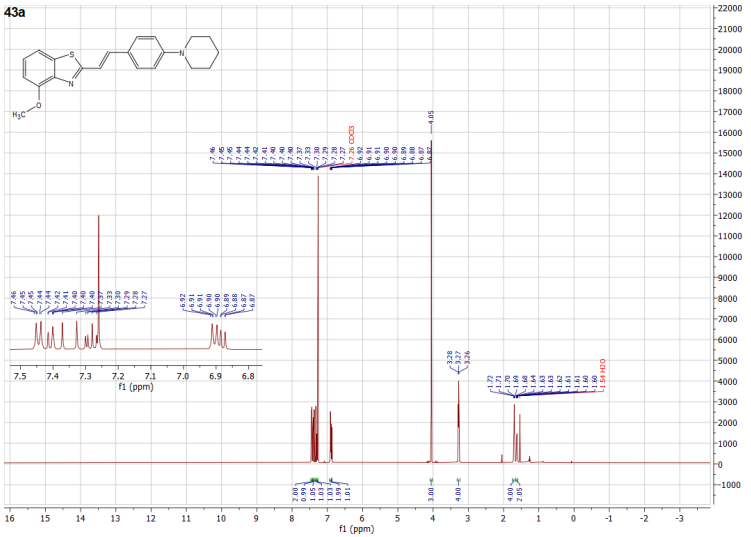
43a
f1 (ppm)

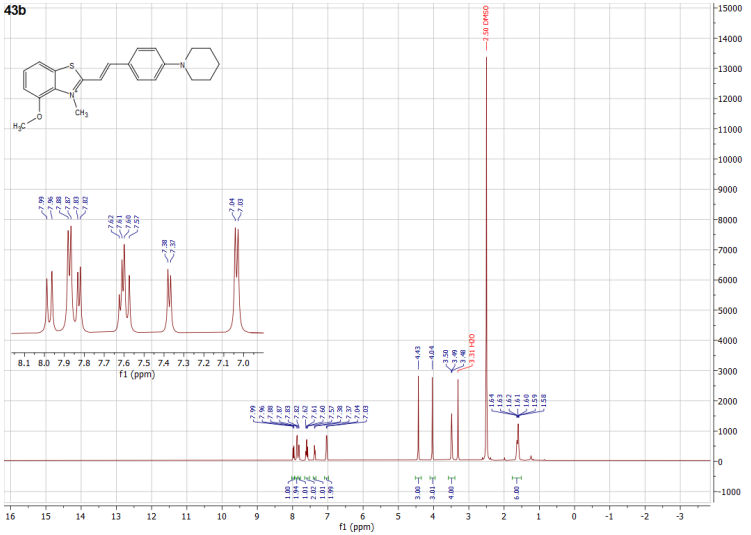
43b
f1 (ppm)

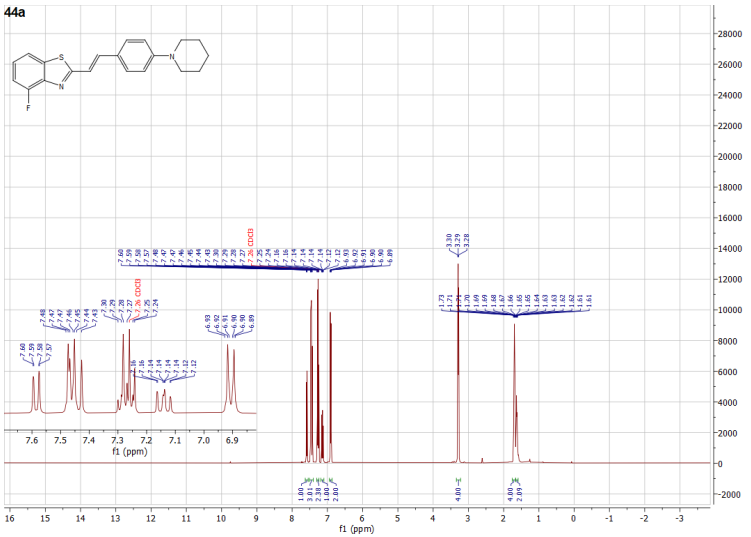
44a
f1 (ppm)

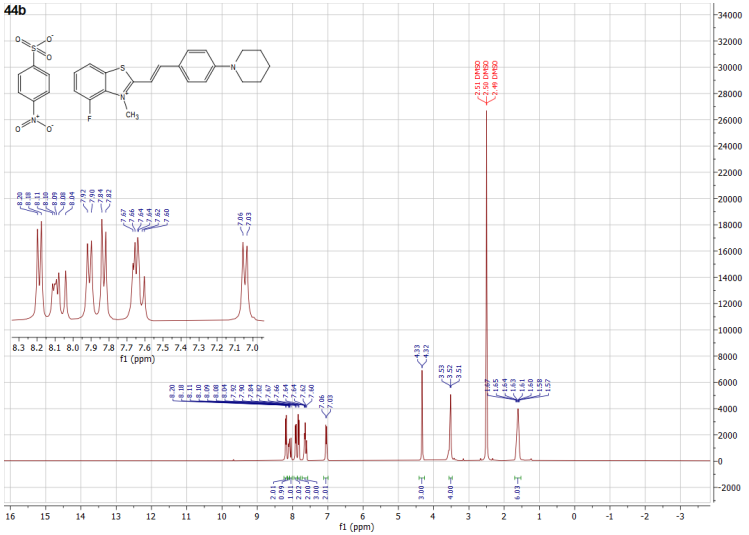
44b
f1 (ppm)

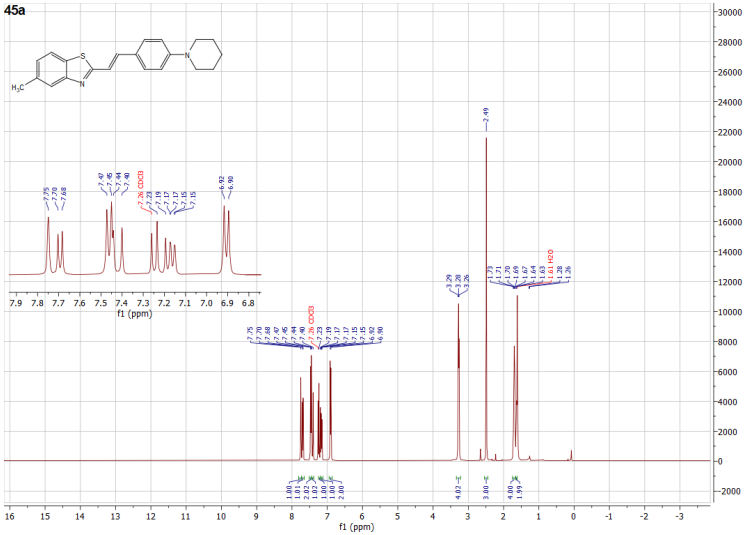
45a
f1 (ppm)

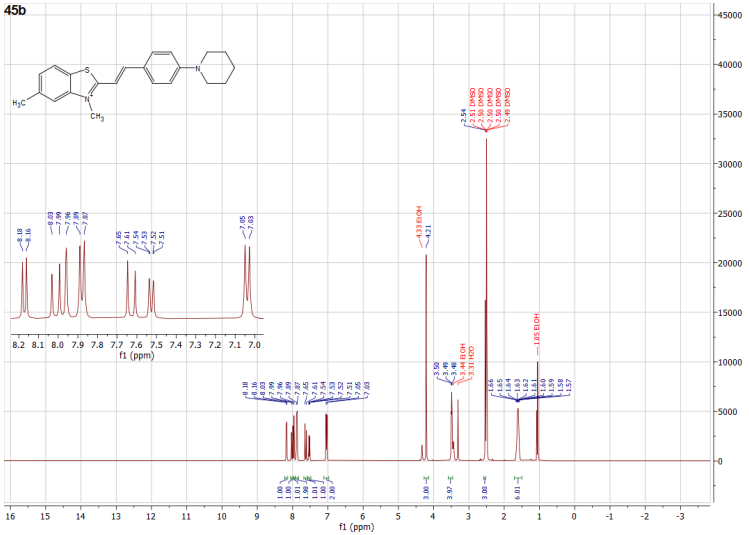
45b
f1 (ppm)

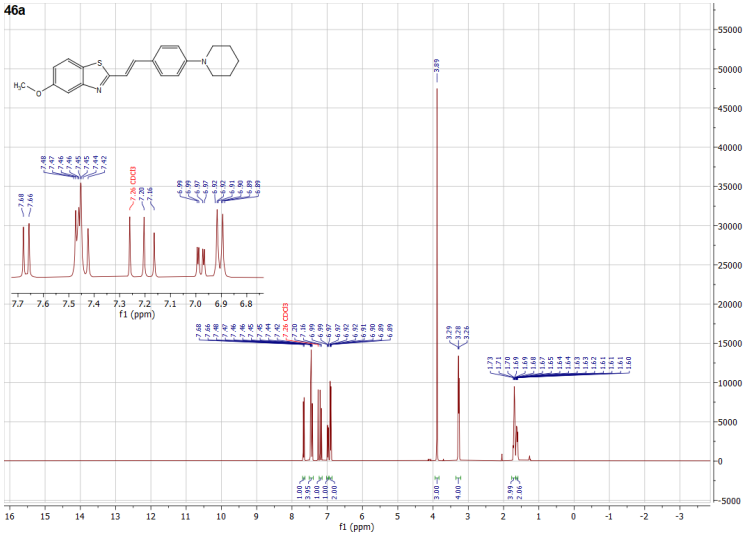
46a
f1 (ppm)

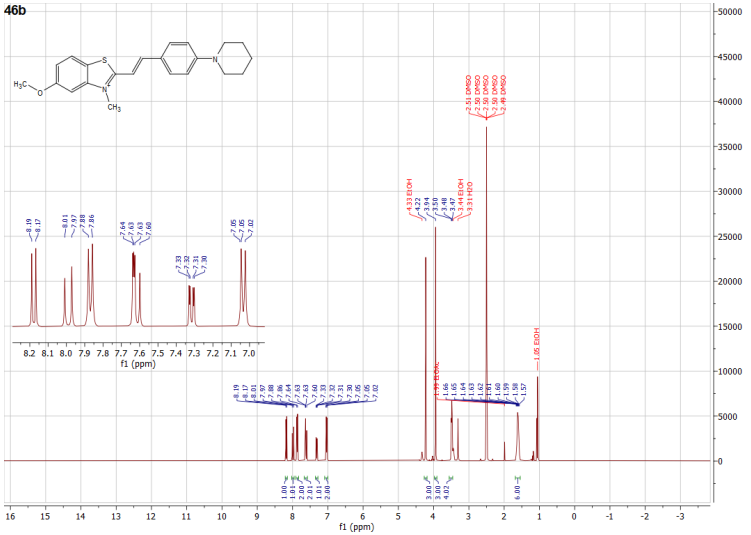
46b
f1 (ppm)

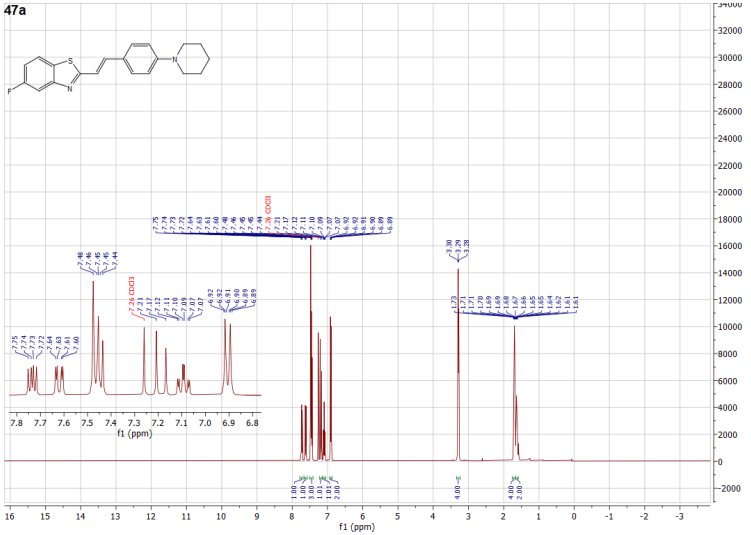
47a
f1 (ppm)

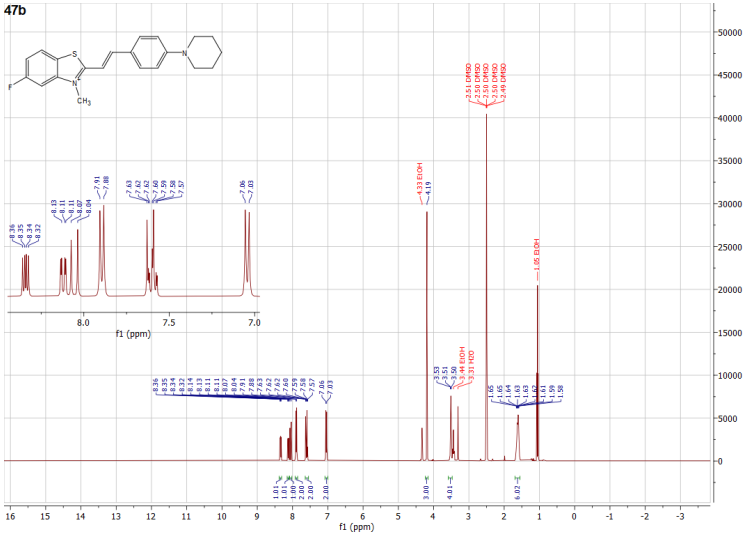
47b
f1 (ppm)

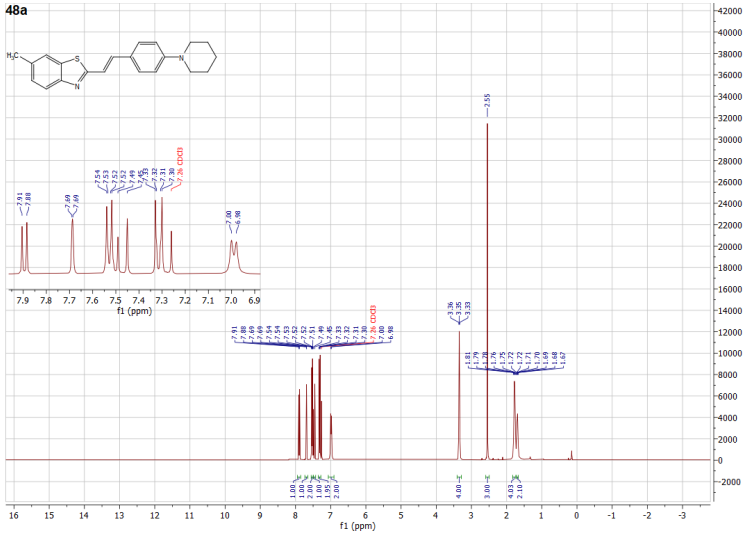
48a
f1 (ppm)

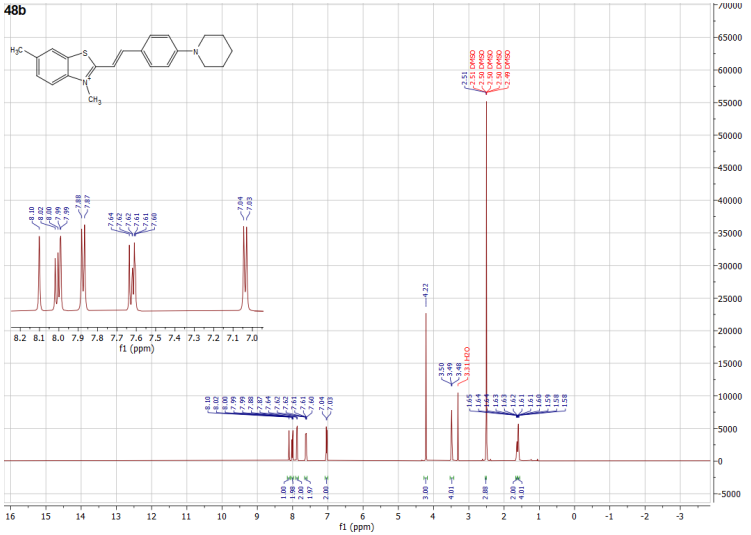
48b
f1 (ppm)

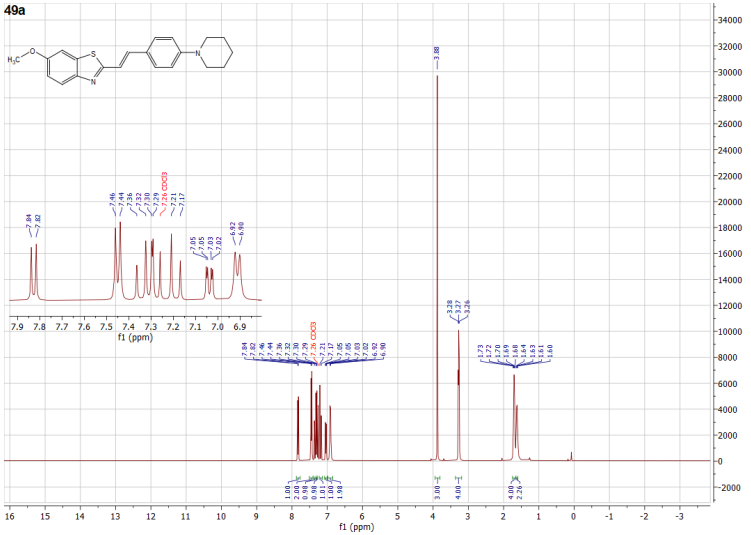
49a
f1 (ppm)

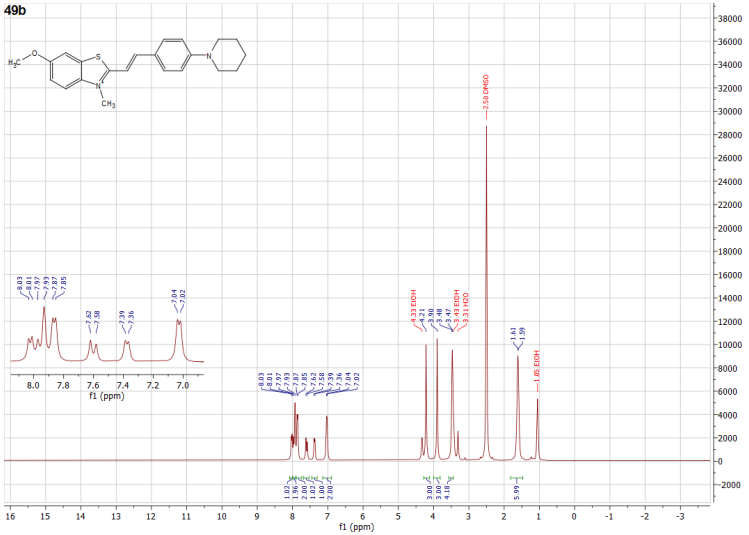
49b
f1 (ppm)

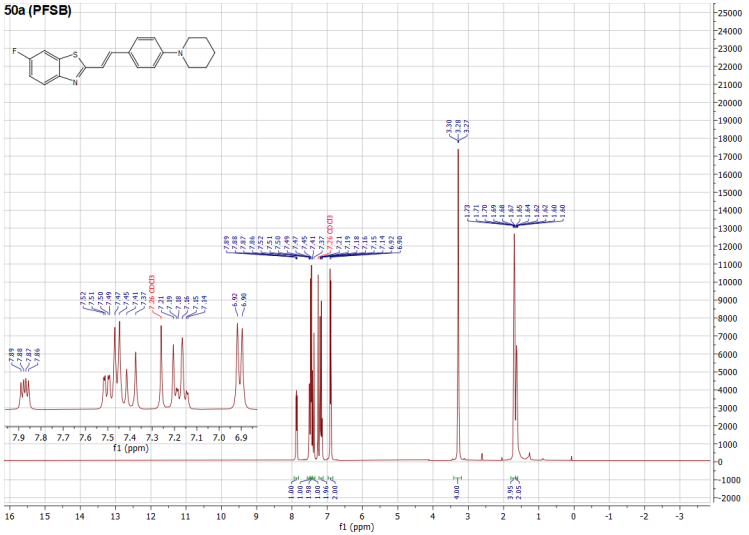
50a (PFSB)
f1 (ppm)

50b

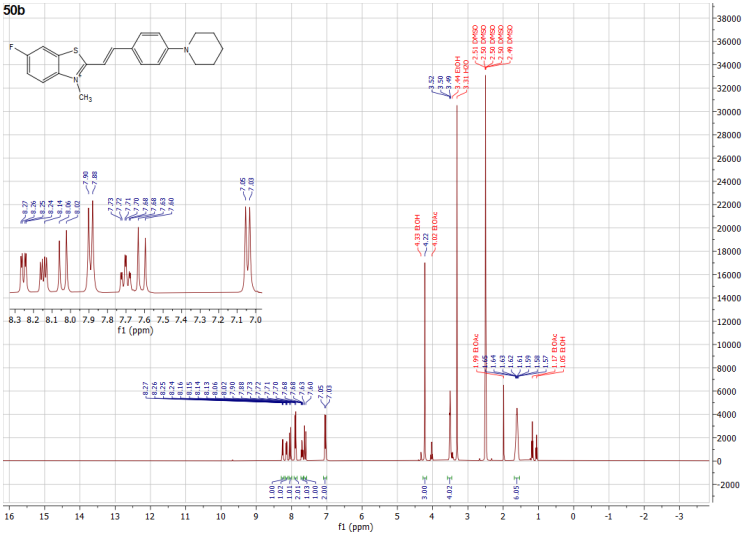

51a

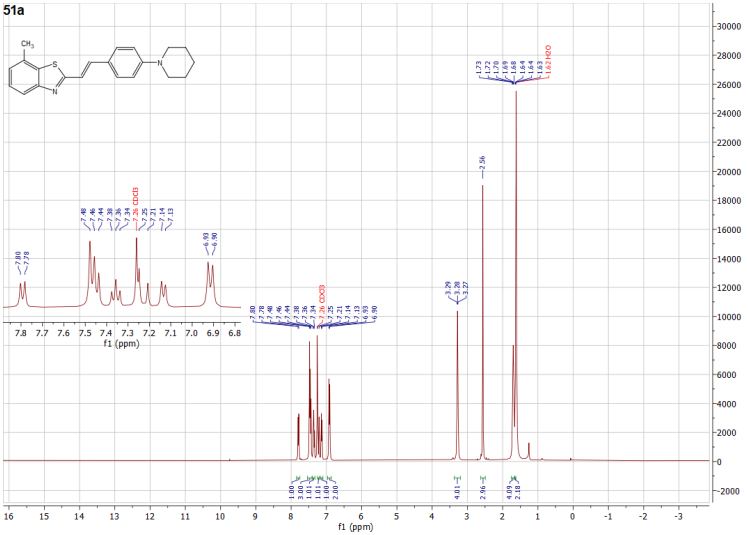

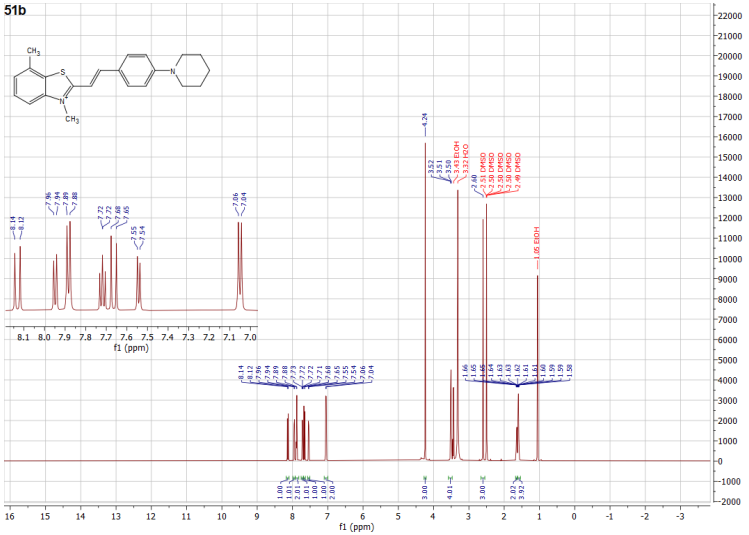
51b
f1 (ppm)

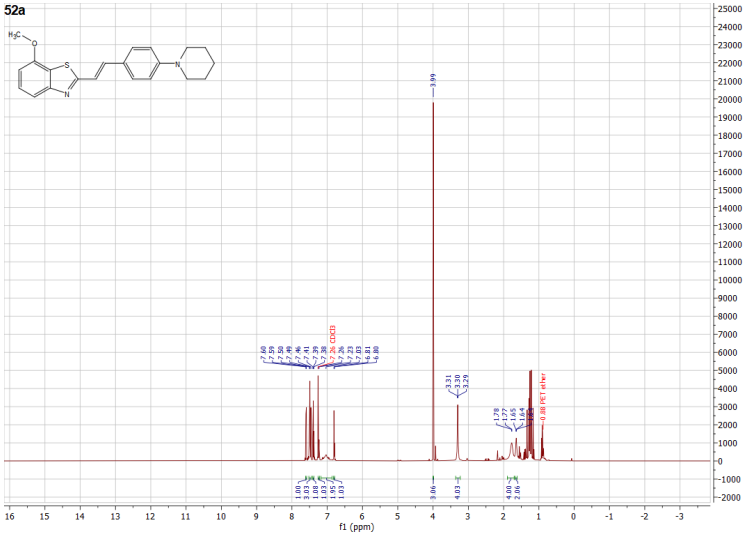
52a
f1 (ppm)

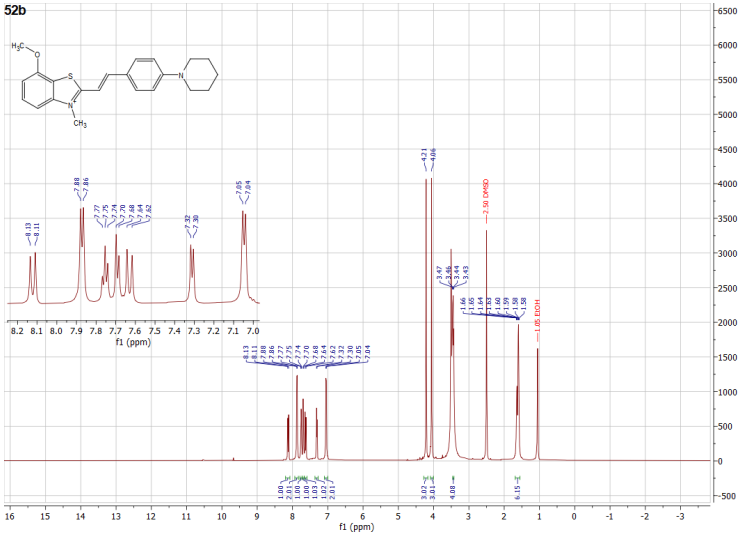
52b
f1 (ppm)

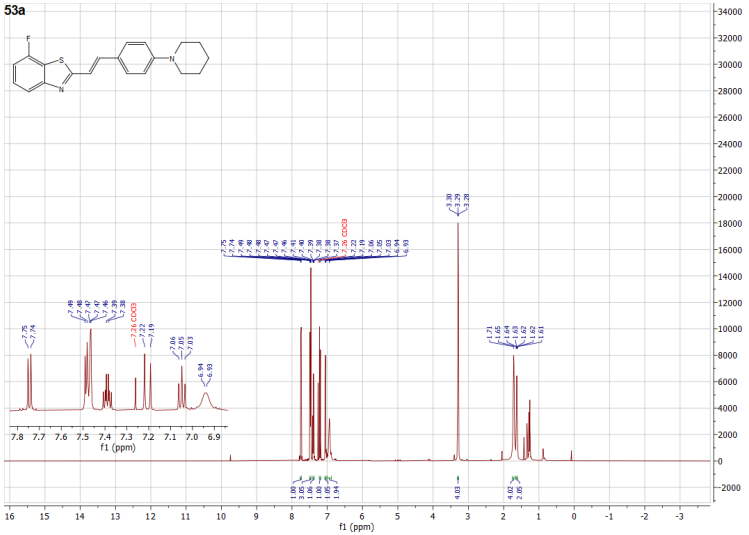
53a
f1 (ppm)

53b

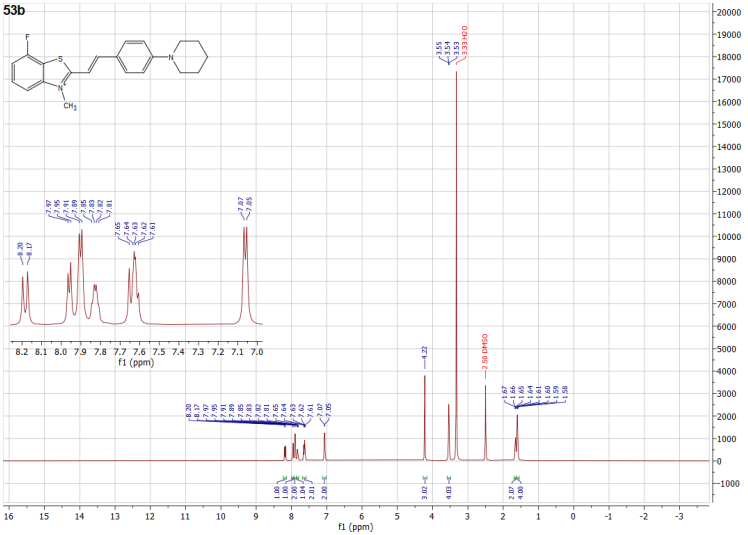

54a

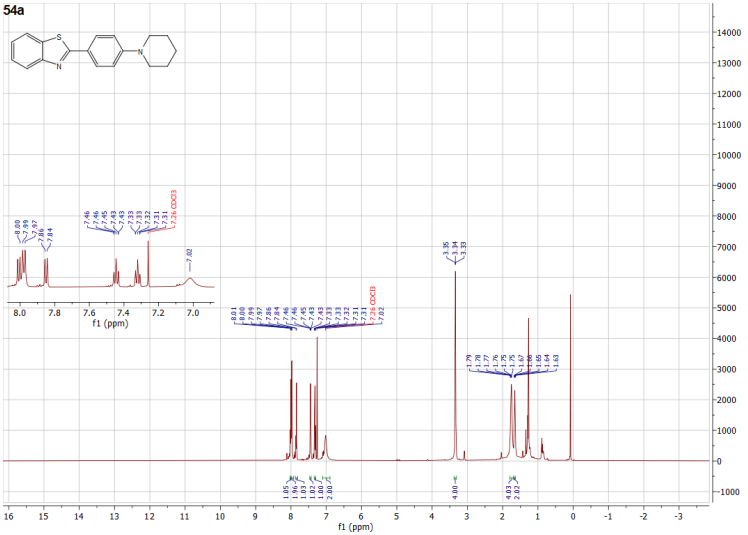

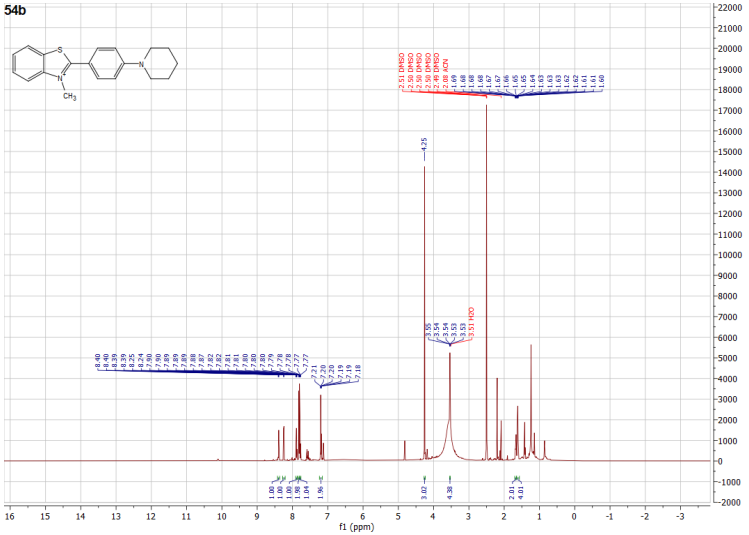
54b
f1 (ppm)

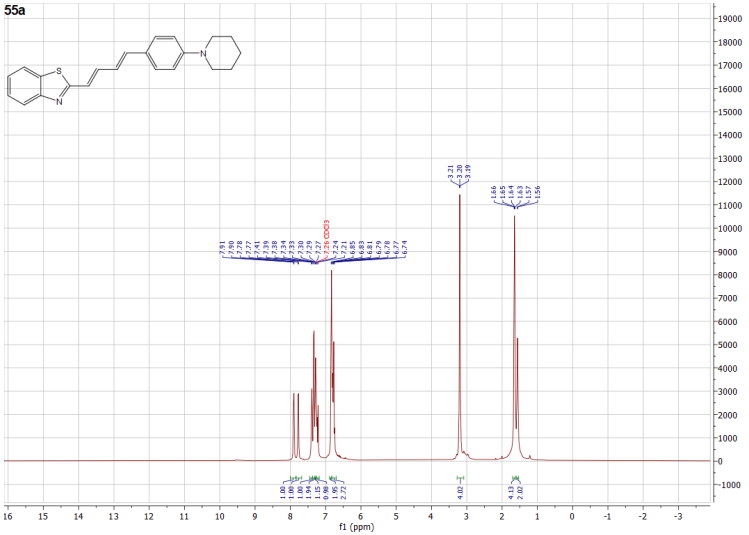
55a
f1 (ppm)

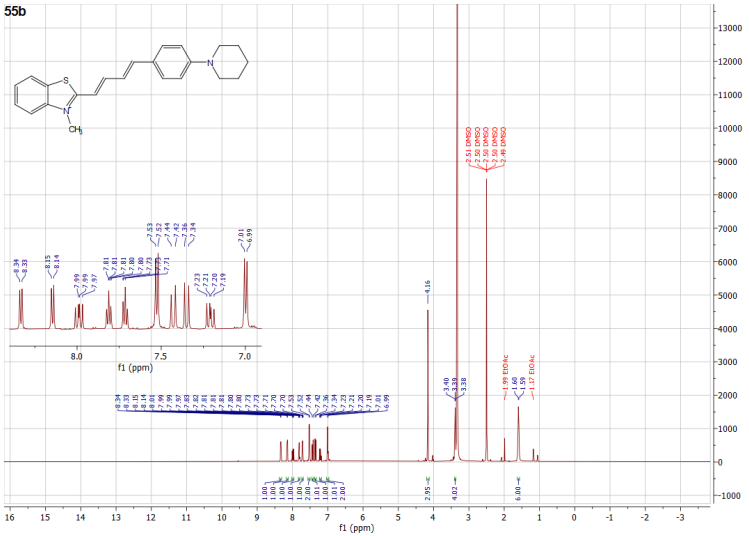
55b
f1 (ppm)

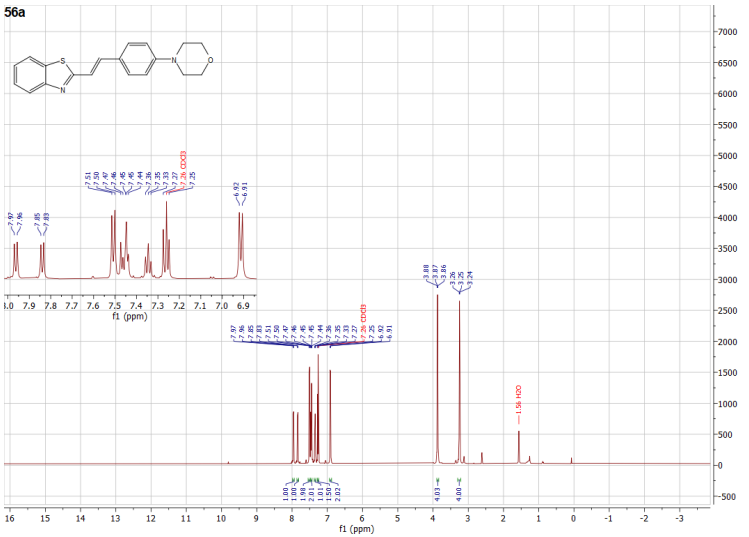
56a
f1 (ppm)

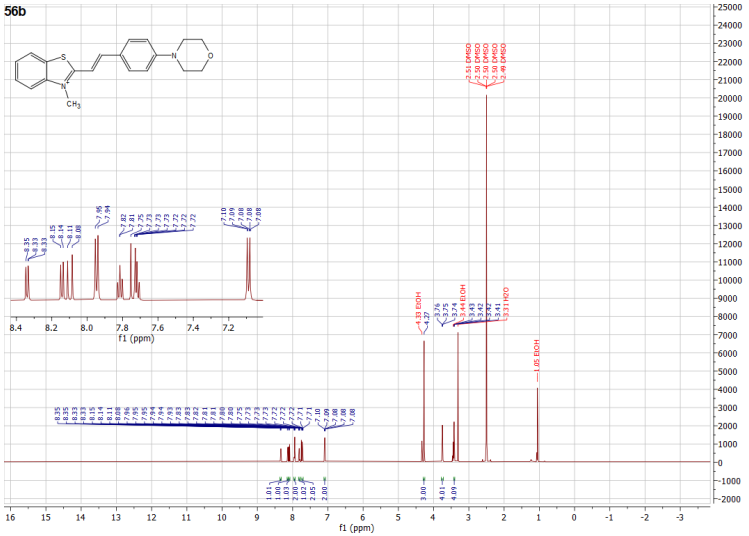
56b
f1 (ppm)

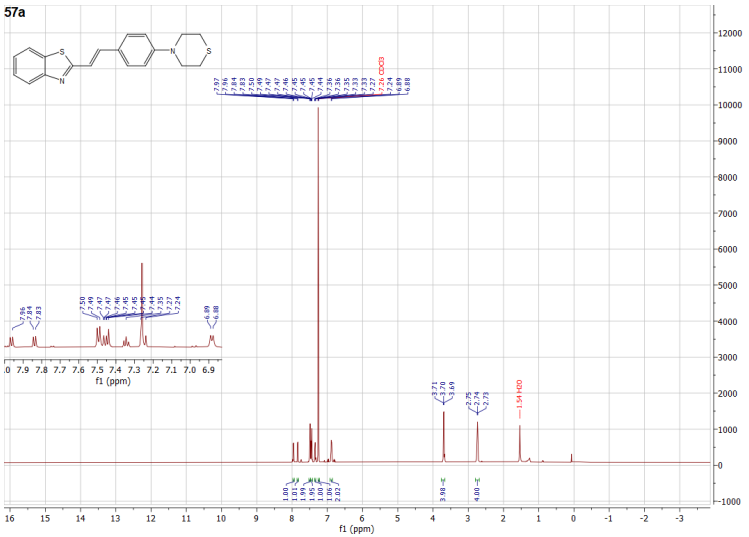
57a
f1 (ppm)

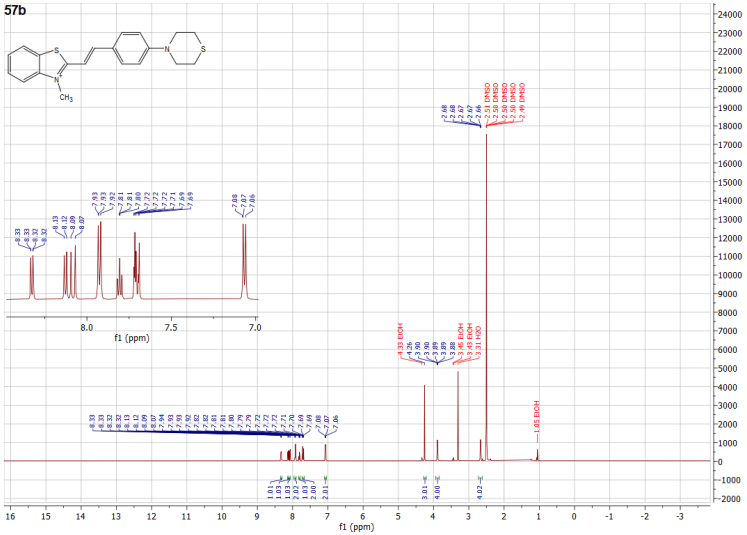
57b
f1 (ppm)

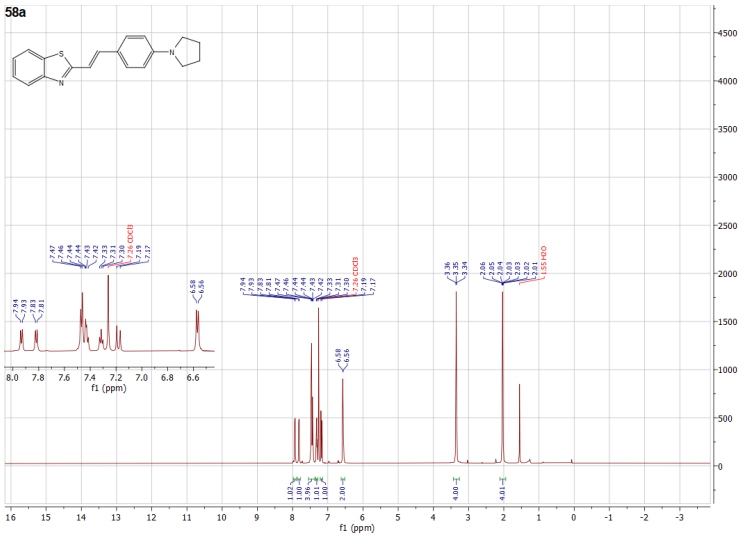
58a
f1 (ppm)

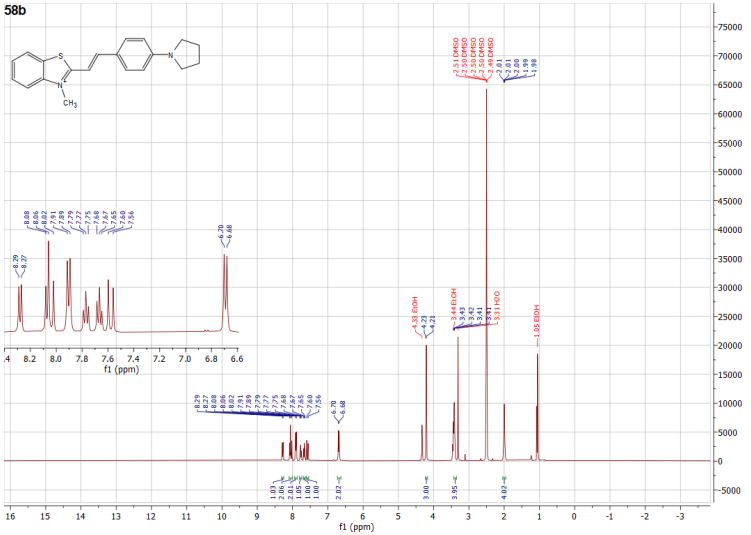
58b
f1 (ppm)

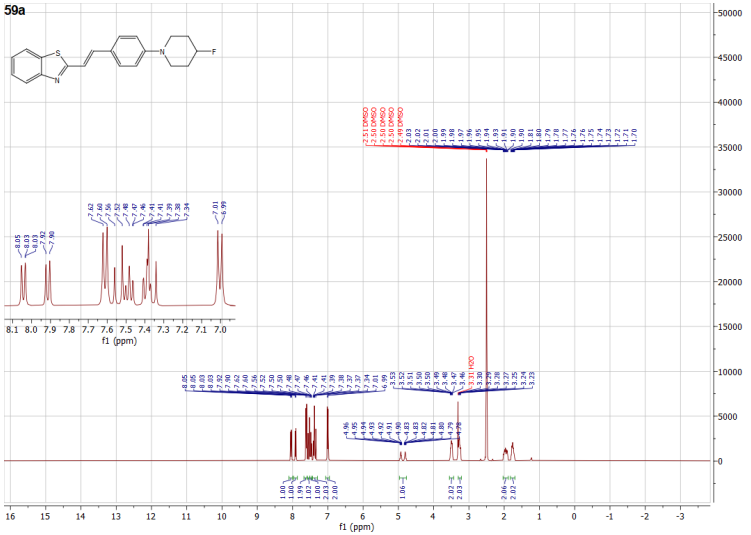
59a
f1 (ppm)

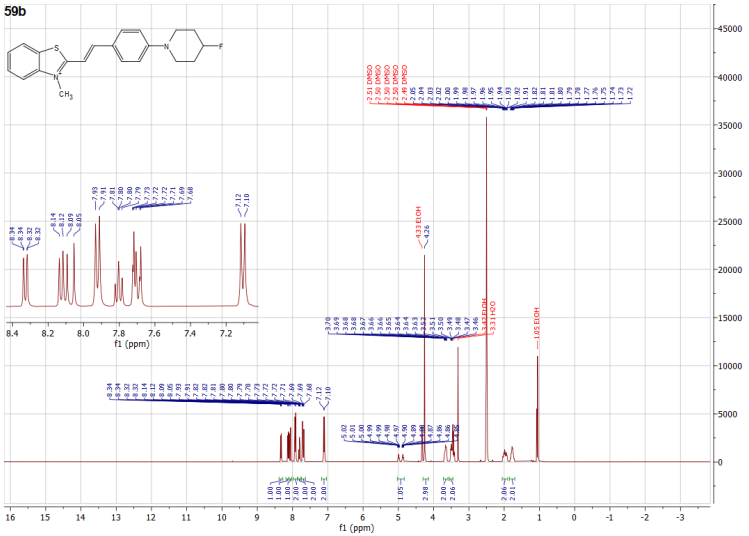
59b
f1 (ppm)

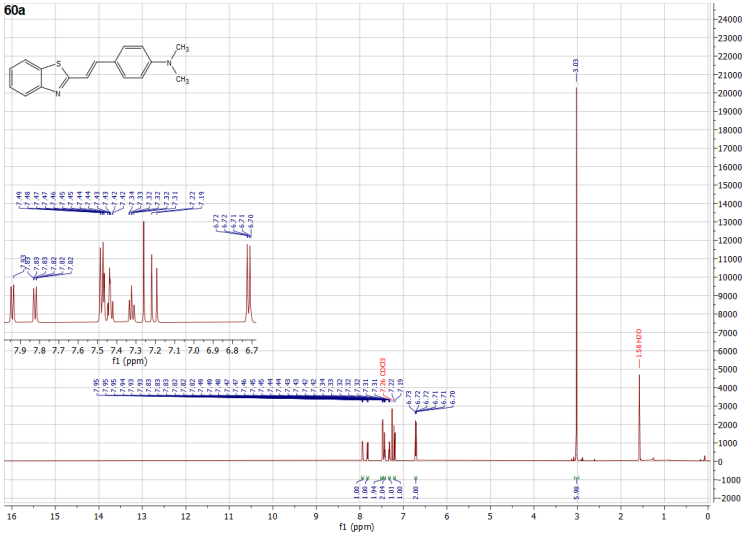
60a
f1 (ppm)

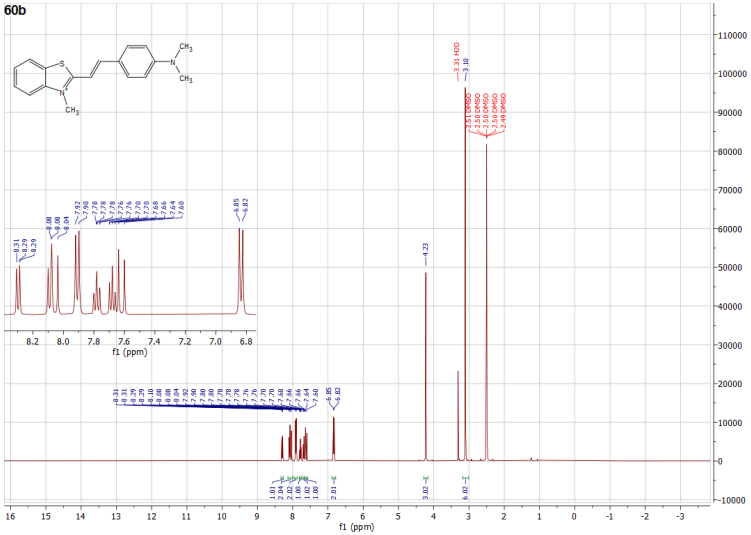
60b
f1 (ppm)

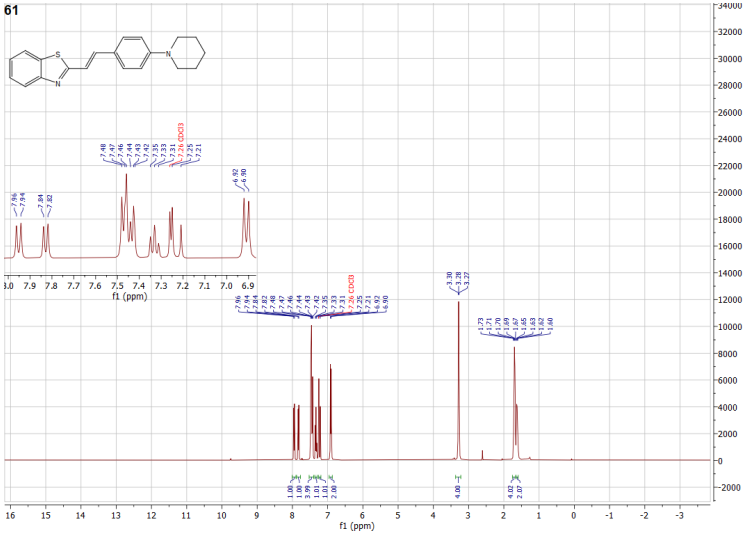
61
f1 (ppm)

62

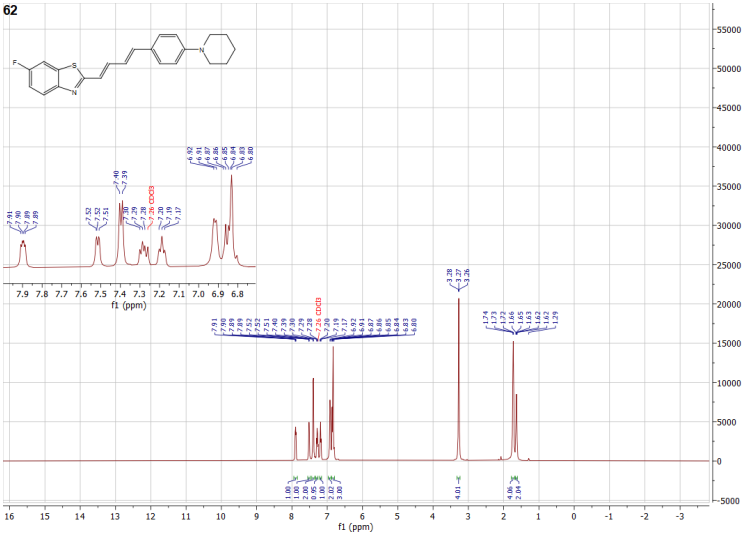

63

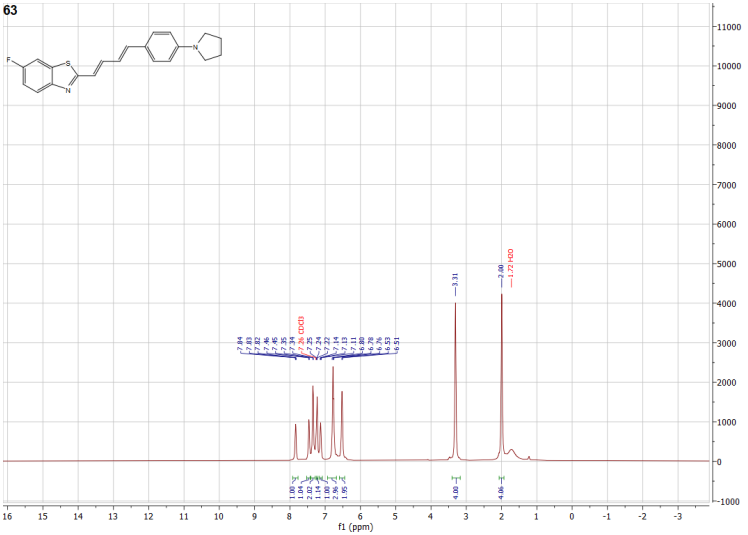

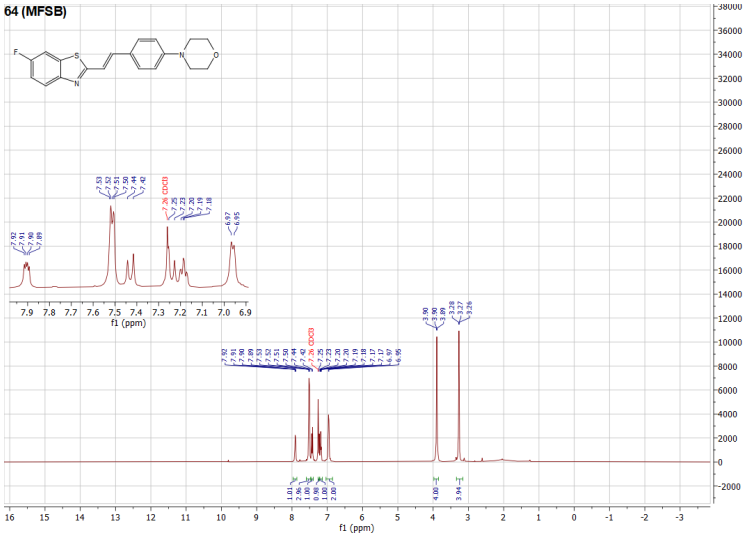
64 (MFSB)
F
S
N
N
O
7.92
7.91
7.90
7.89
7.53
7.52
7.51
7.50
7.44
7.42
7.26 CDCl3
7.25
7.23
7.20
7.19
7.18
6.97
6.95
3.90
3.90
3.28
3.27
3.26
f1 (ppm)

2. ^{1}H NMR spectra of the radiolabeling precursors